

Universal Critical Equation of State and the Chiral Phase Transition in QCD

JÜRGEN BERGES*

*Institut für Theoretische Physik
Universität Heidelberg
Philosophenweg 16
D-69120 Heidelberg, Germany*

Abstract

We employ non-perturbative flow equations to compute the equation of state for two flavor QCD within an effective quark meson model. This yields the temperature and quark mass dependence of quantities like the chiral condensate or the pion mass. Our treatment covers both the chiral perturbation theory domain of validity and the domain of validity of universality associated with critical phenomena: We explicitly connect the physics at zero temperature and realistic quark mass with the universal behavior near the critical temperature T_c and the chiral limit. For realistic quark masses the pion correlation length near T_c turns out to be smaller than its zero temperature value. In the vicinity of T_c and zero quark mass we obtain a precision estimate of the universal critical equation of state. It belongs to the universality class of the three dimensional $O(4)$ symmetric Heisenberg model. We also investigate scalar field theories directly in three dimensions near second order and first order phase transitions. In particular, we obtain the universal equation of state for weak first order phase transitions in scalar matrix models. We also study the coarse grained free energy. Its dependence on the coarse graining scale gives a quantitative criterion for the validity of Langer's theory of spontaneous bubble nucleation.

*Email: J.Berges@thphys.uni-heidelberg.de

Contents

1	Introduction and overview	3
2	Non-perturbative flow equations	14
2.1	Effective average action	14
2.2	Exact flow equation	16
3	Equation of state and second order phase transitions	18
3.1	Introduction	18
3.2	Scale dependence of the effective average potential	19
3.3	Universal critical equation of state	26
3.4	Conclusions	30
4	Equation of state and first order phase transitions	32
4.1	Introduction	32
4.2	Scalar matrix model	34
4.3	Phase structure	36
4.4	Scale dependence of the effective average potential	43
4.5	Solving the flow equation	47
4.6	Renormalization group flow	53
4.7	Universal equation of state for weak first order phase transitions	57
4.8	Coarse graining and Langer's theory of bubble nucleation	61
4.9	Conclusions	69
5	The equation of state for two flavor QCD	72
5.1	Introduction	72
5.2	The quark meson model	78
5.3	A short (scale) history of QCD	79
5.4	Flow equations and infrared stability	84
5.5	Thermal equilibrium and dimensional reduction	92
5.6	Equation of state and the chiral phase transition	95
5.7	Universal critical equation of state	102
5.8	Conclusions	107
6	Outlook	111
7	Acknowledgments	113
A	Threshold functions	114
B	Temperature dependent threshold functions	115
C	Pole structure of the l_n^d integrals	118
D	The quark mass term	120

1 Introduction and overview

Quantum chromodynamics (QCD) describes qualitatively different physics at different length scales. The theory is asymptotically free [1] and at short distances or high energies the strong interaction dynamics of quarks and gluons can be determined from perturbation theory. On the other hand, at scales of a few hundred MeV confinement sets in and the spectrum of the theory consists only of color neutral states. A further important aspect of strong interaction dynamics is spontaneous chiral symmetry breaking. In the limit of vanishing current quark masses the classical or “short distance” QCD action does not couple left- and right-handed quarks. As a consequence, for N_f massless quark flavors the classical QCD action exhibits a global chiral invariance under $U_L(N_f) \times U_R(N_f) = SU_L(N_f) \times SU_R(N_f) \times U_V(1) \times U_A(1)$, with different unitary transformations acting on the left- and right-handed quark fields. However, this symmetry is not fully observed in the hadron spectrum. It is phenomenologically well established that in the quantum theory the symmetry $SU_L(N_f) \times SU_R(N_f)$ is spontaneously broken to the diagonal $SU_V(N_f)$ vector-like subgroup. For $N_f = 2$ the isospin symmetry is realized in the hadron spectrum to a very good approximation. The comparably stronger explicit symmetry breaking due to non-zero current quark masses makes the realization of the $SU_V(3)$ symmetry less accurate. In addition, the axial abelian subgroup $U_A(1)$ is broken in the quantum theory by an anomaly of the axial-vector current [2]. (The abelian $U_V(1)$ subgroup corresponds to baryon number conservation.)

Extrapolating QCD from short distance to long distance scales is clearly a non-perturbative problem. The strong gauge coupling α_s changes with scale, growing with increased distance. However, not only effective couplings but also the relevant degrees of freedom can change with scale. Indeed, at low energies an essential part of strong interaction dynamics can be encoded in the masses and interactions of mesons. Prominent examples of systematic effective descriptions are the successes of chiral perturbation theory [3, 4] based on the non-linear sigma model or a description within the linear sigma model [5]¹. The success of any analytical approach to bridge the gap between short distance and long distance QCD may depend on the ability to introduce field variables for composite objects such as mesons at a certain “compositeness” scale (cf. section 5).

An even more challenging subject is finite temperature QCD [8]. In view of present and future heavy-ion collision experiments [9], but also for its cosmological relevance [10], there is an increased interest in the thermal properties of QCD. It was realized early [11] that in a thermal equilibrium situation at sufficiently high temperature or density QCD may differ in important aspects from the corresponding zero temperature or vacuum properties. If one considers the phase structure of QCD as a function of temperature one expects at a critical temperature around $T_c \simeq 100 - 200$ MeV two types of phase transitions or crossover phenomena². First, there is the expectation that the confined quarks and gluons at zero

¹It has been demonstrated recently [6, 7] that the results of chiral perturbation theory can be reproduced within the linear meson model once certain higher dimensional operators in its effective action are taken into account.

²Transitions are expected for both increasing density and increasing temperature [12, 13]. We will

temperature become deconfined at sufficiently high temperature where the hot state is conventionally called the quark–gluon plasma. In the pure gauge theory, or equivalently in the limit of infinite quark masses, a high temperature deconfinement phase transition is well–established [14, 15]. Second, the spontaneously broken chiral symmetry in the limit of vanishing quark masses and zero temperature is expected to be restored in a high temperature phase. It is not yet clear whether these phase transitions occur at the same temperature or whether they persist for realistic quark masses or rather turn into smooth crossover.

Such a transition must have occurred during the early stages of the evolution of the universe. According to the standard hot big bang cosmology the transition took place about a microsecond after the big bang, where the temperature dropped to the order of 100 MeV. Three orders of magnitude higher the previous transition occurred, related to the dynamics of the electroweak interactions³, and for most of its evolution the early universe was to a good approximation in thermal equilibrium [10].

A promising prospect is to reproduce the QCD transition in heavy–ion collisions in the laboratory at sufficiently high energy. Present fixed target heavy–ion collision experiments at the AGS accelerator (BNL) and at the CERN SPS accelerator have produced heavy–ion beams with energies that could yield initial temperatures above T_c [20]. Here the initial temperature refers to a frequently used scenario in which the central rapidity region reaches a stage of local thermal equilibrium, preceded by an intermediate pre–equilibrium stage after the first instant of nuclear contact [21, 22]. In this scenario the thermalized⁴ central region is characterized by a large number ratio of mesons to baryons [22], thus QCD at finite temperature and zero baryon number density would be of relevance for its description. Whereas SPS realizes for very heavy ion Pb beams a center–of–mass energy of 160 GeV per nucleon, future colliders, RHIC with 200 GeV per nucleon (gold on gold) and the LHC with 6300 GeV per nucleon (lead on lead), will allow to produce temperatures substantially larger than the typical time scales of 10^{-23} sec. or distances of 1 fm associated with the QCD transition [25].

Of particular interest is the order of a possible phase transition which may have far–reaching phenomenological consequences. One reason is that a first order phase transition may create an out of equilibrium situation. For a first order transition the (coarse grained) free energy as a function of a suitable order parameter exhibits two distinct minima near the critical temperature T_c . If in a heavy–ion collision of sufficiently high energy a region of the high temperature phase is created, it then cools through the phase transition. The initial high temperature phase becomes a local minimum of the free energy and the lowest minimum corresponds to the low temperature phase. However, a barrier separating both

restrict the discussion here to QCD at non–zero temperature.

³Existence and properties of the electroweak phase transition depend strongly on the mass of the Higgs scalar M_H . For Higgs boson masses around $M_H \gtrsim 80$ GeV there is no phase transition but rather a smooth crossover [16, 17, 18, 19].

⁴Thermalization enters as an assumption that remains to be justified. There are results from the parton cascade model [23, 24] which give some support to the idea that there will be enough time in a RHIC collision for local thermal equilibrium to be established.

minima prevents a smooth transition at T_c . At a first order phase transition, typically the conversion proceeds in a short dramatic period through the nucleation and growth of “bubbles” (droplets) of the low temperature phase (cf. section 4).

In contrast to the discontinuous behavior at a first order transition, at a second order phase transition the order parameter changes continuously (but non-analytically) from one phase to the other. In particular, there is no mass scale present at a second order phase transition which corresponds to infinite correlation lengths. Large correlation lengths may yield distinctive, qualitative signatures in a relativistic heavy-ion collision. It has been argued [26, 27] that in the central rapidity region a large correlation length may be responsible for the creation of large domains, in which the pion field has a non-zero expectation value pointing in a fixed direction in isospin space (“disoriented chiral condensate” [28]). The observational consequences would be strong fluctuations in the number ratio of neutral to charged pions. Such a phenomenon was even related [26, 27] to the prominent Centauro events [29] in high energy cosmic ray experiments. Apart from the phenomenological implications, a large correlation length opens the spectacular possibility that the QCD phase transition is characterized by universal properties! The notion of universality for critical phenomena is well-established in statistical physics [30]. Universal properties are independent of the details, like short distance couplings, of the model under investigation. They only depend on the symmetries, the dimensionality of space and the number of field degrees of freedom. As a consequence a whole class of models is described by the same universal form of the equation of state in the vicinity of the critical temperature. The range of applicability typically covers very different physical systems in condensed matter physics and high temperature quantum field theory (cf. section 3).

Finally there is the possibility of no true phase transition at all. For such a crossover phenomenon quantities may change rapidly in the transition region, and the phenomenological consequences may be almost indistinguishable from a situation with a true phase transition. However, for a crossover there occurs no non-analytical behavior and all correlation lengths remain finite.

Large correlation lengths near a second order (or weak first order) phase transition are appealing both from the theoretical and the experimental point of view. For the experimentalist they may yield a unique, distinctive signature that a QCD phase transition has occurred. The theoretical challenge is to find a method that describes both the known low-energy zero temperature properties of QCD and the possible universal behavior associated with a large correlation length near the critical temperature of a second order phase transition. The link between the zero temperature and the universal critical properties is crucial. One may think of separating the problem into two parts: First, one considers a tractable, easier model than the original one where both models belong to the same universality class. The simplified description can develop enormous predictive power because of the universal properties of the equation of state near the critical temperature. For instance, a number of stimulating contributions [31, 26, 27] pointed out that for sufficiently small up and down quark masses and sufficiently large strange quark mass the chiral phase transition is expected to be in the universality class of the three dimensional $O(4)$ symmetric Heisenberg

model⁵. This model is known to exhibit a second order phase transition, where universal properties can be observed. Apart from the expected observational consequences, a number of interesting conclusions have been drawn from universality arguments [26, 27], e.g. that the pion mass increases with temperature around T_c . In particular, near the critical temperature only the pions and the sigma resonance play a role for the behavior of the chiral condensate and long-distance correlation functions. Here the chiral condensate, i.e. the expectation value of the quark bilinear $\langle\bar{\psi}\psi\rangle$, plays the role of an order parameter for the chiral transition in the limit of vanishing current quark masses. However, the questions how small the up and down quark mass m_u and m_d would have to be in order to obtain a large correlation length near T_c and if the drawn conclusions are valid for realistic quark mass values remained unanswered. Nothing can be inferred from universality arguments about the absolute magnitude of correlation lengths. Likewise the question of the value of the critical temperature is non-universal in nature. The non-universal amplitudes crucially depend on the zero temperature properties of the theory under investigation. In a second step one therefore finally has to link the universal behavior near T_c and zero current quark mass on one hand with the known physical properties at $T = 0$ for realistic quark masses on the other hand.

One reason for the “missing link” is the breakdown of chiral perturbation theory for temperatures exceeding about one third of the zero temperature pion mass $m_\pi = 135$ MeV (cf. section 5). Exploring the universal region in lattice QCD, on the other hand, is limited by present computer resources, though the use of improved actions seems promising [34]. Since decreasing quark masses increase the computational cost, simulations are typically done with unphysically heavy quarks where extrapolation to realistic values or to the chiral limit is needed.

Equation of state for two flavor QCD

It is a major result of this work to provide the equation of state for two flavor QCD which covers *both* the chiral perturbation theory domain of validity and the domain of validity of universality associated with critical phenomena [33]. The equation of state connects in a temperature range below $\simeq 170$ MeV the derivative of the free energy or the effective potential with the average light current quark mass $\hat{m} = (m_u + m_d)/2$. It therefore allows to study the temperature and quark mass dependence of various quantities, like the pion mass m_π or the chiral condensate $\langle\bar{\psi}\psi\rangle$ or the pion decay constant f_π etc. In addition, we obtain a precision estimate of the universal critical equation of state of the three dimensional $O(4)$ symmetric Heisenberg model in the vicinity of the critical temperature and the chiral limit. From the scaling form of the equation of state we extract universal critical exponents, amplitude ratios and couplings. Recent lattice simulations for the universal critical equation of state of the three dimensional $O(4)$ model show agreement with our results at the few per cent level (cf. section 5). In addition, we find all non-

⁵We note that for two flavors the relevant chiral symmetry $SU(2) \times SU(2)$ is locally isomorphic to $O(4)$. This does not hold in the case of a speculative “effective restoration” [31, 32] of the axial $U_A(1)$ at temperatures around T_c .

universal information to be encoded in two independent amplitudes that are properly computed for the two flavor case.

Though these results will be presented in the text in more detail we point out two important answers one obtains from this study: First of all, for a thermal equilibrium situation the chiral transition gives no indication for strong fluctuations of pions with long wavelength⁶. In the presence of light quark masses the second order phase transition is turned into a smooth crossover: The expectation value of the quark bilinear $\langle \bar{\psi}\psi \rangle$ decreases smoothly as the temperature is increased. The longest correlation lengths near the “crossover temperature” T_{pc} , which turns out to be around 130 MeV for realistic quark masses, even becomes smaller than at $T = 0$. (It should be emphasized, however, that a tricritical behavior with a massless excitation remains possible for three flavors. This would not be characterized by the universal behavior of the $O(4)$ model; see the discussion below.) The second answer concerns the applicability of universal, i.e. almost model independent, arguments for a description of the chiral phase transition. Though the quark masses are fixed in nature, varying the average current quark mass to zero allows us to observe critical behavior independent from the realistic physical situation. In this way one can probe to what extent universality approximately is realized for realistic or even heavier quark masses. Universality has been assumed e.g. in two flavor lattice QCD simulations to guide extrapolation to realistic quark mass values or even to the chiral limit [36]. Despite the observed comparably short correlation lengths at non-zero temperature, we find the approximate validity of the $O(4)$ scaling behavior over a large temperature interval near and above $T_c = 100.7$ MeV even for quark masses slightly larger than the realistic ones (cf. section 5).

Our approach is based on the use of an exact non-perturbative flow equation for a scale dependent effective action Γ_k [37, 38], which is the generating functional of the $1PI$ Green functions in the presence of an infrared cutoff $\sim k$. In a thermal equilibrium context the so-called effective average action Γ_k becomes temperature dependent and describes a coarse grained free energy with a coarse graining length scale $\sim k^{-1}$. The coarse grained description allows us to consider the relevant physics at a given momentum-like scale k . The approach is closely connected to the Wilsonian renormalization group [30, 39, 40, 41, 42, 43], often also called exact renormalization group. An introduction to the method is given in section 2.

The flow equation for Γ_k can be supplemented by an exact formalism for the introduction of composite field variables or, more generally, a change of degrees of freedom at some given scale k [44]. We employ for scales below a “compositeness scale” of $k_\Phi \simeq 600$ MeV a description in terms of quark and scalar mesonic degrees of freedom. This effective quark meson model can be obtained from QCD in principle by “integrating out” the gluon degrees of freedom and by introducing fields for composite operators [44, 45] (cf. the discussion in sections 5 and 6). In this picture the scale k_Φ is associated to the scale at which the

⁶We have restricted the discussion to the thermal equilibrium properties of QCD. The question of strong fluctuations of pions with long wavelength has been investigated in the context of a chiral QCD phase transition far from equilibrium [26, 35].

formation of mesonic bound states can be observed [44] in the flow of the momentum dependent four-quark interaction. Though considerable progress has been made, a reliable quantitative derivation of the effective quark meson model from QCD is still missing. We emphasize, however, that the quantitative aspects of this derivation will be of minor relevance for our practical calculations in the mesonic sector: If the effective Yukawa coupling between the quarks and the mesons turns out to be strong at the compositeness scale we observe a fast approach of the scale dependent effective couplings to approximate partial infrared fixed points [46, 33]. This behavior is discussed in section 5.4. As a consequence, the detailed form of the meson potential at k_Φ becomes unimportant, except for the value of one relevant scalar mass term \overline{m}_{k_Φ} . In this work we fix \overline{m}_{k_Φ} from phenomenological input such that $f_\pi = 92.4$ MeV (for $m_\pi = 135$ MeV) which sets our unit of mass for two flavor QCD. The only other input parameter we use is the constituent quark mass M_q to determine the scale k_Φ . We consider a range $300 \text{ MeV} \lesssim M_q \lesssim 350 \text{ MeV}$ and find a rather weak dependence of our results on the precise value of M_q . We point out that though a strong Yukawa coupling at k_Φ is phenomenologically suggested by the comparably large value of the constituent quark mass M_q it enters our description as a (consistent) assumption. On the present level of approximation the quark meson model for two flavors can be reduced to the well known $O(4)$ symmetric Gell-Mann–Levy linear sigma model [5] for the three pions and the “sigma resonance”, however, it is coupled to quarks now. The meson degrees of freedom can be understood as quark–antiquark bound states. Spontaneous chiral symmetry breaking is described by a non-vanishing expectation value of the meson field in absence of quark masses. The non-perturbative flow equations for the quark–meson model are obtained from a suitable truncation of the exact flow equation for Γ_k . We solve them numerically. Further details about the model and the applied approximations can be found in section 5.

Quark mass dependent phase structure

The details of a possible QCD phase transition, like the order or the “strength” of the transition, crucially depend on the number of flavors and the current quark masses. Though the number of flavors and the quark masses are fixed in nature, on the theoretical side it is possible to adjust them in order to get more insight into the phase structure of QCD. A considerable amount of information about the phase structure of non-zero temperature QCD has been provided by lattice Monte Carlo simulations whose results will be instructive in the following. The majority of lattice simulations incorporating dynamical fermions have been done with two or four flavors of equal mass quarks. There are a few simulations carried out for two light and one heavier quark which comes closest to the physical light quark mass ratios. To save computational cost, however, simulations are typically done with unphysically heavy quarks.

Lattice QCD simulations in the limit of two light quark flavors show no signs of a first order deconfinement phase transition [47, 36]. The expectation value of the Polyakov loop⁷ increases smoothly with increased temperature when dynamical fermions are present.

⁷We note that the Polyakov loop represents no order parameter for a possible deconfinement phase

There is no sharply defined transition, but rather a smooth crossover from one regime to the other. In accordance with our results, the chiral transition for two small, non-zero quark masses is found to be described by a crossover phenomenon [47, 36]. The lattice results indicate that both crossover, associated to the deconfinement and to the chiral transition, occur at the same temperature approximately around⁸ 140 – 150 MeV. This qualitative picture almost remains the same for the more realistic case of two light and one heavier quark. Simulations with “2+1” flavors carried out by the Columbia group in the staggered fermion scheme find a first order signal from the chiral condensate for three light flavors. However, the first order transition disappears for an increased strange quark mass, even before the strange quark adopts its physical mass value [48]. In contrast, from a Wilson fermion approach the Tsukuba group finds results that indicate a first order chiral phase transition for realistic quark masses[49]. However, simulations with Wilson fermions in this context are difficult because they break chiral symmetry completely away from the continuum limit. Though no final conclusion can be drawn from the lattice results by now, if there is a first order phase transition at all it is very likely to be weak. In addition, lattice data seem to indicate that QCD exhibits a (smooth) transition which is dominated by the approximate restoration of chiral symmetry.

Our results and the results from lattice simulations are compatible with the following picture proposed from effective sigma model considerations [31, 50, 26, 51]: For three massless quark flavors the chiral phase transition is first order in nature. If the strange quark mass m_s is raised the phase space shows a line of first order transitions which ends in a tricritical point with a massless excitation. For larger strange quark masses the transition remains of second order. If one takes into account that the up and down quark masses are non-zero this second order phase transition is smoothed into a crossover phenomenon. However, there remains a line of tricritical points separating the first order region for small m_s and the crossover region for large m_s . It has been pointed out [51, 52] that the QCD chiral phase transition may be close to a tricritical point with a massless excitation.

Effective three dimensional behavior at high temperature

Our investigations have ruled out the appearance of a large correlation length at the equilibrium chiral transition in the two flavor case, corresponding to an infinite mass limit for the remaining quark flavors. However, we have seen that a chiral transition with a large correlation length remains possible through the influence of the strange quark. In particular, along the mentioned line of tricritical points the transition is expected to be in the universality class of the Ising model [51]. In this case, as has been discussed above, in a first step one may learn as much as possible about the phase transition only relying on universality arguments. This alone typically poses a complicated non-perturbative problem. The problems are related to the effectively three dimensional behavior of high

transition in the presence of light quarks. Only in the limit of infinite quark masses, or equivalently in the pure gauge theory, it is an order parameter for the spontaneous breaking of the center $Z(N)$ of the gauge group $SU(N)$ at high temperature [14].

⁸Here the zero temperature ρ meson mass is used to set the energy scale.

temperature quantum field theory in four dimensions. Quantum field theory at non-zero temperature T can be formulated in terms of an Euclidean functional integral where the “time” dimension is compactified on a torus with radius T^{-1} [53]. Accordingly, non-zero temperature results in (anti-) periodic boundary conditions for (fermionic) bosonic fields in the Euclidean “time” direction with periodicity T^{-1} . As a consequence, the zeroth component of the Euclidean four-momentum becomes discrete, i.e. $q_0 = 2l\pi T$ for bosons and $q_0 = (2l + 1)\pi T$ for fermions with integers⁹ l . It is suggestive that if the relevant correlation length becomes much larger than the inverse temperature the compactified “time” dimension cannot be resolved anymore. This phenomenon is known as “dimensional reduction” [54]. The effective three dimensional behavior of the theory can also be understood from the observation that for sufficiently high temperature the theory is dominated by classical statistical fluctuations. In particular, the critical exponents which describe the singular behavior of various quantities near a second order phase transition are those of the corresponding classical system¹⁰ [55] (cf. section 5). An important particularity of the dimensionally reduced theory is the absence of fermionic degrees of freedom. This can be seen as a consequence of the fact that the “lightest” fermionic excitation is of the order πT , whereas there exists a zero mode ($l = 0$) for a bosonic field. We have explicitly verified the phenomenon of dimensional reduction and the absence of fermions within the effective quark meson model at high temperature (cf. section 5).

Near a second order (or a sufficiently weak first order) phase transition we therefore have to deal with a purely bosonic three dimensional theory. Standard high temperature perturbation theory can give a reliable description only if the relevant dimensionless couplings remain small near the transition. In three dimensions the (effective) scalar quartic coupling $\bar{\lambda}$ has positive canonical mass dimension. If one denotes by m_R the relevant mass at the critical temperature, standard perturbation theory corresponds to an expansion in the dimensionless effective coupling $\bar{\lambda}/m_R$. For a given fixed coupling $\bar{\lambda}$ a perturbative expansion will only converge if m_R is sufficiently large, $m_R \gg \bar{\lambda}$. In consequence, standard perturbation theory is not applicable to second order ($m_R = 0$) or weak first order ($m_R \ll \bar{\lambda}$) phase transitions due to the apparent infrared divergences in a perturbative treatment. Obviously in a suitable non-perturbative treatment a “running” effective renormalized coupling λ_R has to be introduced. The running coupling approaches zero at a second order phase transition, with λ_R/m_R going to a constant as the correlation length m_R^{-1} tends to infinity. Typically no small effective coupling characterizes the interactions at the phase transition (cf. section 3).

The three dimensional systems may be treated within the ϵ -expansion [56] or by the use of perturbation series at fixed dimension [57]. Most of the lattice results come from the analysis of high temperature expansions [58] or from Monte Carlo simulations [59]. For the critical equation of state of the three dimensional $O(4)$ model a result from the ϵ -expansion up to second order in $\epsilon = 4 - d$ ($d = 3$) is available [60]. The reliability of this

⁹These are commonly called Matsubara frequencies.

¹⁰In the vicinity of the critical temperature of a second order phase transition the correlation length of the relevant bosonic field is $\xi \sim T_c^{-1}(|T - T_c|/T_c)^{-\nu}$ with a (positive) exponent ν , and one *always* faces a high temperature situation for $T \rightarrow T_c$, i.e. $\xi \gg T^{-1}$.

expansion is not guaranteed a priori and results from a lattice Monte Carlo simulation [61] that has recently been obtained show substantial deviations from the ϵ -expansion results (cf. section 5). The lattice simulations are quite demanding in the vicinity of the critical temperature of a second order (or weak first order) phase transition and require careful correction for finite size effects. As has been pointed out above our results agree quite well with the lattice study.

The use of non-perturbative flow equations within the framework of the effective average action is particularly suitable for dealing with theories which are plagued by infrared problems in perturbation theory. The employed formulation is both infrared and ultraviolet finite in arbitrary dimensions. In particular, the method is not restricted to an expansion in small couplings which has been crucial for the treatment of the effective quark meson model.

Equation of state for second order and (weak) first order transitions

The first two parts of this work are devoted to the study of scalar field theories near the critical temperature of second order and first order phase transitions. These investigations are performed directly in three dimensions. We obtain a detailed quantitative picture of the critical equation of state in the vicinity of the second order phase transition of the $O(N)$ symmetric N -component model [62, 63, 64]. Similar to the case $N = 4$, for $N = 1$ our results have been confirmed by lattice simulations [65, 66] while there remains a considerable discrepancy to the ϵ -expansion results¹¹. We point out that our approximations are based on a derivative expansion for the effective average action that takes into account the *most general* non-derivative, i.e. potential, term consistent with the symmetries. It does not rely on any restriction of the potential to a polynomial form. It therefore allows to study the complete non-analytic behavior of the effective potential, or equivalently the free energy, near the critical temperature of the second order phase transition. For $N = 4$ our universal results in three dimensions are found to correspond to the results from the quark meson model near the critical temperature and the chiral limit. This correspondence is a manifestation of the phenomenon of dimensional reduction. The $O(N)$ model has a wide range of different applications in statistical physics and high temperature quantum field theory. For $N = 4$ the model also describes the scalar sector of the electroweak standard model in the limit of vanishing gauge and Yukawa couplings. In condensed matter physics $N = 3$ corresponds to the well known Heisenberg model used to describe the ferromagnetic phase transition. There are other applications like the helium superfluid transition ($N = 2$), liquid-vapor transition ($N = 1$) or statistical properties of long polymer chains ($N = 0$) [67]. The critical properties of these systems are presented in section 3.

The second part of this work provides a detailed investigation of first order phase transitions. In particular weak first order phase transitions are a much less thoroughly studied subject in the literature than second order transitions. This becomes especially desirable in the context of a possible weak first order chiral phase transition in QCD. We consider [68, 69] models with $U(N) \times U(N)$ symmetry with a scalar field in the (\bar{N}, N)

¹¹For $N = 1$ the ϵ -expansion for the scaling equation of state is available up to order ϵ^3 [67].

representation, described by an arbitrary complex $N \times N$ matrix. We compute the equation of state for $N = 2$ which can be used for an effective description of two flavor QCD in the case of a speculative “effective restoration” [31, 32] of the chiral anomaly at high temperature. The considered theory also has a relation to the electroweak phase transition in models with two Higgs doublets. In certain limiting cases the model describes a non-linear matrix model for unitary matrices or one for singular 2×2 matrices (cf. section 4).

For a large part of the parameter space the $U(2) \times U(2)$ symmetric matrix model exhibits a weak first order phase transition. Though the corresponding classical or short distance action indicates a second order phase transition, the transition becomes first order once fluctuations are taken into account. The fluctuation induced first order phase transition is known in four dimensions as the Coleman–Weinberg phenomenon [70]. A reliable method for a description of this phenomenon in three dimensions may be of relevance for the QCD chiral phase transition. For the realistic case of three flavors it has been argued that the chiral transition can be mainly fluctuation induced [51, 52].

We put special emphasis on the investigation of (approximate) universal properties near weak first order phase transitions. Whereas for second order transitions the universal equation of state can be expressed as a function of only one scaling variable (cf. section 3), due to an additional mass scale at a first order transition there is a second dimensionless ratio. The equation of state or, equivalently, the effective potential or free energy therefore depends on two independent scaling variables in the universal region. We have succeeded to describe this situation [68] for the present matrix models and present the universal equation of state in section 4.7.

Coarse graining and first order transitions

Another challenging problem is the discussion of the dynamics of a first order phase transition [71] which usually relies on the study of a non-convex potential or free energy. The decay of metastable states is associated either with tunneling fluctuations through barriers in the potential [72], or, at non-zero temperature, with thermal fluctuations above them [73]. However, the effective potential [75], which seems at first sight a natural tool for such studies, is expected to be a convex quantity with no barrier. The resolution of this paradox lies in the realization that the effective potential is convex because the tunneling or thermal fluctuations are incorporated in it. These fluctuations are associated with low frequency modes, while the non-convex part of the potential is related to the classical potential and the integration of high frequency modes. A natural approach to the study of first order phase transitions separates the problem in two parts. First, the high frequency modes are integrated out, with the possible generation of new minima of the potential through radiative symmetry breaking [70]. Subsequently, the decay of metastable states is discussed with semiclassical techniques [72, 73], using the non-convex potential that has resulted from the first step. This leads one to the notion of the coarse grained free energy, which is fundamental in statistical physics. Every physical system has a characteristic length scale associated with it. The dynamics of smaller length scales is integrated out, and is incorporated in the parameters of the free energy one uses for the study of the

behavior at larger length scales. Here we note that by construction, i.e. the inclusion of fluctuations with characteristic momenta larger than a given infrared cutoff $\sim k$, the effective average action Γ_k is the appropriate quantity for the study of physics at a scale k (cf. section 2). It therefore realizes the concept of a coarse grained free energy in the sense of Langer [71].

The use of the effective average action will allow us to address the old question of the validity [68, 69] of the standard theory of spontaneous bubble nucleation proposed by Langer [71]. This requires first a meaningful definition of a coarse grained free energy with a coarse graining scale k and second the validity of a saddle point approximation for the treatment of fluctuations around the “critical bubble” (cf. section 4.8). Here only fluctuations with momenta smaller than k must be included. Both issues turn out to be closely related. The validity of the saddle point approximation typically requires small dimensionless couplings. On the other hand we observe for large effective couplings that the form of the relevant coarse grained effective potential U_k depends strongly on the coarse graining scale k . This means that the lowest order in the saddle point approximation (classical contribution) depends strongly on the details of the coarse graining procedure. Since the final results as nucleation rates etc. must be independent of the coarse graining prescription this is only compatible with a large contribution from the higher orders of the saddle point expansion. We will consider this issue in section 4.8 in a quantitative way.

This work is organized as follows. We provide an introduction into the non-perturbative effective average action method in section 2. The two following sections concern our studies of second order and first order phase transitions in three dimensional scalar field theories. These parts are based on refs. [62, 63, 64] and [68, 69] respectively. Section 5 is devoted to the chiral phase transition for two flavor QCD within the effective quark meson model. This part is based on refs. [33, 74]. Each section is supposed to be rather self-contained with a short introduction and conclusions to allow for a selective approach to the presented material. Section 6 presents an outlook. The acknowledgments are found in section 7. The three appendices A–C contain a discussion and definitions of threshold functions used in preceding sections. In appendix D the connection of the average current quark mass with the effective source term of the quark meson model is established. This is used in section 5.

2 Non-perturbative flow equations

2.1 Effective average action

We will introduce here the effective average action [37] Γ_k with an infrared cutoff $\sim k$. The effective average action is based on the quantum field theoretical concept of the effective action [75] Γ , i.e. the generating functional of the *1PI* Green functions. The field equations derived from Γ include all quantum effects. For a field theoretical description of thermal equilibrium this concept is easily generalized to a temperature dependent effective action which includes in addition the thermal fluctuations. In statistical physics Γ describes the free energy as a functional of some (space dependent) order parameter. In particular, for a constant order parameter, Γ yields the effective potential which encodes the equation of state. The effective average action Γ_k is a simple generalization of the effective action, with the distinction that only fluctuations with momenta $q^2 \gtrsim k^2$ are included. In the language of statistical physics, Γ_k is a coarse grained free energy with a coarse graining scale k . Lowering k results in a successive inclusion of fluctuations with momenta $q^2 \gtrsim k^2$ and therefore permits to explore the theory on larger and larger length scales. We note that Γ_k is closely related to an effective action for averages of fields [37], where the average is taken over a volume of size $\sim k^{-d}$ and which is similar in spirit to the block-spin action [76, 30] in lattice theories. In a theory with a physical ultraviolet cutoff Λ we can associate Γ_Λ with the microscopic or classical action S since no fluctuations below Λ are effectively included. For example, in statistical systems on a lattice the scale Λ plays the role of the inverse lattice spacing. In the context of dimensional reduction in high temperature quantum field theory Λ appears as the ultraviolet cutoff scale for the effective three dimensional models (cf. section 5.5). By definition, the effective average action equals the effective action for $k = 0$, i.e. $\Gamma_0 = \Gamma$, since the infrared cutoff is absent. Thus Γ_k interpolates between the classical action S and the effective action Γ as k is lowered from Λ to zero. The ability to follow the evolution to $k \rightarrow 0$ is equivalent to the ability to solve the theory. The dependence of the effective average action on the scale k is described by an exact flow equation which is presented in section 2.2.

To be explicit we consider the path integral representation of the generating functional for the connected Green functions in d Euclidean dimensions with N real scalar fields χ_a ($a = 1 \dots N$), classical action S and sources J_a . We introduce a k -dependent generating functional

$$W_k[J] = \ln \int D\chi \exp \left(-S[\chi] - \Delta_k S[\chi] + \int d^d x J_a(x) \chi^a(x) \right), \quad (2.1)$$

with an additional infrared cutoff term which is quadratic in the fields and reads in momentum space¹²

$$\Delta_k S[\chi] = \frac{1}{2} \int \frac{d^d q}{(2\pi)^d} R_k(q) \chi_a(-q) \chi^a(q). \quad (2.2)$$

¹²In order to avoid a proliferation of symbols we distinguish functions or operators in position space and their Fourier transforms according to their arguments, with the convention $\chi_a(q) = \int d^d x \exp(-iq_\mu x^\mu) \chi_a(x)$.

Without this term W_k equals the usual generating functional for the connected Green functions. Here the infrared cutoff function R_k is required to vanish for $k \rightarrow 0$ and to diverge for $k \rightarrow \Lambda$ and fixed q^2 . For $\Lambda \rightarrow \infty$ this can be achieved, for example, by the choice

$$R_k(q) = \frac{Z_k q^2 e^{-q^2/k^2}}{1 - e^{-q^2/k^2}}. \quad (2.3)$$

Here Z_k denotes an appropriate wave function renormalization constant which will be defined later. For fluctuations with small momenta $q^2 \ll k^2$ the cutoff $R_k \simeq Z_k k^2$ acts like an additional mass term. For $q^2 \gg k^2$ the infrared cutoff vanishes such that the functional integration of the high momentum modes is not disturbed. The expectation value of χ in the presence of $\Delta_k S[\chi]$ and J reads

$$\phi^a(x) \equiv \langle \chi^a(x) \rangle = \frac{\delta W_k[J]}{\delta J_a(x)}. \quad (2.4)$$

In terms of W_k the effective average action is defined via a modified Legendre transform

$$\Gamma_k[\phi] = -W_k[J] + \int d^d x J_a(x) \phi^a(x) - \Delta_k S[\phi]. \quad (2.5)$$

The subtraction of the infrared cutoff piece in (2.5) guarantees that the only difference between Γ_k and Γ is the effective infrared cutoff in the fluctuations. For $k > 0$ this allows the interpretation of Γ_k as a reasonable coarse grained free energy (cf. sections 2.2 and 4.8). Furthermore, one observes that Γ_k does not need to be convex whereas the standard effective action $\Gamma = \lim_{k \rightarrow 0} \Gamma_k$ is a convex functional by its definition as a Legendre transform. To establish the property $\Gamma_\Lambda = S$ one may consider an alternative integral equation for Γ_k . Using

$$J_a(x) = \frac{\delta(\Gamma_k + \Delta_k S)[\phi]}{\delta \phi^a(x)} \quad (2.6)$$

and eqs. (2.1), (2.5) one finds

$$\exp(-\Gamma_k[\phi]) = \int D\chi \exp\left(-S[\chi] - \Delta_k S[\chi - \phi] + \int d^d x \frac{\delta \Gamma_k[\phi]}{\delta \phi^a} [\chi^a - \phi^a]\right). \quad (2.7)$$

For $k > 0$ the term $\exp(-\Delta_k S[\chi - \phi])$ constrains the functional integral and behaves $\sim \delta[\chi - \phi]$ for $k \rightarrow \Lambda$ thus leading to the property $\Gamma_k \rightarrow S$ in this limit [38]. One will often not consider the limit $\Lambda \rightarrow \infty$, but rather keep this scale fixed and associate it with a physical ultraviolet cutoff for the validity of the investigated field theory. In particular, near second order or weak first order phase transitions the universal properties of the theory become independent of the precise form of Γ_Λ .

The formulation of the effective average action can be easily generalized to fermionic degrees of freedom. In particular, it is possible to incorporate chiral fermions since a chirally invariant cutoff R_k can be formulated [77]. Possible local gauge symmetries can be treated along similar lines [78, 17, 79, 80, 81, 45, 82, 83]. Here $\Delta_k S$ may not be gauge invariant and the usual Ward identities receive corrections [81] which vanish for $k \rightarrow 0$.

2.2 Exact flow equation

The dependence of the effective average action Γ_k on the coarse graining scale k is described by an exact flow equation which can be derived in a straightforward way [38]. From eq. (2.5) and (2.4) one finds

$$\begin{aligned} \partial_t \Gamma_k|_\phi &\equiv k \frac{\partial}{\partial k} \Gamma_k|_\phi = -\partial_t W_k|_J - \partial_t \Delta_k S[\phi] \\ &= \frac{1}{2} \text{Tr} \left\{ W_k^{(2)} \partial_t R_k \right\}. \end{aligned} \quad (2.8)$$

The trace in momentum space reads $\text{Tr} = \sum_a \int d^d q / (2\pi)^d$ and $W_k^{(2)}$ denotes the k -dependent connected two-point function

$$\begin{aligned} (W_k^{(2)})_{ab}(q, q') &= \frac{\delta^2 W_k[J]}{\delta J^a(-q) \delta J^b(q')} \\ &= \langle \chi_a(q) \chi_b(-q') \rangle - \langle \chi_a(q) \rangle \langle \chi_b(-q') \rangle. \end{aligned} \quad (2.9)$$

With the help of eq. (2.4) differentiated with respect to ϕ and (2.6) with respect to J one finds that eq. (2.8) can be rewritten as

$$\partial_t \Gamma_k[\phi] = \frac{1}{2} \text{Tr} \left\{ \left[\Gamma_k^{(2)}[\phi] + R_k \right]^{-1} \partial_t R_k \right\}. \quad (2.10)$$

The exact flow equation (2.10) describes the scale dependence of Γ_k in terms of the inverse average propagator $\Gamma_k^{(2)}$ as given by the second functional derivative of Γ_k with respect to the field components

$$\left(\Gamma_k^{(2)} \right)_{ab}(q, q') = \frac{\delta^2 \Gamma_k}{\delta \phi^a(-q) \delta \phi^b(q')}. \quad (2.11)$$

The trace in eq. (2.10) involves only one momentum integration as well as the summation over the internal indices. The additional cutoff function R_k with a form like the one given in eq. (2.3) renders the momentum integration both infrared and ultraviolet finite. In particular, the direct implementation of the additional mass-like term $R_k \simeq Z_k k^2$ for $q^2 \ll k^2$ into the inverse average propagator makes the formulation suitable for dealing with theories which are plagued by infrared problems in perturbation theory. Up to exponentially small corrections the integration of the high momentum modes with $q^2 \gg k^2$ is not affected by the infrared cutoff. We note that the derivation of the exact flow equation does not depend on the particular choice of the cutoff function and it may sometimes be technically easier to use a different infrared cutoff function, as e.g. $R_k \sim k^2$. Ultraviolet finiteness, however, is related to a fast decay of $\partial_t R_k$ for $q^2 \gg k^2$. For a rapidly decaying cutoff function R_k like the one given in eq. (2.3) only fluctuations with momenta in a small ‘‘window’’ around $q^2 \simeq k^2$ effectively contribute to the trace on the r.h.s. of eq. (2.10) for given k . Accordingly, the large momentum fluctuations with $q^2 \gtrsim k^2$, which are not affected by the infrared cutoff, have already been integrated out. Since the momentum integrations for $q^2 \lesssim k^2$ are effectively cut off, Γ_k realizes the concept of a coarse grained free energy in the

sense of Langer [71] (cf. section 4.8). Of course, the particular choice for the infrared cutoff function should have no effect on the physical results for $k \rightarrow 0$. Different choices of R_k correspond to different trajectories in the space of effective actions along which the unique infrared limit Γ_0 is reached. Nevertheless, once approximations are applied not only the trajectory but also its end point may depend on the precise definition of the function R_k . This dependence may be used to study the robustness of the approximation.

The flow equation (2.10) closely resembles a one-loop equation: Replacing $\Gamma_k^{(2)}$ by the second functional derivative of the classical action, $S^{(2)}$, one obtains the corresponding one-loop result. The “renormalization group improvement” $S^{(2)} \rightarrow \Gamma_k^{(2)}$ turns the one-loop flow equation into an *exact* non-perturbative flow equation. It also turns the equation into a functional differential equation. Possible methods for its solution include standard perturbation theory in the case of a small coupling, the $1/N$ -expansion or the ϵ -expansion. Particularly suitable for our purposes is the derivative expansion. We will allow for an arbitrary field dependence of the non-derivative term, i.e. the effective potential. This enables us to study the non-analytic behavior of the equation of state near second order phase transitions or the simultaneous description of degenerate minima at first order transitions. With the help of the derivative expansion the functional differential equation (2.10) can be transformed into a coupled set of non-linear partial differential equations. If one does not want to resort to further approximations at this level, one needs appropriate tools for solving this type of partial differential equations. Analytical solutions can be found only in certain limiting cases and for most purposes numerical solutions seem the adequate tool. We have developed suitable numerical algorithms which will be addressed to in section 4.5.

We emphasize that the flow equation (2.10) is closely connected to the Wilsonian (exact) renormalization group equation¹³ [30, 39, 40, 41, 42, 43]. The latter describes how the Wilsonian effective action S_Λ^W changes with the ultraviolet cutoff Λ . Polchinski’s continuum version of the Wilsonian flow equation [42] can be transformed into eq. (2.10) by means of a Legendre transform and a suitable variable redefinition [85, 86]. In contrast to the effective average action the Wilsonian effective action does not generate the $1PI$ Green functions [87]. We also note that eq. (2.10) is compatible with all symmetries of the model. Extensions of the flow equations to gauge fields [78, 17, 79, 80, 81, 45, 82, 83] and fermions [77, 120] (cf. section 5) are available. The exact flow equation can be supplemented by an exact formalism for the introduction of composite field variables or, more generally, a change of variables [44]. We will exploit this crucial feature for a description of low-energy QCD in section 5.

¹³The exact flow equation may also be interpreted as a differential form of the Schwinger-Dyson equations [84].

3 Equation of state and second order phase transitions

3.1 Introduction

The prototype for investigations concerning the restoration of a spontaneously broken symmetry at high temperature is the N -component scalar field theory with $O(N)$ symmetry. For $N = 4$ it describes the scalar sector of the electroweak standard model in the limit of vanishing gauge and Yukawa couplings. It is also used as an effective model for the chiral phase transition in QCD in the limit of two quark flavors [31, 50, 26, 27]. In condensed matter physics $N = 3$ corresponds to the well known Heisenberg model used to describe the ferromagnetic phase transition. There are other applications like the helium superfluid transition ($N = 2$), liquid-vapor transition ($N = 1$) or statistical properties of long polymer chains ($N = 0$) [67].

The equation of state (EOS) for a magnetic system is specified by the free energy density (here denoted by U) as a function of arbitrary magnetization ϕ and temperature T . All thermodynamic quantities can be derived from the function $U(\phi, T)$. For example, the response of the system to a homogeneous magnetic field H follows from $\partial U / \partial \phi = H$. This permits the computation of ϕ for arbitrary H and T . There is a close analogy to quantum field theory at non-vanishing temperature. Here U corresponds to the temperature dependent effective potential as a function of a scalar field ϕ . For instance, in the $O(4)$ symmetric model for the chiral phase transition in two flavor QCD the meson field ϕ has four components. In this picture, the average light quark mass \hat{m} is associated with the source $H \sim \hat{m}$ and one is interested in the behavior during the phase transition (or crossover) for $H \neq 0$. The temperature and source dependent meson masses and zero momentum interactions are given by derivatives of U (cf. section 5).

The applicability of the $O(N)$ symmetric scalar model to a wide class of very different physical systems in the vicinity of the critical temperature T_c at which the phase transition occurs is a manifestation of universality of critical phenomena. There exists a universal scaling form of the EOS in the vicinity of the second order phase transition which is not accessible to standard perturbation theory. The main reason is the effective three dimensional behavior of high temperature quantum field theory already discussed in section 1. In particular, the critical exponents which describe the singular behavior of various quantities near the phase transition are those of the corresponding classical statistical system (cf. section 5).

The quantitative description of the scaling form of the EOS will be the main topic of this section [62, 63, 64]. The calculation of the effective potential $U(\phi, T)$ in the vicinity of the critical temperature of a second order phase transition is an old problem. One can prove through a general renormalization group analysis [30] the Widom scaling form [88]

of the EOS¹⁴

$$H = \phi^\delta \tilde{f} \left((T - T_c) / \phi^{1/\beta} \right). \quad (3.1)$$

Only the limiting cases $\phi \rightarrow 0$ and $\phi \rightarrow \infty$ are quantitatively well described by critical exponents and amplitudes. The critical exponents β and δ have been computed with high accuracy [67, 89, 90] but the scaling function \tilde{f} is more difficult to access. A particular difficulty for a perturbative computation in three dimensions arises from the singularities induced by massless Goldstone modes in the phase with spontaneous symmetry breaking for models with continuous symmetry ($N \neq 1$). The scaling function \tilde{f} has been computed within the ϵ -expansion up to second order in ϵ [60] (third order for $N = 1$ [67]). Recently, the scaling form of the EOS has also been studied for $N = 1$ and $N = 4$ using lattice Monte-Carlo simulations [66, 65, 61]. We will observe that the lattice results agree quite well with those obtained from the effective average action method, while there appears a considerable discrepancy to the ϵ -expansion results.

In the following we compute the scaling EOS for $O(N)$ symmetric scalar N -component models directly in three dimensions [62, 63, 64]. Section 3.2 presents a computation of the effective potential $U = \lim_{k \rightarrow 0} U_k$ from a derivative expansion of the effective average action. The approximation takes into account the most general field dependence of the potential term. This will allow us to compute the non-analytic behavior of U in the vicinity of the second order phase transition. From U the universal scaling form of the equation of state is extracted in section 3.3. We conclude in section 3.4.

3.2 Scale dependence of the effective average potential

In this section we compute the effective average potential $U_k(\rho)$ for an $O(N)$ symmetric scalar field theory directly in three dimensions [62, 63, 64]. Here $\rho = \frac{1}{2} \phi^a \phi_a$ and ϕ^a denotes the N -component real scalar field. For $k \rightarrow 0$ one obtains the effective potential (Helmholtz free energy) $U_0(\rho) \equiv U(\rho)$. In the phase with spontaneous symmetry breaking the minimum of the potential occurs for $k = 0$ at $\rho_0 \neq 0$. In the symmetric phase the minimum of $U_k(\rho)$ ends at $\rho_0 = 0$ for $k = 0$. The two phases are separated by a scaling solution for which U_k/k^3 becomes independent of k once expressed in terms of a suitably rescaled field variable and the corresponding phase transition is of second order.

Though the evolution equation (2.10) for the effective average action is exact, it remains a complicated functional differential equation. In practice, one has to find a truncation for Γ_k in order to obtain approximate solutions. An important feature of the exact flow equation is therefore its simple and intuitive form which helps to find a non-perturbative approximation scheme. The r.h.s. of eq. (2.10) expresses the scale dependence of Γ_k in terms of the exact propagator. Known properties of the propagator can be used as a guide to find an appropriate truncation for the effective average action. For a scalar theory the propagator is a matrix characterized by mass terms and kinetic terms $\sim Zq^2$. The mass matrix is given by the second derivative of the potential U_k with respect to the fields. In

¹⁴We frequently suppress in our notation an appropriate power of a suitable “microscopic” length scale Λ^{-1} which is used to render quantities dimensionless.

general Z can be a complicated function of the fields and momenta. We may exploit the fact that the function Z plays the role of a field and momentum dependent wave function renormalization factor. For second order phase transitions and approximately for weak first order phase transitions the behavior of Z is governed by the anomalous dimension η . Typically for three dimensional scalar theories η is small. One therefore expects a weak dependence of Z on the fields and momenta (cf. also the discussion in section 6).

Our truncation is the lowest order in a systematic derivative expansion of Γ_k [37, 55, 92, 93, 94, 62, 63, 95]

$$\Gamma_k = \int d^d x \left\{ U_k(\rho) + \frac{1}{2} Z_k \partial^\mu \phi_a \partial_\mu \phi^a \right\}. \quad (3.2)$$

We keep for the potential term the most general $O(N)$ symmetric form $U_k(\rho)$, whereas the wave function renormalization is approximated by one k -dependent parameter. Next order in the derivative expansion would be the generalization to a ρ -dependent wavefunction renormalization $Z_k(\rho)$ plus a function $Y_k(\rho)$ accounting for a possible different index structure of the kinetic term for $N \geq 2$ [37, 92, 95] (cf. section 6). Going further would require the consideration of terms with four derivatives and so on. The weak ρ -dependence of the wave function renormalization factor employed in the ansatz (3.2) has been established explicitly for the scaling solution [93, 95] and also recently for the equation of state ($N = 1$) [96].

If the ansatz (4.2) is inserted into the evolution equation for the effective average action (2.10) one can extract flow equations for the effective average potential $U_k(\rho)$ and for the wave function renormalization constant Z_k (or equivalently the anomalous dimension η)¹⁵. For a study of the behavior in the vicinity of the phase transition it is convenient to work with dimensionless renormalized fields¹⁶

$$\begin{aligned} \tilde{\rho} &= Z_k k^{2-d} \rho, \\ u_k(\tilde{\rho}) &= k^{-d} U_k(\rho). \end{aligned} \quad (3.3)$$

With the truncation of eq. (3.2) the exact evolution equation for $u'_k \equiv \partial u_k / \partial \tilde{\rho}$ [55, 92, 63] reduces then to the partial differential equation

$$\begin{aligned} \frac{\partial u'_k}{\partial t} &= (-2 + \eta) u'_k + (d - 2 + \eta) \tilde{\rho} u''_k \\ &\quad - 2v_d (N - 1) u''_k l_1^d(u'_k; \eta) - 2v_d (3u''_k + 2\tilde{\rho} u'''_k) l_1^d(u'_k + 2\tilde{\rho} u''_k; \eta), \end{aligned} \quad (3.4)$$

where $t = \ln(k/\Lambda)$, with Λ the ultraviolet cutoff of the theory. The anomalous dimension η is defined by

$$\eta = -\frac{\partial}{\partial t} \ln Z_k \quad (3.5)$$

and

$$v_d^{-1} = 2^{d+1} \pi^{\frac{d}{2}} \Gamma\left(\frac{d}{2}\right), \quad (3.6)$$

¹⁵Details of the calculation may be found in section 4 for the discussion of scalar matrix models which covers the considerations involved here.

¹⁶We keep the number of dimensions d arbitrary and specialize only later to $d = 3$.

with $v_3 = 1/8\pi^2$. The “threshold” functions $l_n^d(w; \eta)$ result from the momentum integration on the r.h.s. of eq. (2.10), and read for $n \geq 1$, with $y = q^2/k^2$

$$l_n^d(w; \eta) = -n \int_0^\infty dy y^{\frac{d}{2}+1} \frac{\partial r(y)}{\partial y} [y(1+r(y)) + w]^{-(n+1)} - \frac{n}{2} \eta \int_0^\infty dy y^{\frac{d}{2}} r(y) [y(1+r(y)) + w]^{-(n+1)}. \quad (3.7)$$

Here $r(y)$ depends on the choice of the momentum dependence of the infrared cutoff and we employ according to eq. (2.3)

$$r(y) = \frac{e^{-y}}{1 - e^{-y}}. \quad (3.8)$$

This choice has the property $\lim_{q^2 \rightarrow 0} R_k/Z_k k^2 = \lim_{y \rightarrow 0} yr(y) = 1$, whereas for $q^2 \gg k^2$ the effect of the infrared cutoff is exponentially suppressed. The “threshold” functions l_n^d decrease rapidly for increased w and account for the decoupling of modes with mass term $w \gg 1$. We evaluate these functions numerically. Finally, the anomalous dimension is given in our truncation by¹⁷ [55, 92, 63]

$$\eta(k) = \frac{16v_d}{d} \kappa \lambda^2 m_{2,2}^d(2\lambda\kappa), \quad (3.9)$$

with κ the location of the minimum of the potential and λ the quartic coupling

$$\begin{aligned} u'_k(\kappa) &= 0, \\ u''_k(\kappa) &= \lambda. \end{aligned} \quad (3.10)$$

The function $m_{2,2}^d$ is given by

$$m_{2,2}^d(w) = \int_0^\infty dy y^{\frac{d}{2}-2} \frac{1+r+y\frac{\partial r}{\partial y}}{(1+r)^2 [(1+r)y+w]^2} \left\{ 2y \frac{\partial r}{\partial y} + 2 \left(y \frac{\partial}{\partial y} \right)^2 r - 2y^2 \left(1+r+y\frac{\partial r}{\partial y} \right) \frac{\partial r}{\partial y} \left[\frac{1}{(1+r)y} + \frac{1}{(1+r)y+w} \right] \right\}. \quad (3.11)$$

We point out that the argument $2\lambda\kappa$ turns out generically to be of order one for the scaling solution. Therefore, $\kappa \sim \lambda^{-1}$ and the mass effects are important, in contrast to perturbation theory where they are treated as small quantities $\sim \lambda$.

At a second order phase transition there is no mass scale present in the theory. In particular, one expects a scaling behavior of the rescaled effective average potential $u_k(\tilde{\rho})$. This can be studied by following the trajectory describing the scale dependence of $u_k(\tilde{\rho})$

¹⁷We neglect here for simplicity the implicit, linear η -dependence of the function $m_{2,2}^d$. We have numerically verified this approximation to have only a minor effect on the value of η .

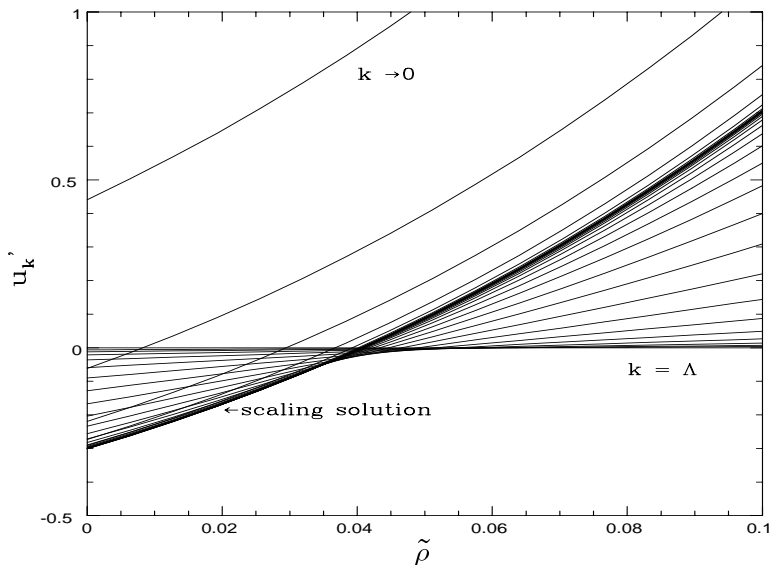


Figure 1: The evolution of $u'_k(\tilde{\rho})$ as k is lowered from Λ to zero for $N = 1$. The initial conditions (bare couplings) have been chosen such that the scaling solution is approached before the system evolves towards the symmetric phase with $u'_k(0) > 0$.

as k is lowered from Λ to zero. Near the phase transition the trajectory spends most of the “time” t in the vicinity of the k -independent scaling solution of eq. (3.4) given by $\partial_t u'_*(\tilde{\rho}) = 0$.¹⁸ Only at the end of the running the “near-critical” trajectories deviate from the scaling solution. For $k \rightarrow 0$ they either end up in the symmetric phase with $\kappa = 0$ and positive constant mass term m^2 such that $u'_k(0) \sim m^2/k^2$; or they lead to a non-vanishing constant ρ_0 indicating spontaneous symmetry breaking with $\kappa \rightarrow Z_0 k^{2-d} \rho_0$. The equation of state involves the potential $U_0(\rho)$ for temperatures away from the critical temperature. Its computation requires the solution for the running away from the critical trajectory which involves the full partial differential equation (3.4). We have developed two alternative algorithms for its numerical solution which will be discussed in section 4.5.

In fig. 1 we present the results of the numerical integration of eq. (3.4) for $d = 3$ and $N = 1$. The function $u'_k(\tilde{\rho})$ is plotted for various values of $t = \ln(k/\Lambda)$. The evolution starts at $k = \Lambda$ ($t = 0$) where the average potential is equal to the classical potential (no effective integration of modes has been performed). We start with a quartic classical potential parameterized as

$$u'_\Lambda(\tilde{\rho}) = \lambda_\Lambda(\tilde{\rho} - \kappa_\Lambda). \quad (3.12)$$

We arbitrarily choose $\lambda_\Lambda = 0.1$ and fine tune κ_Λ so that a scaling solution is approached at later stages of the evolution. There is a critical value $\kappa_{cr} \simeq 6.396 \times 10^{-2}$ for which the evolution leads to the scaling solution. For the results in fig. 1 a value κ_Λ slightly smaller than κ_{cr} is used. As k is lowered (and t turns negative), $u'_k(\tilde{\rho})$ deviates from its

¹⁸The resulting ordinary differential equation for $u_*(\tilde{\rho})$ has already been solved numerically for a somewhat different choice of the infrared cutoff [93, 94, 95].

initial linear shape. Subsequently it evolves towards a form which is independent of k and corresponds to the scaling solution $\partial_t u'_*(\tilde{\rho}) = 0$. It spends a long “time” t - which can be rendered arbitrarily long through appropriate fine tuning of κ_Λ - in the vicinity of the scaling solution. During this “time”, the minimum of the potential $u'_k(\tilde{\rho})$ takes a fixed value κ_* , while the minimum of $U_k(\rho)$ evolves towards zero according to

$$\rho_0(k) = k\kappa_*/Z_k. \quad (3.13)$$

The longer $u'_k(\tilde{\rho})$ stays near the scaling solution, the smaller the resulting value of $\rho_0(k)$ when the system deviates from it. As this value determines the mass scale for the renormalized theory at $k = 0$, the scaling solution governs the behavior of the system very close to the phase transition, where the characteristic mass scale goes to zero. Another important property of the “near-critical” trajectories, which spend a long “time” t near the scaling solution, is that they become insensitive to the details of the classical theory which determine the initial conditions for the evolution. After $u'_k(\tilde{\rho})$ has evolved away from its scaling form $u'_*(\tilde{\rho})$, its shape is independent of the choice of λ_Λ for the classical theory. This property gives rise to the universal behavior near second order phase transitions. For the solution depicted in fig. 1, $u_k(\tilde{\rho})$ evolves in such a way that its minimum runs to zero with $u'_k(0)$ subsequently increasing. Eventually the theory settles down in the symmetric phase with a positive constant renormalized mass term $m^2 = k^2 u'_k(0)$ as $k \rightarrow 0$. Another possibility is that the system ends up in the phase with spontaneous symmetry breaking. In this case κ grows in such a way that $\rho_0(k)$ approaches a constant value for $k \rightarrow 0$.

The approach to the scaling solution and the deviation from it can also be seen in fig. 2. The evolution of the running parameters $\kappa(t)$, $\lambda(t)$ starts with their initial classical values, leads to fixed point values κ_* , λ_* near the scaling solution, and finally ends up in the symmetric phase (κ runs to zero). Similarly the anomalous dimension $\eta(k)$, which is given by eq. (3.9), takes a fixed point value η_* when the scaling solution is approached. During this part of the evolution the wave function renormalization is given by

$$Z_k \sim k^{-\eta_*} \quad (3.14)$$

according to eq. (3.5). When the parts of the evolution towards and away from the fixed point become negligible compared to the evolution near the fixed point - that is, very close to the phase transition - eq. (3.14) becomes a very good approximation for sufficiently low k . This indicates that η_* can be identified with the critical exponent η . For the solution of fig. 2 ($N = 1$) we find $\kappa_* = 4.07 \times 10^{-2}$, $\lambda_* = 9.04$ and $\eta_* = 4.4 \times 10^{-2}$.

As we have already mentioned the details of the renormalized theory in the vicinity of the phase transition are independent of the classical coupling λ_Λ . Also the initial form of the potential does not have to be of the quartic form of eq. (3.12) as long as the symmetries are respected. Moreover, the critical theory can be parameterized in terms of critical exponents [56], an example of which is the anomalous dimension η . These exponents are universal quantities which depend only on the dimensionality of the system and its internal symmetries. For our three-dimensional theory they depend only on the value of N and can be easily extracted from our results. We concentrate here on the exponent ν , which

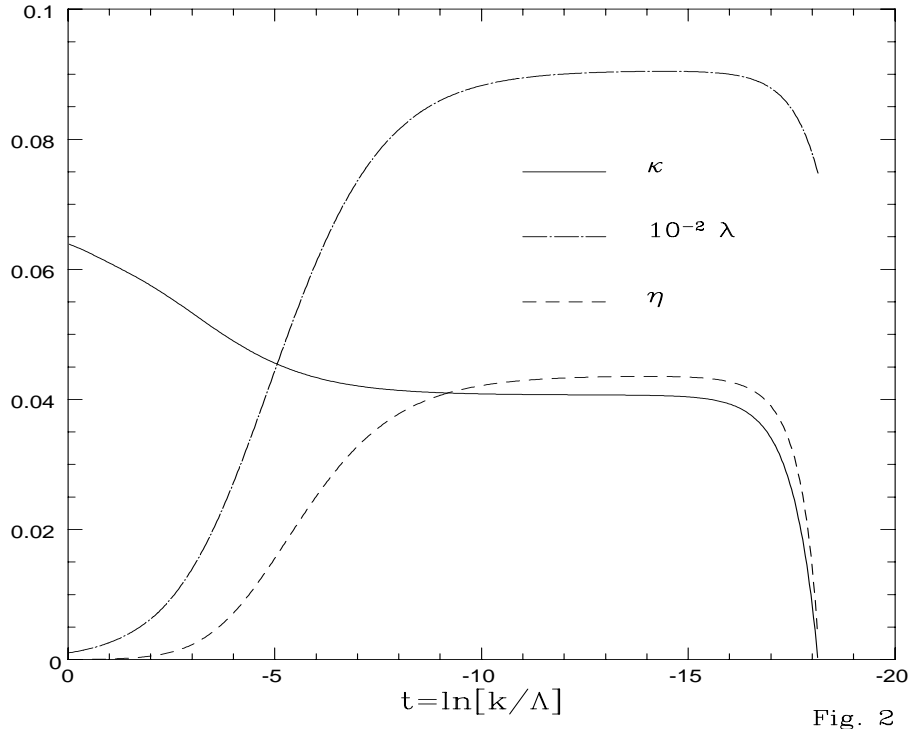


Figure 2: The evolution of κ , λ and η for the solution of fig. 1.

parameterizes the behavior of the renormalized mass in the critical region. Other exponents are computed in sections 3.3 and 5.7 along with the critical equation of state. The other exponents are not independent quantities, but can be determined from η and ν through universal scaling laws [56]. We define the exponent ν through the renormalized mass term in the symmetric phase

$$m^2 = \frac{1}{Z_k} \frac{dU_k(0)}{d\rho} = k^2 u'_k(0) \quad \text{for } k \rightarrow 0. \quad (3.15)$$

The behavior of m^2 in the critical region depends only on the distance from the phase transition, which can be expressed in terms of the difference of κ_Λ from the critical value κ_{cr} for which the renormalized theory has exactly $m^2 = 0$. The exponent ν is determined from the relation

$$m^2 \sim |\delta\kappa_\Lambda|^{2\nu} = |\kappa_\Lambda - \kappa_{cr}|^{2\nu}. \quad (3.16)$$

For a determination of ν from our results we calculate m^2 for various values of κ_Λ near κ_{cr} . We subsequently plot $\ln(m^2)$ as a function of $\ln|\delta\kappa_\Lambda|$. This curve becomes linear for $\delta\kappa_\Lambda \rightarrow 0$ and we obtain ν from the constant slope. In the past the critical exponents of the $O(N)$ symmetric theory were calculated from truncated versions of the partial differential equation (3.4) [55, 92]. The strategy was to turn eq. (3.4) into an infinite system of ordinary differential equations for the coefficients of a Taylor expansion around the “running” minimum of the potential. This infinite system was approximately solved by neglecting

$\tilde{\rho}$ -derivatives of $u_k(\tilde{\rho})$ higher than a given order. The apparent convergence of the procedure was checked by enlarging the level of truncation. We now have an alternative way of estimating the accuracy of this method. Our numerical solution of the partial differential equation (3.4) corresponds to an infinite level of truncation where all the higher derivatives are taken into account. In table 1 we present results obtained through the procedure of successive truncations and through our numerical solution for $N = 3$. We give the values

	κ_*	λ_*	$u_*^{(3)}$	η	ν
a	6.57×10^{-2}	11.5			0.745
b	8.01×10^{-2}	7.27	52.8		0.794
c	7.86×10^{-2}	6.64	42.0	3.6×10^{-2}	0.760
d	7.75×10^{-2}	6.94	43.5	3.8×10^{-2}	0.753
e	7.71×10^{-2}	7.03	43.4	3.8×10^{-2}	0.752
f	7.64×10^{-2}	7.07	44.2	3.8×10^{-2}	0.747

Table 1: The minimum κ of the potential $u_k(\tilde{\rho})$, the derivatives $\lambda = u''(\kappa)$, $u_k^{(3)}(\kappa)$ for the scaling solution, and the critical exponents η and ν , in various approximations: (a)-(e) from refs. [55, 92] and (f) from the present section [63, 62]. $N = 3$.

- a) Truncation where only the evolution of κ and λ is considered and higher derivatives of the potential and the anomalous dimension are neglected.
- b) κ , λ , $u_k^{(3)}(\kappa)$ are included.
- c) κ , λ , $u_k^{(3)}(\kappa)$ are included and η is approximated by eq. (3.9).
- d) with five parameters: κ , λ , $u_k^{(3)}(\kappa)$, $u_k^{(4)}(\kappa)$ and η .
- e) as in d) and in addition $u_k^{(5)}(\kappa)$, $u_k^{(6)}(\kappa)$ are estimated.
- f) The partial differential equation (3.4) for $u'_k(\tilde{\rho})$ is solved numerically and η is approximated by eq. (3.9).

of κ , λ , $u_k^{(3)}(\kappa)$ for the scaling solution and the critical exponents η , ν . We observe how the results stabilize as more $\tilde{\rho}$ -derivatives of $u_k(\tilde{\rho})$ at $\tilde{\rho} = \kappa$ and the anomalous dimension are taken into account. The last line gives the results of our numerical solution of eq. (3.4). By comparing with the previous line we conclude that the inclusion of all the $\tilde{\rho}$ -derivatives higher than $u_k^{(6)}(\kappa)$ and the term $\sim \eta$ in the “threshold” function of eq. (3.7) generates an improvement of less than 1 % for the results. This is smaller than the error induced by the omission of the higher derivative terms in the average action, which typically generates an uncertainty of the order of the anomalous dimension. In table 2 we compare our values for the critical exponents with results obtained from other methods¹⁹ (such as the

¹⁹See also ref. [95] and references therein for a calculation of critical exponents using similar methods as in this work.

ϵ -expansion, perturbation series at fixed dimension, lattice high temperature expansions and the $1/N$ -expansion). As expected η is rather poorly determined since it is the quan-

N	ν		η	
0	0.589	$0.5880(15)^a$	0.040	$0.027(4)^a$
		$0.5880(15)^b$		$0.0320(25)^b$
		$0.5878(6)^c$		
1	0.643	$0.6300(15)^a$	0.044	$0.032(3)^a$
		$0.6310(15)^b$		$0.0375(25)^b$
		$0.6315(8)^c$		
2	0.697	$0.6695(20)^a$	0.042	$0.033(4)^a$
		$0.671(5)^b$		$0.040(3)^b$
		$0.675(2)^c$		
3	0.747	$0.705(3)^a$	0.038	$0.033(4)^a$
		$0.710(7)^b$		$0.040(3)^b$
		$0.716(2)^c$		
4	0.787	$0.73(2)^{a*}$	0.034	$0.03(1)^{a*}$
		$0.759(3)^c$		
10	0.904	$0.894(4)^c$	0.019	
		0.877^d		0.025^d
100	0.990	0.989^d	0.002	0.003^d

Table 2: Critical exponents ν and η for various values of N . For comparison we list results obtained with other methods as summarized in [67], [97] and [89]:

- a) From perturbation series at fixed dimension to six-loop (*seven-loop [98]) order.
- b) From the ϵ -expansion at order ϵ^5 .
- c) From lattice high temperature expansions.
- d) From the $1/N$ -expansion at order $1/N^2$.

tity most seriously affected by the omission of the higher derivative terms in the average action. The exponent ν is in agreement with the known results at the 1-5 % level, with a discrepancy roughly equal to the value of η for various N .

In conclusion, the shape of the average potential is under good quantitative control for every scale k . This permits a quantitative understanding of the most important properties of the system at every length scale. We will exploit this in the following to extract the scaling form of the equation of state which is the main result here.

3.3 Universal critical equation of state

In this section we extract the Widom scaling form of the equation of state (EOS) from a solution [62, 64] of eqs. (3.4), (3.9) for the three dimensional $O(N)$ model. Its asymptotic behavior yields the universal critical exponents and amplitude ratios. We also present fits for the scaling function for $N = 1$ and $N = 3$. (See in addition section 5.7 for $N = 4$.) An

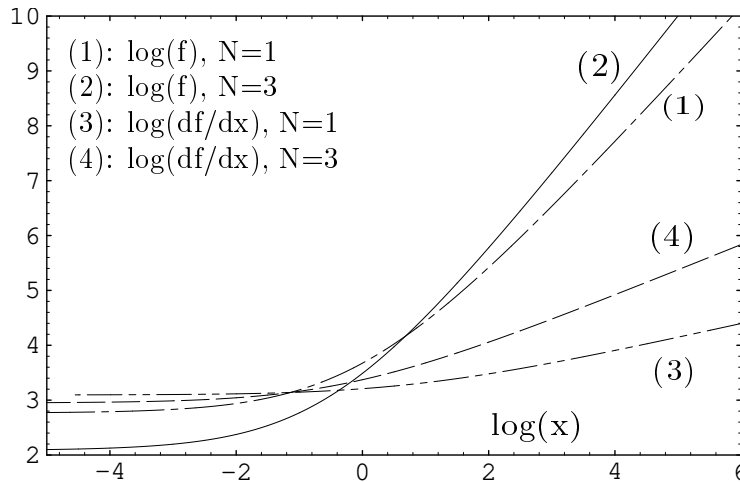


Figure 3: Logarithmic plot of f and df/dx for $x > 0$.

alternative parameterization of the equation of state in terms of renormalized quantities is used in order to compute universal couplings.

Eq. (3.1) establishes the scaling properties of the EOS. The external field H is related to the derivative of the effective potential $U' = \partial U / \partial \rho$ by $H_a = U' \phi_a$. The critical equation of state, relating the temperature, the external field and the order parameter, can then be written in the scaling form ($\phi = \sqrt{2\rho}$)

$$\frac{U'}{\phi^{\delta-1}} = f(x), \quad x = \frac{-\delta\kappa_\Lambda}{\phi^{1/\beta}}, \quad (3.17)$$

with critical exponents δ and β . A measure of the distance from the phase transition is the difference $\delta\kappa_\Lambda = \kappa_\Lambda - \kappa_{cr}$. If κ_Λ is interpreted as a function of temperature, the deviation $\delta\kappa_\Lambda$ is proportional to the deviation from the critical temperature, i.e. $\delta\kappa_\Lambda = A(T)(T_{cr} - T)$ with $A(T_{cr}) > 0$. For $\phi \rightarrow \infty$ our numerical solution for U' obeys $U' \sim \phi^{\delta-1}$ with high accuracy. The inferred value of δ is displayed in table 3, and we have checked the scaling relation $\delta = (5 - \eta)/(1 + \eta)$. The value of the critical exponent η is obtained from eq. (3.4) for the scaling solution. We have also verified explicitly that f depends only on the scaling variable x for the value of β given in table 3. In figs. 1 and 2 we plot $\log(f)$ and $\log(df/dx)$ as a function of $\log|x|$ for $N = 1$ and $N = 3$. Fig. 1 corresponds to the symmetric phase ($x > 0$), and fig. 2 to the phase with spontaneous symmetry breaking ($x < 0$). This is our main result of this section.

One can easily extract the asymptotic behavior from the logarithmic plots and compare with known values of critical exponents and amplitudes. The curves become constant, both for $x \rightarrow 0^+$ and $x \rightarrow 0^-$ with the same value, consistently with the regularity of $f(x)$ at $x = 0$. For the universal function one obtains

$$\lim_{x \rightarrow 0} f(x) = D, \quad (3.18)$$

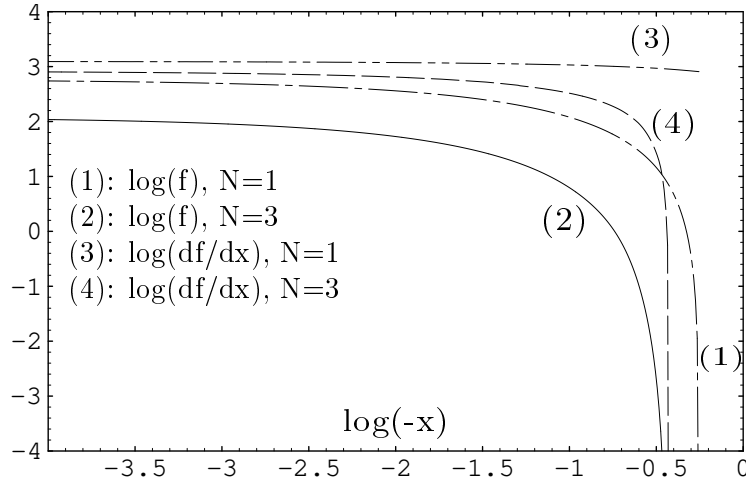


Figure 4: Logarithmic plot of f and df/dx for $x < 0$.

and $H = D\phi^\delta$ on the critical isotherm. For $x \rightarrow \infty$ one observes that $\log(f)$ becomes a linear function of $\log(x)$ with constant slope γ . In this limit the universal function takes the form

$$\lim_{x \rightarrow \infty} f(x) = (C^+)^{-1} x^\gamma. \quad (3.19)$$

The amplitude C^+ and the critical exponent γ characterize the behavior of the 'unrenormalized' squared mass or inverse susceptibility

$$\bar{m}^2 = \chi^{-1} = \lim_{\phi \rightarrow 0} \left(\frac{\partial^2 U}{\partial \phi^2} = (C^+)^{-1} |\delta\kappa_\Lambda|^\gamma \phi^{\delta-1-\gamma/\beta} \right). \quad (3.20)$$

We have verified the scaling relation $\gamma/\beta = \delta - 1$ that connects γ with the exponents β and δ appearing in the Widom scaling form (3.1). One observes that the zero-field magnetic susceptibility, or equivalently the inverse unrenormalized squared mass $\bar{m}^{-2} = \chi$, is non-analytic for $\delta\kappa_\Lambda \rightarrow 0$ in the symmetric phase: $\chi = C^+ |\delta\kappa_\Lambda|^{-\gamma}$. In this phase we find that the correlation length $\xi = (Z_0 \chi)^{1/2}$, which is equal to the inverse of the renormalized mass m_R , behaves as $\xi = \xi^+ |\delta\kappa_\Lambda|^{-\nu}$ with $\nu = \gamma/(2 - \eta)$.

The spontaneously broken phase is characterized by a nonzero value ϕ_0 of the minimum of the effective potential U with $H = (\partial U / \partial \phi)(\phi_0) = 0$. The appearance of spontaneous symmetry breaking below T_c implies that $f(x)$ has a zero $x = -B^{-1/\beta}$ and one observes a singularity of the logarithmic plot in fig. 2. In particular, according to eq. (3.1) the minimum behaves as $\phi_0 = B(\delta\kappa_\Lambda)^\beta$. Below the critical temperature, the longitudinal and transversal susceptibilities χ_L and χ_T are different for $N > 1$

$$\chi_L^{-1} = \frac{\partial^2 U}{\partial \phi^2} = \phi^{\delta-1} \left(\delta f(x) - \frac{x}{\beta} f'(x) \right), \quad \chi_T^{-1} = \frac{1}{\phi} \frac{\partial U}{\partial \phi} = \phi^{\delta-1} f(x) \quad (3.21)$$

(with $f' = df/dx$). This is related to the existence of massless Goldstone modes in the $(N - 1)$ transverse directions, which causes the transversal susceptibility to diverge for

vanishing external field. Fluctuations of these modes induce the divergence of the zero-field longitudinal susceptibility. This can be concluded from the singularity of $\log(f')$ for $N = 3$ in fig. 2. The first x -derivative of the universal function vanishes as $H \rightarrow 0$, i.e. $f'(x = -B^{-1/\beta}) = 0$ for $N > 1$. For $N = 1$ there is a non-vanishing constant value for $f'(x = -B^{-1/\beta})$ with a finite zero-field susceptibility $\chi = C^-(\delta\kappa_\Lambda)^{-\gamma}$, where $(C^-)^{-1} = B^{\delta-1-1/\beta} f'(-B^{-1/\beta})/\beta$. For a non-vanishing physical infrared cutoff k , the longitudinal susceptibility remains finite also for $N > 1$: $\chi_L \sim (k\rho_0)^{-1/2}$. For $N = 1$ in the ordered phase, the correlation length behaves as $\xi = \xi^-(\delta\kappa_\Lambda)^{-\nu}$, and the renormalized minimum $\rho_{0R} = Z_0\rho_0$ of the potential U scales as $\rho_{0R} = E(\delta\kappa_\Lambda)^\nu$.

The amplitudes of singularities near the phase transition D , C^\pm , ξ^\pm , B and E are given in table 3. They are not universal. There are two independent scales in the vicinity of the transition point which can be related to the deviation from the critical temperature and to the external source. All models in the same universality class can be related by a multiplicative rescaling of ϕ and $\delta\kappa_\Lambda$ or $(T_c - T)$. Accordingly there are only two independent amplitudes and exponents respectively. Ratios of amplitudes which are invariant under this rescaling are universal. We display the universal combinations C^+/C^- , ξ^+/ξ^- , $R_\chi = C^+DB^{\delta-1}$, $\tilde{R}_\xi = (\xi^+)^{\beta/\nu}D^{1/(\delta+1)}B$ and ξ^+E in table 3.

N	β	γ	δ	ν	η	λ_R/m_R	ν_R	$\hat{\lambda}_R/\rho_{0R}$	$\hat{\nu}_R$	
1	0.336	1.258	4.75	0.643	0.044	9.69	108	61.6	107	
3	0.388	1.465	4.78	0.747	0.038	7.45	57.4	0	$\simeq 250$	
	C^+	D	B	ξ^+	E	C^+/C^-	ξ^+/ξ^-	R_χ	\tilde{R}_ξ	ξ^+E
1	0.0742	15.88	1.087	0.257	0.652	4.29	1.86	1.61	0.865	0.168
3	0.0743	8.02	1.180	0.263	0.746	-	-	1.11	0.845	0.196

Table 3: Parameters for the equation of state.

The asymptotic behavior observed for the universal function can be used in order to obtain a semi-analytical expression for $f(x)$. We find that the following fit reproduces the numerical values for both f and df/dx with a 1% accuracy (apart from the immediate vicinity of the zero of f for $N = 3$):

$$f_{fit}(x) = D(1 + B^{1/\beta}x)^a(1 + \Theta x)^\Delta(1 + cx)^{\gamma-a-\Delta}, \quad (3.22)$$

with $c = (C^+DB^{a/\beta}\Theta^\Delta)^{-1/(\gamma-a-\Delta)}$ and $a = 1$ ($a = 2$) for $N = 1$ ($N > 1$). The fitting parameters are chosen as $\Theta = 0.569$ (1.312) and $\Delta = 0.180$ (-0.595) for $N = 1$ (3).

There is an alternative parameterization of the equation of state in terms of renormalized quantities. In the symmetric phase ($\delta\kappa_\Lambda < 0$) we consider the dimensionless quantity

$$F(s) = \frac{U'_R}{m_R^2} = C^+x^{-\gamma}f(x), \quad s = \frac{\rho_R}{m_R} = \frac{1}{2}(\xi^+)^3(C^+)^{-1}x^{-2\beta}, \quad (3.23)$$

with $\rho_R = Z_0\rho$ and $U_R^{(n)} = Z_0^{-n}U^{(n)}$. The derivatives of F at $s = 0$ yield the universal couplings

$$\frac{dF}{ds}(0) = \frac{U_R''(0)}{m_R} \equiv \frac{\lambda_R}{m_R}, \quad \frac{d^2F}{ds^2}(0) = U_R'''(0) \equiv \nu_R, \quad (3.24)$$

and similarly for higher derivatives. We confirm that the potential U is well approximated by a ϕ^6 (or ρ^3) polynomial [55, 92, 66]. For $N = 1$, our value for ν_R in the symmetric phase agrees with the results of a numerical simulation [66] within the expected accuracy (related to the size of the anomalous dimension η). However, λ_R/m_R seems to be too small. This may be connected to the more crude approximation for the anomalous dimension in the symmetric phase, as compared to the ordered one. For a recent detailed comparison of the dimensionless renormalized couplings in the symmetric phase with results obtained from other methods we refer the reader to ref. [99]. Small field expansions of the effective potential have also been used to reconstruct the equation of state ($N = 1$) within summed perturbation series at fixed dimension or from high temperature expansions [100]. A comparison including the results obtained here can be found in ref. [100].

In the ordered phase ($\delta\kappa_\Lambda > 0$) we consider the ratio

$$G(\tilde{s}) = \frac{U'_R}{\rho_{0R}^2} = \frac{1}{2}B^2E^{-3}(-x)^{-\gamma}f(x), \quad \tilde{s} = \frac{\rho_R}{\rho_{0R}} = B^{-2}(-x)^{-2\beta}. \quad (3.25)$$

The values for the universal couplings

$$\frac{dG}{d\tilde{s}}(1) = \frac{U_R''(\rho_{0R})}{\rho_{0R}} \equiv \frac{\hat{\lambda}_R}{\rho_{0R}}, \quad \frac{d^2G}{d\tilde{s}^2}(1) = U_R'''(\rho_{0R}) \equiv \hat{\nu}_R, \quad (3.26)$$

as well as λ_R/m_R and ν_R are given in table 3. One observes that for $N > 1$ the renormalized quartic coupling $\hat{\lambda}_R$ vanishes in the ordered phase. The coupling $\hat{\nu}_R$ takes a finite value and higher derivatives $d^nG/d\tilde{s}^n(1)$ (for $n \leq 3$) diverge. This is due to the presence of massless fluctuations.

For comparison, figure 5 is taken from ref. [65] which presents results from a lattice Monte Carlo investigation of the equation of state for $N = 1$ (curve V), along with our results (curve W) and those from the ϵ -expansion to order $\epsilon^0, \dots, \epsilon^3$ (curves 0 – 3). The plot shows very good agreement of the lattice study with our results and the fit of eq. (3.22) in the phase with spontaneous symmetry breaking, whereas it deviates substantially from the results of the ϵ -expansion. We also have computed the equation of state for $N = 4$. We present these results in section 5.7 where we obtain the universal critical equation of state within a study of an effective quark meson model at non-zero temperature. Comparison of our $N = 4$ results with a recent lattice Monte-Carlo simulation [61] shows agreement for the scaling function within a few percent in the symmetric and the spontaneously broken phase (cf. section 5.7).

3.4 Conclusions

In summary, our numerical solution of eq. (3.3) gives a very detailed picture of the critical equation of state of the three dimensional $O(N)$ model. The numerical uncertainties are es-

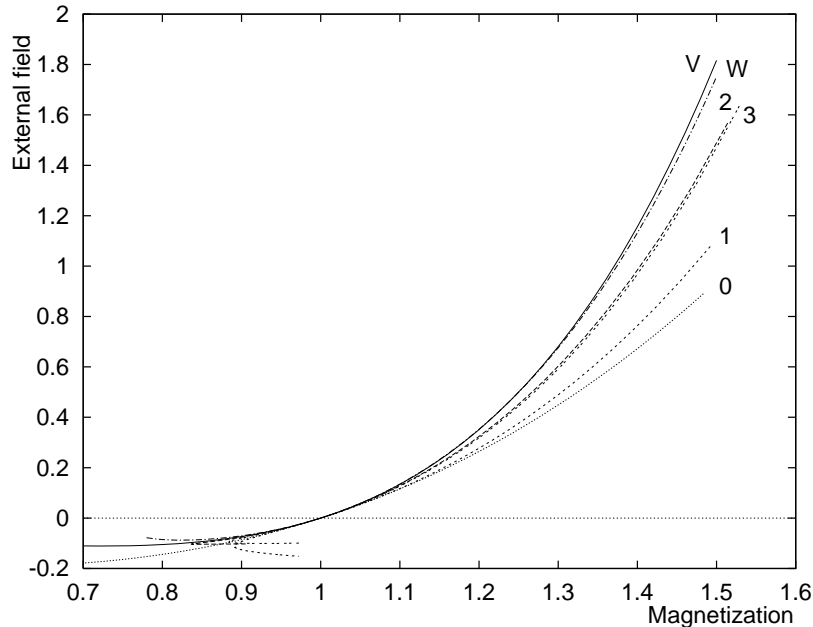


Figure 5: The plot shows the “Ising equation of state” ($N = 1$) computed by different methods. The external source $\hat{j} = \partial\hat{U}/\partial\hat{\phi}$ is plotted as a function of the magnetization $\hat{\phi}$. In contrast to the parameters used in the text here all curves are normalized by the conditions $\partial\hat{U}/\partial\hat{\phi}(1) = 0$ and $\partial^2\hat{U}/\partial(\hat{\phi})^2(1) = 1$. The curves 0 – 3 are from the ϵ -expansion in the parametric representation of the equation of state [67], in orders $\epsilon^0, \dots, \epsilon^3$, respectively. The curve W represents our result and the curve V denotes the lattice result of ref. [65] where this plot is taken from.

timated by comparison of results obtained through two independent integration algorithms [63, 68] (cf. section 4.5). They are small, typically less than 0.3% for critical exponents and (1 – 3)% for amplitudes. The scaling relations between the critical exponents are fulfilled within a deviation of 2×10^{-4} . The dominant quantitative error stems from the truncation of the exact flow equation and is related to the size of the anomalous dimension $\eta \simeq 4\%$ (cf. also the discussion in section 6).

We have obtained a precise description of the universal equation of state in the vicinity of the critical temperature of a second order phase transition. We will see in the next section that universal properties can also be observed for weak first order phase transitions. In particular, we will compute the universal equation of state for weak first order phase transitions in scalar matrix models in section 4.7.

4 Equation of state and first order phase transitions

4.1 Introduction

Matrix models are extensively discussed in statistical physics. Beyond the $O(N)$ symmetric Heisenberg models (“vector models”), which we have discussed in the previous section, they correspond to the simplest scalar field theories. There is a wide set of different applications as the metal insulator transition [101] or liquid crystals [102] or strings and random surfaces [103]. The universal behavior of these models in the vicinity of a second order or weak first order phase transition is determined by the symmetries and the field content of the corresponding field theories. We will consider here [68] models with $U(N) \times U(N)$ symmetry with a scalar field in the (\bar{N}, N) representation, described by an arbitrary complex $N \times N$ matrix φ . We do not impose nonlinear constraints for φ a priori but rather use a “classical” potential. This enforces nonlinear constraints in certain limiting cases. Among those, our model describes a nonlinear matrix model for unitary matrices or one for singular 2×2 matrices. The universal critical behavior does not depend on the details of the classical potential and there is no difference between the linear and nonlinear models in the vicinity of the limiting cases. We concentrate here on three dimensions, relevant for statistical physics and critical phenomena in high temperature field theory.

The cases $N = 2, 3$ have a relation to high temperature strong interaction physics. At vanishing temperature the four dimensional models can be used for a description of the pseudoscalar and scalar mesons for N quark flavors (cf. section 5). For $N = 3$ the antihermitean part of φ describes here the pions, kaons, η and η' whereas the hermitean part accounts for the nonet of scalar 0^{++} mesons.²⁰ For nonzero temperature T the effects of fluctuations with momenta $p^2 \lesssim (\pi T)^2$ are described by the corresponding three dimensional models. These models account for the long distance physics and obtain after integrating out the short distance fluctuations by virtue of dimensional reduction which will be treated in detail in section 5.5. In particular, the three dimensional models embody the essential dynamics in the immediate vicinity of a second order or weak first order chiral phase transition [31, 50, 26, 27]. The four dimensional models at nonvanishing temperature have also been used for investigations of the temperature dependence of meson masses [105, 52]. The simple model investigated in this section is not yet realistic – it neglects the effect of the axial anomaly which reduces the chiral flavor symmetry to $SU(N) \times SU(N)$. For simplicity we will concentrate here on $N = 2$, but our methods can be generalized to $N = 3$ and the inclusion of the axial anomaly.

The case $N = 2$ also has a relation to the electroweak phase transition in models with two Higgs doublets. Our model corresponds here to the critical behavior in a special class of left-right symmetric theories in the limit where the gauge couplings are neglected. Even though vanishing gauge couplings are not a good approximation for typical realistic models one would like to understand this limiting case reliably.

For the present matrix models one wants to know if the phase transition becomes

²⁰See ref. [104] for a recent phenomenological analysis.

second order in certain regions of parameter space. In the context of flow equations this is equivalent to the question if the system of running couplings admits a fixed point which is infrared stable (except one relevant direction corresponding to $T - T_c$). We will employ here the average action method introduced in section 2. We find that the phase transition for the investigated matrix models with $N = 2$ and symmetry breaking pattern $U(2) \times U(2) \rightarrow U(2)$ is always (fluctuation induced) first order, except for a boundary case with enhanced $O(8)$ symmetry. For a large part of parameter space the transition is weak and one finds large renormalized dimensionless couplings near the critical temperature. If the running of the couplings towards approximate fixed points (there are no exact fixed points) is sufficiently fast the large distance physics loses memory of the details of the short distance or classical action. In this case the physics near the phase transition is described by an universal equation of state.

Besides the possible practical applications it is a theoretical challenge to find the universal equation of state for weak first order phase transitions. Whereas for second order transitions the universal equation of state can be expressed as a function of only one scaling variable (cf. section 3.3), the additional mass scale at a first order transition induces a second dimensionless ratio. The equation of state or, equivalently, the effective potential or free energy therefore depends on two different scaling variables in the universal region. We have succeeded to describe this situation for the present matrix models and give the universal equation of state in section 4.7.

An important aspect in the study of first order phase transitions is the possible creation of an out of equilibrium situation, as has been discussed in section 1. An old and challenging problem in this context concerns the question of the validity of Langer's theory [71] of spontaneous bubble nucleation. In Langer's approach the decay of metastable states is described in terms of a steady state solution of the associated Fokker-Planck equation. The nucleation rate is obtained from the integrated probability current flowing across the saddle point ("critical bubble") of a suitably defined coarse grained free energy. The treatment requires first a meaningful definition of a coarse grained free energy with a coarse graining scale k . Second, the validity of a saddle point approximation for the treatment of fluctuations around the critical bubble has to be ensured. Here only fluctuations with momenta smaller than k must be included. We will see that the two issues are closely related. The validity of the saddle point approximation typically requires small dimensionless couplings. On the other hand we observe for large couplings that the form of the coarse grained effective potential U_k depends strongly on k even for scales where the location of the minima of U_k is essentially independent of k . This means that the lowest order in the saddle point approximation (classical contribution) depends strongly on the details of the coarse graining procedure. Since the final results as nucleation rates etc. must be independent of the coarse graining prescription this is only compatible with a large contribution from the higher orders of the saddle point expansion. Section 4.8 deals with this issue in a quantitative way.

The text is organized as follows. In section 4.2 we define the $U(2) \times U(2)$ symmetric matrix model and we establish the connection to a matrix model for unitary matrices and to one for singular complex 2×2 matrices. There we also give an interpretation of the

model as the coupled system of two $SU(2)$ -doublets for the weak interaction Higgs sector. Section 4.3 is devoted to an overview over the phase structure and the coarse grained effective potential U_k for the three dimensional theory. The evolution equation for U_k and its scaling form is computed in section 4.4. A method for its numerical solution is discussed in section 4.5 which also contains the flow equation for the wave function renormalization constant or the anomalous dimension η . A detailed account on the renormalization group flow is presented in section 4.6. We compute the universal form of the equation of state for weak first order phase transitions in section 4.7 and we extract critical exponents and the corresponding index relations. The dependence of the coarse grained effective potential on the coarse graining scale is studied in detail in section 4.8. The quantitative analysis is applied to Langer's theory of bubble formation. Section 4.9 contains the conclusions.

4.2 Scalar matrix model

We consider a $U(2) \times U(2)$ symmetric effective action for a scalar field φ which transforms in the $(2, 2)$ representation with respect to the subgroup $SU(2) \times SU(2)$. Here φ is represented by a complex 2×2 matrix and the transformations are

$$\begin{aligned}\varphi &\rightarrow U\varphi V^\dagger, \\ \varphi^\dagger &\rightarrow V\varphi^\dagger U^\dagger\end{aligned}\tag{4.1}$$

where U and V are unitary 2×2 matrices corresponding to the two distinct $U(2)$ factors.

We classify the invariants for the construction of the effective average action by the number of derivatives. The lowest order in a systematic derivative expansion [92, 93] of Γ_k is given by

$$\Gamma_k = \int d^d x \left\{ U_k(\varphi, \varphi^\dagger) + Z_k \partial_\mu \varphi_{ab}^* \partial^\mu \varphi^{ab} \right\} \quad (a, b = 1, 2).\tag{4.2}$$

The term with no derivatives defines the scalar potential U_k which is an arbitrary function of traces of powers of $\varphi^\dagger \varphi$. The most general $U(2) \times U(2)$ symmetric scalar potential can be expressed as a function of only two independent invariants,

$$\begin{aligned}\rho &= \text{tr}(\varphi^\dagger \varphi) \\ \tau &= 2 \text{tr} \left(\varphi^\dagger \varphi - \frac{1}{2} \rho \right)^2 = 2 \text{tr}(\varphi^\dagger \varphi)^2 - \rho^2.\end{aligned}\tag{4.3}$$

Here we have used for later convenience the traceless matrix $\varphi^\dagger \varphi - \frac{1}{2} \rho$ to construct the second invariant. Higher invariants, $\text{tr} \left(\varphi^\dagger \varphi - \frac{1}{2} \rho \right)^n$ for $n > 2$, can be expressed as functions of ρ and τ [46].

For the derivative part we consider a standard kinetic term with a scale dependent wave function renormalization constant Z_k . The first correction to the kinetic term would include field dependent wave function renormalizations $Z_k(\rho, \tau)$ plus functions not specified in eq. (4.2) which account for a different index structure of invariants with two derivatives. These wave function renormalizations may be defined at zero momentum. The next level

involves invariants with four derivatives and so on. We define Z_k at the minimum ρ_0, τ_0 of U_k and at vanishing momenta q^2 ,

$$Z_k = Z_k(\rho = \rho_0, \tau = \tau_0; q^2 = 0). \quad (4.4)$$

The factor Z_k appearing in the definition of the infrared cutoff R_k in eq. (2.3) is identified with (4.4). The k -dependence of this function is given by the anomalous dimension

$$\eta(k) = -\frac{d}{dt} \ln Z_k. \quad (4.5)$$

If the ansatz (4.2) is inserted into the flow equation for the effective average action (2.10) one obtains flow equations for the effective average potential $U_k(\rho, \tau)$ and for the wave function renormalization constant Z_k (or equivalently the anomalous dimension η). This is done in sections 4.4 and 4.5. These flow equations have to be integrated starting from some short distance scale Λ and one has to specify U_Λ and Z_Λ as initial conditions. At the scale Λ , where Γ_Λ can be taken as the classical or short distance action, no integration of fluctuations has been performed. The short distance potential is taken to be a quartic potential which is parametrized by two quartic couplings $\bar{\lambda}_{1\Lambda}, \bar{\lambda}_{2\Lambda}$ and a mass term. We start in the spontaneously broken regime where the minimum of the potential occurs at a nonvanishing field value and there is a negative mass term at the origin of the potential ($\bar{\mu}_\Lambda^2 > 0$),

$$U_\Lambda(\rho, \tau) = -\bar{\mu}_\Lambda^2 \rho + \frac{1}{2} \bar{\lambda}_{1\Lambda} \rho^2 + \frac{1}{4} \bar{\lambda}_{2\Lambda} \tau^2 \quad (4.6)$$

and $Z_\Lambda = 1$. The potential is bounded from below provided $\bar{\lambda}_{1\Lambda} > 0$ and $\bar{\lambda}_{2\Lambda} > -2\bar{\lambda}_{1\Lambda}$. For $\bar{\lambda}_{2\Lambda} > 0$ one observes the potential minimum for the configuration $\varphi_{ab} = \varphi \delta_{ab}$ corresponding to the spontaneous symmetry breaking down to the diagonal $U(2)$ subgroup of $U(2) \times U(2)$. For negative $\bar{\lambda}_{2\Lambda}$ the potential is minimized by the configuration $\varphi_{ab} = \varphi \delta_{a1} \delta_{ab}$ which corresponds to the symmetry breaking pattern $U(2) \times U(2) \rightarrow U(1) \times U(1) \times U(1)$. In the special case $\bar{\lambda}_{2\Lambda} = 0$ the theory exhibits an enhanced $O(8)$ symmetry. This constitutes the boundary between two phases with different symmetry breaking patterns.

The limits of infinite couplings correspond to nonlinear constraints in the matrix model. For $\bar{\lambda}_{1\Lambda} \rightarrow \infty$ with fixed ratio $\bar{\mu}_\Lambda^2 / \bar{\lambda}_{1\Lambda}$ one finds the constraint $\text{tr}(\varphi^\dagger \varphi) = \bar{\mu}_\Lambda^2 / \bar{\lambda}_{1\Lambda}$. By a convenient choice of Z_Λ (rescaling of φ) this can be brought to the form $\text{tr}(\varphi^\dagger \varphi) = 2$. On the other hand, the limit $\bar{\lambda}_{2\Lambda} \rightarrow +\infty$ enforces the constraint $\varphi^\dagger \varphi = \frac{1}{2} \text{tr}(\varphi^\dagger \varphi)$. Combining the limits $\bar{\lambda}_{1\Lambda} \rightarrow \infty, \bar{\lambda}_{2\Lambda} \rightarrow \infty$ the constraint reads $\varphi^\dagger \varphi = 1$ and we deal with a matrix model for unitary matrices. (These considerations generalize to arbitrary N .) Another interesting limit obtains for $\bar{\lambda}_{1\Lambda} = -\frac{1}{2} \bar{\lambda}_{2\Lambda} + \Delta_\lambda, \Delta_\lambda > 0$ if $\bar{\lambda}_{2\Lambda} \rightarrow -\infty$. In this case the nonlinear constraint reads $(\text{tr} \varphi^\dagger \varphi)^2 = \text{tr}(\varphi^\dagger \varphi)^2$ which implies for $N = 2$ that $\det \varphi = 0$. This is a matrix model for singular complex 2×2 matrices.

One can also interpret our model as the coupled system of two $SU(2)$ -doublets for the weak interaction Higgs sector. This is simply done by decomposing the matrix φ_{ab} into two two-component complex fundamental representations of one of the $SU(2)$ subgroups,

$\varphi_{ab} \rightarrow \varphi_{1b}, \varphi_{2b}$. The present model corresponds to a particular left-right symmetric model with interactions specified by

$$\begin{aligned}\rho &= \varphi_1^\dagger \varphi_1 + \varphi_2^\dagger \varphi_2 \\ \tau &= \left(\varphi_1^\dagger \varphi_1 - \varphi_2^\dagger \varphi_2 \right)^2 + 4 \left(\varphi_1^\dagger \varphi_2 \right) \left(\varphi_2^\dagger \varphi_1 \right).\end{aligned}\tag{4.7}$$

We observe that for a typical weak interaction symmetry breaking pattern the expectation values of φ_1 and φ_2 should be aligned in the same direction or one of them should vanish. In the present model this corresponds to the choice $\bar{\lambda}_{2\Lambda} < 0$. The phase structure of a related model without the term $\sim (\varphi_1^\dagger \varphi_2)(\varphi_2^\dagger \varphi_1)$ has been investigated previously [108] and shows second or first order transitions²¹. Combining these results with the outcome of this work leads already to a detailed qualitative overview over the phase pattern in a more general setting with three independent couplings for the quartic invariants $(\varphi_1^\dagger \varphi_1 + \varphi_2^\dagger \varphi_2)^2$, $(\varphi_1^\dagger \varphi_1 - \varphi_2^\dagger \varphi_2)^2$ and $(\varphi_1^\dagger \varphi_2)(\varphi_2^\dagger \varphi_1)$. We also note that the special case $\bar{\lambda}_{2\Lambda} = 2\bar{\lambda}_{1\Lambda}$ corresponds to two Heisenberg models interacting only by a term sensitive to the alignment between φ_1 and φ_2 , i.e. a quartic interaction of the form $(\varphi_1^\dagger \varphi_1)^2 + (\varphi_2^\dagger \varphi_2)^2 + 2(\varphi_1^\dagger \varphi_2)(\varphi_2^\dagger \varphi_1)$.

The model is now completely specified and it remains to extract the flow equations for U_k and Z_k . Before this is carried out in sections 4.4 and 4.5 we present an overview over the phase structure in the next section. These results are obtained from a numerical solution of the evolution equations.

4.3 Phase structure

In this section we consider the $U(2) \times U(2)$ symmetric model in three space dimensions. The aim is to give an overview of our results concerning the phase structure and the effective average potential. We concentrate here on the spontaneous symmetry breaking with a residual $U(2)$ symmetry group. This symmetry breaking can be observed for a configuration which is proportional to the identity and with (4.3) one finds $\tau = 0$. In this case we shall use an expansion of $U_k(\rho, \tau)$ around $\tau = 0$ keeping only the linear term in τ . This amounts to assuming

$$\frac{\partial^n U_k}{\partial \tau^n}(\rho, \tau = 0) = 0 \quad \text{for } n \geq 2.\tag{4.8}$$

We will motivate this truncation in section 4.5 where we present a more detailed analysis. We make no expansion of $U_k(\rho, \tau)$ in terms of ρ . This allows the description of a first order phase transition where a second local minimum of $U_k(\rho) \equiv U_k(\rho, \tau = 0)$ appears. The ρ -dependence also gives information about the equation of state of the system.

For the considered symmetry breaking pattern the short distance potential U_Λ given in eq. (4.6) is parametrized by positive quartic couplings,

$$\bar{\lambda}_{1\Lambda}, \bar{\lambda}_{2\Lambda} > 0\tag{4.9}$$

²¹First order phase transitions and coarse graining have also been discussed in a multi-scalar model with Z_2 symmetry [109].

and the location of its minimum is given by

$$\rho_{0\Lambda} = \bar{\mu}_\Lambda^2 / \bar{\lambda}_{1\Lambda}. \quad (4.10)$$

To study the phase structure of the model we integrate the flow equation for the effective average potential U_k (cf. sect. 4.4, 4.5) for a variety of initial conditions $\rho_{0\Lambda}, \bar{\lambda}_{1\Lambda}$ and $\bar{\lambda}_{2\Lambda}$. In particular, for general $\bar{\lambda}_{1\Lambda}, \bar{\lambda}_{2\Lambda} > 0$ we are able to find a critical value $\rho_{0\Lambda} = \rho_{0c}$ for which the system exhibits a first order phase transition. In this case the evolution of U_k leads at some scale $k_2 < \Lambda$ to the appearance of a second local minimum at the origin of the effective average potential and both minima become degenerate in the limit $k \rightarrow 0$. If $\rho_0(k) > 0$ denotes the k -dependent outer minimum of the potential ($U'_k(\rho_0) = 0$, where the prime on U_k denotes the derivative with respect to ρ at fixed k) at a first order phase transition one has

$$\lim_{k \rightarrow 0} (U_k(0) - U_k(\rho_0)) = 0. \quad (4.11)$$

A measure of the distance from the phase transition is the difference $\delta\kappa_\Lambda = (\rho_{0\Lambda} - \rho_{0c})/\Lambda$. If $\bar{\mu}_\Lambda^2$ and therefore $\rho_{0\Lambda}$ is interpreted as a function of temperature, the deviation $\delta\kappa_\Lambda$ is proportional to the deviation from the critical temperature T_c , i.e. $\delta\kappa_\Lambda = A(T)(T_c - T)$ with $A(T_c) > 0$.

We consider in the following the effective average potential U_k for a nonzero scale k . This allows to observe the nonconvex part of the potential (cf. sect. 4.8). As an example we show in fig. 6 the effective average potential $U_{k=k_f}$ for $\lambda_{1\Lambda} = \bar{\lambda}_{1\Lambda}/\Lambda = 0.1$ and $\lambda_{2\Lambda} = \bar{\lambda}_{2\Lambda}/\Lambda = 2$ as a function of the renormalized field $\varphi_R = (\rho_R/2)^{1/2}$ with $\rho_R = Z_{k=k_f}\rho$. The scale k_f is some characteristic scale below which the location of the minimum $\rho_0(k)$ becomes essentially independent of k . Its precise definition is given below. We have normalized U_{k_f} and φ_R to powers of the renormalized minimum $\varphi_{0R}(k_f) = (\rho_{0R}(k_f)/2)^{1/2}$ with $\rho_{0R}(k_f) = Z_{k_f}\rho_0(k_f)$. The potential is shown for various values of deviations from the critical temperature or $\delta\kappa_\Lambda$. For the given examples $\delta\kappa_\Lambda = -0.03, -0.015$ the minimum at the origin becomes the absolute minimum and the system is in the symmetric (disordered) phase. Here φ_{0R} denotes the minimum in the metastable ordered phase. In contrast, for $\delta\kappa_\Lambda = 0.04, 0.1$ the absolute minimum is located at $\varphi_R/\varphi_{0R} = 1$ which characterizes the spontaneously broken phase. For large enough $\delta\kappa_\Lambda$ the local minimum at the origin vanishes. For $\delta\kappa_\Lambda = 0$ the two distinct minima are degenerate in height²². As a consequence the order parameter makes a discontinuous jump at the phase transition which characterizes the transition to be first order. It is instructive to consider some characteristic values of the effective average potential. In fig. 7 we consider for $\lambda_{1\Lambda} = 0.1, \lambda_{2\Lambda} = 2$ the value of the renormalized minimum $\rho_{0R}(k_f)$ and the radial mass term as a function of $-\delta\kappa_\Lambda$ or temperature. In the spontaneously broken phase the renormalized radial mass squared is given by (cf. section 4.4)

$$m_R^2(k_f) = 2Z_{k_f}^{-1}\rho_0 U''_{k_f}(\rho_0), \quad (4.12)$$

²²We note that the critical temperature is determined by condition (4.11) in the limit $k \rightarrow 0$. Nevertheless for the employed nonvanishing scale $k = k_f$ the minima of U_k become almost degenerate at the critical temperature.

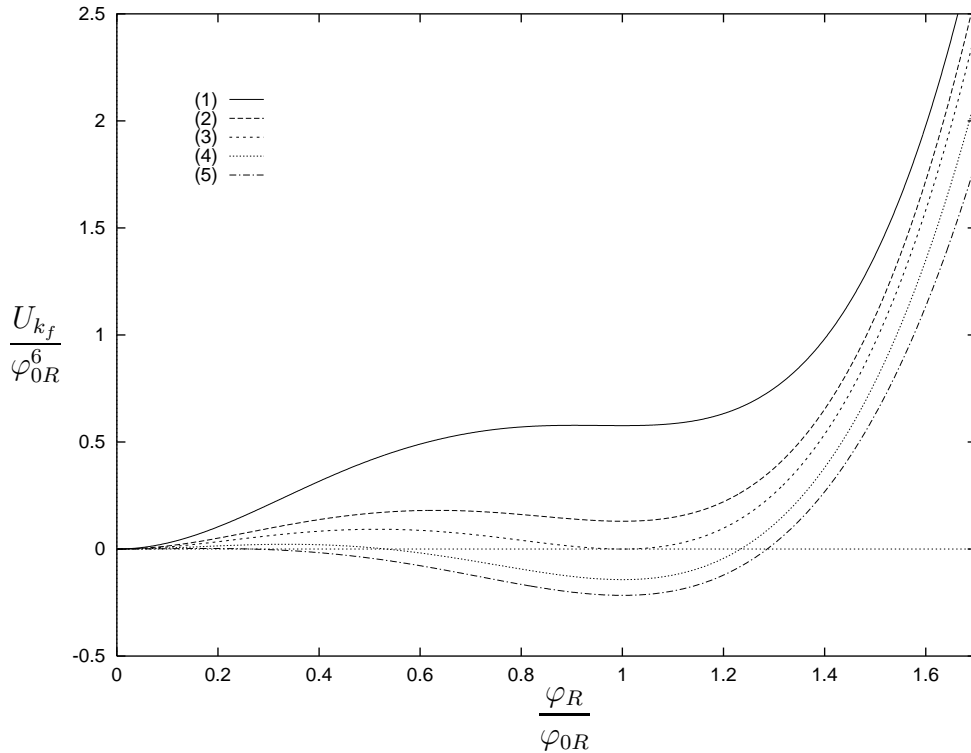


Figure 6: The effective average potential $U_{k=k_f}$ as a function of the renormalized field φ_R . The potential is shown for various values of $\delta\kappa_\Lambda \sim T_c - T$. The parameters for the short distance potential U_Λ are (1) $\delta\kappa_\Lambda = -0.03$, (2) $\delta\kappa_\Lambda = -0.015$, (3) $\delta\kappa_\Lambda = 0$, (4) $\delta\kappa_\Lambda = 0.04$, (5) $\delta\kappa_\Lambda = 0.1$ and $\lambda_{1\Lambda} = 0.1$, $\lambda_{2\Lambda} = 2$.

in the symmetric phase the renormalized mass term reads

$$m_{0R}^2(k_f) = Z_{k_f}^{-1} U'_{k_f}(0). \quad (4.13)$$

At the critical temperature ($\delta\kappa_\Lambda = 0$) one observes the discontinuity $\Delta\rho_{0R} = \rho_{0R}(k_f)$ and the jump in the mass term $\Delta m_R = m_R(k_f) - m_{0R}(k_f) = m_R^c - m_{0R}^c$. (Here the index “c” denotes $\delta\kappa_\Lambda = 0$). The ratio $\Delta\rho_{0R}/\Lambda$ is a rough measure for the “strength” of the first order transition. For $\Delta\rho_{0R}/\Lambda \ll 1$ the phase transition is weak in the sense that typical masses are small compared to Λ . In consequence, the long-wavelength fluctuations play a dominant role and the system exhibits universal behavior, i.e. it becomes largely independent of the details at the short distance scale Λ^{-1} . We will discuss the universal behavior in more detail below.

In order to characterize the strength of the phase transition for arbitrary positive values of $\lambda_{1\Lambda}$ and $\lambda_{2\Lambda}$ we consider lines of constant $\Delta\rho_{0R}/\Lambda$ in the $\lambda_{1\Lambda}, \lambda_{2\Lambda}$ plane. In fig. 8 this is done for the logarithms of these quantities. For fixed $\lambda_{2\Lambda}$ one observes that the discontinuity at the phase transition weakens with increased $\lambda_{1\Lambda}$. On the other hand for given $\lambda_{1\Lambda}$ one finds a larger jump in the order parameter for increased $\lambda_{2\Lambda}$. This is true up to a saturation point where $\Delta\rho_{0R}/\Lambda$ becomes independent of $\lambda_{2\Lambda}$. In the plot this can be observed from

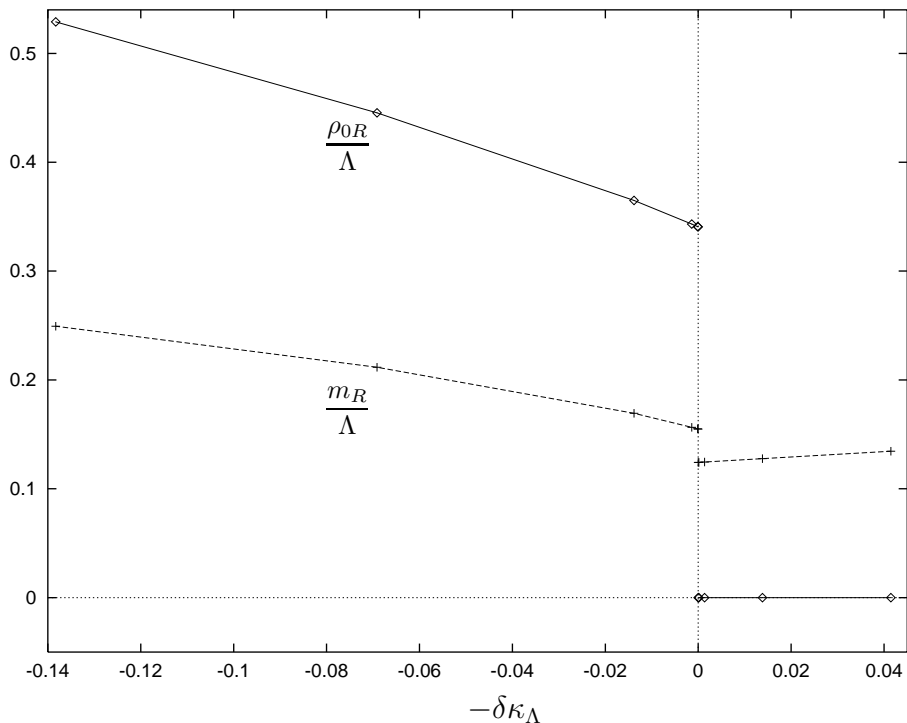


Figure 7: The minimum ρ_{0R} and the mass term m_R in units of the momentum scale Λ as a function of $-\delta\kappa_\Lambda$ or temperature ($\lambda_{1\Lambda} = 0.1$, $\lambda_{2\Lambda} = 2$, $k = k_f$). For $\delta\kappa_\Lambda = 0$ one observes the jump in the renormalized order parameter $\Delta\rho_{0R}$ and mass Δm_R .

the vertical part of the line of constant $\ln(\Delta\rho_{0R}/\Lambda)$. This phenomenon occurs for arbitrary nonvanishing $\Delta\rho_{0R}/\Lambda$ in the strong $\lambda_{2\Lambda}$ coupling limit and is discussed in section 4.6.

In the following we give a detailed quantitative description of the first order phase transitions and a separation in weak and strong transitions. We consider some characteristic quantities for the effective average potential in dependence on the short distance parameters $\lambda_{1\Lambda}$ and $\lambda_{2\Lambda}$ for $\delta\kappa_\Lambda = 0$. We consider the discontinuity in the renormalized order parameter $\Delta\rho_{0R}$ and the inverse correlation lengths (mass terms) m_R^c and m_{0R}^c in the ordered and the disordered phase respectively. Fig. 9 shows the logarithm of $\Delta\rho_{0R}$ in units of Λ as a function of the logarithm of the initial coupling $\lambda_{2\Lambda}$. We have connected the calculated values obtained for various fixed $\lambda_{1\Lambda} = 0.1$, 2 and $\lambda_{1\Lambda} = 4$ by straight lines. The values are listed in table 4. For $\lambda_{2\Lambda}/\lambda_{1\Lambda} \lesssim 1$ the curves show constant positive slope. In this range $\Delta\rho_{0R}$ follows a power law behavior

$$\Delta\rho_{0R} = R (\lambda_{2\Lambda})^\theta, \quad \theta = 1.93. \quad (4.14)$$

The critical exponent θ is obtained from the slope of the curve in fig. 9 for $\lambda_{2\Lambda}/\lambda_{1\Lambda} \ll 1$. The exponent is universal and, therefore, does not depend on the specific value for $\lambda_{1\Lambda}$. On the other hand, the amplitude R grows with decreasing $\lambda_{1\Lambda}$. For vanishing $\lambda_{2\Lambda}$ the order parameter changes continuously at the transition point and one observes a second order

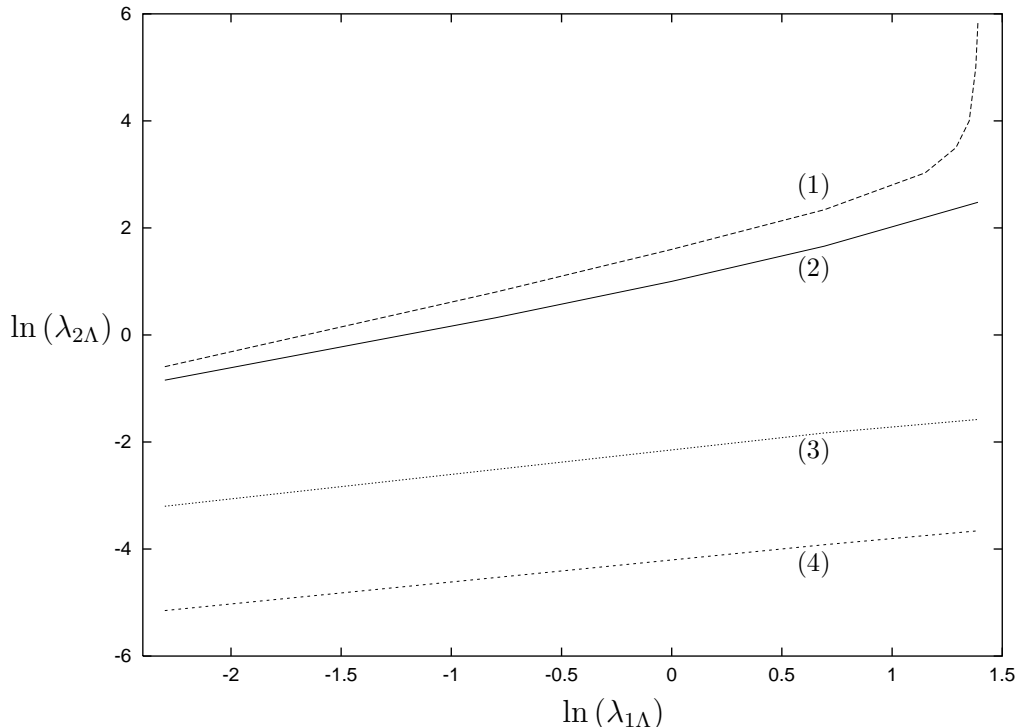


Figure 8: Lines of constant jump of the renormalized order parameter $\Delta\rho_{0R}/\Lambda$ at the phase transition in the $\ln(\lambda_{1\Lambda}), \ln(\lambda_{2\Lambda})$ plane. The curves correspond to (1) $\ln(\Delta\rho_{0R}/\Lambda) = -4.0$, (2) $\ln(\Delta\rho_{0R}/\Lambda) = -4.4$, (3) $\ln(\Delta\rho_{0R}/\Lambda) = -10.2$, (4) $\ln(\Delta\rho_{0R}/\Lambda) = -14.3$.

phase transition as expected for the $O(8)$ symmetric vector model. As $\lambda_{2\Lambda}/\lambda_{1\Lambda}$ becomes larger than one the curves deviate substantially from the linear behavior. The deviation depends on the specific choice of the short distance potential. For $\lambda_{2\Lambda}/\lambda_{1\Lambda} \gg 1$ the curves flatten. In this range $\Delta\rho_{0R}$ becomes insensitive to a variation of the quartic coupling $\lambda_{2\Lambda}$.

In addition to the jump in the order parameter we present the mass terms m_R^c and m_{0R}^c which we normalize to $\Delta\rho_{0R}$. In fig. 10 these ratios are plotted versus the logarithm of the ratio of the initial quartic couplings $\lambda_{2\Lambda}/\lambda_{1\Lambda}$. Again values obtained for fixed $\lambda_{1\Lambda} = 0.1, 2$ and $\lambda_{1\Lambda} = 4$ are connected by straight lines. The universal range is set by the condition $m_R^c/\Delta\rho_{0R} \simeq \text{const}$ (equivalently for $m_{0R}^c/\Delta\rho_{0R}$). The universal ratios are $m_R^c/\Delta\rho_{0R} = 1.69$ and $m_{0R}^c/\Delta\rho_{0R} = 1.26$ as can be seen from table 4. For the given curves universality holds approximately for $\lambda_{2\Lambda}/\lambda_{1\Lambda} \lesssim 1/2$ and becomes “exact” in the limit $\lambda_{2\Lambda}/\lambda_{1\Lambda} \rightarrow 0$. In this range we obtain

$$m_R^c = S(\lambda_{2\Lambda})^\theta, \quad m_{0R}^c = \tilde{S}(\lambda_{2\Lambda})^\theta. \quad (4.15)$$

The universal features of the system are not restricted to the weak coupling region of $\lambda_{2\Lambda}$. This is demonstrated in fig. 10 for values up to $\lambda_{2\Lambda} \simeq 2$. The ratios $m_R^c/\Delta\rho_{0R}$ and $m_{0R}^c/\Delta\rho_{0R}$ deviate from the universal values as $\lambda_{2\Lambda}/\lambda_{1\Lambda}$ is increased. For fixed $\lambda_{2\Lambda}$ a larger $\lambda_{1\Lambda}$ results in a weaker transition concerning $\Delta\rho_{0R}/\Lambda$. The ratio $m_R^c/\Delta\rho_{0R}$ increases with

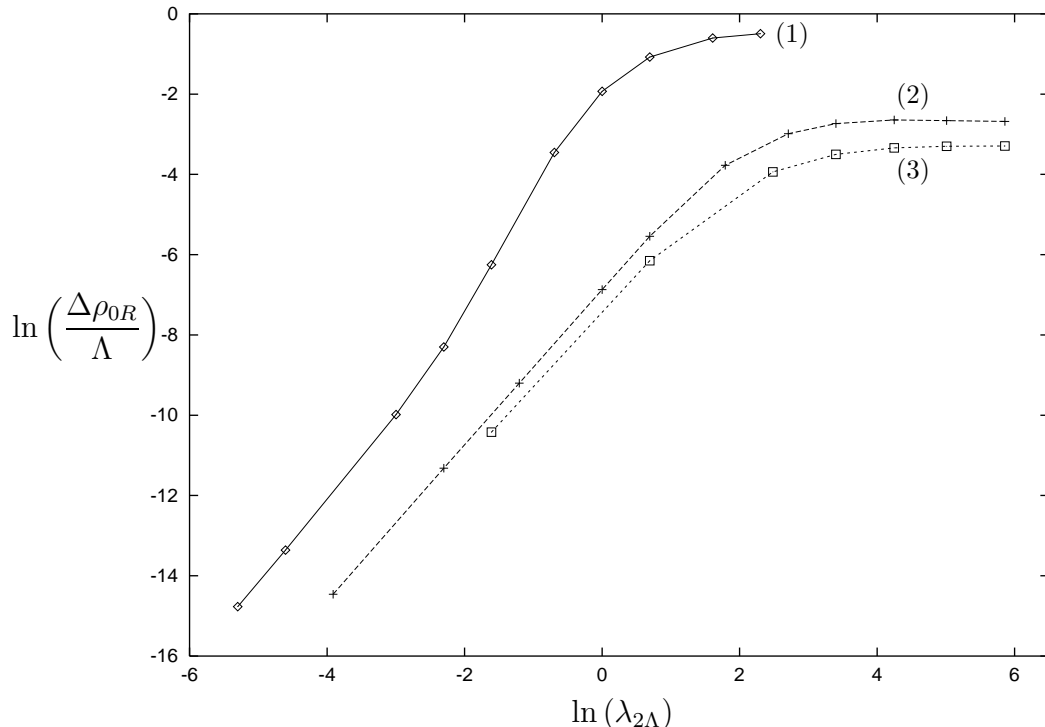


Figure 9: The logarithm of the discontinuity of the renormalized order parameter $\Delta\rho_{0R}/\Lambda$ as a function of $\ln(\lambda_{2\Lambda})$. Data points for fixed (1) $\lambda_{1\Lambda} = 0.1$, (2) $\lambda_{1\Lambda} = 2$, (3) $\lambda_{1\Lambda} = 4$ are connected by straight lines.

$\lambda_{1\Lambda}$ for small fixed $\lambda_{2\Lambda}$ whereas in the asymptotic region, $\lambda_{2\Lambda}/\lambda_{1\Lambda} \gg 1$, one observes from fig. 10 that this tendency is reversed and $m_R^c/\Delta\rho_{0R}$, $m_{0R}^c/\Delta\rho_{0R}$ start to decrease at about $\lambda_{1\Lambda} \simeq 2$.

In summary, the above results show that though the short distance potential U_Λ indicates a second order phase transition, the transition becomes first order once fluctuations are taken into account. This fluctuation induced first order phase transition is known in four dimensions as the Coleman-Weinberg phenomenon [70]. Previous studies of the three dimensional $U(2) \times U(2)$ symmetric model using the ϵ -expansion [110, 31] already indicated that the phase transition should be a fluctuation induced first order transition. The validity of the ϵ -expansion for weak first order transitions is, however, not clear a priori since the expansion parameter is not small – there are known cases where it fails to predict correctly the order of the transition [111]. The question of the order of the phase transition has been addressed also in lattice studies [112] and in high-temperature expansion [113]. All studies are consistent with the first order nature of the transition and with the absence of nonperturbative infrared stable fixed points. It is, however, notoriously difficult to distinguish by these methods between weak first order and second order transitions. Our method gives here a clear and unambiguous answer and allows a detailed quantitative description of the phase transition. The universal form of the equation of state for weak first order phase transitions is presented in section 4.7.

$\lambda_{1\Lambda}$	$\lambda_{2\Lambda}$	$\frac{\Delta\rho_{0R}}{\Lambda}$	$\frac{m_R^c}{\Delta\rho_{0R}}$	$\frac{m_{0R}^c}{\Delta\rho_{0R}}$	$\lambda_{1\Lambda}$	$\lambda_{2\Lambda}$	$\frac{\Delta\rho_{0R}}{\Lambda}$	$\frac{m_R^c}{\Delta\rho_{0R}}$	$\frac{m_{0R}^c}{\Delta\rho_{0R}}$
0.1	0.005	0.386×10^{-6}	1.69	1.26	2	2	0.392×10^{-2}	1.66	1.24
0.1	0.01	0.158×10^{-5}	1.68	1.26	2	6	0.230×10^{-1}	1.68	1.25
0.1	0.05	0.461×10^{-4}	1.66	1.23	2	15	0.505×10^{-1}	1.80	1.35
0.1	0.1	0.249×10^{-3}	1.58	1.17	2	30	0.649×10^{-1}	1.91	1.45
0.1	0.2	0.193×10^{-2}	1.34	0.992	2	70	0.712×10^{-1}	2.01	1.60
0.1	0.5	0.316×10^{-1}	0.772	0.571	2	150	0.699×10^{-1}	2.02	1.65
0.1	1	0.145	0.527	0.395	2	350	0.685×10^{-1}	2.03	1.68
0.1	2	0.341	0.455	0.360	4	0.2	0.298×10^{-4}	1.69	1.26
0.1	5	0.547	0.450	0.414	4	2	0.213×10^{-2}	1.70	1.27
0.1	10	0.610	0.462	0.490	4	12	0.195×10^{-1}	1.80	1.35
2	0.02	0.523×10^{-6}	1.69	1.26	4	30	0.302×10^{-1}	1.89	1.43
2	0.1	0.121×10^{-4}	1.69	1.26	4	70	0.355×10^{-1}	1.96	1.49
2	0.3	0.101×10^{-3}	1.69	1.25	4	150	0.369×10^{-1}	1.98	1.55
2	1	0.104×10^{-2}	1.66	1.25	4	350	0.372×10^{-1}	1.97	1.57

Table 4: The discontinuity in the renormalized order parameter $\Delta\rho_{0R}$ and the critical inverse correlation lengths m_R^c and m_{0R}^c in the ordered and the disordered phase respectively. For small $\lambda_{2\Lambda}/\lambda_{1\Lambda}$ the ratios $m_R^c/\Delta\rho_{0R}$ and $m_{0R}^c/\Delta\rho_{0R}$ become universal.

In the following we specify the scale k_f for which we have given the effective average potential U_k . We observe that U_k depends strongly on the infrared cutoff k as long as k is larger than the scale k_2 where the second minimum of the potential appears. Below k_2 the two minima start to become almost degenerate for T near T_c and the running of $\rho_0(k)$ stops rather soon. The nonvanishing value of k_2 induces a physical infrared cutoff and represents a characteristic scale for the first order phase transition. We stop the integration of the flow equation for the effective average potential at a scale $k_f < k_2$ which is determined in terms of the curvature (mass term) at the top of the potential barrier that separates the two local minima of U_k at the origin and at $\rho_0(k)$. The top of the potential barrier at $\rho_B(k)$ is determined by

$$U'_k(\rho_B) = 0 \quad (4.16)$$

for $0 < \rho_B(k) < \rho_0(k)$ and for the renormalized mass term at $\rho_B(k)$ one obtains

$$m_{B,R}^2(k) = 2Z_k^{-1} \rho_B U''_k(\rho_B) < 0. \quad (4.17)$$

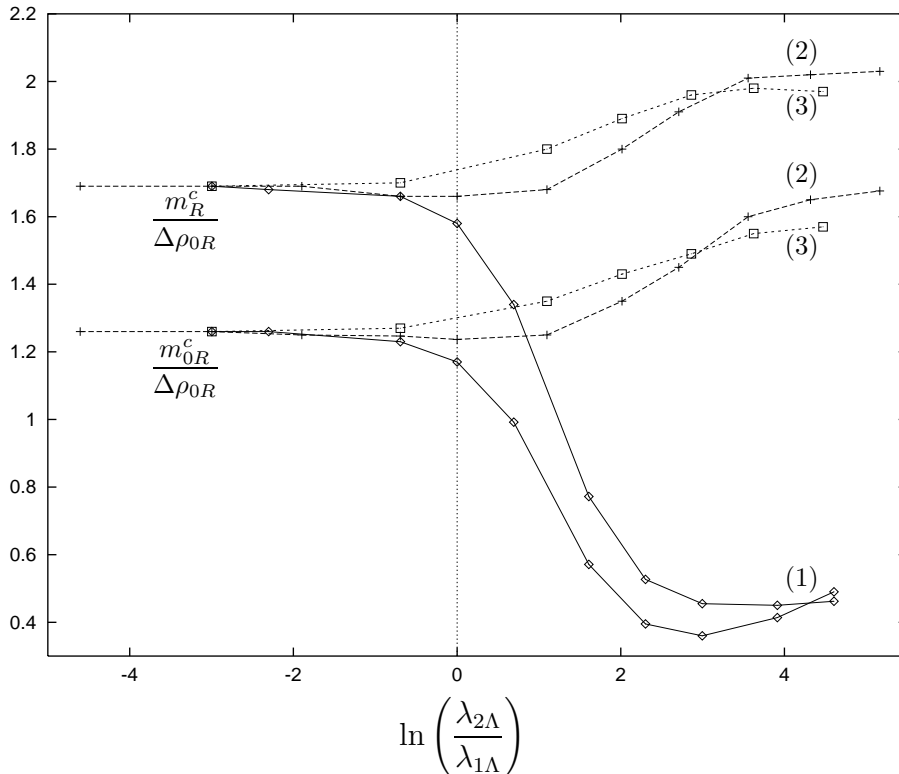


Figure 10: The inverse correlation lengths m_R^c and m_{0R}^c in the ordered and the disordered phase respectively. They are normalized to $\Delta\rho_{0R}$ and given as a function of $\ln(\lambda_{2\Lambda}/\lambda_{1\Lambda})$. Data points for fixed (1) $\lambda_{1\Lambda} = 0.1$, (2) $\lambda_{1\Lambda} = 2$, (3) $\lambda_{1\Lambda} = 4$ are connected by straight lines.

We fix our final value for the running by

$$\frac{k_f^2 - |m_{B,R}^2(k_f)|}{k_f^2} = 0.01 \quad (4.18)$$

For this choice the coarse grained effective potential U_{k_f} essentially includes all fluctuations with momenta larger than the mass $|m_{B,R}|$ at the top of the potential barrier. It is a nonconvex function which is the appropriate quantity for the study of physical processes such as tunneling or inflation. The nonconvex part of U_k is considered in detail in section 4.8. There we will also discuss that the appropriate choice for a coarse graining scale k is often far from obvious.

4.4 Scale dependence of the effective average potential

In this section we derive the flow equation for the effective average potential U_k . We point out a related investigation of the four dimensional $SU(N) \times SU(N)$ symmetric linear sigma model coupled to fermions that has been studied previously within the framework of the

effective average action [46]. There the flow equations for a polynomial approximation of U_k can be found for arbitrary dimension d . To study the equation of state of the three dimensional theory we keep here the most general form for U_k .

We define U_k by evaluating the average action for a constant field with $\Gamma_k = \Omega U_k$ where Ω denotes the volume. To evaluate the r.h.s. of (2.10) with the ansatz (4.2) we expand Γ_k around a constant background configuration. With the help of the $U(2) \times U(2)$ transformations the matrix field φ can be turned into a standard diagonal form with real nonnegative eigenvalues. Without loss of generality the evolution equation for the effective potential can therefore be obtained by calculating the trace in (2.10) for small field fluctuations χ_{ab} around a constant background configuration which is real and diagonal,

$$\varphi_{ab} = \varphi_a \delta_{ab}, \quad \varphi_a^* = \varphi_a. \quad (4.19)$$

We separate the fluctuation field into its real and imaginary part, $\chi_{ab} = \frac{1}{\sqrt{2}}(\chi_{Rab} + i\chi_{Iab})$ and perform the second functional derivatives of Γ_k with respect to the eight real components. For the constant configuration (4.19) it turns out that $\Gamma_k^{(2)}$ has a block diagonal form because mixed derivatives with respect to real and imaginary parts of the field vanish. The remaining submatrices $\delta^2\Gamma_k/\delta\chi_R^{ab}\delta\chi_R^{cd}$ and $\delta^2\Gamma_k/\delta\chi_I^{ab}\delta\chi_I^{cd}$ can be diagonalized in order to find the inverse of $\Gamma_k^{(2)} + R_k$ under the trace occurring in eq. (2.10). Here the momentum independent part of $\Gamma_k^{(2)}$ defines the mass matrix by the second functional derivatives of U_k . The eight eigenvalues of the mass matrix are

$$\begin{aligned} (M_1^\pm)^2 &= U'_k + 2(\rho \pm (\rho^2 - \tau)^{1/2}) \partial_\tau U_k, \\ (M_2^\pm)^2 &= U'_k \pm 2\tau^{1/2} \partial_\tau U_k \end{aligned} \quad (4.20)$$

corresponding to second derivatives with respect to χ_I and

$$\begin{aligned} (M_3^\pm)^2 &= (M_1^\pm)^2, \\ (M_4^\pm)^2 &= U'_k + \rho U''_k + 2\rho \partial_\tau U_k + 4\tau \partial_\tau U'_k + 4\rho\tau \partial_\tau^2 U_k \\ &\quad \pm \left\{ \tau (U''_k + 4\partial_\tau U_k + 4\rho \partial_\tau U'_k + 4\tau \partial_\tau^2 U_k)^2 \right. \\ &\quad \left. + (\rho^2 - \tau) (U''_k - 2\partial_\tau U_k - 4\tau \partial_\tau^2 U_k)^2 \right\}^{1/2} \end{aligned} \quad (4.21)$$

corresponding to second derivatives with respect to χ_R . Here the eigenvalues are expressed in terms of the invariants ρ and τ using

$$\varphi_1^2 = \frac{1}{2}(\rho + \tau^{1/2}), \quad \varphi_2^2 = \frac{1}{2}(\rho - \tau^{1/2}) \quad (4.22)$$

and we adopt the convention that a prime on $U_k(\rho, \tau)$ denotes the derivative with respect to ρ at fixed τ and k and $\partial_\tau^n U_k \equiv \partial^n U_k / (\partial \tau)^n$.

The flow equation for the effective average potential is simply expressed in terms of the

mass eigenvalues

$$\begin{aligned} \frac{\partial}{\partial t} U_k(\rho, \tau) &= \frac{1}{2} \int \frac{d^d q}{(2\pi)^d} \frac{\partial}{\partial t} R_k(q) \\ &\left\{ \frac{2}{P_k(q) + (M_1^+(\rho, \tau))^2} + \frac{2}{P_k(q) + (M_1^-(\rho, \tau))^2} + \frac{1}{P_k(q) + (M_2^+(\rho, \tau))^2} \right. \\ &\left. + \frac{1}{P_k(q) + (M_2^-(\rho, \tau))^2} + \frac{1}{P_k(q) + (M_4^+(\rho, \tau))^2} + \frac{1}{P_k(q) + (M_4^-(\rho, \tau))^2} \right\}. \end{aligned} \quad (4.23)$$

On the right hand side of the evolution equation appears the (massless) inverse average propagator

$$P_k(q) = Z_k q^2 + R_k(q) = \frac{Z_k q^2}{1 - e^{-q^2/k^2}} \quad (4.24)$$

which incorporates the infrared cutoff function R_k given by eq. (2.3). The only approximation so far is due to the derivative expansion (4.2) of Γ_k which enters into the flow equation (4.23) through the form of P_k . The mass eigenvalues (4.20) and (4.21) appearing in the above flow equation are exact since we have kept for the potential the most general form $U_k(\rho, \tau)$.

Spontaneous symmetry breaking and mass spectra

In the following we consider spontaneous symmetry breaking patterns and the corresponding mass spectra for a few special cases. For the origin at $\varphi_{ab} = 0$ all eigenvalues equal $U'_k(0, 0)$. If the origin is the absolute minimum of the potential we are in the symmetric regime where all excitations have mass squared $U'_k(0, 0)$.

Spontaneous symmetry breaking to the diagonal $U(2)$ subgroup of $U(2) \times U(2)$ can be observed for a field configuration which is proportional to the identity matrix, i.e. $\varphi_{ab} = \varphi \delta_{ab}$. The invariants (4.3) take on values $\rho = 2\varphi^2$ and $\tau = 0$. The relevant information for this symmetry breaking pattern is contained in $U_k(\rho) \equiv U_k(\rho, \tau = 0)$. In case of spontaneous symmetry breaking there is a nonvanishing value for the minimum ρ_0 of the potential. With $U'_k(\rho_0) = 0$ one finds the expected four massless Goldstone bosons with $(M_1^-)^2 = (M_2^\pm)^2 = (M_3^-)^2 = 0$. In addition there are three massive scalars in the adjoint representation of the unbroken diagonal $SU(2)$ with mass squared $(M_1^+)^2 = (M_3^+)^2 = (M_4^-)^2 = 4\rho_0 \partial_\tau U_k$ and one singlet with mass squared $(M_4^+)^2 = 2\rho_0 U''_k$. The situation corresponds to chiral symmetry breaking in two flavor QCD in absence of quark masses and the chiral anomaly. The Goldstone modes are the pseudoscalar pions and the η (or η'), the scalar triplet has the quantum numbers of a_0 and the singlet is the so-called σ -field.

Another interesting case is the spontaneous symmetry breaking down to a residual $U(1) \times U(1) \times U(1)$ subgroup of $U(2) \times U(2)$ which can be observed for the configuration $\varphi_{ab} = \varphi \delta_{a1} \delta_{ab}$ ($\rho = \varphi^2$, $\tau = \varphi^4 = \rho^2$). Corresponding to the number of broken generators one observes the five massless Goldstone bosons $(M_1^\pm)^2 = (M_2^+)^2 = (M_3^\pm)^2 = 0$ for the minimum of the potential at $U'_k + 2\rho_0 \partial_\tau U_k = 0$. In addition there are two scalars with mass

squared $(M_2^-)^2 = (M_4^-)^2 = U'_k - 2\rho_0\partial_\tau U_k$ and one with $(M_4^+)^2 = U'_k + 2\rho_0 U''_k + 6\rho_0\partial_\tau U_k + 8\rho_0^2\partial_\tau U'_k + 8\rho_0^3\partial_\tau^2 U_k$.

We finally point out the special case where the potential is independent of the second invariant τ . In this case there is an enhanced $O(8)$ symmetry instead of $U(2) \times U(2)$. With $\partial_\tau^n U_k \equiv 0$ and $U'_k(\rho_0) = 0$ one observes the expected seven massless Goldstone bosons and one massive mode with mass squared $2\rho_0 U''_k$.

Scaling form of the flow equation

For the $O(8)$ symmetric model in the limit $\bar{\lambda}_{2\Lambda} = 0$ one expects a region of the parameter space which is characterized by renormalized masses much smaller than the ultraviolet cutoff or inverse microscopic length scale of the theory. In particular, in the absence of a mass scale one expects a scaling behavior of the effective average potential U_k . The behavior of U_k at or near a second order phase transition is most conveniently studied using the scaling form of the evolution equation. This form is also appropriate for an investigation that has to deal with weak first order phase transitions as encountered in the present model for $\bar{\lambda}_{2\Lambda} > 0$. The remaining part of this section is devoted to the derivation of the scaling form (4.33) of the flow equation (4.23).

In the present form of eq. (4.23) the r.h.s. shows an explicit dependence on the scale k once the momentum integration is performed. By a proper choice of variables we cast the evolution equation into a form where the scale no longer appears explicitly. We introduce a dimensionless potential $u_k = k^{-d}U_k$ and express it in terms of dimensionless renormalized fields

$$\begin{aligned}\tilde{\rho} &= Z_k k^{2-d} \rho, \\ \tilde{\tau} &= Z_k^2 k^{4-2d} \tau.\end{aligned}\tag{4.25}$$

The derivatives of u_k are given by

$$\partial_{\tilde{\tau}}^n u_k^{(m)}(\tilde{\rho}, \tilde{\tau}) = Z_k^{-2n-m} k^{(2n+m-1)d-4n-2m} \partial_\tau^n U_k^{(m)}(\rho, \tau).\tag{4.26}$$

(Note that $u_k^{(m)}$ denotes m derivatives with respect to $\tilde{\rho}$ at fixed $\tilde{\tau}$ and k , while $U_k^{(m)}$ denotes m derivatives with respect to ρ at fixed τ and k). With

$$\begin{aligned}\frac{\partial}{\partial t} u_k(\tilde{\rho}, \tilde{\tau})|_{\tilde{\rho}, \tilde{\tau}} &= -du_k(\tilde{\rho}, \tilde{\tau}) + (d-2+\eta)\tilde{\rho}u'_k(\tilde{\rho}, \tilde{\tau}) + (2d-4+2\eta)\tilde{\tau}\partial_{\tilde{\tau}}u_k(\tilde{\rho}, \tilde{\tau}) \\ &\quad + k^{-d}\frac{\partial}{\partial t} U_k(\rho(\tilde{\rho}), \tau(\tilde{\tau}))|_{\rho, \tau}\end{aligned}\tag{4.27}$$

one obtains from (4.23) the evolution equation for the dimensionless potential. Here the anomalous dimension η arises from the t -derivative acting on Z_k and is given by eq. (4.5). It is convenient to introduce dimensionless integrals by

$$\frac{1}{2} \int \frac{d^d q}{(2\pi)^d} \frac{\partial R_k}{\partial t} \frac{1}{P_k + Z_k k^2 \omega} = 2v_d k^d [l_0^d(\omega) - \eta \hat{l}_0^d(\omega)]\tag{4.28}$$

where

$$v_d^{-1} = 2^{d+1} \pi^{\frac{d}{2}} \Gamma\left(\frac{d}{2}\right).\tag{4.29}$$

The explicit form of l_0^d and \hat{l}_0^d reads

$$\begin{aligned} l_0^d(\omega) &= - \int_0^\infty dy y^{\frac{d}{2}+1} \frac{\partial r(y)}{\partial y} [y(1+r(y)) + \omega]^{-1}, \\ \hat{l}_0^d(\omega) &= \frac{1}{2} \int_0^\infty dy y^{\frac{d}{2}} r(y) [y(1+r(y)) + \omega]^{-1} \end{aligned} \quad (4.30)$$

with the dimensionless infrared cutoff function

$$r(y) = \frac{e^{-y}}{1 - e^{-y}}. \quad (4.31)$$

The behavior of these functions is discussed in section 4.5 where we also consider their derivatives with respect to ω . Using the notation

$$l_0^d(\omega; \eta) = l_0^d(\omega) - \eta \hat{l}_0^d(\omega) \quad (4.32)$$

one obtains the flow equation for the dimensionless potential

$$\begin{aligned} \frac{\partial}{\partial t} u_k(\tilde{\rho}, \tilde{\tau}) &= -du_k(\tilde{\rho}, \tilde{\tau}) + (d-2+\eta)\tilde{\rho}u'_k(\tilde{\rho}, \tilde{\tau}) + (2d-4+2\eta)\tilde{\tau}\partial_{\tilde{\tau}}u_k(\tilde{\rho}, \tilde{\tau}) \\ &+ 4v_d l_0^d((m_1^+(\tilde{\rho}, \tilde{\tau}))^2; \eta) + 4v_d l_0^d((m_1^-(\tilde{\rho}, \tilde{\tau}))^2; \eta) + 2v_d l_0^d((m_2^+(\tilde{\rho}, \tilde{\tau}))^2; \eta) \\ &+ 2v_d l_0^d((m_2^-(\tilde{\rho}, \tilde{\tau}))^2; \eta) + 2v_d l_0^d((m_4^+(\tilde{\rho}, \tilde{\tau}))^2; \eta) + 2v_d l_0^d((m_4^-(\tilde{\rho}, \tilde{\tau}))^2; \eta) \end{aligned} \quad (4.33)$$

where the dimensionless mass terms are related to (4.21) according to

$$(m_i^\pm(\tilde{\rho}, \tilde{\tau}))^2 = \frac{(M_i^\pm(\rho(\tilde{\rho}), \tau(\tilde{\tau})))^2}{Z_k k^2}. \quad (4.34)$$

Eq. (4.33) is the scaling form of the flow equation we are looking for. For a $\tilde{\tau}$ -independent potential it reduces to the evolution equation for the $O(8)$ symmetric model [92, 93]. The potential u_k at a second order phase transition is given by a k -independent (scaling) solution $\partial u_k / \partial t = 0$ [92, 93]. For this solution all the k -dependent functions on the r.h.s. of eq. (4.33) become independent of k . For a weak first order phase transition these functions will show a weak k -dependence for k larger than the inherent mass scale of the system (cf. section 4.6). There is no particular advantage of the scaling form of the flow equation for strong first order phase transitions.

4.5 Solving the flow equation

Eq. (4.33) describes the scale dependence of the effective average potential u_k by a nonlinear partial differential equation for the three variables t , $\tilde{\rho}$ and $\tilde{\tau}$. A particular difficulty for its analytical study is that the integral $l_0^d(\omega; \eta)$ (cf. eq. (4.30)) can be done analytically only for

certain limits of the arguments. The complicated form of the equation therefore suggests a numerical solution. We will use a method that relies on a simultaneous expansion of the potential around a number of field values $\tilde{\rho}_i, \tilde{\tau}_j$, $i = 1, \dots, l$, $j = 1, \dots, l'$ for given numbers l, l' . The expansions around different points are matched to obtain the general field dependence of the potential. As a consequence we cast the partial differential equation (4.33) into a system of ordinary differential equations. The method is developed in [63] for a computation of the critical equation of state for $O(N)$ symmetric Heisenberg models [62] (cf. section 3). The generalization to the present model is described below. This approach has some favorable aspects. The main advantage is that it allows a very efficient integration of the differential equations using a standard Runge-Kutta algorithm without the occurrence of numerical instabilities²³. The coupled set of ordinary differential equations describes the flow of couplings defined as derivatives of the potential at given points, e.g. at the minimum of the potential. These couplings often allow direct physical interpretation and some of their properties can be read off from the analytic structure of their flow equations. We will exploit this fact to explain the results we obtain from the numerical solution in section 4.6.

We concentrate in the following on spontaneous symmetry breaking with a residual $U(2)$ symmetry group. As we have already pointed out in section 4.2 this symmetry breaking can be observed for a configuration which is proportional to the identity and we have $\tilde{\tau} = 0$. In this case the eigenvalues (4.20) and (4.21) of the mass matrix with (4.34) are given by

$$\begin{aligned} (m_1^-)^2 &= (m_2^\pm)^2 = (m_3^-)^2 = u'_k, \\ (m_1^+)^2 &= (m_3^+)^2 = (m_4^-)^2 = u'_k + 4\tilde{\rho}\tilde{\partial}_\tau u_k, \\ (m_4^+)^2 &= u'_k + 2\tilde{\rho}u''_k \end{aligned} \tag{4.35}$$

and on the r.h.s. of the partial differential equation (4.33) for $u_k(\tilde{\rho}) \equiv u_k(\tilde{\rho}, \tilde{\tau} = 0)$ only the functions $u'_k(\tilde{\rho})$, $u''_k(\tilde{\rho})$ and $\partial_\tau u_k(\tilde{\rho})$ appear. At fixed $\tilde{\rho} = \tilde{\rho}_i$ the k -dependence of u_k is then determined by the couplings $u'_k(\tilde{\rho}_i)$, $u''_k(\tilde{\rho}_i)$ and $\partial_\tau u_k(\tilde{\rho}_i)$. We determine these couplings through the use of flow equations which are obtained by taking the derivative in eq. (4.33) with respect to $\tilde{\rho}$ and $\tilde{\tau}$ evaluated at $\tilde{\rho} = \tilde{\rho}_i$, $\tilde{\tau} = 0$. These flow equations for u'_k , u''_k and $\partial_\tau u_k$ involve also higher derivatives of the potential as u'''_k , $u_k^{(4)}$, $\partial_\tau u'_k$ and $\partial_\tau u''_k$. The procedure will be to evaluate the flow equations for u'_k and u''_k at different points $\tilde{\rho}_i$, $\tilde{\tau} = 0$ for $i = 1, \dots, l$ and to estimate the higher $\tilde{\rho}$ -derivatives appearing on the right hand side of the flow equations by imposing matching conditions. The same procedure can be applied to $\partial_\tau u_k$ and in order to obtain an equivalent matching we also consider the flow equation for $\partial_\tau u'_k$. One could proceed in a similar way for $\partial_\tau^2 u_k$ which appears on the right hand side of the evolution equation of $\partial_\tau u_k$ and so on. However, since we are interested in the

²³These instabilities arise through the inevitable small round-off errors at every integration step. The standard discretised version of eq. (4.33), using finite difference quotients for the derivatives, becomes strongly oscillating after a few integration steps. Already for the most simple linear partial differential equations one finds that the resulting error may grow exponentially with the number of steps (see e.g. ref. [114] for an analytically solved example). A possible finite difference scheme uses “backward” difference quotients as we have exemplified in ref. [63].

$\tilde{\rho}$ -dependence of the potential at $\tilde{\tau} = 0$ we shall use a truncated expansion²⁴ in $\tilde{\tau}$ with

$$\partial_{\tilde{\tau}}^n u_k(\tilde{\rho}, \tilde{\tau} = 0) = 0 \quad \text{for } n \geq 2. \quad (4.36)$$

In three space dimensions the neglected ($\tilde{\rho}$ -dependent) operators have negative canonical mass dimension. We make no expansion in terms of $\tilde{\rho}$ since the general $\tilde{\rho}$ -dependence allows a description of a first order phase transition where a second local minimum of $u_k(\tilde{\rho})$ appears. The approximation (4.36) only affects the flow equations for $\partial_{\tilde{\tau}} u_k$ and $\partial_{\tilde{\tau}} u'_k$ (cf. eqs. (4.43) and (4.44)). The form of the flow equations for u'_k and u''_k is not affected by the truncation (cf. eqs. (4.41) and (4.42)). From u'_k we obtain the effective average potential u_k by simple integration. We have tested the sensitivity of our results for u'_k to a change in $\partial_{\tilde{\tau}} u_k$ by neglecting the $\tilde{\rho}$ -dependence of the $\tilde{\tau}$ -derivative. We observed no qualitative change of the results. We expect that the main truncation error is due to the derivative expansion (4.2) for the effective average action.

To simplify notation we introduce

$$\begin{aligned} \epsilon(\tilde{\rho}) &= u'_k(\tilde{\rho}, \tilde{\tau} = 0), \\ \lambda_1(\tilde{\rho}) &= u''_k(\tilde{\rho}, \tilde{\tau} = 0), \\ \lambda_2(\tilde{\rho}) &= 4\partial_{\tilde{\tau}} u_k(\tilde{\rho}, \tilde{\tau} = 0). \end{aligned} \quad (4.37)$$

Higher derivatives are denoted by primes on the $\tilde{\rho}$ -dependent quartic ‘‘couplings’’, i.e. $\lambda'_1 = u'''_k$, $\lambda'_2 = \partial_{\tilde{\tau}} u'_k$ etc. It is convenient to introduce functions $l_n^d(\omega; \eta)$ that can be related to $l_0^d(\omega; \eta)$ (4.30) by differentiation with respect to the mass argument:

$$\begin{aligned} l_1^d(\omega; \eta) &= l_1^d(\omega) - \eta \hat{l}_1^d(\omega) \\ &= -\frac{\partial}{\partial \omega} l_0^d(\omega; \eta), \\ l_{n+1}^d(\omega; \eta) &= -\frac{1}{n} \frac{\partial}{\partial \omega} l_n^d(\omega; \eta) \quad \text{for } n \geq 1. \end{aligned} \quad (4.38)$$

The explicit form of l_n^d and \hat{l}_n^d is given in eq. (C.1) in the appendix. For $\omega \geq -1$ they are positive, monotonically decreasing functions of ω . In leading order l_n^d and \hat{l}_n^d vanish $\sim \omega^{-(n+1)}$ for arguments $\omega \gg 1$. They introduce a ‘‘threshold’’ behavior that accounts for the decoupling of modes with mass squared larger than the infrared cutoff $Z_k k^2$. For vanishing argument they are of order unity. As $\omega \rightarrow -1$ the functions l_n^d , \hat{l}_n^d exhibit a pole for $d < 2(n+1)$. The pole structure is discussed in the appendix. We also use two-parameter functions $l_{n_1, n_2}^d(\omega_1, \omega_2; \eta)$ [46]. For $n_1 = n_2 = 1$ their relation to the functions $l_n^d(\omega; \eta)$ can be expressed as

$$\begin{aligned} l_{1,1}^d(\omega_1, \omega_2; \eta) &= \frac{1}{\omega_2 - \omega_1} \left[l_1^d(\omega_1; \eta) - l_1^d(\omega_2; \eta) \right] \quad \text{for } \omega_1 \neq \omega_2, \\ l_{1,1}^d(\omega, \omega; \eta) &= l_2^d(\omega; \eta) \end{aligned} \quad (4.39)$$

²⁴In principle one could also consider points with $\tilde{\tau} \neq 0$ in the neighborhood of $\tilde{\tau} = 0$ and use the additional information to estimate the higher $\tilde{\tau}$ -derivatives as it is done for the higher $\tilde{\rho}$ -derivatives.

and

$$l_{n_1+1, n_2}^d(\omega_1, \omega_2; \eta) = -\frac{1}{n_1} \frac{\partial}{\partial \omega_1} l_{n_1, n_2}^d(\omega_1, \omega_2; \eta), \quad l_{n_1, n_2}^d(\omega_1, \omega_2; \eta) = l_{n_2, n_1}^d(\omega_2, \omega_1; \eta). \quad (4.40)$$

With the help of these functions the scale dependence of ϵ is described by

$$\begin{aligned} \frac{\partial \epsilon}{\partial t} = & (-2 + \eta)\epsilon + (d - 2 + \eta)\tilde{\rho}\lambda_1 - 6v_d(\lambda_1 + \lambda_2 + \tilde{\rho}\lambda_2')l_1^d(\epsilon + \tilde{\rho}\lambda_2; \eta) \\ & - 2v_d(3\lambda_1 + 2\tilde{\rho}\lambda_1')l_1^d(\epsilon + 2\tilde{\rho}\lambda_1; \eta) - 8v_d\lambda_1 l_1^d(\epsilon; \eta) \end{aligned} \quad (4.41)$$

and for λ_1 one finds

$$\begin{aligned} \frac{\partial \lambda_1}{\partial t} = & (d - 4 + 2\eta)\lambda_1 + (d - 2 + \eta)\tilde{\rho}\lambda_1' \\ & + 6v_d \left[(\lambda_1 + \lambda_2 + \tilde{\rho}\lambda_2')^2 l_2^d(\epsilon + \tilde{\rho}\lambda_2; \eta) - (\lambda_1' + 2\lambda_2' + \tilde{\rho}\lambda_2'') l_1^d(\epsilon + \tilde{\rho}\lambda_2; \eta) \right] \\ & + 2v_d \left[(3\lambda_1 + 2\tilde{\rho}\lambda_1')^2 l_2^d(\epsilon + 2\tilde{\rho}\lambda_1; \eta) - (5\lambda_1' + 2\tilde{\rho}\lambda_1'') l_1^d(\epsilon + 2\tilde{\rho}\lambda_1; \eta) \right] \\ & + 8v_d \left[(\lambda_1)^2 l_2^d(\epsilon; \eta) - \lambda_1' l_1^d(\epsilon; \eta) \right]. \end{aligned} \quad (4.42)$$

Similarly the scale dependence of λ_2 is given by

$$\begin{aligned} \frac{\partial \lambda_2}{\partial t} = & (d - 4 + 2\eta)\lambda_2 + (d - 2 + \eta)\tilde{\rho}\lambda_2' - 4v_d(\lambda_2)^2 l_{1,1}^d(\epsilon + \tilde{\rho}\lambda_2, \epsilon; \eta) \\ & + 2v_d \left[3(\lambda_2)^2 + 12\lambda_1\lambda_2 + 8\tilde{\rho}\lambda_2'(\lambda_1 + \lambda_2) + 4\tilde{\rho}^2(\lambda_2')^2 \right] l_{1,1}^d(\epsilon + \tilde{\rho}\lambda_2, \epsilon + 2\tilde{\rho}\lambda_1; \eta) \\ & - 14v_d\lambda_2' l_1^d(\epsilon + \tilde{\rho}\lambda_2; \eta) - 2v_d(5\lambda_2' + 2\tilde{\rho}\lambda_2'') l_1^d(\epsilon + 2\tilde{\rho}\lambda_1; \eta) \\ & + 2v_d \left[(\lambda_2)^2 l_2^d(\epsilon; \eta) - 4\lambda_2' l_1^d(\epsilon; \eta) \right] \end{aligned} \quad (4.43)$$

and for λ_2' it reads

$$\begin{aligned} \frac{\partial \lambda_2'}{\partial t} = & (2d - 6 + 3\eta)\lambda_2' + (d - 2 + \eta)\tilde{\rho}\lambda_2'' \\ & + 4v_d(\lambda_2)^2 \left[(\lambda_1 + \lambda_2 + \tilde{\rho}\lambda_2') l_{2,1}^d(\epsilon + \tilde{\rho}\lambda_2, \epsilon; \eta) + \lambda_1 l_{1,2}^d(\epsilon + \tilde{\rho}\lambda_2, \epsilon; \eta) \right] \\ & - 2v_d \left[3\lambda_2(4\lambda_1 + \lambda_2) + 4\tilde{\rho}\lambda_2'(2\lambda_1 + 2\lambda_2 + \tilde{\rho}\lambda_2') \right] \left[(\lambda_1 + \lambda_2 + \tilde{\rho}\lambda_2') \right. \\ & \left. l_{2,1}^d(\epsilon + \tilde{\rho}\lambda_2, \epsilon + 2\tilde{\rho}\lambda_1; \eta) + (3\lambda_1 + 2\tilde{\rho}\lambda_1') l_{1,2}^d(\epsilon + \tilde{\rho}\lambda_2, \epsilon + 2\tilde{\rho}\lambda_1; \eta) \right] \\ & + 4v_d \left[\lambda_2'(7\lambda_2 + 10\lambda_1) + 6\lambda_2\lambda_1' + 4\tilde{\rho} \left(\lambda_2''(\lambda_1 + \lambda_2 + \tilde{\rho}\lambda_2') + \lambda_2'(2\lambda_2' + \lambda_1') \right) \right] \\ & l_{1,1}^d(\epsilon + \tilde{\rho}\lambda_2, \epsilon + 2\tilde{\rho}\lambda_1; \eta) - 8v_d\lambda_2\lambda_2' l_{1,1}^d(\epsilon + \tilde{\rho}\lambda_2, \epsilon; \eta) \\ & + 2v_d(3\lambda_1 + 2\tilde{\rho}\lambda_1')(5\lambda_2' + 2\tilde{\rho}\lambda_2'') l_2^d(\epsilon + 2\tilde{\rho}\lambda_1; \eta) + 14v_d\lambda_2'(\lambda_1 + \lambda_2 + \tilde{\rho}\lambda_2') \\ & l_2^d(\epsilon + \tilde{\rho}\lambda_2; \eta) - 2v_d(7\lambda_2'' + 2\tilde{\rho}\lambda_2''') l_1^d(\epsilon + 2\tilde{\rho}\lambda_1; \eta) - 14v_d\lambda_2'' l_1^d(\epsilon + \tilde{\rho}\lambda_2; \eta) \\ & - 4v_d(\lambda_2)^2 \lambda_1 l_3^d(\epsilon; \eta) + 4v_d\lambda_2'(2\lambda_1 + \lambda_2) l_2^d(\epsilon; \eta) - 8v_d\lambda_2'' l_1^d(\epsilon; \eta). \end{aligned} \quad (4.44)$$

We evaluate the above flow equations at different points $\tilde{\rho}_i$ for $i = 1, \dots, l$ and use a set of matching conditions that has been proposed in ref. [63]. The generalization of these conditions to the present model is obtained by considering fourth order polynomial expansions of $\epsilon(\tilde{\rho})$ and $\lambda_2(\tilde{\rho})$ around some arbitrary point $\tilde{\rho}_i$,

$$\begin{aligned} (\epsilon)_i(\tilde{\rho}) &= \epsilon_i + \lambda_{1,i}(\tilde{\rho} - \tilde{\rho}_i) + \frac{1}{2}\lambda'_{1,i}(\tilde{\rho} - \tilde{\rho}_i)^2 + \frac{1}{6}\lambda''_{1,i}(\tilde{\rho} - \tilde{\rho}_i)^3, \\ (\lambda_2)_i(\tilde{\rho}) &= \lambda_{2,i} + \lambda'_{2,i}(\tilde{\rho} - \tilde{\rho}_i) + \frac{1}{2}\lambda''_{2,i}(\tilde{\rho} - \tilde{\rho}_i)^2 + \frac{1}{6}\lambda'''_{2,i}(\tilde{\rho} - \tilde{\rho}_i)^3 \end{aligned} \quad (4.45)$$

with $\epsilon_i = \epsilon(\tilde{\rho}_i)$, $\lambda_{2,i} = \lambda_2(\tilde{\rho}_i)$ etc. Using similar expressions for

$$(\lambda_1)_i(\tilde{\rho}) = \frac{\partial}{\partial \tilde{\rho}}(\epsilon)_i(\tilde{\rho}) \quad , \quad (\lambda'_2)_i(\tilde{\rho}) = \frac{\partial}{\partial \tilde{\rho}}(\lambda_2)_i(\tilde{\rho}) \quad (4.46)$$

the matching is done by imposing continuity at half distance between neighboring expansion points,

$$\begin{aligned} (\epsilon)_i \left(\frac{\tilde{\rho}_i + \tilde{\rho}_{i+1}}{2} \right) &= (\epsilon)_{i+1} \left(\frac{\tilde{\rho}_i + \tilde{\rho}_{i+1}}{2} \right) \quad , \quad (\lambda_1)_i \left(\frac{\tilde{\rho}_i + \tilde{\rho}_{i+1}}{2} \right) = (\lambda_1)_{i+1} \left(\frac{\tilde{\rho}_i + \tilde{\rho}_{i+1}}{2} \right), \\ (\lambda_2)_i \left(\frac{\tilde{\rho}_i + \tilde{\rho}_{i+1}}{2} \right) &= (\lambda_2)_{i+1} \left(\frac{\tilde{\rho}_i + \tilde{\rho}_{i+1}}{2} \right) \quad , \quad (\lambda'_2)_i \left(\frac{\tilde{\rho}_i + \tilde{\rho}_{i+1}}{2} \right) = (\lambda'_2)_{i+1} \left(\frac{\tilde{\rho}_i + \tilde{\rho}_{i+1}}{2} \right) \end{aligned} \quad (4.47)$$

for $i = 1, \dots, l-1$ and

$$(\lambda'_1)_j \left(\frac{\tilde{\rho}_j + \tilde{\rho}_{j+1}}{2} \right) = (\lambda'_1)_{j+1} \left(\frac{\tilde{\rho}_j + \tilde{\rho}_{j+1}}{2} \right) \quad , \quad (\lambda''_2)_j \left(\frac{\tilde{\rho}_j + \tilde{\rho}_{j+1}}{2} \right) = (\lambda''_2)_{j+1} \left(\frac{\tilde{\rho}_j + \tilde{\rho}_{j+1}}{2} \right) \quad (4.48)$$

for the initial and end points, $j = 1$ and $j = l-1$. Together these $4(l-1)$ conditions (4.47) for all $l-1 \geq 2$ intermediate points and the four conditions (4.48) make up two independent algebraic systems of each $2l$ equations. From the first set of equations one obtains a unique solution for $\lambda'_{1,i}$ and $\lambda''_{1,i}$. The second set is identical in structure and $\lambda''_{2,i}$, $\lambda'''_{2,i}$ can be obtained from the solutions for $\lambda'_{1,i}$ and $\lambda''_{1,i}$ with the substitutions $\epsilon_j \rightarrow \lambda_{2,j}$, $\lambda_{1,j} \rightarrow \lambda'_{2,j}$, $\lambda'_{1,j} \rightarrow \lambda''_{2,j}$, $\lambda''_{1,j} \rightarrow \lambda'''_{2,j}$ for $j = 1, \dots, l$. With the help of these algebraic solutions we eliminate $\lambda'_1(\tilde{\rho})$, $\lambda''_1(\tilde{\rho})$, $\lambda'_2(\tilde{\rho})$ and $\lambda''_2(\tilde{\rho})$ in the flow equations (4.41) - (4.44) for all l points $\tilde{\rho}_i$.²⁵ Therefore, equations (4.41) - (4.44) are turned into a closed system of $4l$ ordinary differential equations for the unknowns $\epsilon(\tilde{\rho}_i)$, $\lambda_1(\tilde{\rho}_i)$, $\lambda_2(\tilde{\rho}_i)$ and $\lambda'_2(\tilde{\rho}_i)$.

²⁵The algebraic solutions $\lambda'_{1,i}$ and $\lambda''_{1,i}$ (equivalently $\lambda''_{2,i}$ and $\lambda'''_{2,i}$) do incorporate information from the whole range of points $\tilde{\rho}_j$ with $j = 1, \dots, l$. It is a feature of the matching conditions (4.47), (4.48) that the contributions from points $\tilde{\rho}_{j \neq i}$ to $\lambda'_{1,i}$, $\lambda''_{1,i}$ rapidly decrease with increasing $|i-j|$. For equal spacings between neighboring expansion points contributions from points $\tilde{\rho}_j$ with $j > i+1$ ($j < i-1$) are typically suppressed by a factor $\lesssim 10^{-|i-j|+1}$ as compared to the contribution from the nearest neighbor point $\tilde{\rho}_{i+1}$ ($\tilde{\rho}_{i-1}$). As a consequence solutions $\lambda'_{1,i}$, $\lambda''_{1,i}$ for inner points with $1 \ll i \ll l$ become independent from boundary points. We observe approximate translational invariance for inner point solutions, i.e. $\lambda'_{1,i \pm n}$ and $\lambda''_{1,i \pm n}$ are approximately obtained from the solutions $\lambda'_{1,i}$ and $\lambda''_{1,i}$ with the substitutions $\epsilon_j \rightarrow \epsilon_{j \pm n}$, $\lambda_{1,j} \rightarrow \lambda_{1,j \pm n}$ for $1 \leq j \leq l$ if i and $i \pm n$ are sufficiently far away from the boundaries. The decoupling from distant points and the translational invariance for inner points can be used to obtain approximate

If there is a minimum of the potential at nonvanishing $\kappa \equiv \tilde{\rho}_0$ we use expansion points that are proportional to the minimum, i.e. $\tilde{\rho}_i = \frac{i-1}{n}\kappa$ with $i = 1, \dots, l$ and fixed integer n . The condition $\epsilon(\kappa) = 0$ can be used to obtain the scale dependence of $\kappa(k)$:

$$\begin{aligned} \frac{d\kappa}{dt} &= -[\lambda_1(\kappa)]^{-1} \frac{\partial \epsilon}{\partial t} \Big|_{\tilde{\rho}=\kappa} \\ &= -(d-2+\eta)\kappa + 6v_d \left(1 + \frac{\lambda_2(\kappa) + \kappa \lambda_2'(\kappa)}{\lambda_1(\kappa)} \right) l_1^d(\kappa \lambda_2(\kappa); \eta) \\ &\quad + 2v_d \left(3 + \frac{2\kappa \lambda_1'(\kappa)}{\lambda_1(\kappa)} \right) l_1^d(2\kappa \lambda_1(\kappa); \eta) + 8v_d l_1^d(0; \eta). \end{aligned} \quad (4.49)$$

To make contact with β -functions for the couplings at the potential minimum κ we point out the relation

$$\frac{d\lambda_{1,2}^{(m)}(\kappa)}{dt} = \frac{\partial \lambda_{1,2}^{(m)}}{\partial t} \Big|_{\tilde{\rho}=\kappa} + \lambda_{1,2}^{(m+1)}(\kappa) \frac{d\kappa}{dt}. \quad (4.50)$$

Similar relations hold for $\epsilon(\tilde{\rho}_i)$, $\lambda_1(\tilde{\rho}_i)$ etc., e.g.

$$\begin{aligned} \frac{d\epsilon(\tilde{\rho}_i)}{dt} &= \frac{\partial \epsilon}{\partial t} \Big|_{\tilde{\rho}=\tilde{\rho}_i} + \frac{i-1}{n} \lambda_1(\tilde{\rho}_i) \frac{d\kappa}{dt}, \\ \frac{d\lambda_1(\tilde{\rho}_i)}{dt} &= \frac{\partial \lambda_1}{\partial t} \Big|_{\tilde{\rho}=\tilde{\rho}_i} + \frac{i-1}{n} \lambda_1'(\tilde{\rho}_i) \frac{d\kappa}{dt}. \end{aligned} \quad (4.51)$$

We integrate the $4l-1$ differential equations (4.41) - (4.44) for the couplings $\epsilon(\tilde{\rho}_i)$, $\lambda_1(\tilde{\rho}_i)$, $\lambda_2(\tilde{\rho}_i)$ and $\lambda_2'(\tilde{\rho}_i)$ (with $\partial/\partial t$ replaced by d/dt according to (4.51)) and the one for κ (4.49) with a fifth-order Runge-Kutta algorithm using the embedded fourth-order method for precision control. The general $\tilde{\rho}$ -dependence is recovered by patching the simultaneous expansions around different points at half distance between neighboring expansion points. The polynomial patching improves with decreasing distance which is used to check the stability of numerical results. In order to check for systematic errors the algorithm has been verified by comparison with a conventional ‘‘backward’’ finite difference method [63].

It remains to compute the anomalous dimension η defined in (4.5) which describes the scale dependence of the wave function renormalization Z_k . We consider a space dependent distortion of the constant background field configuration (4.19) of the form

$$\varphi_{ab}(x) = \varphi_a \delta_{ab} + [\delta\varphi e^{-iQx} + \delta\varphi^* e^{iQx}] \Sigma_{ab}. \quad (4.52)$$

Insertion of the above configuration into the parametrization (4.2) of Γ_k yields

$$Z_k = Z_k(\rho, \tau, Q^2 = 0) = \frac{1}{2} \frac{1}{\Sigma_{ab}^* \Sigma_{ab}} \lim_{Q^2 \rightarrow 0} \frac{\partial}{\partial Q^2} \frac{\delta \Gamma_k}{\delta(\delta\varphi \delta\varphi^*)} \Big|_{\delta\varphi=0}. \quad (4.53)$$

expressions which become useful if a large number of expansion points is considered. We use the exact algebraic solution for $l = 10$ points. For $l > 10$ we apply the approximate translational invariance to generate from $\lambda'_{1,5}$, $\lambda'_{1,6}$ additional solutions $\lambda'_{1,5+2i}$, $\lambda'_{1,6+2i}$ for $i = 1, \dots, (l-10)/2$ with l even and equivalently for $\lambda''_{1,5}$, $\lambda''_{1,6}$. With $\lambda'_{1,l-3}, \dots, \lambda'_{1,l}$ and $\lambda''_{1,l-3}, \dots, \lambda''_{1,l}$ from the calculation with 10 points one obtains the desired generalization. We have used runs with different choices of l in order to check the stability of the numerical results.

To obtain the flow equation of the wave function renormalization one expands the effective average action around a configuration of the form (4.52) and evaluates the r.h.s. of eq. (2.10). This computation has been done in ref. [46] for a ‘‘Goldstone’’ configuration with

$$\Sigma_{ab} = \delta_{a1}\delta_{b2} - \delta_{a2}\delta_{b1} \quad (4.54)$$

and $\varphi_a\delta_{ab} = \varphi\delta_{ab}$ corresponding to a symmetry breaking pattern with residual $U(2)$ symmetry. The result of ref. [46] can be easily generalized to arbitrary fixed field values of $\tilde{\rho}$ and we find

$$\eta(k) = 4\frac{v_d}{d}\tilde{\rho} \left[4(\lambda_1)^2 m_{2,2}^d(\epsilon, \epsilon + 2\tilde{\rho}\lambda_1; \eta) + (\lambda_2)^2 m_{2,2}^d(\epsilon, \epsilon + \tilde{\rho}\lambda_2; \eta) \right]. \quad (4.55)$$

The definition of the threshold function

$$m_{2,2}^d(\omega_1, \omega_2; \eta) = m_{2,2}^d(\omega_1, \omega_2) - \eta \hat{m}_{2,2}^d(\omega_1, \omega_2) \quad (4.56)$$

can be found in appendix A. For vanishing arguments the functions $m_{2,2}^d$ and $\hat{m}_{2,2}^d$ are of order unity. They are symmetric with respect to their arguments and in leading order $m_{2,2}^d(0, \omega) \sim \hat{m}_{2,2}^d(0, \omega) \sim \omega^{-2}$ for $\omega \gg 1$. According to eq. (4.4) we use $\tilde{\rho} = \kappa$ to define the uniform wave function renormalization

$$Z_k \equiv Z_k(\kappa). \quad (4.57)$$

We point out that according to our truncation of the effective average action with eq. (4.55) the anomalous dimension η is exactly zero at $\tilde{\rho} = 0$. This is an artefact of the truncation and we expect the symmetric phase to be more affected by truncation errors than the spontaneously broken phase. We typically observe small values for $\eta(k) = -d(\ln Z_k)/dt$ (of the order of a few per cent). The smallness of η is crucial for our approximation of a uniform wave function renormalization to give quantitatively reliable results for the equation of state. For the universal equation of state given in sect. 4.7 one has $\eta = 0.022$ as given by the corresponding index of the $O(8)$ symmetric ‘‘vector’’ model.

4.6 Renormalization group flow

To understand the detailed picture of the phase structure presented in section 4.3 we will consider the flow of some characteristic quantities for the effective average potential as the infrared cutoff k is lowered. We will always consider in this section the trajectories for the critical ‘‘temperature’’, i.e. $\delta\kappa_\Lambda = 0$, and we follow the flow for different values of the short distance parameters $\lambda_{1\Lambda}$ and $\lambda_{2\Lambda}$. The discussion for sufficiently small $\delta\kappa_\Lambda$ is analogous. In particular, we compare the renormalization group flow of these quantities for a weak and a strong first order phase transition. In some limiting cases their behavior can be studied analytically. For the discussion we will frequently consider the flow equations for the quartic ‘‘couplings’’ $\lambda_1(\tilde{\rho})$, $\lambda_2(\tilde{\rho})$ eqs. (4.42), (4.43) and for the minimum κ eq. (4.49).

In fig. 11, 12 we follow the flow of the dimensionless renormalized minimum κ and the radial mass term $\tilde{m}^2 = 2\kappa\lambda_1(\kappa)$ in comparison to their dimensionful counterparts $\rho_{0R} = k\kappa$ and $m_R^2 = k^2\tilde{m}^2$ in units of the momentum scale Λ . We also consider the dimensionless renormalized mass term $\tilde{m}_2^2 = \kappa\lambda_2(\kappa)$ corresponding to the curvature of the potential in the direction of the second invariant $\tilde{\tau}$. The height of the potential barrier $U_B(k) = k^3u_k(\tilde{\rho}_B)$ with $u'_k(\tilde{\rho}_B) = 0$, $0 < \tilde{\rho}_B < \kappa$, and the height of the outer minimum $U_0(k) = k^3u_k(\kappa)$ is also displayed and will be discussed in section 4.8. Fig. 11 shows these quantities as a function of $t = \ln(k/\Lambda)$ for $\lambda_{1\Lambda} = 2$, $\lambda_{2\Lambda} = 0.1$. One observes that the flow can be

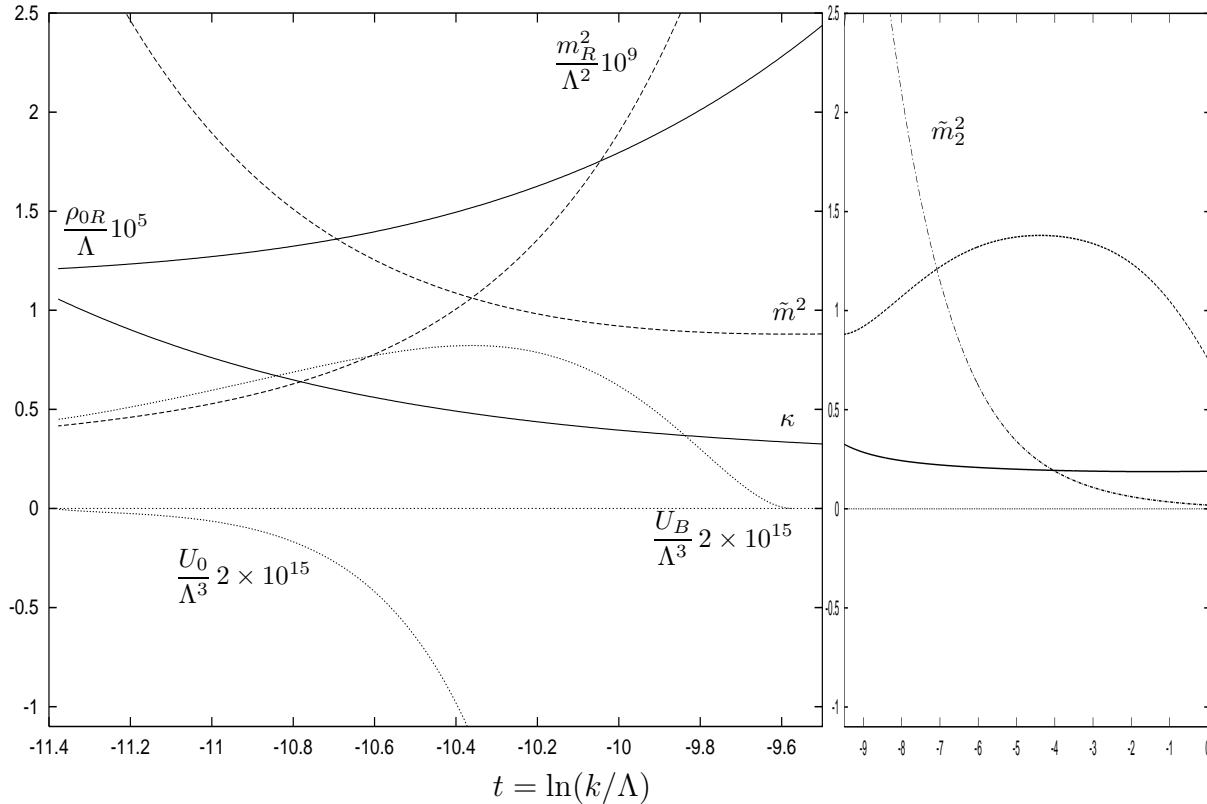


Figure 11: Scale dependence of the dimensionless renormalized masses \tilde{m}^2 , \tilde{m}_2^2 , minimum κ and dimensionful counterparts $m_R^2 = k^2\tilde{m}^2$, $\rho_{0R} = k\kappa$ in units of Λ . We also show $U_B(k)$ and $U_0(k)$, the value of the potential at the top of the potential barrier and at the minimum ρ_{0R} , respectively. The short distance parameters are $\lambda_{1\Lambda} = 2$, $\lambda_{2\Lambda} = 0.1$ and $\delta\kappa_\Lambda = 0$.

separated into two parts. The first part ranging from $t = 0$ to $t \simeq -6$ is characterized by $\kappa \simeq \text{const}$ and small \tilde{m}_2^2 . It is instructive to consider what happens in the case $\tilde{m}_2^2 \equiv 0$. In this case $\lambda_2 \equiv 0$ and the flow is governed by the Wilson-Fisher fixed point of the O(8) symmetric theory. At the corresponding second order phase transition the evolution of u_k leads to the scaling solution of (4.33) which obtains for $\partial u_k / \partial t = 0$. As a consequence u_k becomes a k -independent function that takes on constant (fixed point) values [92, 93]. In particular, the minimum κ of the potential takes on its fixed point value $\kappa(k) = \kappa_*$. The

fixed point is not attractive in the $U(2) \times U(2)$ symmetric theory and $\lambda_{2\Lambda}$ is an additional relevant parameter for the system. For small λ_2 the evolution is governed by an anomalous dimension $d\lambda_2/dt = A\lambda_2$ with $A < 0$, leading to the increasing \tilde{m}_2^2 as k is lowered.

The system exhibits scaling behavior only for sufficiently small λ_2 . As \tilde{m}_2^2 increases the quartic coupling λ_1 and therefore the radial mass term \tilde{m}^2 is driven to smaller values as can be observed from fig. 11. For nonvanishing λ_2 the corresponding qualitative change in the flow equation (4.42) for λ_1 is the occurrence of a term $\sim \lambda_2^2$. It allows to drive λ_1 to negative values in a certain range of $\tilde{\rho} < \kappa$ and, therefore, to create a potential barrier inducing a first order phase transition. We observe from the plot that at $t \lesssim -9.5$ a second minimum arises ($U_B \neq 0$). The corresponding value of $k = \Lambda e^t = k_2$ sets a characteristic scale for the first order phase transition. Below this scale the dimensionless, renormalized quantities approximately scale according to their canonical dimension. The dimensionful quantities like ρ_{0R} or m_R^2 show only a weak scale dependence in this range. In contrast to the above example of a weak first order phase transition with characteristic renormalized masses much smaller than Λ fig. 12 shows the flow of the corresponding quantities for a strong first order phase transition. The short distance parameters employed are $\lambda_{1\Lambda} = 0.1$, $\lambda_{2\Lambda} = 2$. Here the range with $\kappa \simeq \text{const}$ is almost absent and one observes no approximate scaling behavior.

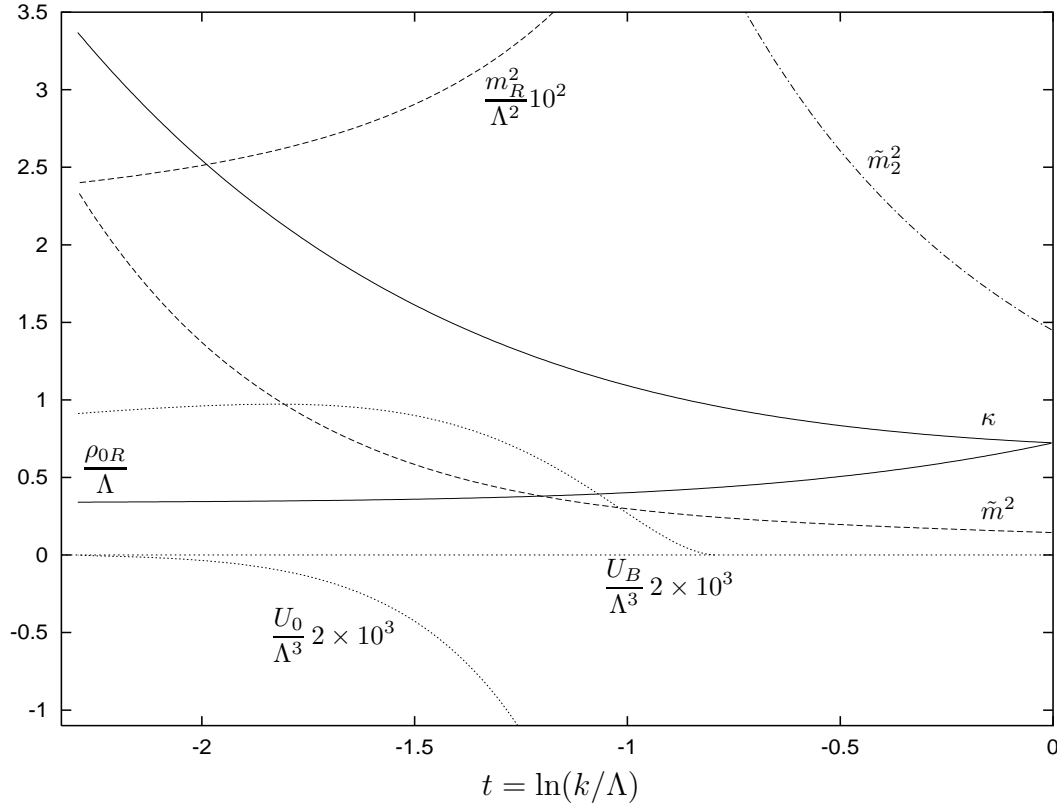


Figure 12: Same as fig. 11 for $\lambda_{1\Lambda} = 0.1$ and $\lambda_{2\Lambda} = 2$.

With the above examples it becomes easy to understand the phase structure presented in section 4.3. For the given curves of figs. 9 and 10 we distinguished between the range $\lambda_{2\Lambda}/\lambda_{1\Lambda} \ll 1$ and $\lambda_{2\Lambda}/\lambda_{1\Lambda} \gg 1$ to denote the weak and the strong first order region. For $\lambda_{2\Lambda}/\lambda_{1\Lambda} \ll 1$ the initial renormalization group flow is dominated by the Wilson-Fisher fixed point of the $O(8)$ symmetric theory. In this range the irrelevant couplings are driven close to the fixed point for some “time” $|t| = -\ln(k/\Lambda)$, losing their memory on the initial conditions given by the short distance potential u_Λ . As a consequence we are able to observe universal behavior as is demonstrated in fig. 10.

To discuss the case $\lambda_{2\Lambda}/\lambda_{1\Lambda} \gg 1$ we consider the flow equations for the couplings at the minimum $\kappa \neq 0$ of the potential given by (4.49) and (4.50) with (4.42), (4.43). In the limit of an infinite mass term $\tilde{m}_2^2 = \kappa\lambda_2(\kappa) \rightarrow \infty$ the β -functions for $\lambda_1(\kappa)$ and κ become independent from $\lambda_2(\kappa)$ due to the threshold functions, with $l_n^3(\kappa\lambda_2) \sim (\kappa\lambda_2)^{-(n+1)}$ for large $\kappa\lambda_2(\kappa)$. As a consequence β_{λ_1} and β_κ equal the β -functions for an $O(5)$ symmetric model. We argue in the following that in this large coupling limit fluctuations of massless Goldstone bosons lead to an attractive fixed point for $\lambda_2(\kappa)$. We take the flow equation (4.50), (4.43) for $\lambda_2(\kappa)$ keeping only terms with positive canonical mass dimension for a qualitative discussion. (This amounts to the approximation $\lambda_1^{(n)}(\kappa) = \lambda_2^{(n)}(\kappa) = 0$ for $n \geq 1$.) To be explicit, one may consider the case for given $\lambda_{1\Lambda} = 2$. The critical cutoff value for the potential minimum is $\kappa_\Lambda \simeq 0.2$ for $\lambda_{2\Lambda} \gg 1$. For $\kappa\lambda_2(\kappa) \gg 1$ and taking $\eta \simeq 0$ the β -function for $\lambda_2(\kappa)$ is to a good approximation given by ($d = 3$)

$$\frac{d\lambda_2(\kappa)}{dt} = -\lambda_2(\kappa) + 2v_3(\lambda_2(\kappa))^2 l_2^3(0). \quad (4.58)$$

The second term on the r.h.s. of eq. (4.58) is due to massless Goldstone modes which give the dominant contribution in the considered range. The solution of (4.58) implies an attractive fixed point for $\lambda_2(\kappa)$ with a value

$$\lambda_{2*}(\kappa) = \frac{1}{2v_3 l_2^3(0)} \simeq 4\pi^2. \quad (4.59)$$

Starting from $\lambda_{2\Lambda}$ one finds for the “time” $|t|$ necessary to reach a given $\lambda_2(\kappa) > \lambda_{2*}(\kappa)$

$$|t| = -\ln \frac{\lambda_2(\kappa) - \lambda_{2*}(\kappa)}{\lambda_2(\kappa) \left(1 - \frac{\lambda_{2*}(\kappa)}{\lambda_{2\Lambda}}\right)}. \quad (4.60)$$

This converges to a finite value for $\lambda_{2\Lambda} \rightarrow \infty$. The further evolution therefore becomes insensitive to the initial value for $\lambda_{2\Lambda}$ in the large coupling limit. The flow of $\lambda_1(\kappa)$ and κ is not affected by the initial running of $\lambda_2(\kappa)$ and quantities like $\Delta\rho_{0R}/\Lambda$ or $m_R/\Delta\rho_{0R}$ become independent of $\lambda_{2\Lambda}$ if the coupling is sufficiently large. This qualitative discussion is confirmed by the numerical solution of the full set of equations presented in figs. 9 and 10. For the fixed point value we obtain $\lambda_{2*}(\kappa) = 38.02$. We point out that an analogous discussion for the large coupling region of $\lambda_{1\Lambda}$ cannot be made. This can be seen by considering the mass term at the origin of the short distance potential (4.6) given by

$u'_\Lambda(0,0) = -\kappa_\Lambda \lambda_{1\Lambda}$. Due to the pole of $l_n^3(\omega, \eta)$ at $\omega = -1$ for $n > 1/2$ (cf. appendix C) one obtains the constraint

$$\kappa_\Lambda \lambda_{1\Lambda} < 1 \quad . \quad (4.61)$$

In the limit $\lambda_{1\Lambda} \rightarrow \infty$ the mass term $2\kappa_\Lambda \lambda_{1\Lambda}$ at the minimum κ of the potential at the critical temperature therefore remains finite.

4.7 Universal equation of state for weak first order phase transitions

We presented in section 4.3 some characteristic quantities for the effective average potential which become universal at the phase transition for a sufficiently small quartic coupling $\lambda_{2\Lambda} = \bar{\lambda}_{2\Lambda}/\Lambda$ of the short distance potential U_Λ (4.6). The aim of this section is to generalize this observation and to find a universal scaling form of the equation of state for weak first order phase transitions. The equation of state relates the derivative of the free energy $U = \lim_{k \rightarrow 0} U_k$ to an external source, $\partial U / \partial \varphi = j$. Here the derivative has to be evaluated in the outer convex region of the potential. For instance, for the meson model of strong interactions the source j is proportional to the average quark mass [31, 6] and the equation of state permits to study the quark mass dependence of properties of the chiral phase transition. We will compute the equation of state for a nonzero coarse graining scale k . It therefore contains information for quantities like the ‘‘classical’’ bubble surface tension in the context of Langer’s theory of bubble formation which will be discussed in section 4.8.

In three dimensions the $U(2) \times U(2)$ symmetric model exhibits a second order phase transition in the limit of a vanishing quartic coupling $\lambda_{2\Lambda}$ due to an enhanced $O(8)$ symmetry. In this case there is no scale present in the theory at the critical temperature. In the vicinity of the critical temperature (small $|\delta\kappa_\Lambda| \sim |T_c - T|$) and for small enough $\lambda_{2\Lambda}$ one therefore expects a scaling behavior of the effective average potential U_k and accordingly a universal scaling form of the equation of state. At the second order phase transition in the $O(8)$ symmetric model there are only two independent scales that can be related to the deviation from the critical temperature and to the external source or φ . As a consequence the properly rescaled potential U/ρ_R^3 or $U/\rho^{(\delta+1)/2}$ (with the usual critical exponent δ) can only depend on one dimensionless ratio. A possible set of variables to represent the two independent scales are the renormalized minimum of the potential $\varphi_{0R} = (\rho_{0R}/2)^{1/2}$ (or the renormalized mass for the symmetric phase) and the renormalized field $\varphi_R = (\rho_R/2)^{1/2}$. The rescaled potential will then only depend on the scaling variable $z = \varphi_R/\varphi_{0R}$ [62]. Another possible choice is the Widom scaling variable $x = -\delta\kappa_\Lambda/\varphi^{1/\beta}$ [88]. In the $U(2) \times U(2)$ symmetric theory $\lambda_{2\Lambda}$ is an additional relevant parameter which renders the phase transition first order and introduces a new scale, e.g. the nonvanishing value for the jump in the renormalized order parameter $\Delta\varphi_{0R} = (\Delta\rho_{0R}/2)^{1/2}$ at the critical temperature or $\delta\kappa_\Lambda = 0$. In the universal range we therefore observe three independent scales and the scaling form of the equation of state will depend on two dimensionless ratios. The rescaled potential

U/φ_{0R}^6 can then be written as a universal function G

$$\frac{U}{\varphi_{0R}^6} = G(z, v) \quad (4.62)$$

which depends on the two scaling variables

$$z = \frac{\varphi_R}{\varphi_{0R}}, \quad v = \frac{\Delta\varphi_{0R}}{\varphi_{0R}}. \quad (4.63)$$

The relation (4.62) is the scaling form of the equation of state we are looking for. At a second order phase transition the variable v vanishes identically and $G(z, 0)$ describes the scaling equation of state for the model with $O(8)$ symmetry [62]. The variable v accounts for the additional scale present at the first order phase transition. We note that $z = 1$ corresponds to a vanishing source and $G(1, v)$ describes the temperature dependence of the free energy for $j = 0$. In this case $v = 1$ denotes the critical temperature T_c whereas for $T < T_c$ one has $v < 1$. Accordingly $v > 1$ obtains for $T > T_c$ and φ_{0R} describes here the local minimum corresponding to the metastable ordered phase. The function $G(z, 1)$ accounts for the dependence of the free energy on j for $T = T_c$.

We consider the scaling form (4.62) of the equation of state for a nonzero coarse graining scale k . The renormalized field is given by $\varphi_R = Z_k^{1/2}\varphi$. We pointed out in section 4.3 that there is a characteristic scale k_2 for the first order phase transition where the second local minimum of the effective average potential appears. For weak first order phase transitions one finds $\rho_{0R} \sim k_2$. To observe the scaling form of the equation of state the infrared cutoff k has to run below k_2 with $k \ll k_2$. For the scale k_f defined in eq. (4.18) we observe universal behavior to high accuracy (cf. fig. 10 and the corresponding universal ratios in table 4 for small $\lambda_{2\Lambda}/\lambda_{1\Lambda}$). The result for the universal function $U_{k_f}/\varphi_{0R}^6 = G_{k_f}(z, v)$ is presented in fig. 13. For $v = 1$ one has $\varphi_{0R}(k_f) = \Delta\varphi_{0R}(k_f)$ which denotes the critical temperature. Accordingly $v > 1$ denotes temperatures above and $v < 1$ temperatures below the critical temperature. One observes that $G_{k_f}(z, 1)$ shows two almost degenerate minima. (They become exactly degenerate in the limit $k \rightarrow 0$). For the given examples $v = 1.18, 1.07$ the minimum at the origin becomes the absolute minimum and the system is in the symmetric phase. In contrast, for $v = 0.90, 0.74$ the absolute minimum is located at $z = 1$ which characterizes the spontaneously broken phase. For small enough v the local minimum at the origin vanishes.

We explicitly verified that the universal function G_{k_f} depends only on the scaling variables z and v by choosing various values for $\delta\kappa_\Lambda$ and for the quartic couplings of the short distance potential, $\lambda_{1\Lambda}$ and $\lambda_{2\Lambda}$. In section 4.3 we observed that the model shows universal behavior for a certain range of the parameter space. For given $\lambda_{1\Lambda}$ and small enough $\lambda_{2\Lambda}$ one always observes universal behavior. For $\lambda_{1\Lambda} = 0.1, 2$ and 4 it is demonstrated that (approximate) universality holds for $\lambda_{2\Lambda}/\lambda_{1\Lambda} \lesssim 1/2$ (cf. fig. 10). For $\lambda_{1\Lambda}$ around 2 one observes from figs. 9, 10 and table 4 that the system is to a good accuracy described by its universal properties for even larger values of $\lambda_{2\Lambda}$. The corresponding phase transitions cannot be considered as particularly weak first order. The universal function G_{k_f} therefore accounts for a quite large range of the parameter space.

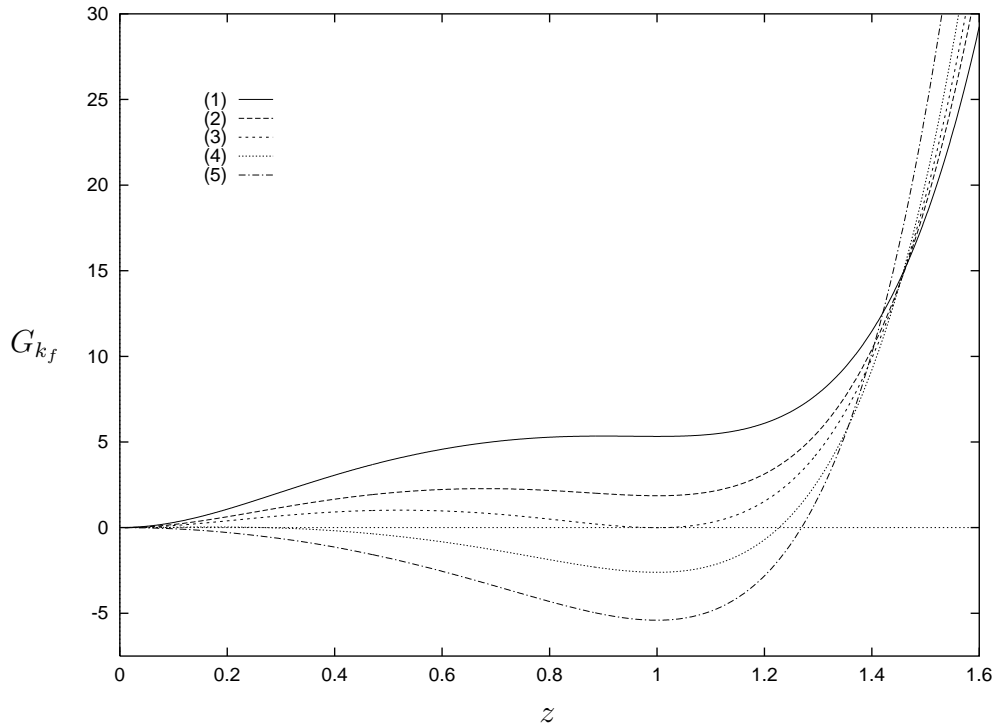


Figure 13: Universal shape of the coarse grained potential ($k = k_f$) as a function of the scaling variable $z = \varphi_R/\varphi_{0R} = (\rho_R/\rho_{0R})^{1/2}$ for different values of $v = \Delta\varphi_{0R}/\varphi_{0R} = (\Delta\rho_{0R}/\rho_{0R})^{1/2}$. The employed values for v are (1) $v = 1.18$, (2) $v = 1.07$, (3) $v = 1$, (4) $v = 0.90$, (5) $v = 0.74$. For vanishing sources one has $z = 1$. In this case $v = 1$ denotes the critical temperature T_c . Similarly $v > 1$ corresponds to $T > T_c$ with φ_{0R} denoting the minimum in the metastable ordered phase.

We emphasize that the universal form of the effective potential given in fig. 13 depends on the scale k_f where the integration of the flow equations is stopped (cf. eq. (4.18)). A different prescription for k_f will, in general, lead to a different form of the effective potential. We may interpret this as a scheme dependence describing the effect of different coarse graining procedures. This is fundamentally different from nonuniversal corrections since G_{k_f} is completely independent of details of the short distance or classical action and in this sense universal. A more quantitative discussion of this scheme dependence will be presented in the next section. We note that fluctuations on scales $k < k_f$ do not influence substantially the location of the minima of the coarse grained potential and the form of $U_k(\varphi_R)$ for $\varphi_R > \varphi_{0R}$ remains almost k -independent. Here $\partial U_{k_f}/\partial\varphi = j(k_f)$ with $j(k_f) \simeq \lim_{k \rightarrow 0} j(k) = j$.²⁶

We have established the scaling equation of state using the renormalized variables φ_R , φ_{0R} and $\Delta\varphi_{0R}$. Alternatively the scaling equation of state can be presented in terms of the short distance parameters $\delta\kappa_\Lambda$, $\lambda_{2\Lambda}$ and the unrenormalized field φ . For the $O(8)$ symmetric

²⁶The role of massless Goldstone boson fluctuations for the universal form of the effective average potential in the limit $k \rightarrow 0$ has been discussed previously for the $O(8)$ symmetric model [62].

model ($\lambda_{2\Lambda} = 0$) this is known as the Widom scaling form of the equation of state [88] and in this case the relation between φ_R , φ_{0R} and φ , $\delta\kappa_\Lambda$ is solely determined by critical exponents and amplitudes [62]. For the $U(2) \times U(2)$ symmetric model the dependence of φ_R , φ_{0R} and $\Delta\varphi_{0R}$ on the parameters $\delta\kappa_\Lambda$, $\lambda_{2\Lambda}$ and the unrenormalized field φ can be expressed in terms of scaling functions. In general, only for limiting cases as $\delta\kappa_\Lambda = 0$ or $\lambda_{2\Lambda} = 0$ the relation is determined by critical exponents and amplitudes. We will consider here these limits.

We consider the renormalized minimum φ_{0R} in two limits which are denoted by $\Delta\varphi_{0R} = \varphi_{0R}(\delta\kappa_\Lambda = 0)$ and $\varphi_{0R}^0 = \varphi_{0R}(\lambda_{2\Lambda} = 0)$. The behavior of $\Delta\varphi_{0R}$ is described in terms of the exponent θ according to eq. (4.14),

$$\Delta\varphi_{0R} \sim (\lambda_{2\Lambda})^{\theta/2}, \quad \theta = 1.93. \quad (4.64)$$

The dependence of the minimum φ_{0R}^0 of the $O(8)$ symmetric potential on the temperature is characterized by the critical exponent ν ,

$$\varphi_{0R}^0 \sim (\delta\kappa_\Lambda)^{\nu/2}, \quad \nu = 0.882. \quad (4.65)$$

The exponent ν for the $O(8)$ symmetric model is determined analogously to θ as described in section 9²⁷. We can also introduce a critical exponent ζ for the jump of the unrenormalized order parameter

$$\Delta\varphi_0 \sim (\lambda_{2\Lambda})^\zeta, \quad \zeta = 0.988. \quad (4.66)$$

With

$$\varphi_0^0 \sim (\delta\kappa_\Lambda)^\beta, \quad \beta = 0.451 \quad (4.67)$$

it is related to θ and ν by the additional index relation

$$\frac{\theta}{\zeta} = \frac{\nu}{\beta} = 1.95. \quad (4.68)$$

We have verified this numerically. For the case $\delta\kappa_\Lambda = \lambda_{2\Lambda} = 0$ one obtains

$$j \sim \varphi^\delta. \quad (4.69)$$

The exponent δ is related to the anomalous dimension η via the usual index relation $\delta = (5 - \eta)/(1 + \eta)$. From the scaling solution of eq. (4.55) we obtain $\eta = 0.0224$.

With the help of the above relations one immediately verifies that for $\lambda_{2\Lambda} = 0$

$$z \sim (-x)^{-\beta}, \quad v = 0 \quad (4.70)$$

and for $\delta\kappa_\Lambda = 0$

$$z \sim y^{-\zeta}, \quad v = 1. \quad (4.71)$$

Here we have used the Widom scaling variable x and the new scaling variable y given by

$$x = \frac{-\delta\kappa_\Lambda}{\varphi^{1/\beta}}, \quad y = \frac{\lambda_{2\Lambda}}{\varphi^{1/\zeta}}. \quad (4.72)$$

²⁷For the $O(8)$ symmetric model ($\lambda_{2\Lambda} = 0$) we consider the minimum φ_{0R}^0 at $k = 0$.

4.8 Coarse graining and Langer's theory of bubble nucleation

The coarse grained effective potential U_k results from the integration of fluctuations with momenta larger than $\sim k$. It is a nonconvex function whereas the standard effective potential $U = \lim_{k \rightarrow 0} U_k$ has to be convex by its definition as a Legendre transform (cf. section 2.2). The difference between U and U_k is due to fluctuations with characteristic length scales larger than the inverse coarse graining scale $\sim k^{-1}$. The role of these fluctuations for the approach to convexity has been established explicitly [106, 68, 69]. The study of first order phase transitions usually relies on the nonconvex “part” of the potential. As an illustration we consider the change of the system from the high temperature to the low temperature phase by bubble nucleation as described by Langer's theory [71]. On the one hand, the approach relies on the definition of a suitable coarse grained free energy Γ_k with a coarse graining scale k and, on the other hand, a saddle point approximation for the treatment of fluctuations around the “critical bubble” is employed. The problem is therefore separated into two parts: One part concerns the treatment of fluctuations with momenta $q^2 \gtrsim k^2$ which are included in the coarse grained free energy. The second part deals with an estimate of fluctuations around the bubble for which only fluctuations with momenta smaller than k must be considered. These issues will be discussed in this section in a quantitative way. In particular, we will give a criterion for the validity of Langer's formula.

One may consider a system that starts at some high temperature $T > T_c$ and investigate what happens as T is lowered as a function of time as for example during the evolution of the early universe [10]. For large enough temperature the origin of the potential ($\varphi = 0$) is the only minimum and the system is therefore originally in the symmetric phase. As T approaches T_c a second local minimum develops at $\varphi_0 > 0$. This becomes the absolute minimum below T_c . Nevertheless, the potential barrier prevents the system to change smoothly to the ordered phase. For a short while where T is in the vicinity of T_c but below T_c the system remains therefore in a state with higher energy density as compared to the state corresponding to the absolute minimum away from the origin. This is the so-called “false vacuum” in high energy physics or the metastable state in statistical physics. Such a state is unstable with respect to fluctuations which penetrate or cross the barrier. The picture is familiar from the condensation of vapor. The false vacuum corresponds to the supercooled vapor phase and the true vacuum to the fluid phase. Bubbles of the true vacuum (droplets) occur through thermal or quantum fluctuations²⁸. If a bubble is large enough so that the decrease in volume energy exceeds the surface energy it will grow. The phase transition is completed once the whole space is filled with the true vacuum. On the other hand, small bubbles shrink due to the surface tension. The critical bubble is just large enough that it does not shrink. To be explicit we consider a spherical bubble where the bubble wall with “thickness” Δ is thin as compared to the bubble radius R , i.e. $\Delta \ll R$. In leading order the coarse grained free energy Γ_k for such a bubble configuration

²⁸In the real world the condensation of vapor is triggered by impurities but this is not the issue here.

can be decomposed in a volume and a surface term [72, 73]

$$\Gamma_k^{(0)} = -\frac{4\pi}{3}R^3\epsilon + 4\pi R^2\sigma_k. \quad (4.73)$$

In the thin wall approximation one obtains for the surface tension σ_k in our conventions

$$\sigma_k = 2 \int_0^{\varphi_0} d\varphi \sqrt{2Z_k U_k(\varphi)}. \quad (4.74)$$

For the difference in the free energy density ϵ one has

$$\epsilon = U(0) - U(\varphi_0) = -\lim_{k \rightarrow 0} U_0(k). \quad (4.75)$$

We include in ϵ fluctuations with arbitrarily small momenta. In contrast, the long wavelength contributions to the true surface tension²⁹ are effectively cut off by the characteristic length scale of the bubble surface. We include for the computation of the “classical” surface tension σ_k only fluctuations with $q^2 \gtrsim k^2$. The modes with $q^2 \lesssim k^2$ contribute to the “fluctuation determinant” A_k (cf. eq. (4.76)). The determination of a suitable coarse graining scale k for the computation of σ_k is discussed below.

The critical bubble maximizes $\Gamma_k^{(0)}$ with respect to the radius. It minimizes the coarse grained free energy with respect to other deformations because the spherical form is energetically favorable. The critical bubble therefore represents a saddle point in the space of possible “bubble configurations”. In Langer’s theory of bubble formation one considers a saddle point expansion around the critical bubble. There is exactly one negative mode that corresponds to the shrinking or growth of the bubble and there are infinitely many positive modes (there are also translational zero modes)³⁰. The bubble nucleation rate $\bar{\Gamma}$, which describes the probability per unit volume per unit time for the transition to the new vacuum, can be written in the form [72, 73, 71]

$$\bar{\Gamma} = A_k \exp(-\Gamma_k^{(0)}[\varphi_b^{(0)}]) = A_k \exp\left(-\frac{16\pi}{3} \frac{\sigma_k^3}{\epsilon^2}\right) \quad (4.76)$$

where $\Gamma_k^{(0)}$ is evaluated for $\varphi_b^{(0)}$ corresponding to the critical bubble and approximated by (4.73). The exponential term with the coarse grained free energy $\Gamma_k^{(0)}$ denotes the lowest order or classical contribution. The prefactor A_k contains several factors that depend on the details of the system under investigation. In particular, A_k accounts for the contribution to the free energy from the fluctuations with momenta smaller than k . It depends on k through the effective ultraviolet cutoff for these fluctuations which is present since fluctuations with

²⁹The true surface tension is a “measurable quantity”. It is independent of k and all fluctuations must be included. It therefore differs, in general, from σ_k which includes only part of the fluctuations.

³⁰Langer’s theory is not restricted to the thin wall approximation which is considered here for simplicity. In particular, the property of the critical bubble to represent a saddle point with exactly one negative mode is independent from the thin wall approximation.

momenta larger than k are already included in $\Gamma_k^{(0)}[\varphi_b^{(0)}]$ ³¹. Langer's formula for bubble nucleation amounts essentially to a perturbative one loop estimate of A_k .

For a determination of a useful choice of k it is convenient to place the discussion in a more general context which does not rely on the thin wall approximation or a saddle point approximation. What one is finally interested in is the free energy $\Gamma[\varphi_b]$ for bubble configurations of a given shape. The "true critical bubble" φ_b^c corresponds to a saddle point in the space of "bubble configurations" which are characterized by boundary conditions connecting the false and the true vacuum. The nucleation rate is then proportional $\exp -\Gamma[\varphi_b^c]$. The coarse graining can be seen as a convenient strategy to evaluate $\Gamma[\varphi_b]$ by separating contributions from different momentum scales. We propose to choose the coarse graining scale k somewhat above but in the vicinity of the inverse thickness Δ^{-1} of the bubble wall. We will argue below that in this case the corrections to the effective surface tension from the prefactor A_k should be best accessible.

In fact, we can write $\bar{\Gamma} = B \exp -\Gamma[\varphi_b^c]$ where B contains dynamical factors and $\Gamma[\varphi_b^c]$ does not include contributions from fluctuations of the negative mode and the translational modes present for the critical bubble. The prefactor in eq. (4.76) can then be written as

$$A_k = B \exp -(\delta_k + \eta_k) \quad (4.77)$$

where

$$\delta_k = \Gamma[\varphi_b^c] - \Gamma_k[\varphi_b^c], \quad \eta_k = \Gamma_k[\varphi_b^c] - \frac{16\pi}{3} \frac{\sigma_k^3}{\epsilon^2}. \quad (4.78)$$

The term η_k includes the difference between the true critical bubble and the configuration used to estimate σ_k as well as a correction term to ϵ to be discussed below. We first concentrate on δ_k which describes the difference between the free energy and the coarse grained free energy for the critical bubble. As mentioned above this is due to fluctuations with momenta $q^2 \lesssim k^2$ and incorporates the dominant k -dependence of A_k . Since the bubble provides for inherent effective infrared cutoff scales $\sim R^{-1}$ or Δ^{-1} the contribution δ_k is both infrared and ultraviolet finite. The larger k , the more fluctuations are included in δ_k and from this point of view one wants to take k as low as possible. On the other hand, k should not be taken smaller than Δ^{-1} if the approximation used for a computation of Γ_k relies on almost constant field configurations rather than real bubbles, as is usually the case. Only for k sufficiently large compared to Δ^{-1} the difference between an evaluation of the potential and kinetic terms in Γ_k for almost constant field configurations (e.g. by a derivative expansion) rather than for bubbles remains small. In this way the technique of course graining combines a relatively simple treatment of the modes with $q^2 \gtrsim k^2$ for which the detailed properties of the bubble are irrelevant with an estimate of fluctuations around the bubble for which the short distance physics ($q^2 \gtrsim k^2$) needs not to be considered anymore. It is clear that k is only a technical construct and for physical quantities the k -dependence of δ_k and $\Gamma_k^{(0)}$ must cancel. More precisely, this concerns the sum $\delta_k + \eta_k + 16\pi\sigma_k^3/3\epsilon^2$. For thin wall bubbles the most important contribution to η_k is easily identified:

³¹The effective average action [37] also provides the formal tool how the ultraviolet cutoff $\sim k$ is implemented in the remaining functional integral for large length scale fluctuations.

By our definition of ϵ we have included contributions from fluctuations with length scales $\gtrsim R$. They should not be present in the effective action for a bubble with finite radius. Therefore η_k contains a correction term $(16\pi/3)\sigma_k^3(\epsilon^{-2}(R) - \epsilon^{-2})$ which replaces effectively ϵ by $\epsilon(R)$ in eq. (4.76). We can evaluate $\epsilon(R)$ in terms of the coarse grained free energy at a scale k_R

$$\epsilon(R) \simeq U_{k_R}(0) - U_{k_R}(\varphi_0) = -U_0(k_R), \quad k_R = \frac{1}{R}. \quad (4.79)$$

For $\Delta \ll R$ one should not confound k_R with the coarse graining scale k since one has the inequality

$$k_R \ll \frac{1}{\Delta} \lesssim k. \quad (4.80)$$

Only for $\Delta \simeq R$ the clear separation between k_R and k disappears. We note that at the critical temperature one has $R \rightarrow \infty$ and therefore $\epsilon(R) = \epsilon$.

Since σ_k enters the nucleation rate (4.76) exponentially even small changes with k will have large effects. If one finds a strong dependence of σ_k on the coarse graining scale k this is only compatible with a large contribution from the higher orders of the saddle point expansion. The k -dependence of σ_k therefore gives direct information about the validity of Langer's formula. We find a strong scale dependence of σ_k if the phase transition is characterized by large effective dimensionless couplings. A weak scale dependence is observed for small effective couplings. This gives a very consistent picture: The validity of the saddle point approximation typically requires small dimensionless couplings. In this case also the details of the coarse graining are not of crucial importance within an appropriate range of k . The remaining part of this section provides a detailed quantitative discussion.

We consider the dependence of the effective average potential U_k and the surface tension σ_k on the coarse graining scale k near the critical temperature T_c for three examples in detail. They are distinguished by different choices for the quartic couplings $\bar{\lambda}_{1\Lambda}$ and $\bar{\lambda}_{2\Lambda}$ of the short distance potential U_Λ given by eq. (4.6). The choice $\bar{\lambda}_{1\Lambda}/\Lambda = 0.1$ and $\bar{\lambda}_{2\Lambda}/\Lambda = 2$ corresponds to a strong first order phase transition with renormalized masses not much smaller than the cutoff scale Λ . The renormalized couplings will turn out small enough such that the notion of a coarse grained potential U_k and a surface tension σ_k can be used without detailed information on the coarse graining scale within a certain range of k . In contrast we give two examples where the dependence of U_k and σ_k on the coarse graining scale becomes of crucial importance. The choice $\bar{\lambda}_{1\Lambda}/\Lambda = 2$ and $\bar{\lambda}_{2\Lambda}/\Lambda = 0.1$ leads to a weak first order phase transition with small renormalized masses and the system shows universal behavior (cf. sect. 4.3). For $\bar{\lambda}_{1\Lambda}/\Lambda = 4$ and $\bar{\lambda}_{2\Lambda}/\Lambda = 70$ one observes a relatively strong first order phase transition. Nevertheless for both examples the coarse grained potential and the surface tension show a similarly high sensitivity on the scale k .

In figs. 14, 15 the scale dependence of U_k is shown for a fixed temperature in the vicinity of $T = T_c$ or $\delta\kappa_\Lambda = 0$. We plot U_k in units of Λ^3 as a function of $\varphi_R/\Lambda^{1/2} = (\rho_R/2\Lambda)^{1/2} = (Z_k\rho/2\Lambda)^{1/2}$ for different values of k . Each curve differs in $k = \Lambda e^t$ by $\Delta t = 1/18$ and the first curve to the left with a negative curvature at the origin corresponds to $t \simeq -0.40$ for fig. 14 ($t \simeq -9.3$ for fig. 15). For $0 \geq t \gtrsim -0.40$ ($0 \geq t \gtrsim -9.3$) there is only

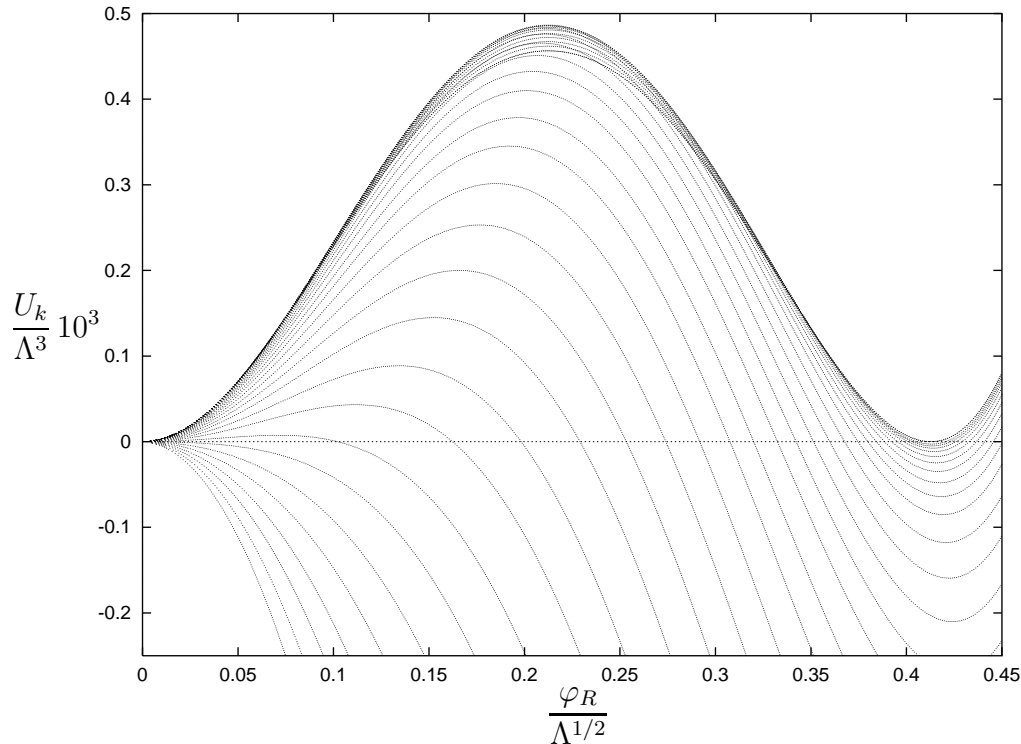


Figure 14: The coarse grained potential in dependence on the coarse graining scale k for fixed (almost critical) temperature. The example corresponds to $\bar{\lambda}_{1\Lambda}/\Lambda = 0.1$, $\bar{\lambda}_{2\Lambda}/\Lambda = 2$.

one minimum of the potential away from the origin which lies below the plotted range in fig. 14 (15). Lowering k results in a successive inclusion of fluctuations on larger length scales and one observes the appearance of a second local minimum at the origin of the potential. The barrier between both minima increases and reaches its maximum value. As k is lowered further the potential barrier starts to decrease whereas the location of the minima becomes almost k -independent and degenerate in height. In this region also the outer convex part of the potential shows an almost stable profile due to the decoupling of the massive modes. We stop the integration at the scale $k = k_f$ given by eq. (4.18). The coarse grained effective potential U_k with $k = k_f$ essentially includes all fluctuations with squared momenta larger than the scale $|m_{B,R}^2|$ given by the curvature at the top of the potential barrier (cf. eq. (4.17)). Successive inclusion of fluctuations with momenta smaller than k_f would result in a further decrease of the potential barrier. The flattening of the barrier is induced by the pole structure of the threshold functions $l_n^3(\omega)$ appearing in the flow equations for the couplings (e.g. $l_1^3(\omega)$ appearing in eq. (4.42) exhibits a pole at $\omega = -1$ according to $l_1^3(\omega) \sim (\omega + 1)^{-1/2}$ for ω near -1 (cf. appendix C)). The argument ω corresponds to dimensionless mass terms as $U_k'(\rho_R)/k^2$ or $(U_k'(\rho_R) + 2\rho_R U_k''(\rho_R))/k^2$. In the nonconvex region of the potential the curvature is negative. Since the pole cannot be crossed, negative U_k' or U_k'' must go to zero with k^2 and as a consequence the potential barrier flattens. For the scalar “vector” model the approach to convexity in the limit $k \rightarrow 0$

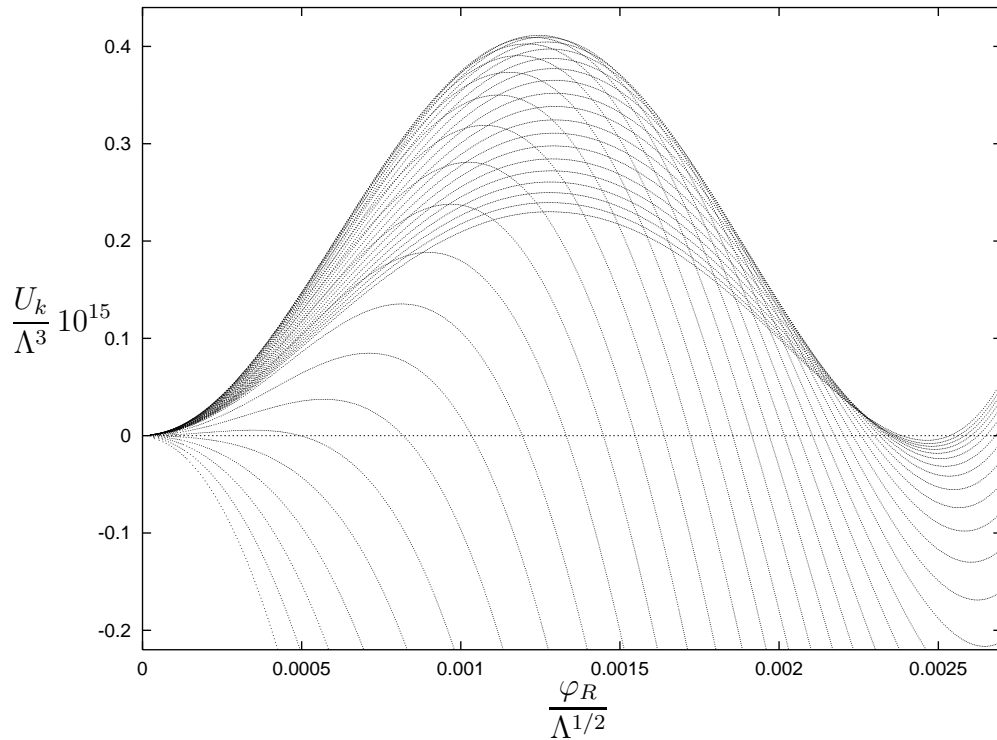


Figure 15: The coarse grained potential for $\bar{\lambda}_{1\Lambda}/\Lambda = 2, \bar{\lambda}_{2\Lambda}/\Lambda = 0.1$.

has been studied analytically previously [106]. Here we are interested in the potential for a nonzero coarse graining scale k .

The most significant difference between fig. 14 and fig. 15 is the k -dependence of the potential barrier in a region where the minima become degenerate and almost independent of k . Fig. 14 shows a barrier with a weak scale dependence in the range of k where the location of the minima stabilizes. In contrast, in fig. 15 one observes a barrier with a strong scale dependence in this region. Figs. 11 and 12 (cf. sect. 4.6) show the relative height $U_0(k) = U_k(\varphi_0) - U_k(0)$ between the two local minima and the height of the potential barrier $U_B(k) = U_k(\varphi_B) - U_k(0)$ ($(\partial U_k / \partial \varphi)(\varphi_B) = 0, 0 < \varphi_B < \varphi_0$) as a function of $t = \ln(k/\Lambda)$. Accordingly one observes that for $\bar{\lambda}_{1\Lambda}/\Lambda = 0.1, \bar{\lambda}_{2\Lambda}/\Lambda = 2$ the top of the potential barrier shows a weak scale dependence in a region of k where $U_0(k)$ is small whereas for $\bar{\lambda}_{1\Lambda}/\Lambda = 2, \bar{\lambda}_{2\Lambda}/\Lambda = 0.1$ the top of the potential barrier depends strongly on the coarse graining scale in this region. The surface tension σ_k is displayed in fig. 16 and shows a corresponding behavior. Here we consider σ_k also for the short distance parameters $\bar{\lambda}_{1\Lambda}/\Lambda = 4, \bar{\lambda}_{2\Lambda}/\Lambda = 70$. In fig. 16 the surface tension σ_k is normalized to σ_{\max} ($\sigma_{\max}/\Lambda^2 = 1.67 \times 10^{-2}(8.41 \times 10^{-11})(1.01 \times 10^{-3})$ for $\bar{\lambda}_{1\Lambda}/\Lambda = 0.1(2)(4), \bar{\lambda}_{2\Lambda}/\Lambda = 2(0.1)(70)$) and given as a function of $\ln(k/k_f)$.³² For $\bar{\lambda}_{1\Lambda}/\Lambda = 0.1, \bar{\lambda}_{2\Lambda}/\Lambda = 2$ the curve exhibits a small

³²The integration according to eq. (4.74) is performed between the two zeros $\varphi = 0$ and $\varphi = \varphi'_0 \lesssim \varphi_0$ of U_k .

curvature around its maximum and $\sigma_{\max} \simeq \sigma_{k=k_f}$. One observes for the second and the third example a comparably large curvature around σ_{\max} and $\sigma_{k=k_f}$ becomes considerably smaller than the maximum. One may consider what happens if this scale dependence is

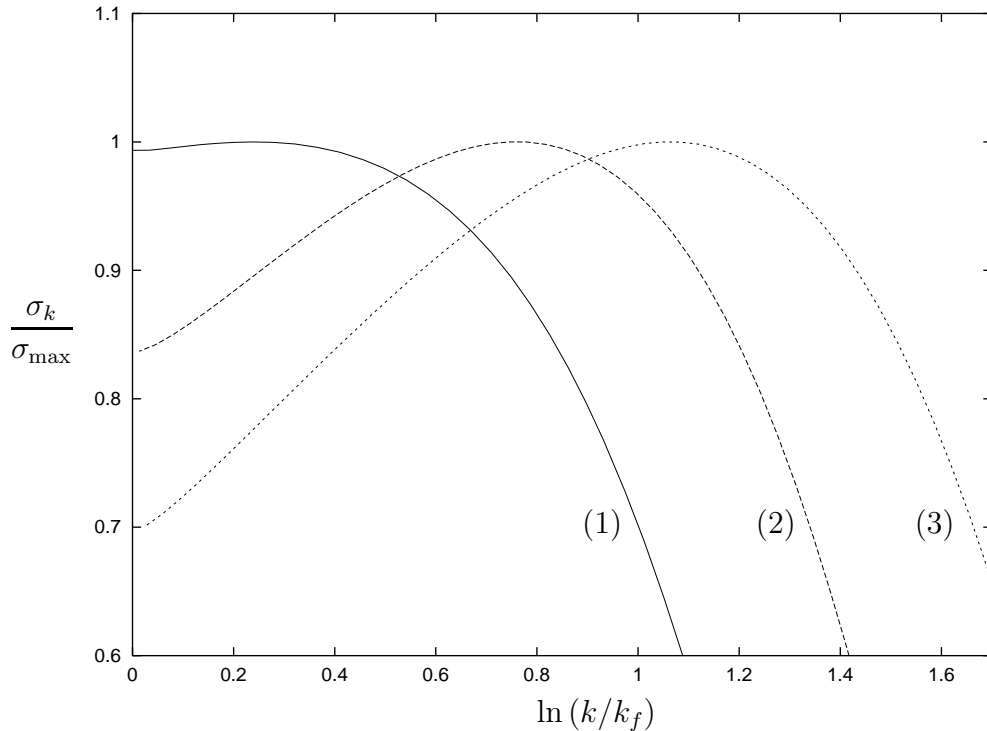


Figure 16: The normalized surface tension σ_k/σ_{\max} as a function of $\ln(k/k_f)$. The short distance parameters are (1) $\bar{\lambda}_{1\Lambda}/\Lambda = 0.1$, $\bar{\lambda}_{2\Lambda}/\Lambda = 2$, (2) $\bar{\lambda}_{1\Lambda}/\Lambda = 2$, $\bar{\lambda}_{2\Lambda}/\Lambda = 0.1$, (3) $\bar{\lambda}_{1\Lambda}/\Lambda = 4$, $\bar{\lambda}_{2\Lambda}/\Lambda = 70$.

not taken into account correctly. If one takes the difference in σ_k from its maximum value to $\sigma_{k=k_f}$ as a rough measure for its uncertainty this is about 30% for the last example. Entering exponentially in eq. (4.76) this would lead to tremendous errors.

We have pointed out above that the coarse graining scale k should not be taken smaller than the inverse bubble wall thickness Δ^{-1} . This ensures that the detailed properties of the bubble are irrelevant for the computation of the “classical” surface tension σ_k . We estimate the bubble wall thickness Δ by

$$\Delta(k) = 2Z_k \frac{\rho_0(k)}{\sigma_k} \quad (4.81)$$

where we have taken the gradient energy as half the total surface energy and approximated the mean field gradient at the bubble wall by φ_0/Δ . For the given examples we observe $\Delta^{-1}(k_f) \simeq k_f/4$. We choose $k \simeq k_f$ as the coarse graining scale.

In order to quantify the differences between the three examples we have displayed some characteristic quantities in table 5. The renormalized couplings

$$\lambda_{1R} = U''_{k_f}(\rho_{0R}), \quad \lambda_{2R} = 4\partial_\tau U_{k_f}(\rho_{0R}) \quad (4.82)$$

$\frac{\bar{\lambda}_{1\Lambda}}{\Lambda}$	$\frac{\bar{\lambda}_{2\Lambda}}{\Lambda}$	$\frac{\lambda_{1R}}{m_R^c}$	$\frac{\lambda_{2R}}{m_R^c}$	$\frac{m_R^c}{m_{2R}^c}$	$\frac{m_R^c}{\Lambda}$	$\frac{m_{2R}^c}{\Lambda}$	$\frac{k_f}{\Lambda}$
0.1	2	0.228	8.26	0.235	1.55×10^{-1}	6.62×10^{-1}	1.011×10^{-1}
2	0.1	0.845	15.0	0.335	2.04×10^{-5}	6.10×10^{-5}	1.145×10^{-5}
4	70	0.980	16.8	0.341	6.96×10^{-2}	2.04×10^{-1}	3.781×10^{-2}

Table 5: The effective dimensionless couplings λ_{1R}/m_R^c and λ_{2R}/m_R^c . The couplings and the mass terms m_R^c , m_{2R}^c are evaluated at the scale k_f and $\delta\kappa_\Lambda = 0$.

are normalized to the mass term

$$m_R^c = (2\rho_{0R}\lambda_{1R})^{1/2}. \quad (4.83)$$

In addition we give the mass term

$$m_{2R}^c = (\rho_{0R}\lambda_{2R})^{1/2} \quad (4.84)$$

corresponding to the curvature of the potential in the direction of the second invariant τ . In comparison with figs. 14–16 one observes that the smaller the effective couplings the weaker the scale dependence of U_k and σ_k . In particular, a reasonably weak scale dependence of U_k and σ_k requires

$$\frac{\lambda_{1R}}{m_R^c} = \frac{1}{2} \frac{m_R^c}{\Delta\rho_{0R}} \ll 1. \quad (4.85)$$

This establishes a quantitative criterion for the range where Langer’s theory can be used without paying too much attention to the precise definition of the coarse graining. Comparison with fig. 10 (cf. sect. 9) shows that this condition is not realized for the range of couplings leading to universal behavior and for large $\bar{\lambda}_{1\Lambda}/\Lambda$. The only region where the saddle point expansion is expected to converge reasonably well is for small $\bar{\lambda}_{1\Lambda}/\Lambda$ and large $\bar{\lambda}_{2\Lambda}/\Lambda$. The second and the third example given in fig. 16, which exhibit a strong k -dependence, show similar values for the effective couplings. More precisely, for the relatively strong phase transition with slightly larger effective couplings one observes an increased scale dependence as compared to the weak phase transition. Therefore, the strength of the transition is not the primary criterion for the convergence of the saddle point expansion. In table 5 also the renormalized masses in units of Λ which indicate the strength of the phase transition and k_f/Λ are presented.

In addition to the dependence on k , the coarse grained free energy depends also on the precise shape of the infrared cutoff function $R_k(q)$ (cf. eq. 4.24). Analytical studies in the Abelian Higgs model indicate [107] that this scheme dependence is rather weak for the effective potential and the surface tension.

In summary, we have shown that the coarse grained free energy cannot be defined without detailed information on the coarse graining scale k unless the effective dimensionless couplings are small. Only for small couplings we observe a weak k -dependence of the surface tension in a range where the location of the minima of the potential remains almost fixed. There is a close relation between the dependence of the coarse grained free energy on the coarse graining scale and the reliability of the saddle point approximation in Langer's theory of bubble nucleation. For a strong k -dependence of U_k a small variation in the coarse graining scale can induce large changes in the predicted nucleation rate in lowest order in a saddle point approximation. In this case the k -dependence of the prefactor A_k has also to be computed. For strong dimensionless couplings a realistic estimate of the nucleation rate therefore needs the capability to compute $\ln A_k$ with the same accuracy as $16\pi\sigma_k^3/3\epsilon^2$ and a check of the cancellation of the k -dependence in the combined expression (4.76). Our observation that the details of the coarse graining prescription become less important in the case of small dimensionless couplings is consistent with the fact that typically small couplings are needed for a reliable saddle point approximation for A_k . For the electroweak high temperature phase transition a small k -dependence of σ_k is found for a small mass M_H of the Higgs scalar whereas for M_H near the W-boson mass the picture resembles our fig. 15 [115]. This corresponds to the observation [116, 117, 118] that the saddle point approximation around the critical bubble converges well only for a small enough mass of the Higgs scalar.

4.9 Conclusions

We have presented in this chapter a detailed investigation of the phase transition in three dimensional models for complex 2×2 matrices. They are characterized by two quartic couplings $\bar{\lambda}_{1\Lambda}$ and $\bar{\lambda}_{2\Lambda}$. In the limit $\bar{\lambda}_{1\Lambda} \rightarrow \infty$, $\bar{\lambda}_{2\Lambda} \rightarrow \infty$ this also covers the model of unitary matrices. The picture arising from this study is unambiguous:

(1) One observes two symmetry breaking patterns for $\bar{\lambda}_{2\Lambda} > 0$ and $\bar{\lambda}_{2\Lambda} < 0$ respectively. The case $\bar{\lambda}_{2\Lambda} = 0$ denotes the boundary between the two phases with different symmetry breaking patterns. In this special case the theory exhibits an enhanced $O(8)$ symmetry. The phase transition is always first order for the investigated symmetry breaking $U(2) \times U(2) \rightarrow U(2)$ ($\bar{\lambda}_{2\Lambda} > 0$). For $\bar{\lambda}_{2\Lambda} = 0$ the $O(8)$ symmetric Heisenberg model is recovered and one finds a second order phase transition.

(2) The strength of the phase transition depends on the size of the classical quartic couplings $\bar{\lambda}_{1\Lambda}/\Lambda$ and $\bar{\lambda}_{2\Lambda}/\Lambda$. They describe the short distance or classical action at a momentum scale Λ . The strength of the transition can be parametrized by m_R^c/Λ with m_R^c a characteristic inverse correlation length at the critical temperature. For fixed $\bar{\lambda}_{2\Lambda}$ the strength of the transition decreases with increasing $\bar{\lambda}_{1\Lambda}$. This is analogous to the Coleman-Weinberg effect in four dimensions.

(3) For a wide range of classical couplings the critical behavior near the phase transition is universal. This means that it becomes largely independent of the details of the classical action once everything is expressed in terms of the relevant renormalized parameters. In particular, characteristic ratios like $m_R^c/\Delta\rho_{0R}$ (critical inverse correlation length in

the ordered phase over discontinuity in the order parameter) or $m_{0R}^c/\Delta\rho_{0R}$ (same for the disordered phase) are not influenced by the addition of new terms in the classical action as far as the symmetries are respected.

(4) The range of short distance parameters $\bar{\lambda}_{1\Lambda}$, $\bar{\lambda}_{2\Lambda}$ for which the phase transition exhibits universal behavior is not only determined by the strength of the phase transition as measured by m_R^c/Λ . For a given $\bar{\lambda}_{1\Lambda}/\Lambda$ and small enough $\bar{\lambda}_{2\Lambda}/\Lambda$ one always observes universal behavior. In the range of small $\bar{\lambda}_{1\Lambda}/\Lambda$ the essential criterion for universal behavior is given by the size of $\bar{\lambda}_{2\Lambda}/\bar{\lambda}_{1\Lambda}$, with approximate universality for $\bar{\lambda}_{2\Lambda} < \bar{\lambda}_{1\Lambda}$. For strong couplings universality extends to larger $\bar{\lambda}_{2\Lambda}/\bar{\lambda}_{1\Lambda}$ and occurs for much larger m_R^c/Λ (cf. table 4).

(5) We have investigated how various characteristic quantities like the discontinuity in the order parameter $\Delta\rho_0$ or the corresponding renormalized quantity $\Delta\rho_{0R}$ or critical correlation lengths depend on the classical parameters. In particular, at the critical temperature one finds universal critical exponents for not too large $\bar{\lambda}_{2\Lambda}$,

$$\begin{aligned}\Delta\rho_{0R} &\sim (\bar{\lambda}_{2\Lambda})^\theta, & \theta &= 1.93, \\ \Delta\rho_0 &\sim (\bar{\lambda}_{2\Lambda})^{2\zeta}, & \zeta &= 0.988.\end{aligned}\tag{4.86}$$

These exponents are related by a scaling relation to the critical correlation length and order parameter exponents ν and β of the $O(8)$ symmetric Heisenberg model according to $\theta/\zeta = \nu/\beta = 1.95$ ($\nu = 0.882$, $\beta = 0.451$ in our calculation for $\bar{\lambda}_{2\Lambda} = 0$). Small values of $\bar{\lambda}_{2\Lambda}$ can be associated with a perturbation of the $O(8)$ symmetric model and θ, ζ are related to the corresponding crossover exponents. On the other hand, $\Delta\rho_{0R}$ ($\Delta\rho_0$) becomes independent of $\bar{\lambda}_{2\Lambda}$ in the infinite coupling limit.

(6) We have computed the universal equation of state. The equation of state relates the derivative of the free energy U to an external source, $\partial U/\partial\varphi = j$. From there one can extract universal ratios e.g. for the jump in the order parameter ($\Delta\rho_{0R}/m_R^c = 0.592$) or for the ratios of critical correlation lengths in the disordered (symmetric) and ordered (spontaneously broken) phase ($m_{0R}^c/m_R^c = 0.746$). It specifies critical couplings ($\lambda_{1R}/m_R^c = 0.845$, $\lambda_{2R}/m_R^c = 15.0$). The universal behavior of the potential for large field arguments $\rho \gg \rho_0$ is $U \sim \rho^{3/(1+\eta)}$ provided ρ_R is sufficiently small as compared to Λ . Here the critical exponent η which characterizes the dependence of the potential on the unrenormalized field ρ is found to be $\eta = 0.022$. For large ρ the universal equation of state equals the one for the $O(8)$ symmetric Heisenberg model and η specifies the anomalous dimension or the critical exponent $\delta = (5 - \eta)/(1 + \eta)$. The equation of state is computed for a nonzero coarse graining scale k . It therefore contains information for quantities like the ‘‘classical’’ bubble surface tension in the context of Langer’s theory of bubble formation.

(7) We have investigated the dependence of the coarse grained effective potential $U_k(\rho)$ and the ‘‘classical’’ surface tension σ_k on the coarse graining scale k with special emphasis on the question of the validity of Langer’s theory of bubble formation. We find a strong scale dependence of U_k and σ_k if the phase transition is characterized by large dimensionless couplings. A weak scale dependence is observed for small effective couplings. There is a close relation between the dependence of the coarse grained free energy on the coarse

graining scale and the reliability of the saddle point approximation in Langer's theory of bubble nucleation. A strong k -dependence of σ_k is only compatible with a large contribution from the higher orders of the expansion. We obtain a very consistent picture: The validity of the saddle point approximation typically requires small dimensionless couplings. In this case also the details of the coarse graining are not of crucial importance within an appropriate range of k . The quantitative criterion for the validity of Langer's formula is in our case $\lambda_{1R}/m_R^c \ll 1$.

(8) Our method is not restricted to the study of the universal behavior. We can compute the effective potential for arbitrary values of the initial parameters and have done this for particular examples.

The uncertainties of our results induced by the numerical integration of the flow equations are well under control and small. They are negligible compared to the expected error induced by our truncation. For a significant improvement of our treatment one would have to include higher order terms in the derivative expansion employed for the effective average action. For weak first order or second order phase transitions we expect the error to be related to the anomalous dimension $\eta = 0.022$. For the special case of the enhanced $O(8)$ symmetry one can compare e.g. with known values for critical exponents obtained by other methods [67, 89, 90]. A comparison of our results for the critical exponents β and ν with the results of the most sophisticated calculations show agreement within a few per cent. The anomalous dimension is also well determined, even though it is most affected by our truncation.

Finally, we should mention that our approach can be extended to systems with reduced $SU(N) \times SU(N)$ symmetry. They obtain by adding to the classical potential a term involving the invariant $\xi = \det \varphi + \det \varphi^\dagger$. (Note that ξ is not invariant with respect to $U(N) \times U(N)$). This will give an even richer pattern of phase transitions and permits a close contact to realistic meson models in QCD where the axial anomaly is incorporated. Finally one can extend the three dimensional treatment to a four dimensional study of field theories at nonvanishing temperature. How this can be used to approach the chiral phase transition in QCD is presented in the next section.

5 The equation of state for two flavor QCD

5.1 Introduction

We have pointed out in section 1 that strong interactions in thermal equilibrium at high temperature T differ in important aspects from the well tested vacuum or zero temperature properties. A phase transition at some critical temperature T_c or a relatively sharp crossover may separate the high and low temperature physics [25]. Many experimental activities at heavy ion colliders [119] search for signs of such a transition. It was realized early that the transition should be closely related to a qualitative change in the chiral condensate according to the general observation that spontaneous symmetry breaking tends to be absent in a high temperature situation. A series of stimulating contributions [31, 26, 27] pointed out that for sufficiently small up and down quark masses, m_u and m_d , and for a sufficiently large mass of the strange quark, m_s , the chiral transition is expected to belong to the universality class of the $O(4)$ Heisenberg model. It was suggested [26, 27] that a large correlation length may be responsible for important fluctuations or lead to a disoriented chiral condensate [28]. The question how small m_u and m_d would have to be in order to see a large correlation length near T_c and if this scenario could be realized for realistic values of the current quark masses remained, however, unanswered. The reason was the missing link between the universal behavior near T_c and zero current quark mass on one hand and the known physical properties at $T = 0$ for realistic quark masses on the other hand.

It is the purpose of the present section to provide this link [33]. We present here the equation of state for two flavor QCD within an effective quark meson model. The equation of state expresses the chiral condensate $\langle \bar{\psi}\psi \rangle$ as a function of temperature and the average current quark mass $\hat{m} = (m_u + m_d)/2$. This connects explicitly the universal critical behavior for $T \rightarrow T_c$ and $\hat{m} \rightarrow 0$ with the temperature dependence for a realistic value \hat{m}_{phys} . Since our discussion covers the whole temperature range $0 \leq T \lesssim 1.7 T_c$ we can fix \hat{m}_{phys} such that the (zero temperature) pion mass is $m_\pi = 135 \text{ MeV}$. The condensate $\langle \bar{\psi}\psi \rangle$ plays here the role of an order parameter. Its precise definition will be given in section 5.2. Figure 17 shows our results for $\langle \bar{\psi}\psi \rangle(T, \hat{m})$: Curve (a) gives the temperature dependence of $\langle \bar{\psi}\psi \rangle$ in the chiral limit $\hat{m} = 0$. Here the lower curve is the full result for arbitrary T whereas the upper curve corresponds to the universal scaling form of the equation of state for the $O(4)$ Heisenberg model. We see perfect agreement of both curves for T sufficiently close to $T_c = 100.7 \text{ MeV}$. This demonstrates the capability of our method to cover the critical behavior and, in particular, to reproduce the critical exponents of the $O(4)$ -model. We have determined (cf. section 5.7) the universal critical equation of state as well as the non-universal amplitudes. This provides the full functional dependence of $\langle \bar{\psi}\psi \rangle(T, \hat{m})$ for small $T - T_c$ and \hat{m} . The curves (b), (c) and (d) are for non-vanishing values of the average current quark mass \hat{m} . Curve (c) corresponds to \hat{m}_{phys} or, equivalently, $m_\pi(T = 0) = 135 \text{ MeV}$. One observes a crossover in the range $T = (1.2 - 1.5)T_c$. The $O(4)$ universal equation of state (upper curve) gives a reasonable approximation in this

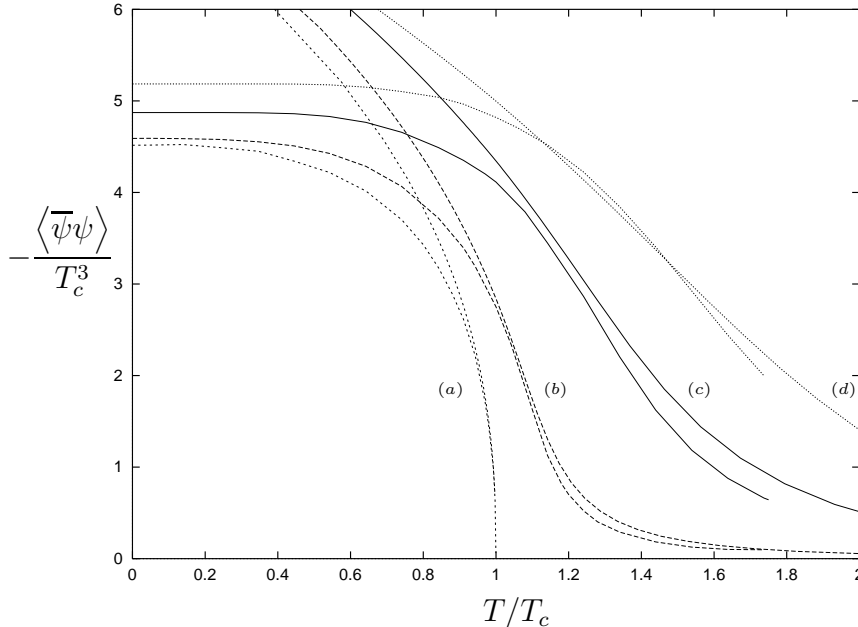


Figure 17: The plot shows the chiral condensate $\langle \bar{\psi}\psi \rangle$ as a function of temperature T . Lines (a), (b), (c), (d) correspond at zero temperature to $m_\pi = 0, 45 \text{ MeV}, 135 \text{ MeV}, 230 \text{ MeV}$, respectively. For each pair of curves the lower one represents the full T -dependence of $\langle \bar{\psi}\psi \rangle$ whereas the upper one shows for comparison the universal scaling form of the equation of state for the $O(4)$ Heisenberg model. The critical temperature for zero quark mass is $T_c = 100.7 \text{ MeV}$. The chiral condensate is normalized at a scale $k_\Phi \simeq 620 \text{ MeV}$.

temperature range. The transition turns out to be much less dramatic than for $\hat{m} = 0$. We have also plotted in curve (b) the results for comparably small quark masses $\simeq 1 \text{ MeV}$, i.e. $\hat{m} = \hat{m}_{\text{phys}}/10$, for which the $T = 0$ value of m_π equals 45 MeV . The crossover is considerably sharper but a substantial deviation from the chiral limit remains even for such small values of \hat{m} . In order to facilitate comparison with lattice simulations which are typically performed for larger values of m_π we also present results for $m_\pi(T = 0) = 230 \text{ MeV}$ in curve (d). One may define a “pseudocritical temperature” T_{pc} associated to the smooth crossover as the inflection point of $\langle \bar{\psi}\psi \rangle(T)$ as usually done in lattice simulations. Our results for this definition of T_{pc} are denoted by $T_{pc}^{(1)}$ and are presented in table 6 for the four different values of \hat{m} or, equivalently, $m_\pi(T = 0)$. The value for the pseudocritical temperature for $m_\pi = 230 \text{ MeV}$ compares well with the lattice results for two flavor QCD (cf. section 5.7). One should mention, though, that a determination of T_{pc} according to this definition is subject to sizeable numerical uncertainties for large pion masses as the curve in figure 17 is almost linear around the inflection point for quite a large temperature range. A problematic point in lattice simulations is the extrapolation to realistic values of m_π or even to the chiral limit. Our results may serve here as an analytic guide. The overall picture shows the approximate validity of the $O(4)$ scaling behavior over a large temperature interval in the vicinity of and above T_c once the (non-universal) amplitudes are properly computed.

A second important result of our investigations is the temperature dependence of the

$\frac{m_\pi}{\text{MeV}}$	0	45	135	230
$\frac{T_{pc}^{(1)}}{\text{MeV}}$	100.7	$\simeq 110$	$\simeq 130$	$\simeq 150$
$\frac{T_{pc}^{(2)}}{\text{MeV}}$	100.7	113	128	—

Table 6: The table shows the critical and “pseudocritical” temperatures for various values of the zero temperature pion mass. Here $T_{pc}^{(1)}$ is defined as the inflection point of $\langle \bar{\psi}\psi \rangle(T)$ whereas $T_{pc}^{(2)}$ is the location of the maximum of the sigma correlation length (see section 5.6).

space-like pion correlation length $m_\pi^{-1}(T)$. (We will often call $m_\pi(T)$ the temperature dependent pion mass since it coincides with the physical pion mass for $T = 0$.) The plot for $m_\pi(T)$ in figure 18 again shows the second order phase transition in the chiral limit $\hat{m} = 0$. For $T < T_c$ the pions are massless Goldstone bosons whereas for $T > T_c$ they form with the sigma particle a degenerate vector of $O(4)$ with mass increasing as a function of temperature. For $\hat{m} = 0$ the behavior for small positive $T - T_c$ is characterized by the critical exponent ν , i.e. $m_\pi(T) = (\xi^+)^{-1} T_c ((T - T_c)/T_c)^\nu$ and we obtain $\nu = 0.787$, $\xi^+ = 0.270$. For $\hat{m} > 0$ we find that $m_\pi(T)$ remains almost constant for $T \lesssim T_c$ with only a very slight dip for T near $T_c/2$. For $T > T_c$ the correlation length decreases rapidly and for $T \gg T_c$ the precise value of \hat{m} becomes irrelevant. We see that the universal critical behavior near T_c is quite smoothly connected to $T = 0$. The full functional dependence of $m_\pi(T, \hat{m})$ allows us to compute the overall size of the pion correlation length near the critical temperature and we find $m_\pi(T_{pc}) \simeq 1.7m_\pi(0)$ for the realistic value \hat{m}_{phys} . This correlation length is even smaller than the vacuum ($T = 0$) one and gives no indication for strong fluctuations of pions with long wavelength. It would be interesting to see if a decrease of the pion correlation length at and above T_c is experimentally observable. It should be emphasized, however, that a tricritical behavior with a massless excitation remains possible for three flavors. This would not be characterized by the universal behavior of the $O(4)$ -model. We also point out that the present investigation for the two flavor case does not take into account a speculative “effective restoration” of the axial $U_A(1)$ symmetry at high temperature [31, 32]. We will comment on these issues in section 5.8.

Our method is based on the effective average action Γ_k [37] which has been introduced in section 2. Since in most cases the flow equation (2.10) for Γ_k can not be solved exactly the capacity to devise useful truncations in a non-perturbative context becomes crucial. This requires first of all an identification of the degrees of freedom which are most relevant for a given problem. In the present work we concentrate on the chiral aspects of QCD³³. Spontaneous chiral symmetry breaking occurs through the expectation value of a (complex) scalar field Φ_{ab} which transforms as $(\bar{\mathbf{N}}, \mathbf{N})$ under the chiral flavor group $SU_L(N) \times SU_R(N)$

³³For a study of chiral symmetry breaking in QED using related exact renormalization group techniques see ref. [121].

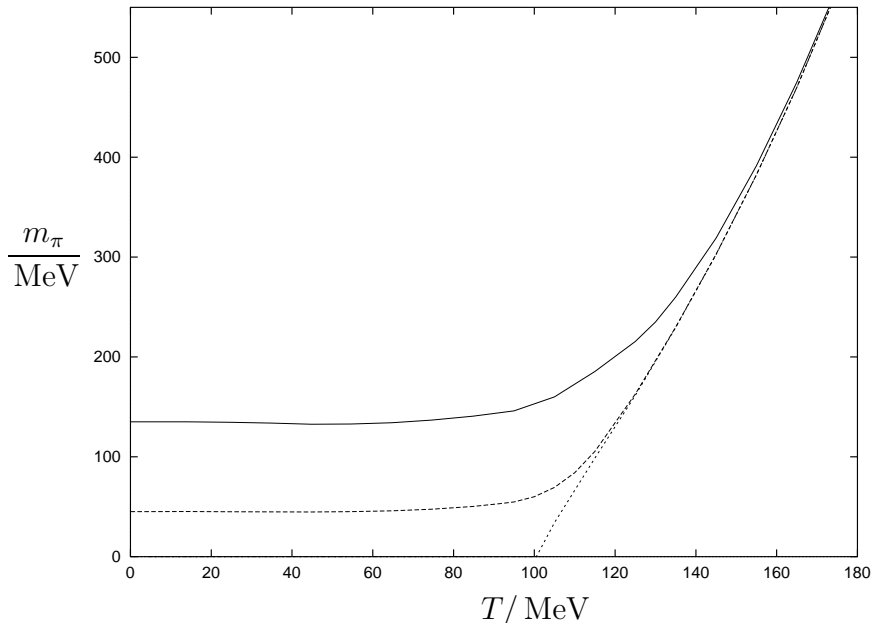


Figure 18: The plot shows m_π as a function of temperature T for three different values of the average light current quark mass \hat{m} . The solid line corresponds to the realistic value $\hat{m} = \hat{m}_{\text{phys}}$ whereas the dotted line represents the situation without explicit chiral symmetry breaking, i.e., $\hat{m} = 0$. The intermediate, dashed line assumes $\hat{m} = \hat{m}_{\text{phys}}/10$.

with N the number of light quark flavors. More precisely, the expectation value

$$\langle \Phi^{ab} \rangle = \bar{\sigma}_0 \delta^{ab} \quad (5.1)$$

induces for $\bar{\sigma}_0 \neq 0$ a spontaneous breaking of the chiral group to a vector-like subgroup, $SU_L(N) \times SU_R(N) \rightarrow SU_{L+R}(N) \equiv SU_V(N)$. In addition, non-vanishing current quark masses m_u, m_d, m_s break the chiral group explicitly and also lift the $SU_V(N)$ degeneracy of the spectrum if they are unequal. The physical degrees of freedom contained in the field Φ_{ab} are pseudoscalar and scalar mesons which can be understood as quark-antiquark bound states. It is obvious that any analytical description of the chiral transition has to include at least part of these (pseudo-)scalar fields as the most relevant degrees of freedom.

In the present work we use for k smaller than a “compositeness scale” $k_\Phi \simeq 600$ MeV a description in terms of Φ_{ab} and quark degrees of freedom. The quarks acquire a constituent quark mass M_q through the chiral condensate $\bar{\sigma}_0$ which forms in our picture for $k_{\chi SB} \simeq 400$ MeV. This effective quark meson model can be obtained from QCD by “integrating out” the gluon degrees of freedom and introducing fields for composite operators [44, 45]. This will be explained in more detail in the first part of section 5.2. In this picture the scale k_Φ is associated to the scale at which the formation of mesonic bound states can be observed in the flow of the effective (momentum dependent) four-quark interaction. We will restrict our discussion here to two flavor QCD with equal quark masses $m_u = m_d \equiv \hat{m}$. Since in this case the scalar triplet a_0 and the pseudoscalar singlet (associated with the

η') have typical masses around³⁴ 1 GeV we will neglect them for $k < k_\Phi$. This reduces the scalar degrees of freedom of our effective model to a four component vector of $O(4)$, consisting of the three pions and the “sigma resonance”.

We imagine that all other degrees of freedom besides the quarks ψ and the scalars Φ are integrated out. This is reflected in the precise form of the effective average action $\Gamma_{k_\Phi}[\psi, \Phi]$ at the scale k_Φ which serves as an initial value for the solution of the flow equation. The flow of $\Gamma_k[\psi, \Phi]$ for $k < k_\Phi$ is then entirely due to the quark and meson fluctuations which are not yet included in $\Gamma_{k_\Phi}[\psi, \Phi]$. Obviously, the initial value Γ_{k_Φ} may be a quite complicated functional of ψ and Φ containing, in particular, important non-local behavior. We will nevertheless use a rather simple truncation in terms of standard kinetic terms and a most general form of the scalar potential U_k , i.e.³⁵

$$\begin{aligned}\hat{\Gamma}_k &= \Gamma_k - \frac{1}{2} \int d^4x \operatorname{tr} (\Phi^\dagger j + j^\dagger \Phi) \\ \Gamma_k &= \int d^4x \left\{ Z_{\psi,k} \bar{\psi}_a i \not{\partial} \psi^a + Z_{\Phi,k} \operatorname{tr} [\partial_\mu \Phi^\dagger \partial^\mu \Phi] + U_k(\Phi, \Phi^\dagger) \right. \\ &\quad \left. + \bar{h}_k \bar{\psi}^a \left(\frac{1 + \gamma_5}{2} \Phi_{ab} - \frac{1 - \gamma_5}{2} (\Phi^\dagger)_{ab} \right) \psi^b \right\}.\end{aligned}\tag{5.2}$$

Here Γ_k is invariant under the chiral flavor symmetry $SU_L(2) \times SU_R(2)$ and the only explicit symmetry breaking arises through the source term $j \sim \hat{m}$. We will consider the flow of the most general form of U_k consistent with the symmetries (without any restriction to a polynomial form as typically used in a perturbative context). On the other hand, our approximations for the kinetic terms are rather crude and parameterized by only two running wave function renormalization constants, $Z_{\Phi,k}$ and $Z_{\psi,k}$. The same holds for the effective Yukawa coupling \bar{h}_k . The main approximations in this work concern

- (i) the simple form of the derivative terms and the Yukawa coupling, in particular, the neglect of higher derivative terms (and terms with two derivatives and higher powers of Φ). This is partly motivated by the observation that at the scale k_Φ and for small temperatures the possible strong non-localities related to confinement affect most likely only the quarks in a momentum range $q^2 \lesssim (300 \text{ MeV})^2$. Details of the quark propagator and interactions in this momentum range are not very important in our context (see section 5.2).
- (ii) the neglect of interactions involving more than two quark fields. This is motivated by the fact that the dominant multi-quark interactions are already incorporated in the mesonic description. Six-quark interactions beyond those contained effectively

³⁴More precisely, because of the anomalous $U_A(1)$ breaking in QCD these mesons are significantly heavier than the remaining degrees of freedom in the range of scales k where the dynamics of the model is strongly influenced by mesonic fluctuations. The situation becomes more involved if the model is considered at high temperature which is discussed in section 5.8.

³⁵Our Euclidean conventions (\bar{h}_k is real) are specified in refs. [46, 77].

in U_k could be related to baryons and play probably only a minor role for the meson physics considered here.

We will choose a normalization of ψ, Φ such that $Z_{\psi, k_\Phi} = \bar{h}_{k_\Phi} = 1$. We therefore need as initial values at the scale k_Φ the scalar wave function renormalization Z_{Φ, k_Φ} and the shape of the potential U_{k_Φ} . We will make here the important assumption that $Z_{\Phi, k}$ is small at the compositeness scale k_Φ (similarly to what is usually assumed in Nambu–Jona-Lasinio-like models). This results in a large value of the renormalized Yukawa coupling $h_k = Z_{\Phi, k}^{-1/2} Z_{\psi, k}^{-1} \bar{h}_k$. A large value of h_{k_Φ} is phenomenologically suggested by the comparably large value of the constituent quark mass M_q . The latter is related to the value of the Yukawa coupling for $k \rightarrow 0$ and the pion decay constant $f_\pi = 92.4 \text{ MeV}$ by $M_q = hf_\pi/2$ (with $h = h_{k=0}$), and $M_q \simeq 300 \text{ MeV}$ implies $h^2/4\pi \simeq 3.4$. For increasing k the value of the Yukawa coupling grows rapidly for $k \gtrsim M_q$. Our assumption of a large initial value for h_{k_Φ} is therefore equivalent to the assumption that the truncation (5.2) can be used up to the vicinity of the Landau pole of h_k . The existence of a strong Yukawa coupling enhances the predictive power of our approach considerably. It implies a fast approach of the running couplings to partial infrared fixed points [46]. In consequence, the detailed form of U_{k_Φ} becomes unimportant, except for the value of one relevant parameter corresponding to the scalar mass term $\bar{m}_{k_\Phi}^2$. In this work we fix $\bar{m}_{k_\Phi}^2$ such that $f_\pi = 92.4 \text{ MeV}$ for $m_\pi = 135 \text{ MeV}$. The possibility of such a choice is highly non-trivial since f_π can actually be predicted [46] in our setting within a relatively narrow range. The value $f_\pi = 92.4 \text{ MeV}$ (for $m_\pi = 135 \text{ MeV}$) sets our unit of mass for two flavor QCD which is, of course, not directly accessible by observation. Besides $\bar{m}_{k_\Phi}^2$ (or f_π) the other input parameter used in this work is the constituent quark mass M_q which determines the scale k_Φ at which h_{k_Φ} becomes very large. We consider a range $300 \text{ MeV} \lesssim M_q \lesssim 350 \text{ MeV}$ and find a rather weak dependence of our results on the precise value of M_q . We also observe that the limit $h_{k_\Phi} \rightarrow \infty$ can be considered as the lowest order of a systematic expansion in $h_{k_\Phi}^{-1}$ which is obviously highly non-perturbative.

A generalization of our method to the realistic case of three light flavors is possible and work in this direction is in progress. For the time being we expect that many features found for $N = 2$ will carry over to the realistic case, especially the critical behavior for $T \rightarrow T_c$ and $\hat{m} \rightarrow 0$ (for fixed $m_s \neq 0$). Nevertheless, some quantities like $\langle \bar{\psi}\psi \rangle (T = 0)$, the difference between f_π for realistic quark masses and $\hat{m} = 0$ or the mass of the sigma resonance at $T = 0$ may be modified. This will also affect the non-universal amplitudes in the critical equation of state and, in particular, the value of T_c . In the picture of the two flavor quark meson model these changes occur through an effective temperature dependence of the initial values of couplings at the scale k_Φ . This effect, which is due to the temperature dependence of effects from fluctuations not considered in the present work is discussed briefly in section 5.8. It remains perfectly conceivable that this additional temperature dependence may result in a first order phase transition or a tricritical behavior for realistic values of \hat{m} for the three flavor case. Details will depend on the strange quark mass. We observe, however, that the temperature dependence in the limit $\hat{m} \rightarrow 0$ involves for $T \leq T_c$ only information from the running of couplings in the range $k \lesssim 300 \text{ MeV}$.

(The running for $k \gtrsim 3T$ effectively drops out in the comparison between the thermal equilibrium results and those for $T = 0$.) In this range of temperatures our model should be quite reliable.

Finally, we mention that we have concentrated here only on the Φ -dependent part of the effective action which is related to chiral symmetry breaking. The Φ -independent part of the free energy also depends on T and only part of this temperature dependence is induced by the scalar and quark fluctuations considered in the present work. Most likely, the gluon degrees of freedom cannot be neglected for this purpose. This is the reason why we do not give results for “overall quantities” like energy density or pressure as a function of T .

The text is organized as follows: In section 5.2 we review the linear quark meson model at vanishing temperature. We begin with an overview of the different scales appearing in strong interaction physics. Subsequently, the flow equations for the linear quark meson model are introduced and their approximate partial fixed point behavior is discussed in detail leading to a “prediction” of the chiral condensate $\langle \bar{\psi}\psi \rangle$. In section 5.5 the exact renormalization group formulation of field theories in thermal equilibrium is given. It is demonstrated how mass threshold functions in the flow equations smoothly decouple all massive Matsubara modes as the temperature increases, therefore leading to a “dimensional reduction” of the model. Section 5.6 contains our results for the linear quark meson model at non-vanishing temperature. Here we discuss the T -dependences of the parameters and physical observables of the linear quark meson model in detail for a temperature range $0 \leq T \lesssim 170 \text{ MeV}$ including the (pseudo)critical temperature T_c of the chiral transition. The critical behavior of the model near T_c and $\hat{m} = 0$, where \hat{m} denotes the light average current quark mass, is carefully analyzed in section 5.7. There we present the universal scaling form of the equation of state including a fit for the corresponding scaling function. Also the universal critical exponents and amplitude ratios are given there. The effects of additional degrees of freedom of strong interaction physics not included in the linear $O(4)$ symmetric quark meson model are addressed in section 5.8. Here we also comment on differences between the linear quark meson model and chiral perturbation theory. Some technical details concerning the quark mass term and the definition of threshold functions at vanishing and non-vanishing temperature are presented in three appendices.

5.2 The quark meson model

Before discussing the finite temperature behavior of strong interaction physics we will review some of its zero temperature features. This will be done within the framework of a linear quark meson model as an effective description for QCD for scales below the mesonic compositeness scale of approximately $k_\Phi \simeq 600 \text{ MeV}$. Relating this model to QCD in a semi-quantitative way in subsection 5.3 will allow us to gain some information on the initial value for the effective average action at the compositeness scale k_Φ . We emphasize, however, that the quantitative aspects of the derivation of the effective quark meson model from QCD will not be relevant for our practical calculations in the mesonic sector. This is related to the “infrared stability” for large Yukawa coupling h_{k_Φ} as discussed in the

introduction and which will be made quantitative in subsection 5.4.

5.3 A short (scale) history of QCD

For an evaluation of the trace on the right hand side of the flow equation (2.10) only a small momentum range $q^2 \simeq k^2$ contributes substantially. One therefore only needs to take into account those fluctuations which are important in this momentum interval. Here we are interested in the description of chiral symmetry breaking. The relevant fluctuations in relation to this phenomenon may change with the scale k and we begin by summarizing the qualitatively different scale intervals which appear for meson physics in QCD. Some of this will be explained in more detail in the remainder of this section whereas other aspects are well known. Details of this discussion may also be found in refs. [44, 46, 122]. We will distinguish five qualitatively different ranges of scales:

1. At sufficiently high momentum scales, say,

$$k \gtrsim k_p \simeq 1.5 \text{ GeV}$$

the relevant degrees of freedom of strong interactions are quarks and gluons and their dynamics is well described by perturbative QCD.

2. For decreasing momentum scales in the range

$$k_\Phi \simeq 600 \text{ MeV} \lesssim k \lesssim k_p \simeq 1.5 \text{ GeV}$$

the dynamical degrees of freedom are still quarks and gluons. Yet, as k is lowered part of their dynamics becomes dominated by effective non-local four quark interactions which cannot be fully accessed perturbatively.

3. At still lower scales this situation changes dramatically. Quarks and gluons are supplemented by mesonic bound states as additional degrees of freedom which are formed at a scale $k_\Phi \simeq 600 \text{ MeV}$. We emphasize that k_Φ is well separated from $\Lambda_{\text{QCD}} \simeq 200 \text{ MeV}$ where confinement sets in and from the constituent masses of the quarks $M_q \simeq (300 - 350) \text{ MeV}$. This implies that below the compositeness scale k_Φ there exists a hybrid description in term of quarks *and* mesons! It is important to note that for scales not too much smaller than k_Φ chiral symmetry remains unbroken. This situation holds down to a scale $k_{\chi_{SB}} \simeq 400 \text{ MeV}$ at which the scalar meson potential develops a non-trivial minimum thus breaking chiral symmetry spontaneously. The meson dynamics within the range

$$k_{\chi_{SB}} \simeq 400 \text{ MeV} \lesssim k \lesssim k_\Phi \simeq 600 \text{ MeV}$$

is dominated by light current quarks with a strong Yukawa coupling $h_k^2/(4\pi) \gg \alpha_s(k)$ to mesons. We will thus assume that the leading gluon effects are included below k_Φ already in the formation of mesons. Near $k_{\chi_{SB}}$ also fluctuations of the light scalar

mesons become important as their initially large renormalized mass approaches zero. Other hadronic bound states like vector mesons or baryons should have masses larger than those of the lightest scalar mesons, in particular near $k_{\chi_{SB}}$, and give therefore only subleading contributions to the dynamics. This leads us to a simple linear model of quarks and scalar mesons as an effective description of QCD for scales below k_{Φ} .

4. As one evolves to scales below $k_{\chi_{SB}}$ the Yukawa coupling decreases whereas α_s increases. Of course, getting closer to Λ_{QCD} it is no longer justified to neglect in the quark sector the QCD effects which go beyond the dynamics of the effective quark meson model in our truncation (5.2). On the other hand, the final IR value of the Yukawa coupling h is fixed by the typical values of constituent quark masses $M_q \simeq 300 \text{ MeV}$ to be $h^2/(4\pi) \simeq 3.4$. One may therefore speculate that the domination of the Yukawa interaction persists even for the interval

$$M_q \simeq 300 \text{ MeV} \lesssim k \lesssim k_{\chi_{SB}} \simeq 400 \text{ MeV}$$

below which the quarks decouple from the evolution of the mesonic degrees of freedom altogether. Of course, details of the gluonic interactions are expected to be crucial for an understanding of quark and gluon confinement. Strong interaction effects may dramatically change the momentum dependence of the quark propagator for k and q^2 around Λ_{QCD} . Yet, there is no coupling of the gluons to the color neutral mesons. As long as one is only interested in the dynamics of the mesons one is led to expect that confinement effects are quantitatively not too important.

5. Because of the effective decoupling of the quarks and therefore of the whole colored sector the details of confinement have only little influence on the mesonic dynamics for scales

$$k \lesssim M_q \simeq 300 \text{ MeV} .$$

Here quarks and gluons disappear effectively from the spectrum and one is left with the pions. They are the only particles whose propagation is not suppressed by a large mass. For scales below the pion mass the flow of the couplings stops.

Let us now try to understand these different ranges of scales in more detail. We may start at $k_p = 1.5 \text{ GeV}$ where we assume that all gluonic degrees of freedom have been integrated out while we have kept an effective infrared cutoff $\sim k_p$ in the quark propagators. Details of this procedure were outlined in ref. [45]. This results in a non-trivial momentum dependence of the quark propagator and effective non-local four and higher quark interactions. Because of the infrared cutoff the resulting effective action for the quarks resembles closely the one for heavy quarks (at least for Euclidean momenta). The dominant effect is the appearance of an effective quark potential similar to the one for the charm quark which describes the effective four quark interactions.

We next have to remove the infrared cutoff for the quarks, $k \rightarrow 0$. This task can be carried out by means of the exact flow equation for quarks only, starting at k_p with an initial value $\Gamma_{k_p}[\psi]$ as obtained after integrating out the gluons. A first investigation in

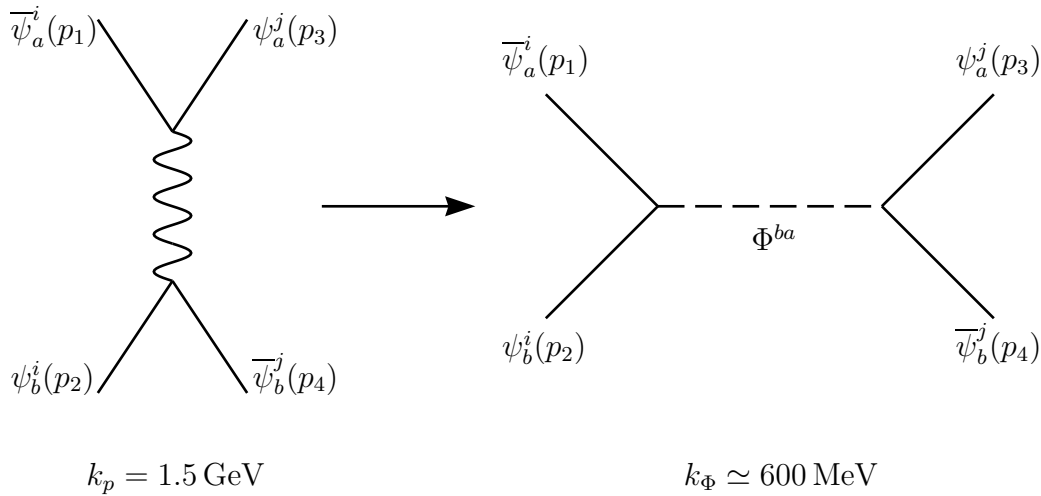


Figure 19: The left diagram represents the one gluon exchange t -channel contribution to the four quark vertex at the scale $k_p \simeq 1.5 \text{ GeV}$. It is assumed here that the gluon propagator is modified such that it accounts for the linearly rising term in the heavy quark potential. The right diagram displays the scalar meson s -channel exchange found at the compositeness scale $k_\Phi \simeq 600 \text{ MeV}$.

this direction [44] used a truncation with a chirally invariant four quark interaction whose most general momentum dependence was retained. A crucial point is, of course, the initial value for this momentum dependence at k_p . The ansatz used in ref. [44] is obtained by Fierz transforming the heavy quark potential and keeping, for simplicity, only the scalar meson channel while neglecting the ρ -meson and pomeron channels which are also present. The effective heavy quark potential was approximated there by a one gluon exchange term $\sim \alpha_s(k_p)$ supplemented by a linearly rising string tension term. This ansatz corresponds to the four quark interaction generated by the flavor neutral t -channel one gluon exchange depicted in figure 19 with an appropriately modified gluon propagator and quark gluon vertex in order to account for the linearly rising part of the potential.

The evolution equation for the four quark interaction can be derived from the fermionic version of eq. (2.10). It is by far not clear that the evolution of the effective four quark vertex will lead at lower scales to a momentum dependence representing the (s -channel) exchange of colorless mesonic bound states. Yet, at the compositeness scale

$$k_\Phi \simeq 600 \text{ MeV} \tag{5.3}$$

one finds [44] an approximate Bethe–Salpeter factorization of the four quark amplitude with precisely this property. This situation is described by the right Feynman diagram in figure 19. In particular, it was possible to extract the amputated Bethe–Salpeter wave function as well as the mesonic bound state propagator displaying a pole-like structure in the s -channel if it is continued to negative $s = (p_1 + p_2)^2$. In the limit where the momentum dependence

of the Bethe–Salpeter wave function and the bound state propagator is neglected the effective action Γ_{k_Φ} resembles³⁶ the Nambu–Jona-Lasinio model [123, 124]. It is therefore not surprising that our description of the dynamics for $k < k_\Phi$ will parallel certain aspects of the investigations of this model, even though we are not bound to the approximations used typically in such studies (large- N_c expansion, perturbative renormalization group, etc.).

It is clear that for scales $k \lesssim k_\Phi$ a description of strong interaction physics in terms of quark fields alone would be rather inefficient. Finding physically reasonable truncations of the effective average action should be much easier once composite fields for the mesons are introduced. The exact renormalization group equation can indeed be supplemented by an exact formalism for the introduction of composite field variables or, more generally, a change of variables [44]. In the context of QCD this amounts to the replacement of the dominant part of the four quark interactions by scalar meson fields with Yukawa couplings to the quarks. In turn, this substitutes the effective quark action at the scale k_Φ by the effective quark meson action given in eq. (5.2) in the introduction³⁷. The term in the effective potential U_{k_Φ} which is quadratic in Φ , $U_{k_\Phi} = \bar{m}_{k_\Phi}^2 \text{tr} \Phi^\dagger \Phi + \dots$, turns out to be positive as a consequence of the attractiveness of the four quark interaction inducing it. Its value was found for the simple truncations used in ref. [44] to be $\bar{m}_{k_\Phi} \simeq 120 \text{ MeV}$. The higher order terms in U_{k_Φ} cannot be determined in the four quark approximation since they correspond to terms involving six or more quark fields. (Their values will not be needed for our quantitative investigations as is discussed in subsection 5.4). The initial value of the (bare) Yukawa coupling corresponds to the amputated Bethe–Salpeter wave function. Neglecting its momentum dependence it can be normalized to $\bar{h}_{k_\Phi} = 1$. Moreover, the quark wave function renormalization $Z_{\psi,k}$ is normalized to one at the scale k_Φ for convenience. One may add that we have refrained here for simplicity from considering four quark operators with vector and pseudo–vector spin structure. Their inclusion is straightforward and would lead to vector and pseudo–vector mesons in the effective action.

In view of the possible large truncation errors made in ref. [44] we will take (5.3) and the above value of \bar{m}_{k_Φ} only as order of magnitude estimates. Furthermore, we will assume, as motivated in the introduction and usually done in large- N_c computations within the NJL model, that

$$Z_{\Phi,k_\Phi} \ll 1. \quad (5.4)$$

As a consequence, the initial value of the renormalized Yukawa coupling $h_{k_\Phi} = Z_{\Phi,k_\Phi}^{-1/2} Z_{\psi,k_\Phi}^{-1} \bar{h}_{k_\Phi}$ is much larger than one and we will be able to exploit the infrared stable features of the flow equations. As a typical coupling we take $h_{k_\Phi} = 100$ in order to simulate the limit $h_{k_\Phi} \rightarrow \infty$. The effective potential $U_k(\Phi)$ must be invariant under the chiral $SU_L(N) \times SU_R(N)$ flavor symmetry. In fact, the axial anomaly of QCD breaks the Abelian $U_A(1)$

³⁶Our solution of the flow equation for Γ_k with $Z_{\Phi,k_\Phi} = 0$ (see below) may be considered as a solution of the NJL model with a particular form of the ultraviolet cutoff dictated by the shape of $R_k(q^2)$ as given in eq. (2.3).

³⁷We note that no double counting problem arises in this procedure.

symmetry. The resulting $U_A(1)$ violating multi-quark interactions³⁸ lead to corresponding $U_A(1)$ violating terms in $U_k(\Phi)$. Accordingly, the most general effective potential U_k is a function of the $N + 1$ independent C and P conserving $SU_L(N) \times SU_R(N)$ invariants

$$\begin{aligned}\rho &= \text{tr } \Phi^\dagger \Phi , \\ \tau_i &\sim \text{tr} \left(\Phi^\dagger \Phi - \frac{1}{N} \rho \right)^i , \quad i = 2, \dots, N , \\ \xi &= \det \Phi + \det \Phi^\dagger .\end{aligned}\tag{5.5}$$

For a given initial form of U_k all quantities in our truncation of Γ_k (5.2) are now fixed and we may follow the flow of Γ_k to $k \rightarrow 0$. In this context it is important that the formalism for composite fields [44] also induces an infrared cutoff in the meson propagator. The flow equations are therefore exactly of the form (2.10), with quarks and mesons treated on an equal footing. At the compositeness scale the quadratic term of $U_{k_\Phi} = \overline{m}_{k_\Phi}^2 \text{Tr } \Phi^\dagger \Phi + \dots$ is positive and the minimum of U_{k_Φ} therefore occurs for $\Phi = 0$. Spontaneous chiral symmetry breaking is described by a non-vanishing expectation value $\langle \Phi \rangle$ in absence of quark masses. This follows from the change of the shape of the effective potential U_k as k flows from k_Φ to zero. The large renormalized Yukawa coupling rapidly drives the scalar mass term to negative values and leads to a potential minimum away from the origin at some scale $k_{\chi\text{SB}} < k_\Phi$ such that finally $\langle \Phi \rangle = \overline{\sigma}_0 \neq 0$ for $k \rightarrow 0$ [44, 46]. This concludes our overview of the general features of chiral symmetry breaking in the context of flow equations for QCD.

We will concentrate in this work on the two flavor case ($N = 2$) and comment on the effects of including the strange quark in section 5.8. Furthermore we will neglect isospin violation and therefore consider a singlet source term j proportional to the average light current quark mass $\hat{m} \equiv \frac{1}{2}(m_u + m_d)$. Due to the $U_A(1)$ -anomaly there is a mass split for the mesons described by Φ . The scalar triplet (a_0) and the pseudoscalar singlet (η') receive a large mass whereas the pseudoscalar triplet (π) and the scalar singlet (σ) remains light. From the measured values $m_{\eta'}, m_{a_0} \simeq 1 \text{ GeV}$ it is evident that a decoupling of these mesons is presumably a very realistic limit³⁹. It can be achieved in a chirally invariant way and leads to the well known $O(4)$ symmetric Gell-Mann-Levy linear sigma model [5] which is, however, coupled to quarks now. This is the two flavor linear quark meson model which we will study in the remainder of this work. For this model the effective potential U_k is a function of ρ only.

It remains to determine the source j as a function of the average current quark mass \hat{m} . This is carried out in appendix D and we obtain in our normalization with $Z_{\psi, k_\Phi} = 1$, $\overline{h}_{k_\Phi} = 1$,

$$j = 2\overline{m}_{k_\Phi}^2 \hat{m} .\tag{5.6}$$

³⁸A first attempt for the computation of the anomaly term in the fermionic effective average action can be found in ref. [125].

³⁹In thermal equilibrium at high temperature this decoupling is not obvious. We will comment on this point in section 5.8.

It is remarkable that higher order terms do not influence the relation between j and \hat{m} . Only the quadratic term $\overline{m}_{k_\Phi}^2$ enters which is in our scenario the only relevant coupling. This feature is an important ingredient for the predictive power of the model as far as the absolute size of the current quark mass is concerned.

The quantities which are directly connected to chiral symmetry breaking depend on the k -dependent expectation value $\langle \Phi \rangle_k = \overline{\sigma}_{0,k}$ as given by

$$\frac{\partial U_k}{\partial \rho}(\rho = 2\overline{\sigma}_{0,k}^2) = \frac{j}{2\overline{\sigma}_{0,k}}. \quad (5.7)$$

In terms of the renormalized expectation value

$$\sigma_{0,k} = Z_{\Phi,k}^{1/2} \overline{\sigma}_{0,k} \quad (5.8)$$

we obtain the following expressions for phenomenological observables from (5.2) for⁴⁰ $d = 4$

$$\begin{aligned} f_{\pi,k} &= 2\sigma_{0,k}, \\ \langle \overline{\psi}\psi \rangle_k &= -2\overline{m}_{k_\Phi}^2 \left[Z_{\Phi,k}^{-1/2} \sigma_{0,k} - \hat{m} \right], \\ M_{q,k} &= h_k \sigma_{0,k}, \\ m_{\pi,k}^2 &= Z_{\Phi,k}^{-1/2} \frac{\overline{m}_{k_\Phi}^2 \hat{m}}{\sigma_{0,k}} = Z_{\Phi,k}^{-1/2} \frac{j}{2\sigma_{0,k}}, \\ m_{\sigma,k}^2 &= Z_{\Phi,k}^{-1/2} \frac{\overline{m}_{k_\Phi}^2 \hat{m}}{\sigma_{0,k}} + 4\lambda_k \sigma_{0,k}^2. \end{aligned} \quad (5.9)$$

Here we have defined the dimensionless, renormalized couplings

$$\begin{aligned} \lambda_k &= Z_{\Phi,k}^{-2} \frac{\partial^2 U_k}{\partial \rho^2}(\rho = 2\overline{\sigma}_{0,k}^2), \\ h_k &= Z_{\Phi,k}^{-1/2} Z_{\psi,k}^{-1} \overline{h}_k. \end{aligned} \quad (5.10)$$

We will mainly be interested in the ‘‘physical values’’ of the quantities (5.9) in the limit $k \rightarrow 0$ where the infrared cutoff is removed, i.e. $f_\pi = f_{\pi,k=0}$, $m_\pi^2 = m_{\pi,k=0}^2$, etc. We point out that the formalism of composite fields provides the link [44] to the chiral condensate $\langle \overline{\psi}\psi \rangle$ since the expectation value $\overline{\sigma}_0$ is related to the expectation value of a composite quark–antiquark operator.

5.4 Flow equations and infrared stability

At first sight, a reliable computation of $\Gamma_{k \rightarrow 0}$ seems a very difficult task. Without a truncation Γ_k is described by an infinite number of parameters (couplings, wave function

⁴⁰We note that the expressions (5.9) obey the well known Gell-Mann–Oakes–Renner relation $m_\pi^2 f_\pi^2 = -2\hat{m} \langle \overline{\psi}\psi \rangle + \mathcal{O}(\hat{m}^2)$ [126].

renormalizations, etc.) as can be seen if Γ_k is expanded in powers of fields and derivatives. For instance, the sigma mass is obtained as a zero of the exact inverse propagator, $\lim_{k \rightarrow 0} \Gamma_k^{(2)}(q)|_{\Phi=\langle\Phi\rangle}$, which formally receives contributions from terms in Γ_k with arbitrarily high powers of derivatives and the expectation value σ_0 . Realistic non-perturbative truncations of Γ_k which reduce the problem to a manageable size are crucial. We will follow here a twofold strategy:

- Physical observables like meson masses, decay constants, etc., can be expanded in powers of (current) quark masses in a similar way as in chiral perturbation theory [3]. To a given finite order of this expansion only a finite number of terms of a simultaneous expansion of Γ_k in powers of derivatives and Φ are required if the expansion point is chosen properly. Details of this procedure and some results can be found in [104, 6, 7].
- Because of an approximate partial IR fixed point behavior of the flow equations in the symmetric regime, i.e. for $k_{\chi SB} < k < k_\Phi$, the values of many parameters of Γ_k for $k \rightarrow 0$ will be almost independent of their initial values at the compositeness scale k_Φ . For large enough h_{k_Φ} only a few relevant parameters need to be computed accurately from QCD. They can alternatively be determined from phenomenology. Because of the present lack of an explicit QCD computation we will pursue the latter approach.

In combination, these two points open the possibility for a perhaps unexpected degree of predictive power within the linear quark meson model. We wish to stress, however, that a perturbative treatment of the model at hand, e.g., using perturbative RG techniques, cannot be expected to yield reliable results. The renormalized Yukawa coupling is very large at the scale k_Φ . Even the IR value of h_k is still relatively big

$$h_{k=0} = \frac{2M_q}{f_\pi} \simeq 6.5 \quad (5.11)$$

and h_k increases with k . The dynamics of the linear quark meson model is therefore clearly non-perturbative for all scales $k \leq k_\Phi$.

We will now turn to the flow equations for the linear quark meson model. We first note that the flow equations for Γ_k and $\Gamma_k - \frac{1}{2} \int d^4x \text{tr} (j^\dagger \Phi + \Phi^\dagger j)$ are identical. The source term therefore does not need to be considered explicitly and only appears in the condition (5.7) for $\langle\Phi\rangle$. It is convenient to work with dimensionless and renormalized variables therefore eliminating all explicit k -dependence. With

$$u(t, \tilde{\rho}) \equiv k^{-d} U_k(\rho), \quad \tilde{\rho} \equiv Z_{\Phi,k} k^{2-d} \rho \quad (5.12)$$

and using (5.2) as a first truncation of the effective average action Γ_k one obtains the flow equation ($t = \ln(k/k_\Phi)$)

$$\begin{aligned} \frac{\partial}{\partial t} u &= -du + (d-2 + \eta_\Phi) \tilde{\rho} u' \\ &+ 2v_d \left\{ 3l_0^d(u'; \eta_\Phi) + l_0^d(u' + 2\tilde{\rho} u''; \eta_\Phi) - 2^{\frac{d}{2}+1} N_c l_0^{(F)d} \left(\frac{1}{2} \tilde{\rho} h^2; \eta_\psi \right) \right\}. \end{aligned} \quad (5.13)$$

Here $v_d^{-1} \equiv 2^{d+1}\pi^{d/2}\Gamma(d/2)$ and primes denote derivatives with respect to $\tilde{\rho}$. The number of quark colors is denoted as N_c . We will always use in the following $N_c = 3$. Eq. (5.13) is a partial differential equation for the effective potential $u(t, \tilde{\rho})$ which has to be supplemented by the flow equation for the Yukawa coupling and expressions for the anomalous dimensions η_Φ, η_ψ . The symbols $l_n^d, l_n^{(F)d}$ denote bosonic and fermionic mass threshold functions, respectively, which are defined in appendix A. They describe the decoupling of massive modes and provide an important non-perturbative ingredient. For instance, the bosonic threshold functions

$$l_n^d(w; \eta_\Phi) = \frac{n + \delta_{n,0}}{4} v_d^{-1} k^{2n-d} \int \frac{d^d q}{(2\pi)^d} \frac{1}{Z_{\Phi,k}} \frac{\partial R_k}{\partial t} \frac{1}{[P(q^2) + k^2 w]^{n+1}} \quad (5.14)$$

involve the inverse average propagator $P(q^2) = q^2 + Z_{\Phi,k}^{-1} R_k(q^2)$ where the infrared cutoff is manifest. These functions decrease $\sim w^{-(n+1)}$ for $w \gg 1$. Since typically $w = M^2/k^2$ with M a mass of the model, the main effect of the threshold functions is to cut off fluctuations of particles with masses $M^2 \gg k^2$. Once the scale k is changed below a certain mass threshold, the corresponding particle no longer contributes to the evolution and decouples smoothly.

The dimensionless renormalized expectation value $\kappa \equiv 2k^{2-d} Z_{\Phi,k} \bar{\sigma}_{0,k}^2$, with $\bar{\sigma}_{0,k}$ the k -dependent VEV of Φ , may be computed for each k directly from the condition (5.7)

$$u'(t, \kappa) = \frac{J}{\sqrt{2\kappa}} k^{-\frac{d+2}{2}} Z_{\Phi,k}^{-1/2} \equiv \epsilon_g. \quad (5.15)$$

Note that $\kappa \equiv 0$ in the symmetric regime for vanishing source term. Equation (5.15) allows us to follow the flow of κ according to

$$\frac{d}{dt} \kappa = \frac{\kappa}{\epsilon_g + 2\kappa\lambda} \left\{ [\eta_\Phi - d - 2] \epsilon_g - 2 \frac{\partial}{\partial t} u'(t, \kappa) \right\} \quad (5.16)$$

with $\lambda \equiv u''(t, \kappa)$. We define the Yukawa coupling for $\tilde{\rho} = \kappa$ and its flow equation reads [46]

$$\begin{aligned} \frac{d}{dt} h^2 &= (d - 4 + 2\eta_\psi + \eta_\Phi) h^2 - 2v_d h^4 \left\{ 3l_{1,1}^{(FB)d} \left(\frac{1}{2} h^2 \kappa, \epsilon_g; \eta_\psi, \eta_\Phi \right) \right. \\ &\quad \left. - l_{1,1}^{(FB)d} \left(\frac{1}{2} h^2 \kappa, \epsilon_g + 2\lambda\kappa; \eta_\psi, \eta_\Phi \right) \right\}. \end{aligned} \quad (5.17)$$

Similarly, the scalar and quark anomalous dimensions are inferred from

$$\begin{aligned}
\eta_\Phi &\equiv -\frac{d}{dt} \ln Z_{\Phi,k} = 4\frac{v_d}{d} \left\{ 4\kappa\lambda^2 m_{2,2}^d(\epsilon_g, \epsilon_g + 2\lambda\kappa; \eta_\Phi) \right. \\
&\quad \left. + 2^{\frac{d}{2}} N_c h^2 m_4^{(F)d} \left(\frac{1}{2} h^2 \kappa; \eta_\psi \right) \right\}, \\
\eta_\psi &\equiv -\frac{d}{dt} \ln Z_{\psi,k} = 2\frac{v_d}{d} h^2 \left\{ 3m_{1,2}^{(FB)d} \left(\frac{1}{2} h^2 \kappa, \epsilon_g; \eta_\psi, \eta_\Phi \right) \right. \\
&\quad \left. + m_{1,2}^{(FB)d} \left(\frac{1}{2} h^2 \kappa, \epsilon_g + 2\lambda\kappa; \eta_\psi, \eta_\Phi \right) \right\},
\end{aligned} \tag{5.18}$$

which is a linear set of equations for the anomalous dimensions. The threshold functions $l_{n_1, n_2}^{(FB)d}$, m_{n_1, n_2}^d , $m_4^{(F)d}$ and $m_{n_1, n_2}^{(FB)d}$ are also specified in appendix A.

The flow equations (5.13), (5.16)—(5.18), constitute a coupled system of ordinary and partial differential equations which can be integrated numerically. Here we take the effective current quark mass dependence of h_k , $Z_{\Phi,k}$ and $Z_{\psi,k}$ into account by stopping the evolution according to eqs. (5.17), (5.18), evaluated for the chiral limit, below the pion mass m_π . (For details of the algorithm used here see refs. [63, 68].) One finds for $d = 4$ that chiral symmetry breaking indeed occurs for a wide range of initial values of the parameters including the presumably realistic case of large renormalized Yukawa coupling and a bare mass \overline{m}_{k_Φ} of order 100 MeV. Driven by the strong Yukawa coupling, the renormalized mass term $u'(t, \tilde{\rho} = 0)$ decreases rapidly and goes through zero at a scale $k_{\chi_{\text{SB}}}$ not far below k_Φ . Here the system enters the spontaneously broken regime and the effective average potential develops an absolute minimum away from the origin. The evolution of the potential minimum $\sigma_{0,k}^2 = k^2 \kappa / 2$ turns out to be reasonably stable already before $k \simeq m_\pi$ where it stops. We take this result as an indication that our truncation of the effective action Γ_k leads at least qualitatively to a satisfactory description of chiral symmetry breaking. The reason for the relative stability of the IR behavior of the VEV (and all other couplings) is that the quarks acquire a constituent mass $M_q = h\sigma_0 \simeq 300$ MeV in the spontaneously broken regime. As a consequence they decouple once k becomes smaller than M_q and the evolution is then dominantly driven by the light Goldstone bosons. This is also important for our approximation of neglecting the residual gluonic interactions in the quark sector of the model as outlined in subsection 5.3.

Most importantly, one finds that the system of flow equations exhibits an approximate IR fixed point behavior in the symmetric regime [46]. To see this explicitly we study the flow equations (5.13), (5.16)—(5.18) subject to the condition (5.4). For the relevant range of $\tilde{\rho}$ both $u'(t, \tilde{\rho})$ and $u'(t, \tilde{\rho}) + 2\tilde{\rho}u''(t, \tilde{\rho})$ are then much larger than $\tilde{\rho}h^2(t)$ and we may therefore neglect in the flow equations all scalar contributions with threshold functions

involving these large masses. This yields the simplified equations ($d = 4, v_4^{-1} = 32\pi^2$)

$$\begin{aligned}\frac{\partial}{\partial t}u &= -4u + (2 + \eta_\Phi) \tilde{\rho}u' - \frac{N_c}{2\pi^2} l_0^{(F)4} \left(\frac{1}{2} \tilde{\rho} h^2\right), \\ \frac{d}{dt}h^2 &= \eta_\Phi h^2 m, \\ \eta_\Phi &= \frac{N_c}{8\pi^2} m_4^{(F)4}(0) h^2, \\ \eta_\psi &= 0.\end{aligned}\tag{5.19}$$

Of course, it should be clear that this approximation is only valid for the initial range of running below k_Φ before the (dimensionless) renormalized scalar mass squared $u'(t, \tilde{\rho} = 0)$ approaches zero near the chiral symmetry breaking scale. The system (5.19) is exactly soluble. Using $m_4^{(F)4}(0) = 1$ which holds independently of the choice of the IR cutoff we find

$$\begin{aligned}h^2(t) &= Z_\Phi^{-1}(t) = \frac{h_I^2}{1 - \frac{N_c}{8\pi^2} h_I^2 t}, \\ u(t, \tilde{\rho}) &= e^{-4t} u_I(e^{2t} \tilde{\rho} \frac{h^2(t)}{h_I^2}) - \frac{N_c}{2\pi^2} \int_0^t dr e^{-4r} l_0^{(F)4} \left(\frac{1}{2} h^2(t) \tilde{\rho} e^{2r}\right).\end{aligned}\tag{5.20}$$

(The integration over r on the right hand side of the solution for u can be carried out by first exchanging it with the one over momentum implicit in the definition of the threshold function $l_0^{(F)4}$ (see appendix A.) Here $u_I(\tilde{\rho}) \equiv u(0, \tilde{\rho})$ denotes the effective average potential at the compositeness scale and h_I^2 is the initial value of h^2 at k_Φ , i.e. for $t = 0$. For simplicity we will use an expansion of the initial value effective potential $u_I(\tilde{\rho})$ in powers of $\tilde{\rho}$ around $\tilde{\rho} = 0$

$$u_I(\tilde{\rho}) = \sum_{n=0}^{\infty} \frac{u_I^{(n)}(0)}{n!} \tilde{\rho}^n\tag{5.21}$$

even though this is not essential for the forthcoming reasoning. Expanding also $l_0^{(F)4}$ in eq. (5.20) in powers of its argument one finds for $n > 2$

$$\frac{u^{(n)}(t, 0)}{h^{2n}(t)} = e^{2(n-2)t} \frac{u_I^{(n)}(0)}{h_I^{2n}} + \frac{N_c}{\pi^2} \frac{(-1)^n (n-1)!}{2^{n+2} (n-2)} l_n^{(F)4}(0) [1 - e^{2(n-2)t}].\tag{5.22}$$

For decreasing $t \rightarrow -\infty$ the initial values $u_I^{(n)}$ become rapidly unimportant and $u^{(n)}/h^{2n}$ approaches a fixed point. For $n = 2$, i.e., for the quartic coupling, one finds

$$\frac{u^{(2)}(t, 0)}{h^2(t)} = 1 - \frac{1 - \frac{u_I^{(2)}(0)}{h_I^2}}{1 - \frac{N_c}{8\pi^2} h_I^2 t}\tag{5.23}$$

leading to a fixed point value $(u^{(2)}/h^2)_* = 1$. As a consequence of this fixed point behavior the system loses all its “memory” on the initial values $u_I^{(n \geq 2)}$ at the compositeness scale

k_Φ ! This typically happens before the approximation $u'(t, \tilde{\rho}), u'(t, \tilde{\rho}) + 2\tilde{\rho}u''(t, \tilde{\rho}) \gg \tilde{\rho}h^2(t)$ breaks down and the solution (5.20) becomes invalid. Furthermore, the attraction to partial infrared fixed points continues also for the range of k where the scalar fluctuations cannot be neglected anymore. The initial value for the bare dimensionless mass parameter

$$\frac{u'_I(0)}{h_I^2} = \frac{\overline{m}_{k_\Phi}^2}{k_\Phi^2} \quad (5.24)$$

is never negligible. (In fact, using the values for $\overline{m}_{k_\Phi}^2$ and k_Φ computed in ref. [44] one obtains $\overline{m}_{k_\Phi}^2/k_\Phi^2 \simeq 0.036$.) For large h_I (and dropping the constant piece $u_I(0)$) the solution (5.20) therefore behaves with growing $|t|$ as

$$\begin{aligned} Z_\Phi(t) &\simeq -\frac{N_c}{8\pi^2}t, \\ h^2(t) &\simeq -\frac{8\pi^2}{N_c t}, \\ u(t, \tilde{\rho}) &\simeq \frac{u'_I(0)}{h_I^2}e^{-2t}h^2(t)\tilde{\rho} - \frac{N_c}{2\pi^2} \int_0^t dr e^{-4r} l_0^{(F)4} \left(\frac{1}{2}h^2(t)\tilde{\rho}e^{2r} \right). \end{aligned} \quad (5.25)$$

In other words, for $h_I \rightarrow \infty$ the IR behavior of the linear quark meson model will depend (in addition to the value of the compositeness scale k_Φ and the quark mass \hat{m}) only on one parameter, $\overline{m}_{k_\Phi}^2$. We have numerically verified this feature by starting with different values for $u_I^{(2)}(0)$. Indeed, the differences in the physical observables were found to be small. This IR stability of the flow equations leads to a perhaps surprising degree of predictive power! For definiteness we will perform our numerical analysis of the full system of flow equations (5.13), (5.16)–(5.18) with the idealized initial value $u_I(\tilde{\rho}) = u'_I(0)\tilde{\rho}$ in the limit $h_I^2 \rightarrow \infty$. It should be stressed, though, that deviations from this idealization will lead only to small numerical deviations in the IR behavior of the linear quark meson model as long as the condition (5.4) holds, say for $h_I \gtrsim 15$ [46].

With this knowledge at hand we may now fix the remaining three parameters of our model, k_Φ , $\overline{m}_{k_\Phi}^2$ and \hat{m} by using $f_\pi = 92.4$ MeV, the pion mass $M_\pi = 135$ MeV and the constituent quark mass M_q as phenomenological input. Because of the uncertainty regarding the precise value of M_q we give in table 7 the results for several values of M_q . The first line of table 7 corresponds to the choice of M_q and $\lambda_I \equiv u''_I(\kappa)$ which we will use for the forthcoming analysis of the model at finite temperature. As argued analytically above the dependence on the value of λ_I is weak for large enough h_I as demonstrated numerically by the second line. Moreover, we notice that our results, and in particular the value of j , are rather insensitive with respect to the precise value of M_q . It is remarkable that the values for k_Φ and $\overline{m}_{k_\Phi}^2$ are not very different from those computed in ref. [44]. As compared to the analysis of ref. [46] the present truncation of Γ_k is of a higher level of accuracy: We now consider an arbitrary form of the effective average potential instead of a polynomial approximation and we have included the pieces in the threshold functions which are proportional to the anomalous dimensions. It is encouraging that the results are rather robust with respect to these improvements of the truncation.

$\frac{M_q}{\text{MeV}}$	$\frac{\lambda_I}{h_I^2}$	$\frac{k_\Phi}{\text{MeV}}$	$\frac{\overline{m}_{k_\Phi}^2}{k_\Phi^2}$	$\frac{j^{1/3}}{\text{MeV}}$	$\frac{\hat{m}(k_\Phi)}{\text{MeV}}$	$\frac{\hat{m}(1 \text{ GeV})}{\text{MeV}}$	$\frac{\langle \overline{\psi}\psi \rangle(1 \text{ GeV})}{\text{MeV}^3}$	$\frac{f_\pi^{(0)}}{\text{MeV}}$
303	1	618	0.0265	66.8	14.7	11.4	$-(186)^3$	80.8
300	0	602	0.026	66.8	15.8	12.0	$-(183)^3$	80.2
310	0	585	0.025	66.1	16.9	12.5	$-(180)^3$	80.5
339	0	552	0.0225	64.4	19.5	13.7	$-(174)^3$	81.4

Table 7: The table shows the dependence on the constituent quark mass M_q of the input parameters k_Φ , $\overline{m}_{k_\Phi}^2/k_\Phi^2$ and j as well as some of our “predictions”. The phenomenological input used here besides M_q is $f_\pi = 92.4 \text{ MeV}$, $m_\pi = 135 \text{ MeV}$. The first line corresponds to the values for M_q and λ_I used in the remainder of this work. The other three lines demonstrate the insensitivity of our results with respect to the precise values of these parameters.

Once the parameters k_Φ , $\overline{m}_{k_\Phi}^2$ and \hat{m} are fixed there are a number of “predictions” of the linear meson model which can be compared with the results obtained by other methods or direct experimental observation. First of all one may compute the value of \hat{m} at a scale of 1 GeV which is suitable for comparison with results obtained from chiral perturbation theory [127] and sum rules [128]. For this purpose one has to account for the running of this quantity with the normalization scale from k_Φ as given in table 7 to the commonly used value of 1 GeV: $\hat{m}(1 \text{ GeV}) = A^{-1}\hat{m}(k_\Phi)$. A reasonable estimate of the factor A is obtained from the three loop running of \hat{m} in the \overline{MS} scheme [128]. For $M_q \simeq 300 \text{ MeV}$ corresponding to the first two lines in table 7 its value is $A \simeq 1.3$. The results for $\hat{m}(1 \text{ GeV})$ are in acceptable agreement with recent results from other methods [127, 128] even though they tend to be somewhat larger. Closely related to this is the value of the chiral condensate

$$\langle \overline{\psi}\psi \rangle(1 \text{ GeV}) \equiv -A\overline{m}_{k_\Phi}^2 \left[f_\pi Z_{\Phi,k=0}^{-1/2} - 2\hat{m} \right]. \quad (5.26)$$

These results are quite non-trivial since not only f_π and $\overline{m}_{k_\Phi}^2$ enter but also the computed IR value $Z_{\Phi,k=0}$. We emphasize in this context that there may be substantial corrections both in the extrapolation from k_Φ to 1 GeV and in the factor a_q (see (D.1)). The latter is due to the neglected influence of the strange quark which may be important near k_Φ . These uncertainties have only little effect on the physics at lower scales as relevant for our analysis of the temperature effects. Only the value of j which is fixed by m_π enters here.

A further more qualitative test concerns the mass of the sigma resonance or radial mode whose renormalized mass squared may be computed according to (5.9) in the limit $k \rightarrow 0$. From our numerical analysis we obtain $\lambda_{k=0} \simeq 20$ which translates into $m_\sigma \simeq 430 \text{ MeV}$. One should note, though, that this result is presumably not very accurate as we have employed in this work the approximation of using the Goldstone boson wave function renormalization constant also for the radial mode. Furthermore, the explicit chiral symmetry breaking contribution to m_σ^2 is certainly underestimated as long as the strange quark is neglected. In any case, we observe that the sigma meson is significantly heavier than the pions. This is a crucial consistency check for the linear quark meson model. A

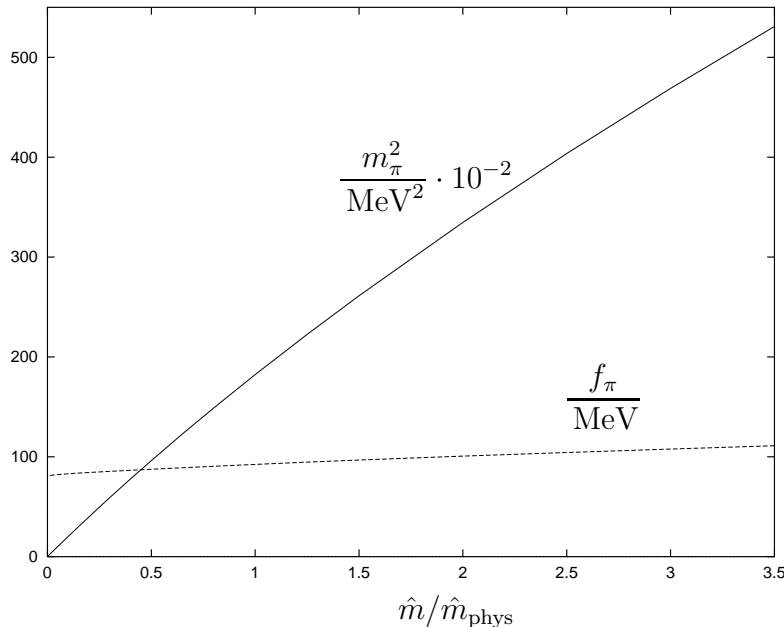


Figure 20: The plot shows m_π^2 (solid line) and f_π (dashed line) as functions of the current quark mass \hat{m} in units of the physical value \hat{m}_{phys} .

low sigma mass would be in conflict with the numerous successes of chiral perturbation theory [3] which requires the decoupling of all modes other than the Goldstone bosons in the IR-limit of QCD. The decoupling of the sigma meson is, of course, equivalent to the limit $\lambda \rightarrow \infty$ which formally describes the transition from the linear to the non-linear sigma model and which appears to be reasonably well realized by the large IR-values of λ obtained in our analysis. We also note that the issue of the sigma mass is closely connected to the value of $f_\pi^{(0)}$, the value of f_π in the chiral limit $\hat{m} = 0$ also given in table 7. To lowest order in $(f_\pi - f_\pi^{(0)})/f_\pi$ or, equivalently, in \hat{m} one has

$$f_\pi - f_\pi^{(0)} = \frac{J}{Z_\Phi^{1/2} m_\sigma^2} = \frac{f_\pi m_\pi^2}{m_\sigma^2}. \quad (5.27)$$

A larger value of m_σ would therefore reduce the difference between $f_\pi^{(0)}$ and f_π .

In figure 20 we show the dependence of the pion mass and decay constant on the average current quark mass \hat{m} . These curves depend very little on the values of the initial parameters as demonstrated in table 7 by $f_\pi^{(0)}$. We observe a relatively large difference of 12 MeV between the pion decay constants at $\hat{m} = \hat{m}_{\text{phys}}$ and $\hat{m} = 0$. According to (5.27) this difference is related to the mass of the sigma particle and will be modified in the three flavor case. We will later find that the critical temperature T_c for the second order phase transition in the chiral limit is almost independent of the initial conditions. The values of $f_\pi^{(0)}$ and T_c essentially determine the non-universal amplitudes in the critical scaling region (cf. section 5.7). In summary, we find that the behavior of our model for small k is quite robust as far as uncertainties in the initial conditions at the scale k_Φ are concerned. We will

see that the difference of observables between non-vanishing and vanishing temperature is entirely determined by the flow of couplings in the range $0 < k \lesssim 3T$.

5.5 Thermal equilibrium and dimensional reduction

The extension of flow equations to thermal equilibrium situations at non-vanishing temperature T is straightforward [55]. In the Euclidean formalism non-zero temperature results in (anti-)periodic boundary conditions for (fermionic) bosonic fields in the Euclidean time direction with periodicity $1/T$ [53]. This leads to the replacement

$$\int \frac{d^d q}{(2\pi)^d} f(q^2) \rightarrow T \sum_{l \in \mathbb{Z}} \int \frac{d^{d-1} \vec{q}}{(2\pi)^{d-1}} f(q_0^2(l) + \vec{q}^2) \quad (5.28)$$

in the trace in (2.10) when represented as a momentum integration, with a discrete spectrum for the zero component

$$q_0(l) = \begin{cases} 2l\pi T & \text{for bosons} \\ (2l+1)\pi T & \text{for fermions} . \end{cases} \quad (5.29)$$

Hence, for $T > 0$ a four-dimensional QFT can be interpreted as a three-dimensional model with each bosonic or fermionic degree of freedom now coming in an infinite number of copies labeled by $l \in \mathbb{Z}$ (Matsubara modes). Each mode acquires an additional temperature dependent effective mass term $q_0^2(l)$. In a high temperature situation where all massive Matsubara modes decouple from the dynamics of the system one therefore expects to observe an effective three-dimensional theory with the bosonic zero modes as the only relevant degrees of freedom. In other words, if the characteristic length scale associated with the physical system is much larger than the inverse temperature the compactified Euclidean “time” dimension cannot be resolved anymore. This phenomenon is known as “dimensional reduction” [54].

The formalism of the effective average action automatically provides the tools for a smooth decoupling of the massive Matsubara modes as the scale k is lowered from $k \gg T$ to $k \ll T$. It therefore allows us to directly link the low- T , four-dimensional QFT to the effective three-dimensional high- T theory. The replacement (5.28) in (2.10) manifests itself in the flow equations (5.13), (5.16)—(5.18) only through a change to T -dependent threshold functions. For instance, the dimensionless functions $l_n^d(w; \eta_\Phi)$ defined in eq. (5.14) are replaced by

$$l_n^d(w, \frac{T}{k}; \eta_\Phi) \equiv \frac{n + \delta_{n,0}}{4} v_d^{-1} k^{2n-d} T \sum_{l \in \mathbb{Z}} \int \frac{d^{d-1} \vec{q}}{(2\pi)^{d-1}} \left(\frac{1}{Z_{\Phi,k}} \frac{\partial R_k(q^2)}{\partial t} \right) \frac{1}{[P(q^2) + k^2 w]^{n+1}} \quad (5.30)$$

where $q^2 = q_0^2 + \vec{q}^2$ and $q_0 = 2\pi l T$. A list of the various temperature dependent threshold functions appearing in the flow equations can be found in appendix B. There we also discuss some subtleties regarding the definition of the Yukawa coupling and the anomalous dimensions for $T \neq 0$. In the limit $k \gg T$ the sum over Matsubara modes approaches the

integration over a continuous range of q_0 and we recover the zero temperature threshold function $l_n^d(w; \eta_\Phi)$. In the opposite limit $k \ll T$ the massive Matsubara modes ($l \neq 0$) are suppressed and we expect to find a $d - 1$ dimensional behavior of l_n^d . In fact, one obtains from (5.30)

$$\begin{aligned} l_n^d(w, T/k; \eta_\Phi) &\simeq l_n^d(w; \eta_\Phi) && \text{for } T \ll k, \\ l_n^d(w, T/k; \eta_\Phi) &\simeq \frac{T}{k} \frac{v_{d-1}}{v_d} l_n^{d-1}(w; \eta_\Phi) && \text{for } T \gg k. \end{aligned} \quad (5.31)$$

For our choice of the infrared cutoff function R_k , eq. (2.3), the temperature dependent Matsubara modes in $l_n^d(w, T/k; \eta_\Phi)$ are exponentially suppressed for $T \ll k$ whereas the behavior is more complicated for other threshold functions appearing in the flow equations (5.13), (5.16)—(5.18). Nevertheless, all bosonic threshold functions are proportional to T/k for $T \gg k$ whereas those with fermionic contributions vanish in this limit⁴¹. This behavior is demonstrated in figure 21 where we have plotted the quotients $l_1^4(w, T/k)/l_1^4(w)$ and $l_1^{(F)4}(w, T/k)/l_1^{(F)4}(w)$ of bosonic and fermionic threshold functions, respectively. One observes that for $k \gg T$ both threshold functions essentially behave as for zero temperature. For growing T or decreasing k this changes as more and more Matsubara modes decouple until finally all massive modes are suppressed. The bosonic threshold function l_1^4 shows for $k \ll T$ the linear dependence on T/k derived in eq. (5.31). In particular, for the bosonic excitations the threshold function for $w \ll 1$ can be approximated with reasonable accuracy by $l_n^4(w; \eta_\Phi)$ for $T/k < 0.25$ and by $(4T/k)l_n^3(w; \eta_\Phi)$ for $T/k > 0.25$. The fermionic threshold function $l_1^{(F)4}$ tends to zero for $k \ll T$ since there is no massless fermionic zero mode, i.e. in this limit all fermionic contributions to the flow equations are suppressed. On the other hand, the fermions remain quantitatively relevant up to $T/k \simeq 0.6$ because of the relatively long tail in figure 21b. The transition from four to three-dimensional threshold functions leads to a *smooth dimensional reduction* as k is lowered from $k \gg T$ to $k \ll T$! Whereas for $k \gg T$ the model is most efficiently described in terms of standard four-dimensional fields Φ a choice of rescaled three-dimensional variables $\Phi_3 = \Phi/\sqrt{T}$ becomes better adapted for $k \ll T$. Accordingly, for high temperatures one will use a potential

$$u_3(t, \tilde{\rho}_3) = \frac{k}{T} u(t, \tilde{\rho}); \quad \tilde{\rho}_3 = \frac{k}{T} \tilde{\rho}. \quad (5.32)$$

In this regime $\Gamma_{k \rightarrow 0}$ corresponds to the free energy of classical statistics and $\Gamma_{k > 0}$ is a classical coarse grained free energy.

For our numerical calculations at non-vanishing temperature we exploit the discussed behavior of the threshold functions by using the zero temperature flow equations in the range $k \geq 10T$. For smaller values of k we approximate the infinite Matsubara sums (cf. eq. (5.30)) by a finite series such that the numerical uncertainty at $k = 10T$ is better than 10^{-4} . This approximation becomes exact in the limit $k \ll 10T$.

⁴¹For the present choice of R_k the temperature dependence of the threshold functions is considerably smoother than in ref. [55].

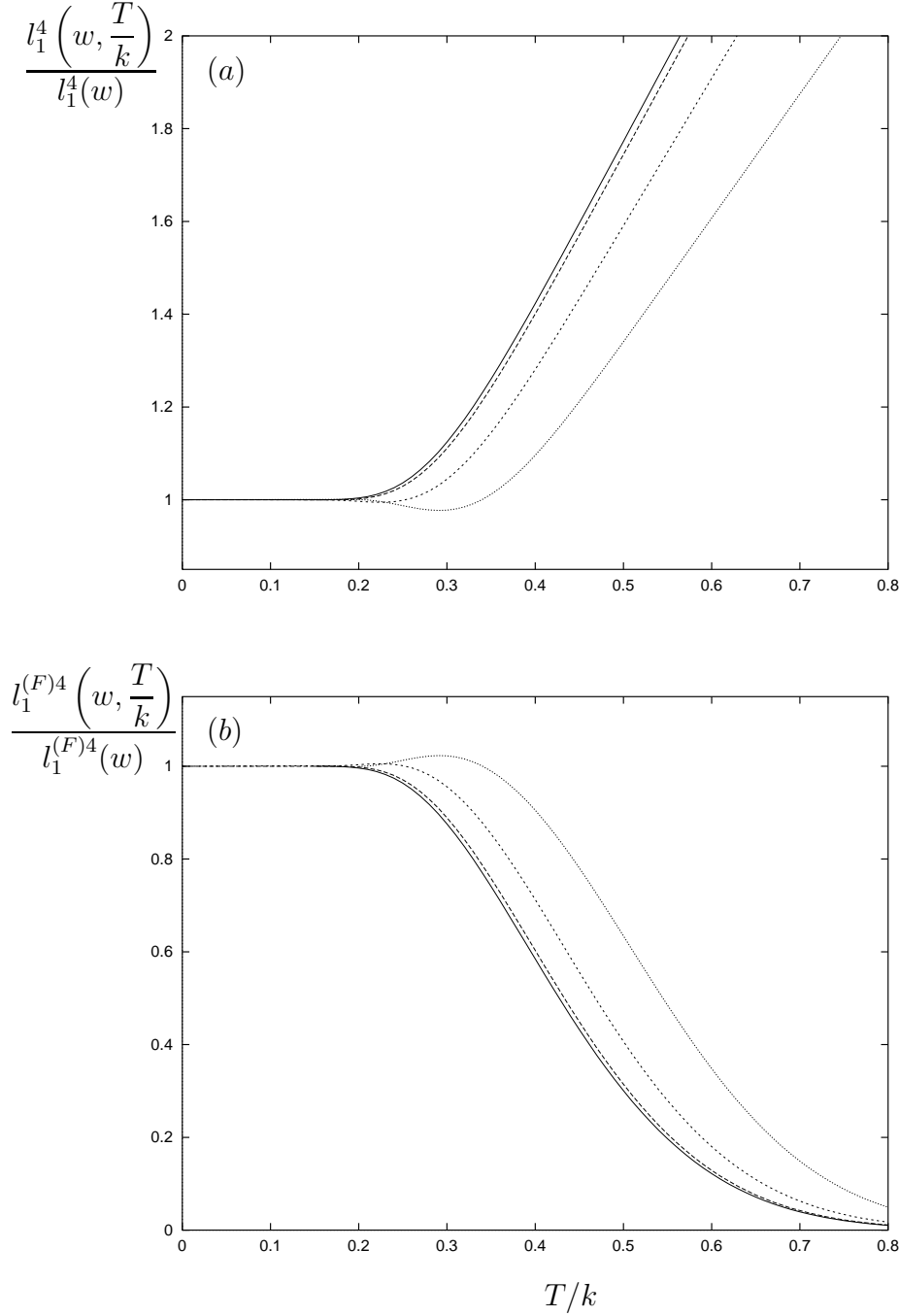


Figure 21: The plot shows the temperature dependence of the bosonic (a) and the fermionic (b) threshold functions $l_1^A(w, T/k)$ and $l_1^{(F)A}(w, T/k)$, respectively, for different values of the dimensionless mass term w . The solid line corresponds to $w = 0$ whereas the dotted ones correspond to $w = 0.1$, $w = 1$ and $w = 10$ with decreasing size of the dots. For $T \gg k$ the bosonic threshold function becomes proportional to T/k whereas the fermionic one tends to zero. In this range the theory with properly rescaled variables behaves as a classical three-dimensional theory.

5.6 Equation of state and the chiral phase transition

In section 5.3 we have considered the relevant fluctuations that contribute to the flow of Γ_k in dependence on the scale k . In a thermal equilibrium situation Γ_k also depends on the temperature T and one may ask for the relevance of thermal fluctuations at a given scale k . In particular, for not too high values of T (cf. sect. 5.8) the “initial condition” Γ_{k_Φ} for the solution of the flow equations should essentially be independent of temperature. This will allow us to fix Γ_{k_Φ} from phenomenological input at $T = 0$ and to compute the temperature dependent quantities in the infrared ($k \rightarrow 0$). We note that the thermal fluctuations which contribute to the r.h.s. of the flow equation for the meson potential (5.13) are effectively suppressed for $T \lesssim k/4$ (cf. section 5.5). Clearly for $T \gtrsim k_\Phi/3$ temperature effects become important at the compositeness scale. We expect the linear quark meson model with a compositeness scale $k_\Phi \simeq 600$ MeV to be a valid description for two flavor QCD below a temperature of about⁴² 170 MeV.

We compute the quantities of interest for temperatures $T \lesssim 170$ MeV by solving numerically the T -dependent version of the flow equations (5.13), (5.16)—(5.18) (cf. section 5.5 and appendix B) by lowering k from k_Φ to zero. For this range of temperatures we use the initial values as given in the first line of table 7. This corresponds to choosing the zero temperature pion mass and the pion decay constant ($f_\pi = 92.4$ MeV for $m_\pi = 135$ MeV) as phenomenological input. The only further input is the constituent quark mass M_q which we vary in the range $M_q \simeq 300 - 350$ MeV. We observe only a minor dependence of our results on M_q for the considered range of values. In particular, the value for the critical temperature T_c of the model remains almost unaffected by this variation.

We have plotted in figure 22 the renormalized expectation value $2\sigma_0$ of the scalar field as a function of temperature for three different values of the average light current quark mass \hat{m} . (We remind that $2\sigma_0(T = 0) = f_\pi$.) For $\hat{m} = 0$ the order parameter σ_0 of chiral symmetry breaking continuously goes to zero for $T \rightarrow T_c = 100.7$ MeV characterizing the phase transition to be of second order. The universal behavior of the model for small $T - T_c$ and small \hat{m} is discussed in more detail in section 5.7. We point out that the value of T_c corresponds to $f_\pi^{(0)} = 80.8$ MeV, i.e. the value of the pion decay constant for $\hat{m} = 0$, which is significantly lower than $f_\pi = 92.4$ MeV obtained for the realistic value \hat{m}_{phys} . If we would fix the value of the pion decay constant to be 92.4 MeV also in the chiral limit ($\hat{m} = 0$), the value for the critical temperature would raise to 115 MeV. The nature of the transition changes qualitatively for $\hat{m} \neq 0$ where the second order transition is replaced by a smooth crossover. The crossover for a realistic \hat{m}_{phys} or $m_\pi(T = 0) = 135$ MeV takes place in a temperature range $T \simeq (120 - 150)$ MeV. The middle curve in figure 22 corresponds to a value of \hat{m} which is only a tenth of the physical value, leading to a zero temperature pion mass $m_\pi = 45$ MeV. Here the crossover becomes considerably sharper but there remain substantial deviations from the chiral limit even for such small quark masses $\hat{m} \simeq 1$ MeV.

⁴²There will be an effective temperature dependence of Γ_{k_Φ} induced by the fluctuations of other degrees of freedom besides the quarks, the pions and the sigma which are taken into account here. We will comment on this issue in section 5.8. For realistic three flavor QCD the thermal kaon fluctuations will become important for $T \gtrsim 170$ MeV.

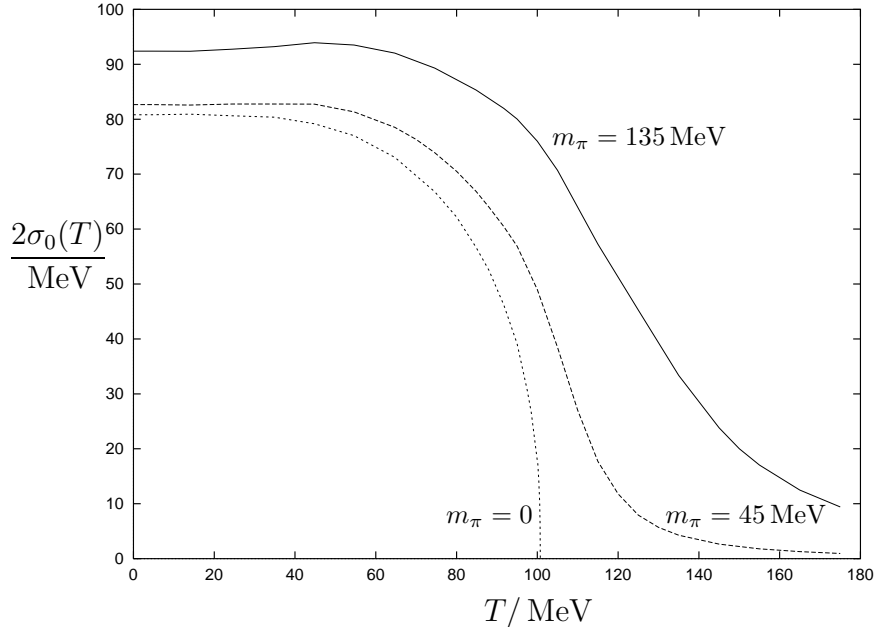


Figure 22: The expectation value $2\sigma_0$ is shown as a function of temperature T for three different values of the zero temperature pion mass.

The temperature dependence of m_π has already been mentioned in the introduction (see fig. 18) for the same three values of \hat{m} . As expected, the pions behave like true Goldstone bosons for $\hat{m} = 0$, i.e. their mass vanishes for $T \leq T_c$. Interestingly, m_π remains almost constant as a function of T for $T < T_c$ before it starts to increase monotonically. We therefore find for two flavors no indication for a substantial decrease of m_π around the critical temperature.

The dependence of the mass of the sigma resonance m_σ on the temperature is displayed in figure 23 for the above three values of \hat{m} . In the absence of explicit chiral symmetry breaking, $\hat{m} = 0$, the sigma mass vanishes for $T \leq T_c$. For $T < T_c$ this is a consequence of the presence of massless Goldstone bosons in the Higgs phase which drive the renormalized quartic coupling λ to zero. In fact, λ runs linearly with k for $T \gtrsim k/4$ and only evolves logarithmically for $T \lesssim k/4$. Once $\hat{m} \neq 0$ the pions acquire a mass even in the spontaneously broken phase and the evolution of λ with k is effectively stopped at $k \sim m_\pi$. Because of the temperature dependence of $\sigma_{0,k=0}$ (cf. figure 22) this leads to a monotonically decreasing behavior of m_σ with T for $T \lesssim T_c$. This changes into the expected monotonic growth once the system reaches the symmetric phase for⁴³ $T > T_c$. For low enough \hat{m} one may use the minimum of $m_\sigma(T)$ for an alternative definition of the (pseudo-)critical temperature denoted as $T_{pc}^{(2)}$. Table 6 in the introduction shows our results for the pseudocritical temperature for different values of \hat{m} or, equivalently, $m_\pi(T = 0)$. For a zero temperature pion mass $m_\pi = 135$ MeV we find $T_{pc}^{(2)} = 128$ MeV. At larger pion masses of about 230 MeV we observe no longer a characteristic minimum for m_σ apart from a very broad, slight dip at

⁴³See section 5.4 for a discussion of the zero temperature sigma mass.

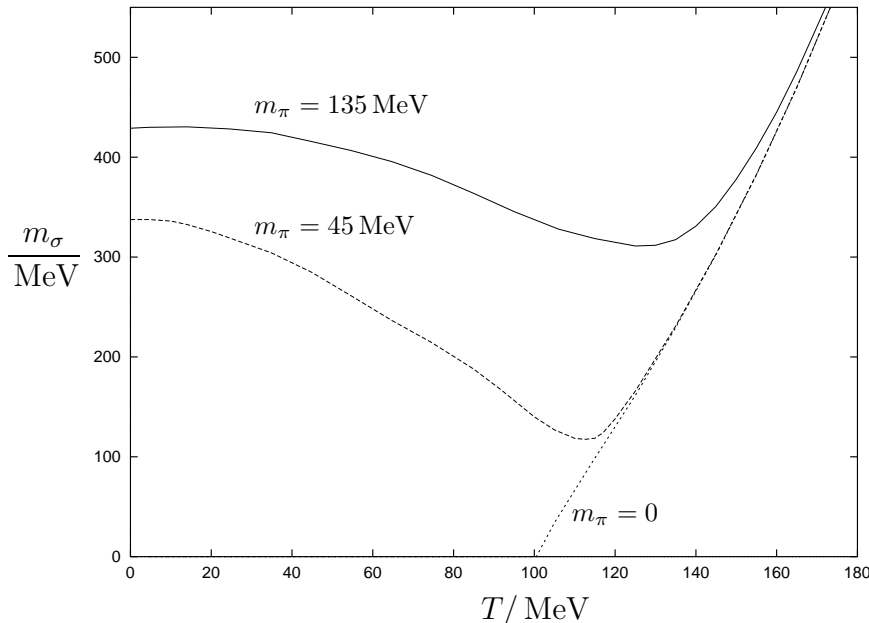


Figure 23: The plot shows the m_σ as a function of temperature T for three different values of the zero temperature pion mass.

$T \simeq 90$ MeV. A comparison of our results with lattice data is given in section 5.7. In fig. 24 we show the renormalized quartic coupling λ as a function of temperature for two fixed values of the average current quark mass. The upper curve corresponds to the physical value of \hat{m} or, equivalently, $m_\pi(T=0) = 135$ MeV whereas the lower curve shows λ for $\hat{m} = 0$. One observes the vanishing of the renormalized quartic coupling in the chiral limit for $T \leq T_c$ as discussed above. The renormalized scalar Φ^6 self interaction

$$U_3(T) = Z_\Phi^{-3} \frac{\partial^3 U(\rho, T)}{\partial \rho^3} (\rho = 2\bar{\sigma}_0^2(T)) \quad (5.33)$$

assumes a small negative value for realistic quark masses in the temperature range $T \lesssim 35$ MeV with $2U_3(T)\sigma_0^2(T) \simeq -0.5 \ll \lambda(T)$ and $2U_3(T)\sigma_0^2(T) \simeq 8.0, 8.5, 1.5$ for $T = 80, 120, 160$ MeV. We display $U_3(T)$ in figure 25 for the chiral limit where one observes a discontinuity of $U_3(T)$ at the critical temperature T_c .

Our results for the chiral condensate $\langle \bar{\psi}\psi \rangle$ as a function of temperature for different values of the average current quark mass are presented in figure 17 in the introduction. We will compare $\langle \bar{\psi}\psi \rangle(T, \hat{m})$ with its universal scaling form for the $O(4)$ Heisenberg model in section 5.7. Another interesting quantity is the temperature dependence of the constituent quark mass. Figure 26 shows $M_q(T)$ for $\hat{m} = 0$, $\hat{m} = \hat{m}_{\text{phys}}/10$ and $\hat{m} = \hat{m}_{\text{phys}}$, respectively. Its behavior is related to the temperature dependence of the renormalized order parameter $\sigma_0(T) \equiv \sigma_{0,k=0}(T)$ and the renormalized Yukawa coupling $h(T) \equiv h_{k=0}(T)$. The temperature dependence of h in the chiral limit can be found in fig. 27. Near the critical temperature one notices a characteristic dip. This results from the long wavelength pion fluctuations through a non-analytic behavior of the mesonic wave function renormalization

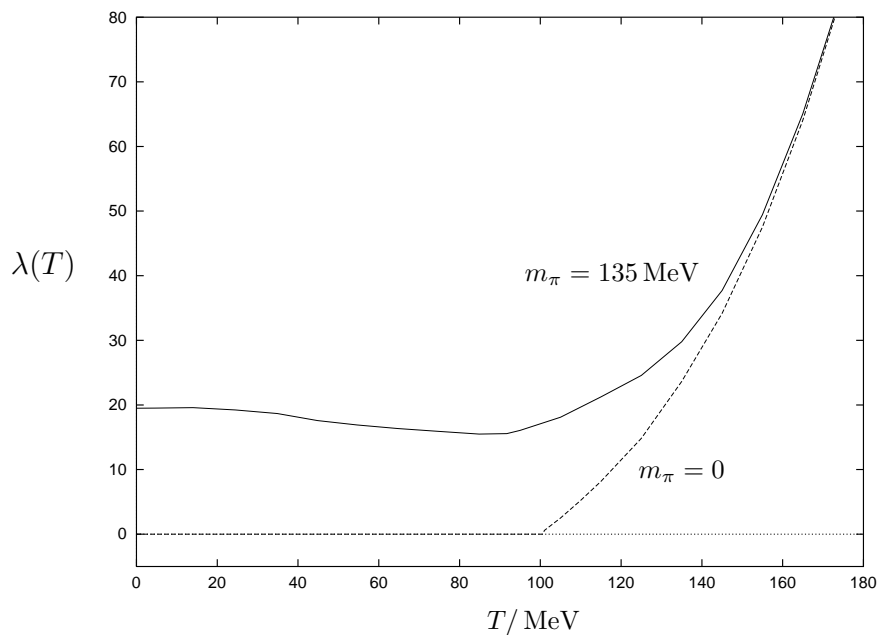


Figure 24: The plot shows the renormalized quartic scalar self coupling λ as a function of temperature T for the physical value of \hat{m} (solid line) as well as for $\hat{m} = 0$ (dashed line).

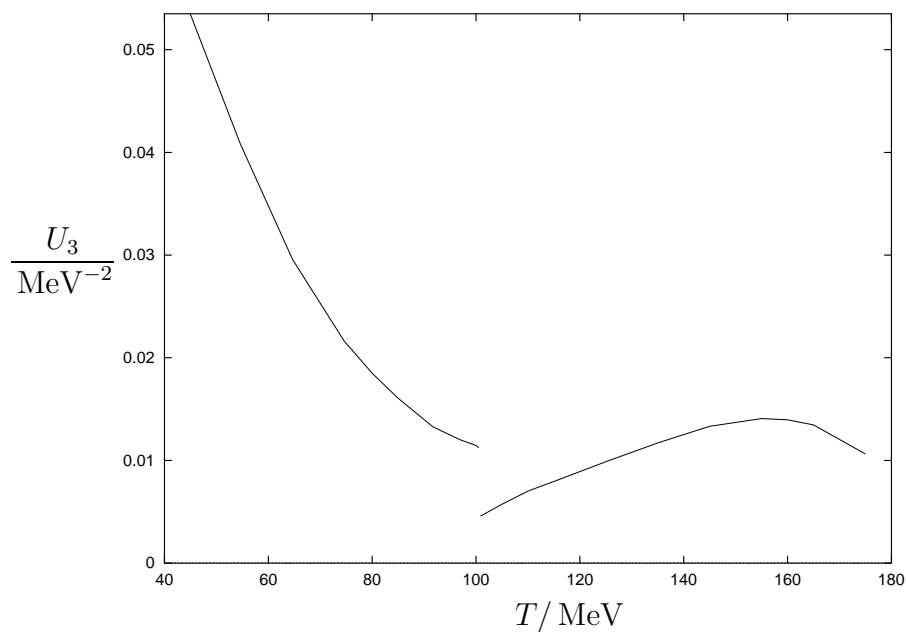


Figure 25: The plot shows the renormalized Φ^6 scalar self coupling U_3 as a function of temperature T in the chiral limit.

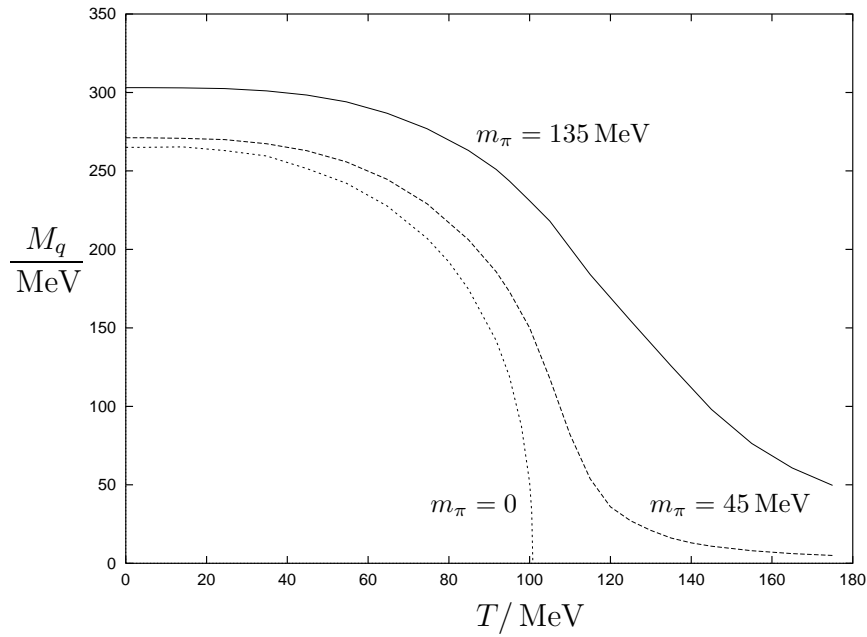


Figure 26: The plot shows the constituent quark mass M_q as a function of T for three different values of the average light current quark mass \hat{m} . The solid line corresponds to the realistic value $\hat{m} = \hat{m}_{\text{phys}}$ whereas the dotted line represents the situation without explicit chiral symmetry breaking, i.e., $\hat{m} = 0$. The intermediate, dashed line assumes $\hat{m} = \hat{m}_{\text{phys}}/10$.

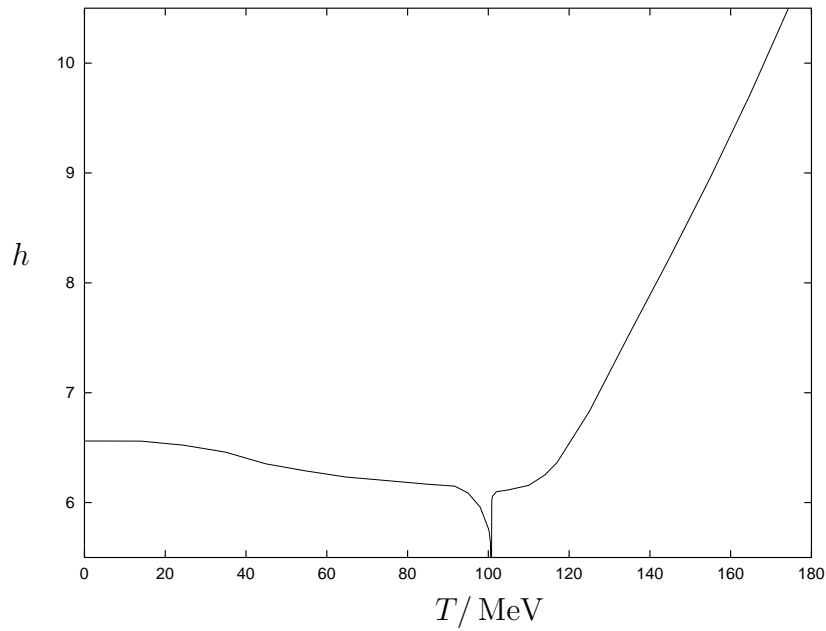


Figure 27: The plot shows the Yukawa coupling, h , as a function of temperature T in the chiral limit.

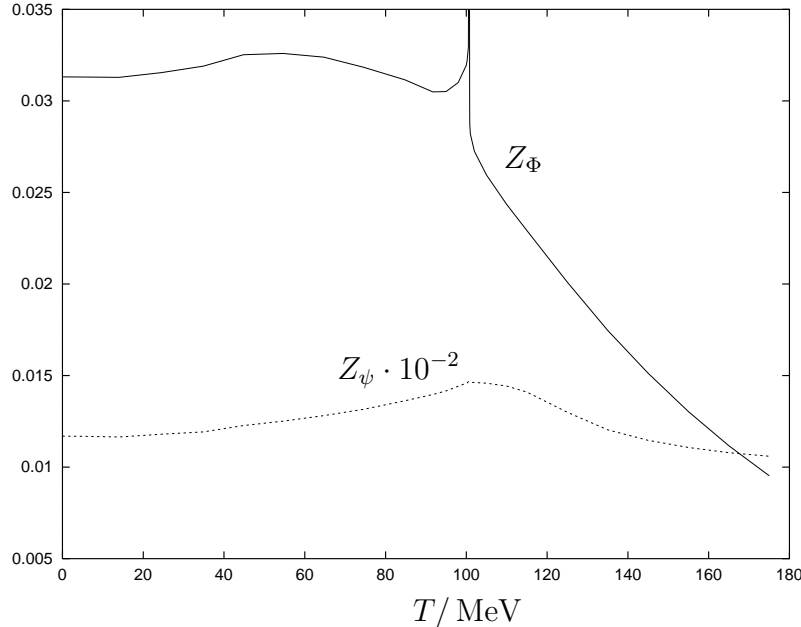


Figure 28: The plot shows the scalar (solid line) and quark (dashed line) wave function renormalization constants, $Z_\Phi(T)$ and $Z_\psi(T) \cdot 10^{-2}$, respectively, as functions of temperature T for $\hat{m} = 0$.

$Z_\Phi(T) \equiv Z_{\Phi,k=0}(T)$ which is displayed in figure 28. There we also present the temperature dependence of the fermionic wave function renormalization $Z_\psi(T) \equiv Z_{\psi,k=0}(T)$. Away from the chiral limit we take the effective quark mass dependence of $h_k(T)$, $Z_{\Phi,k}(T)$ and $Z_{\psi,k}(T)$ into account by stopping their evolution when k reaches the temperature dependent pion mass. In this way we observe no substantial quark mass dependence of these quantities except for $Z_\Phi(T)$, and consequently for $h(T)$, in the vicinity of the critical temperature. A more complete truncation would incorporate field dependent wave function renormalization constants and a field dependent Yukawa coupling.

Our ability to compute the complete temperature dependent effective meson potential U is demonstrated in fig. 29 where we display the derivative of the potential with respect to the renormalized field $\phi_R = (Z_\Phi \rho / 2)^{1/2}$, for different values of T . The curves cover a temperature range $T = (5-175)$ MeV. The first one to the left corresponds to $T = 175$ MeV and neighboring curves differ in temperature by $\Delta T = 10$ MeV. One observes only a weak dependence of $\partial U(T) / \partial \phi_R$ on the temperature for $T \lesssim 60$ MeV. Evaluated for $\phi_R = \sigma_0$ this function connects the renormalized field expectation value with $m_\pi(T)$, the source j and the mesonic wave function renormalization $Z_\Phi(T)$ according to

$$\frac{\partial U(T)}{\partial \phi_R}(\phi_R = \sigma_0) = \frac{2j}{Z_\Phi^{1/2}(T)} = 4\sigma_0(T)m_\pi^2(T). \quad (5.34)$$

We close this section with a short assessment of the validity of our effective quark meson model as an effective description of two flavor QCD at non-vanishing temperature. The identification of qualitatively different scale intervals which appear in the context of

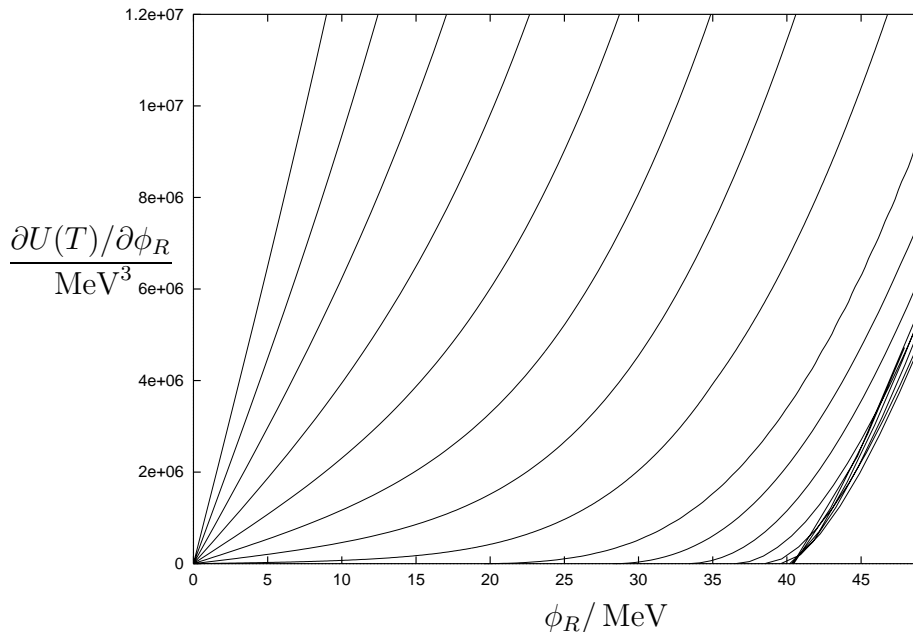


Figure 29: The plot shows the derivative of the meson potential $U(T)$ with respect to the renormalized field $\phi_R = (Z_\Phi \rho/2)^{1/2}$ for different values of T . The first curve on the left corresponds to $T = 175$ MeV. The successive curves to the right differ in temperature by $\Delta T = 10$ MeV down to $T = 5$ MeV.

chiral symmetry breaking, as presented in section 5.3 for the zero temperature case, can be generalized to $T \neq 0$: For scales below k_Φ there exists a hybrid description in terms of quarks and mesons. For $k_{\chi_{SB}} \leq k \lesssim 600$ MeV chiral symmetry remains unbroken where the symmetry breaking scale $k_{\chi_{SB}}(T)$ decreases with increasing temperature. Also the constituent quark mass decreases with T (cf. figure 26). The running Yukawa coupling depends only mildly on temperature for $T \lesssim 120$ MeV (see fig. 27). (Only near the critical temperature and for $\hat{m} = 0$ the running is extended because of massless pion fluctuations.) On the other hand, for $k \lesssim 4T$ the effective three-dimensional gauge coupling increases faster than at $T = 0$ leading to an increase of $\Lambda_{\text{QCD}}(T)$ with T [17]. As k gets closer to the scale $\Lambda_{\text{QCD}}(T)$ it is no longer justified to neglect in the quark sector confinement effects which go beyond the dynamics of our present quark meson model. Here it is important to note that the quarks remain quantitatively relevant for the evolution of the meson degrees of freedom only for scales $k \gtrsim T/0.6$ (cf. fig. 21, section 5.5). In the limit $k \ll T/0.6$ all fermionic Matsubara modes decouple from the evolution of the meson potential according to the temperature dependent version of eq. (5.13). Possible sizeable confinement corrections to the meson physics may occur if $\Lambda_{\text{QCD}}(T)$ becomes larger than the maximum of $M_q(T)$ and $T/0.6$. From fig. 26 we infer that this is particularly dangerous for small \hat{m} in a temperature interval around T_c . Nevertheless, the situation is not dramatically different from the zero temperature case since only a relatively small range of k is concerned. We do not expect that the neglected QCD non-localities lead to qualitative changes. Quantitative modifications, especially for small \hat{m} and $|T - T_c|$ remain possible. This would only effect the non-universal amplitudes (see sect. 5.7). The size of these corrections depends on the

strength of (non–local) deviations of the quark propagator and the Yukawa coupling from the values computed in the quark meson model.

5.7 Universal critical equation of state

In this section we study the linear quark meson model in the vicinity of the critical temperature T_c close to the chiral limit $\hat{m} = 0$. In this region we find that the sigma mass m_σ^{-1} is much larger than the inverse temperature T^{-1} , and one observes an effectively three–dimensional behavior of the high temperature quantum field theory. We also note that the fermions are no longer present in the dimensionally reduced system as has been discussed in section 5.5. We therefore have to deal with a purely bosonic $O(4)$ –symmetric linear sigma model. At the phase transition the correlation length becomes infinite and the effective three–dimensional theory is dominated by classical statistical fluctuations. In particular, the critical exponents which describe the singular behavior of various quantities near the second order phase transition are those of the corresponding classical system.

Many properties of this system are universal, i.e. they only depend on its symmetry ($O(4)$), the dimensionality of space (three) and its degrees of freedom (four real scalar components). Universality means that the long–range properties of the system do not depend on the details of the specific model like its short distance interactions. Nevertheless, important properties as the value of the critical temperature are non–universal. We emphasize that although we have to deal with an effectively three–dimensional bosonic theory, the non–universal properties of the system crucially depend on the details of the four–dimensional theory and, in particular, on the fermions.

Our aim is a computation of the critical equation of state which relates for arbitrary T near T_c the derivative of the free energy or effective potential U to the average current quark mass \hat{m} . The equation of state then permits to study the temperature and quark mass dependence of properties of the chiral phase transition.

At the critical temperature and in the chiral limit there is no scale present in the theory. In the vicinity of T_c and for small enough \hat{m} one therefore expects a scaling behavior of the effective average potential u_k [92] and accordingly a universal scaling form of the equation of state (cf. section 3.3). There are only two independent scales close to the transition point which can be related to the deviation from the critical temperature, $T - T_c$, and to the explicit symmetry breaking through the quark mass \hat{m} . As a consequence, the properly rescaled potential can only depend on one scaling variable. A possible choice for the parameterization of the rescaled “unrenormalized” potential is the use of the Widom scaling variable [88]

$$x = \frac{(T - T_c)/T_c}{(2\bar{\sigma}_0/T_c)^{1/\beta}}. \quad (5.35)$$

Here β is the critical exponent of the order parameter $\bar{\sigma}_0$ in the chiral limit $\hat{m} = 0$ (see equation (5.39)). With $U'(\rho = 2\bar{\sigma}_0^2) = j/(2\bar{\sigma}_0)$ the Widom scaling form of the equation of

state reads [88]

$$\frac{j}{T_c^3} = \left(\frac{2\bar{\sigma}_0}{T_c} \right)^\delta f(x) \quad (5.36)$$

where the exponent δ is related to the behavior of the order parameter according to (5.41). The equation of state (5.36) is written for convenience directly in terms of four-dimensional quantities. They are related to the corresponding effective variables of the three-dimensional theory by appropriate powers of T_c . The source j is determined by the average current quark mass \hat{m} as $j = 2\bar{m}_{k_\Phi}^2 \hat{m}$. The mass term at the compositeness scale, $\bar{m}_{k_\Phi}^2$, also relates the chiral condensate to the order parameter according to $\langle \bar{\psi}\psi \rangle = -2\bar{m}_{k_\Phi}^2 (\bar{\sigma}_0 - \hat{m})$. The critical temperature of the linear quark meson model was found in section 5.6 to be $T_c = 100.7 \text{ MeV}$.

The scaling function f is universal up to the model specific normalization of x and itself. Accordingly, all models in the same universality class can be related by a rescaling of $\bar{\sigma}_0$ and $T - T_c$. The non-universal normalizations for the quark meson model discussed here are defined according to

$$f(0) = D \quad , \quad f(-B^{-1/\beta}) = 0 \quad (5.37)$$

We find $D = 1.82 \cdot 10^{-4}$, $B = 7.41$ and our result for β is given in table 8. Apart from the immediate vicinity of the zero of $f(x)$ we find the following two parameter fit (cf. section 3.3) for the scaling function,

$$f_{\text{fit}}(x) = 1.816 \cdot 10^{-4} (1 + 136.1 x)^2 (1 + 160.9 \theta x)^\Delta (1 + 160.9 (0.9446 \theta^\Delta)^{-1/(\gamma-2-\Delta)} x)^{\gamma-2-\Delta} \quad (5.38)$$

to reproduce the numerical results for f and df/dx at the 1–2% level with $\theta = 0.625$ (0.656), $\Delta = -0.490$ (–0.550) for $x > 0$ ($x < 0$) and γ as given in table 8. The universal properties of the scaling function can be compared with results obtained by other methods for the three-dimensional $O(4)$ Heisenberg model. In figure 30 we display our results along with those obtained from lattice Monte Carlo simulation [61], second order epsilon expansion [60] and mean field theory. We observe a good agreement of average action, lattice and epsilon expansion results within a few per cent for $T < T_c$. Above T_c the average action and the lattice curve go quite close to each other with a substantial deviation from the epsilon expansion and mean field scaling function⁴⁴.

Before we use the scaling function $f(x)$ to discuss the general temperature and quark mass dependent case, we consider the limits $T = T_c$ and $\hat{m} = 0$, respectively. In these limits the behavior of the various quantities is determined solely by critical amplitudes and exponents. In the spontaneously broken phase ($T < T_c$) and in the chiral limit we observe

⁴⁴We note that the question of a better agreement of the curves for $T < T_c$ or $T > T_c$ depends on the chosen non-universal normalization conditions for x and f (cf. eq. (5.37)).

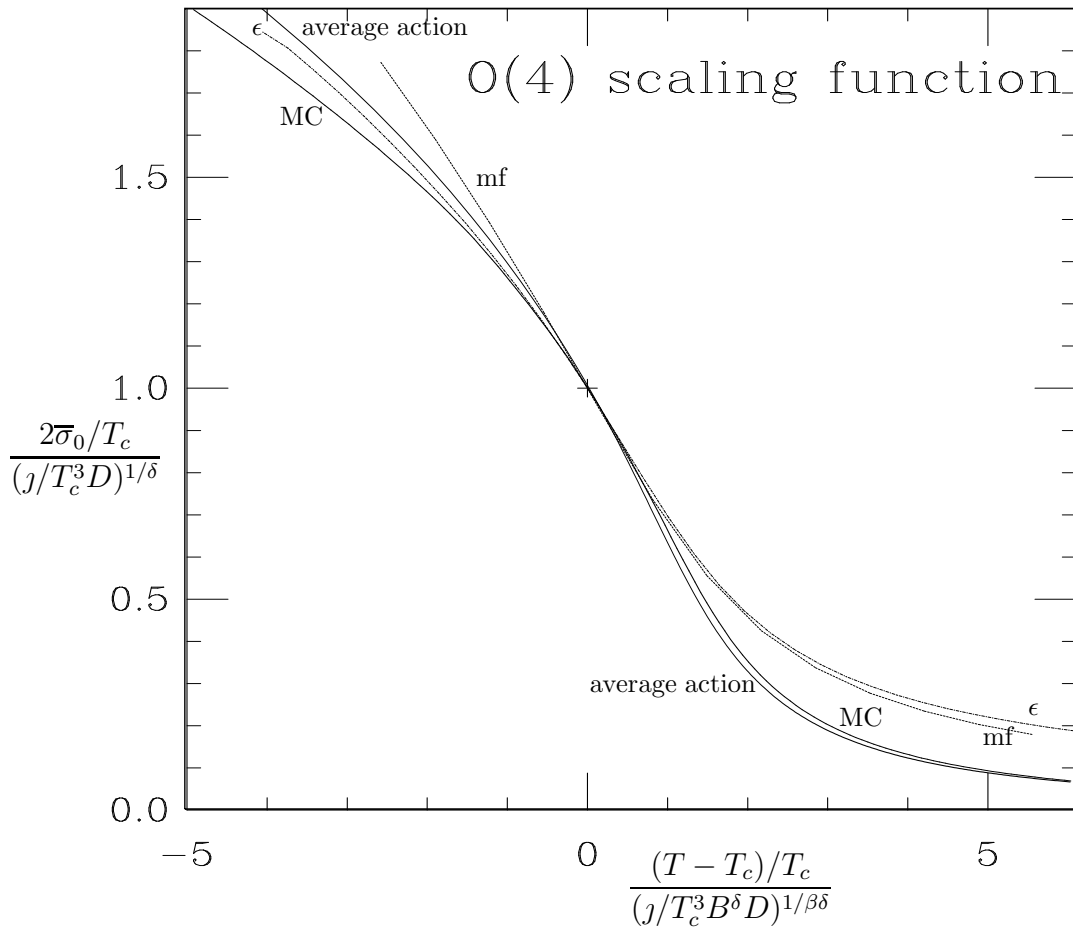


Figure 30: The figure shows a comparison of our results, denoted by “average action”, with results of other methods for the scaling function of the three-dimensional $O(4)$ Heisenberg model. We have labeled the axes for convenience in terms of the expectation value $\bar{\sigma}_0$ and the source j of the corresponding four-dimensional theory. The constants B and D specify the non-universal amplitudes of the model (cf. eq. 5.37). The curve labeled by “MC” represents a fit to lattice Monte Carlo data. The second order epsilon expansion [60] and mean field results are denoted by “ ϵ ” and “mf”, respectively. Apart from our results the curves are taken from ref. [61].

	ν	γ	δ	β	η
average action	0.787	1.548	4.80	0.407	0.0344
FD	0.73(2)	1.44(4)	4.82(5)	0.38(1)	0.03(1)
MC	0.7479(90)	1.477(18)	4.851(22)	0.3836(46)	0.0254(38)

Table 8: The table shows the critical exponents corresponding to the three-dimensional $O(4)$ -Heisenberg model. Our results are denoted by “average action” whereas “FD” labels the exponents obtained from perturbation series at fixed dimension to seven loops [98]. The bottom line contains lattice Monte Carlo results [129].

that the renormalized and unrenormalized order parameters scale according to

$$\begin{aligned}\frac{2\sigma_0(T)}{T_c} &= (2E)^{1/2} \left(\frac{T_c - T}{T_c}\right)^{\nu/2}, \\ \frac{2\bar{\sigma}_0(T)}{T_c} &= B \left(\frac{T_c - T}{T_c}\right)^\beta,\end{aligned}\tag{5.39}$$

respectively, with $E = 0.814$ and the value of B given above. In the symmetric phase the renormalized mass $m = m_\pi = m_\sigma$ and the unrenormalized mass $\bar{m} = Z_\Phi^{1/2} m$ behave as

$$\begin{aligned}\frac{m(T)}{T_c} &= (\xi^+)^{-1} \left(\frac{T - T_c}{T_c}\right)^\nu, \\ \frac{\bar{m}(T)}{T_c} &= (C^+)^{-1/2} \left(\frac{T - T_c}{T_c}\right)^{\gamma/2},\end{aligned}\tag{5.40}$$

where $\xi^+ = 0.270$, $C^+ = 2.79$. For $T = T_c$ and non-vanishing current quark mass we have

$$\frac{2\bar{\sigma}_0}{T_c} = D^{-1/\delta} \left(\frac{J}{T_c^3}\right)^{1/\delta}\tag{5.41}$$

with the value of D given above.

Though the five amplitudes E , B , ξ^+ , C^+ and D are not universal there are ratios of amplitudes which are invariant under a rescaling of $\bar{\sigma}_0$ and $T - T_c$. Our results for the universal amplitude ratios are

$$\begin{aligned}R_\chi &= C^+ D B^{\delta-1} = 1.02, \\ \tilde{R}_\xi &= (\xi^+)^{\beta/\nu} D^{1/(\delta+1)} B = 0.852, \\ \xi^+ E &= 0.220.\end{aligned}\tag{5.42}$$

Those for the critical exponents are given in table 8. Here the value of η is obtained from the temperature dependent version of eq. (5.18) (cf. appendix B) at the critical

temperature. For comparison table 8 also gives the results from perturbation series at fixed dimension to seven-loop order [98, 67] as well as lattice Monte Carlo results [129] which have been used for the lattice form of the scaling function in fig. 30.⁴⁵ There are only two independent amplitudes and critical exponents, respectively. They are related by the usual scaling relations of the three-dimensional scalar $O(N)$ -model [67] which we have explicitly verified by the independent calculation of our exponents.

We turn to the discussion of the scaling behavior of the chiral condensate $\langle \bar{\psi}\psi \rangle$ for the general case of a temperature and quark mass dependence. In figure 17 in the introduction we have displayed our results for the scaling equation of state in terms of the chiral condensate⁴⁶

$$\langle \bar{\psi}\psi \rangle = -\bar{m}_{k_\Phi}^2 T_c \left(\frac{j/T_c^3}{f(x)} \right)^{1/\delta} + j \quad (5.43)$$

as a function of $T/T_c = 1 + x(j/T_c^3 f(x))^{1/\beta\delta}$ for different quark masses or, equivalently, different values of j . The curves shown in figure 17 correspond to quark masses $\hat{m} = 0$, $\hat{m} = \hat{m}_{\text{phys}}/10$, $\hat{m} = \hat{m}_{\text{phys}}$ and $\hat{m} = 3.5\hat{m}_{\text{phys}}$ or, equivalently, to zero temperature pion masses $m_\pi = 0$, $m_\pi = 45$ MeV, $m_\pi = 135$ MeV and $m_\pi = 230$ MeV, respectively (cf. figure 20). One observes that the second order phase transition with a vanishing order parameter at T_c for $\hat{m} = 0$ is turned into a smooth crossover in the presence of non-zero quark masses.

The scaling form (5.43) for the chiral condensate is exact only in the limit $T \rightarrow T_c$, $j \rightarrow 0$. It is interesting to find the range of temperatures and quark masses for which $\langle \bar{\psi}\psi \rangle$ approximately shows the scaling behavior (5.43). This can be inferred from a comparison (see fig. 17) with our full non-universal solution for the T and j dependence of $\langle \bar{\psi}\psi \rangle$ as described in section 5.6. For $m_\pi = 0$ one observes approximate scaling behavior for temperatures $T \gtrsim 90$ MeV. This situation persists up to a pion mass of $m_\pi = 45$ MeV. Even for the realistic case, $m_\pi = 135$ MeV, and to a somewhat lesser extent for $m_\pi = 230$ MeV the scaling curve reasonably reflects the physical behavior for $T \gtrsim T_c$. For temperatures below T_c , however, the zero temperature mass scales become important and the scaling arguments leading to universality break down.

The above comparison may help to shed some light on the use of universality arguments away from the critical temperature and the chiral limit. One observes that for temperatures above T_c the scaling assumption leads to quantitatively reasonable results even for a pion mass almost twice as large as the physical value. This in turn has been used for two flavor lattice QCD as theoretical input to guide extrapolation of results to light current quark masses. From simulations based on a range of pion masses $0.3 \lesssim m_\pi/m_\rho \lesssim 0.7$ and temperatures $0 < T \lesssim 250$ MeV a “pseudocritical temperature” of approximately 140 MeV with a weak quark mass dependence is reported [36]. Here the “pseudocritical temperature” T_{pc} is defined as the inflection point of $\langle \bar{\psi}\psi \rangle$ as a function of temperature. The values of

⁴⁵See also ref. [95] and references therein for a recent calculation of critical exponents using similar methods as in this work. For high precision estimates of the critical exponents see also ref. [89, 90].

⁴⁶In the literature also a different definition of the chiral condensate is used, corresponding to $\langle \bar{\psi}\psi \rangle = -\bar{m}_{k_\Phi}^2 T_c [j/(T_c^3 f(x))]^{1/\delta}$.

the lattice action parameters used in [36] with $N_t = 6$ were $a\hat{m} = 0.0125$, $6/g^2 = 5.415$ and $a\hat{m} = 0.025$, $6/g^2 = 5.445$. For comparison with lattice data we have displayed in figure 17 the temperature dependence of the chiral condensate for a pion mass $m_\pi = 230$ MeV. From the free energy of the linear quark meson model we obtain in this case a pseudocritical temperature of about 150 MeV in reasonable agreement with the results of ref. [36]. In contrast, for the critical temperature in the chiral limit we obtain $T_c = 100.7$ MeV. This value is considerably smaller than the lattice results of about (140 – 150) MeV obtained by extrapolating to zero quark mass in ref. [36]. We point out that for pion masses as large as 230 MeV the condensate $\langle\bar{\psi}\psi\rangle(T)$ is almost linear around the inflection point for quite a large range of temperature. This makes a precise determination of T_c somewhat difficult. Furthermore, figure 17 shows that the scaling form of $\langle\bar{\psi}\psi\rangle(T)$ underestimates the slope of the physical curve. Used as a fit with T_c as a parameter this can lead to an overestimate of the pseudocritical temperature in the chiral limit. We also mention here the results of ref. [130]. There two values of the pseudocritical temperature, $T_{pc} = 150(9)$ MeV and $T_{pc} = 140(8)$, corresponding to $a\hat{m} = 0.0125$, $6/g^2 = 5.54(2)$ and $a\hat{m} = 0.00625$, $6/g^2 = 5.49(2)$, respectively, (both for $N_t = 8$) were computed. These values show a somewhat stronger quark mass dependence of T_{pc} and were used for a linear extrapolation to the chiral limit yielding $T_c = 128(9)$ MeV.

The linear quark meson model exhibits a second order phase transition for two quark flavors in the chiral limit. As a consequence the model predicts a scaling behavior near the critical temperature and the chiral limit which can, in principle, be tested in lattice simulations. For the quark masses used in the present lattice studies the order and universality class of the transition in two flavor QCD remain a partially open question. Though there are results from the lattice giving support for critical scaling [131, 132] there are also recent simulations with two flavors that reveal significant finite size effects and problems with $O(4)$ scaling [133, 134].

5.8 Conclusions

So far we have investigated the chiral phase transition of QCD as described by the linear $O(4)$ -model containing the three pions and the sigma resonance as well as the up and down quarks as degrees of freedom. Of course, it is clear that the spectrum of QCD is much richer than the states incorporated in our model. It is therefore important to ask to what extent the neglected degrees of freedom like the strange quark, strange (pseudo)scalar mesons, (axial)vector mesons, baryons, etc., might be important for the chiral dynamics of QCD. Before doing so it is perhaps instructive to first look into the opposite direction and investigate the difference between the linear quark meson model described here and chiral perturbation theory based on the non-linear sigma model [3]. In some sense, chiral perturbation theory is the minimal model of chiral symmetry breaking containing only the Goldstone degrees of freedom. By construction it is therefore only valid in the spontaneously broken phase and can not be expected to yield realistic results for temperatures close to T_c or for the symmetric phase. However, for small temperatures (and momentum scales) the non-linear model is expected to describe the low-energy and low-temperature

limit of QCD reliably as an expansion in powers of the light quark masses. For vanishing temperature it has been demonstrated recently [6, 7] that the results of chiral perturbation theory can be reproduced within the linear meson model once certain higher dimensional operators in its effective action are taken into account for the three flavor case. Moreover, some of the parameters of chiral perturbation theory (L_4, \dots, L_8) can be expressed and therefore also numerically computed in terms of those of the linear model. For non-vanishing temperature one expects agreement only for low T whereas deviations from chiral perturbation theory should become large close to T_c . Yet, even for $T \ll T_c$ small quantitative deviations should exist because of the contributions of (constituent) quark and sigma meson fluctuations in the linear model which are not taken into account in chiral perturbation theory.

From [135] we infer the three-loop result for the temperature dependence of the chiral condensate in the chiral limit for N light flavors

$$\begin{aligned} \langle \bar{\psi}\psi \rangle(T)_{\chi PT} &= \langle \bar{\psi}\psi \rangle_{\chi PT}(0) \left\{ 1 - \frac{N^2 - 1}{N} \frac{T^2}{12F_0^2} - \frac{N^2 - 1}{2N^2} \left(\frac{T^2}{12F_0^2} \right)^2 \right. \\ &\quad \left. + N(N^2 - 1) \left(\frac{T^2}{12F_0^2} \right)^3 \ln \frac{T}{\Gamma_1} \right\} + \mathcal{O}(T^8). \end{aligned} \quad (5.44)$$

The scale Γ_1 can be determined from the D -wave isospin zero $\pi\pi$ scattering length and is given by $\Gamma_1 = (470 \pm 100)$ MeV. The constant F_0 is (in the chiral limit) identical to the pion decay constant $F_0 = f_\pi^{(0)} = 80.8$ MeV. In figure 31 we have plotted the chiral condensate as a function of T/F_0 for both, chiral perturbation theory according to (5.44) and for the linear quark meson model. As expected the agreement for small T is very good. Nevertheless, the anticipated small numerical deviations present even for $T \ll T_c$ due to quark and sigma meson loop contributions are manifest. For larger values of T , say for $T \gtrsim 0.8f_\pi^{(0)}$ the deviations become significant because of the intrinsic inability of chiral perturbation theory to correctly reproduce the critical behavior of the system near its second order phase transition.

Within the language of chiral perturbation theory the neglected effects of thermal quark fluctuations may be described by an effective temperature dependence of the parameter $F_0(T)$. We notice that the temperature at which these corrections become important equals approximately one third of the constituent quark mass $M_q(T)$ or the sigma mass $m_\sigma(T)$, respectively, in perfect agreement with fig. 21. As suggested by this figure the onset of the effects from thermal fluctuations of heavy particles with a T -dependent mass $m_H(T)$ is rather sudden for $T \gtrsim m_H(T)/3$. These considerations also apply to our two flavor quark meson model. Within full QCD we expect temperature dependent initial values at k_Φ .

The dominant contribution to the temperature dependence of the initial values presumably arises from the influence of the mesons containing strange quarks as well as the strange quark itself. Here the quantity $\bar{m}_{k_\Phi}^2$ seems to be the most important one. (The temperature dependence of higher couplings like $\lambda(T)$ is not very relevant if the IR attractive behavior remains valid, i.e. if Z_{Φ, k_Φ} remains small for the range of temperatures considered. We

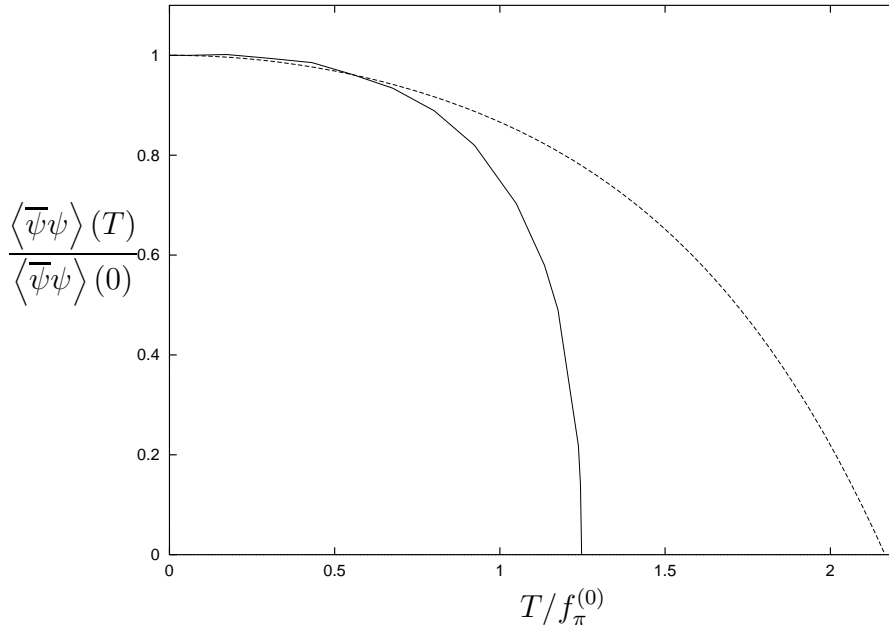


Figure 31: The plot displays the chiral condensate $\langle \bar{\psi}\psi \rangle$ as a function of $T/f_\pi^{(0)}$. The solid line corresponds to our results for vanishing average current quark mass $\hat{m} = 0$ whereas the dashed line shows the corresponding three-loop chiral perturbation theory result for $\Gamma_1 = 470 \text{ MeV}$.

neglect a possible T -dependence of the current quark mass \hat{m} .) In particular, for three flavors the potential U_{k_Φ} contains a term

$$-\frac{1}{2}\bar{\nu}_{k_\Phi} \left(\det \Phi + \det \Phi^\dagger \right) = -\bar{\nu}_{k_\Phi} \varphi_s \Phi_{uu} \Phi_{dd} + \dots \quad (5.45)$$

which reflects the axial $U_A(1)$ anomaly. It yields a contribution to the effective mass term proportional to the expectation value $\langle \Phi_{ss} \rangle \equiv \varphi_s$, i.e.

$$\Delta \bar{m}_{k_\Phi}^2 = -\frac{1}{2}\bar{\nu}_{k_\Phi} \varphi_s. \quad (5.46)$$

Both, $\bar{\nu}_{k_\Phi}$ and φ_s , depend on T . We expect these corrections to become relevant only for temperatures exceeding $m_K(T)/3$ or $M_s(T)/3$. We note that the temperature dependent kaon and strange quark masses, $m_K(T)$ and $M_s(T)$, respectively, may be somewhat different from their zero temperature values but we do not expect them to be much smaller. A typical value for these scales is around 500 MeV. Correspondingly, the thermal fluctuations neglected in our model should become important for $T \gtrsim 170 \text{ MeV}$. It is even conceivable that a discontinuity appears in $\varphi_s(T)$ for sufficiently high T (say $T \simeq 170 \text{ MeV}$). This would be reflected by a discontinuity in the initial values of the $O(4)$ -model leading to a first order transition within this model. Obviously, these questions should be addressed in the framework of the three flavor $SU_L(3) \times SU_R(3)$ quark meson model. Work in this direction is in progress.

We note that the temperature dependence of $\bar{\nu}(T)\varphi_s(T)$ is closely related to the question of an effective high temperature restoration of the axial $U_A(1)$ symmetry [31, 32]. The η'

mass term is directly proportional to this combination, $m_{\eta'}^2(T) - m_\pi^2(T) \simeq \frac{3}{2}\overline{\nu}(T)\varphi_s(T)$ [104]. Approximate $U_A(1)$ restoration would occur if $\varphi_s(T)$ or $\overline{\nu}(T)$ would decrease sizeable for large T . For realistic QCD this question should be addressed by a three flavor study. Within two flavor QCD the combination $\overline{\nu}_k\varphi_s$ is replaced by an effective anomalous mass term $\overline{\nu}_k^{(2)}$. The temperature dependence of $\overline{\nu}^{(2)}(T)$ could be studied by introducing quarks and the axial anomaly in the two flavor matrix model of ref. [68]. We add that this question has also been studied within full two flavor QCD in lattice simulations [133, 136, 137]. So far there does not seem to be much evidence for a restoration of the $U_A(1)$ symmetry near T_c but no final conclusion can be drawn yet.

To summarize, we have found that the effective two flavor quark meson model presumably gives a good description of the temperature effects in two flavor QCD for a temperature range $T \lesssim 170$ MeV. Its reliability should be best for low temperature where our results agree with chiral perturbation theory. However, the range of validity is considerably extended as compared to chiral perturbation theory and includes, in particular, the critical temperature of the second order phase transition in the chiral limit. We have explicitly connected the universal critical behavior for small $|T - T_c|$ and small current quark masses with the renormalized couplings at $T = 0$ and realistic quark masses. The main quantitative uncertainties from neglected fluctuations presumably concern the values of $f_\pi^{(0)}$ and T_c which, in turn, influence the non-universal amplitudes B and D in the critical region. We believe that our overall picture is rather solid. Where applicable our results compare well with numerical simulations of full two flavor QCD.

6 Outlook

The use of non-perturbative flow equations within the framework of the effective average action provides a practical means for non-perturbative studies within a field theoretic context. In this work its application culminated in the computation of the equation of state for two flavor QCD within the effective quark meson model. In particular, the method is free of infrared divergences and allows a precise description of critical phenomena in high temperature quantum field theory or in statistical physics.

It is a valuable merit of the approach presented in this work to yield directly the whole equation of state of the theory under investigation. We have given a detailed quantitative picture of the non-analytic properties of the effective potential or the free energy for second order phase transitions. We have demonstrated that along the lines presented in section 4 also the universal equation of state for weak first order phase transitions can be reliably computed. Furthermore, for $k > 0$ the effective average action realizes the concept of a coarse grained free energy. We, therefore, were able to extract quantities like the “classical” interface tension used in the standard approach to phase conversion by spontaneous bubble nucleation.

Apart from their phenomenological relevance and their intrinsic appeal, critical phenomena also provide a severe test for the reliability of a non-perturbative method. The present level of truncation used in this work is based on a lowest order derivative expansion and the most general potential term⁴⁷. Where available we observe agreement with recent lattice results for the critical equation of state within a few per cent accuracy. So far the main drawback of the method is a precise error estimate which is a natural difficulty in a non-perturbative calculation with couplings that cannot be considered as small. However, the structure of the exact flow equation (2.10) is of considerable help in this context. For instance, for the $O(N)$ symmetric N -component model one easily verifies that the ansatz (cf. section 3 for notation)

$$\Gamma_k = \int d^d x \left\{ U_k(\rho) + \frac{1}{2} \partial^\mu \phi_a Z_k(\rho, -\partial^\nu \partial_\nu) \partial_\mu \phi^a + \frac{1}{4} \partial^\mu \rho Y_k(\rho, -\partial^\nu \partial_\nu) \partial_\mu \rho \right\}. \quad (6.1)$$

contains the most general terms which contribute to $\Gamma_k^{(2)}$ when evaluated for a constant background field [92]. With the above ansatz one therefore obtains an exact flow equation for the effective average potential U_k containing the unknown functions $Z_k(\rho, q^2)$ and $Y_k(\rho, q^2)$, which play the role of field and momentum dependent wave function renormalization constants. Knowledge of these functions would yield an exact critical equation of state from the solution of the flow equation for U_k . These functions involve, however, more complicated momentum dependences of $1PI$ vertices with three or four legs with non-vanishing momenta. Along the lines presented in section 3 recent calculations for the critical equation of state ($N = 1$) have been successively extended to include a wave function renormalization with a most general field dependence⁴⁸ [96]. These results seem

⁴⁷For the scalar matrix models discussed in section 4 we kept the most general form of the potential only for the relevant ρ dependence.

⁴⁸For $N = 1$ the Y_k term is absent.

to improve the exponents and the equation of state within the expected accuracy of a few per cent. In conjunction with the smallness of the anomalous dimension ($\eta \simeq 0.04$) one is lead to expect only small corrections from the momentum dependence of the wave function renormalization. A crucial test for the stability of the results would be to change a given parameterization of the momentum dependence of the wave function renormalization in a reasonable range⁴⁹. In this way we hope to obtain reliable error estimates for the critical equation of state, critical exponents etc.

We also note that the approach is valid for arbitrary dimensions d . All evolution equations presented in this work are formulated for general d . In particular, two dimensional field theories can be treated with this method. This allows, e.g., the comparison with known exact results. We have calculated the critical properties for the two dimensional $O(N)$ model in the “replica limit” [138] $N \rightarrow 0$, which describes the critical swelling of long polymer chains in two space dimensions [139]. For instance, we find the exponent ν (cf. section 3) to be given by $\nu = 0.782$ [140] in the two dimensional model which compares rather well to the exact result $\nu_{(\text{exact})} = 0.75$ [67]. We also note, e.g., that Gräter and Wetterich [141] have used the effective average action method in two dimensions to describe the Kosterlitz–Thouless phase transition by employing an expansion around the minimum of the effective average potential. The validity of the method for arbitrary dimensions d may also be used to get a deeper insight into the ϵ -expansion approach [56].

The investigation of three dimensional scalar models for complex 2×2 matrices in section 4 can be extended in several directions. The generalization to complex $N \times N$ matrices for arbitrary N is straightforward. This opens the possibility to study the large- N behavior and to compare with $1/N$ -expansions⁵⁰. The most interesting generalizations in the context of chiral symmetry breaking are the systems with reduced $SU(N) \times SU(N)$ symmetry (cf. section 5). Another interesting application concerns Anderson localization. The problem of an electron in a random potential can be mapped onto a field theoretic matrix model with e.g. $U(2N)$ symmetry [101]. To get insight into the involved replica limit in the context of flow equations, we have computed the free energy for the three dimensional $O(N)$ model in the limit $N \rightarrow 0$ [140] (cf. also section 3). Further studies are necessary to ensure the validity of this limit for matrix models within the approach presented in this work.

Of course the approach is not restricted to the study of the universal behavior. The ability of the method to cover both the non-universal properties of the four dimensional theory at low temperature and the universal properties near T_c and the chiral limit has been crucial for the investigation of the QCD chiral phase transition in section 5. We expect our results within the effective quark meson model to give a reliable description of the equation of state for two flavor QCD. The employed method can be generalized to the (more) realistic description including the strange quark. The relevant generalizations

⁴⁹One expects a very mild momentum dependence of $Z_k(\rho = \rho_0, q^2)$ for q^2 between zero and k^2 due to the presence of the infrared cutoff. For $q^2 \gg k^2$ the anomalous dimension should determine the behavior near the transition, $Z_k(\rho = \rho_0, q^2) \sim (q^2)^{-\eta/2}$.

⁵⁰See refs. [142, 143] for a renormalization group study within the large- N limit of hermitean matrix models.

have been outlined in section 5 and the investigation is work in progress [74]. We expect our approach to be very well suited to the non-perturbative investigation of the three flavor case. At non-zero temperature we should be able to reliably answer a number of urging questions, like the order of the phase transition or if one has to deal with a crossover phenomenon. Connected to this, we are well prepared to answer the question of a large scale that could lead to a disoriented chiral condensate (cf. section 1). The three flavor results will also give details about the speculative “effective restoration” of the axial $U_A(1)$ around T_c . If the approximate partial infrared fixed point, which we have observed for the two flavor case, is realized for $N_f = 3$ our equation of state will develop a considerable degree of predictive power. Of course, this concerns also the zero temperature low-energy properties of QCD. In particular, these results will be very interesting for the scalar spectrum which is experimentally not very well understood. Further investigations, extending the description in terms of quarks and the low-lying scalar and pseudoscalar mesons, have to include fields for the lightest vector and pseudovector mesons.

We finally note that a computation of the equation of state within QCD, i.e. as a function of $\alpha_s(1 \text{ GeV})$ and the quark masses, depends on a reliable computation of the scalar mass term $\overline{m}^2(k_\Phi)/k_\Phi^2$ and the Yukawa coupling $h(k_\Phi)$ at the compositeness scale. Integrating out the gluons completely for the determination of the quark meson model at k_Φ is, however, a difficult task. Present investigations in this direction within the QCD framework for the effective average action proposed in ref. [45] confirm the relatively simple ansatz at k_Φ for the resulting quark propagator we have used in section 5 [144].

7 Acknowledgments

I first want to thank C. Wetterich. I gained a lot from discussing and working with him. Our collaboration on the topics presented in this work has been always fruitful and fun. I also want to thank F. Wegner for his continuous interest and for his substantial influence on the statistical physics aspects of this work. I have considerably profited from the joined Graduate College of the high energy physics and the statistical physics department of the ITP. I also want to thank D. Jungnickel for many valuable discussions and for collaborating on the QCD chiral phase transition. I am grateful to N. Tetradis for his collaboration on the scaling equation of state and on the coarse grained free energy. In addition I thank J. Adams, S. Bornholdt and F. Freire for their co-operation on numerics. I also thank M. Gräter for many discussions on matrix models. I would like to express my gratitude to all people at the ITP for providing a most stimulating environment.

A Threshold functions

In this appendix we list the various definitions of dimensionless threshold functions appearing in the flow equations and the expressions for the anomalous dimensions for $T = 0$. They involve the inverse scalar average propagator⁵¹ $P(q)$

$$P(q) = \frac{q^2}{1 - \exp\left\{-\frac{q^2}{k^2}\right\}} \quad (\text{A.1})$$

and the corresponding fermionic function P_F which can be chosen as [46]

$$P_F(q) = P(q) \equiv q^2 (1 + r_F(q))^2 . \quad (\text{A.2})$$

We abbreviate

$$x = q^2 , \quad P(x) \equiv P(q) , \quad \dot{P}(x) \equiv \frac{\partial}{\partial x} P(x) , \quad \widehat{\partial} \dot{P} \equiv \frac{\partial}{\partial x} \frac{\widehat{\partial}}{\partial t} P , \quad (\text{A.3})$$

etc., and use the formal definition

$$\frac{\widehat{\partial}}{\partial t} \equiv \frac{1}{Z_{\Phi,k}} \frac{\partial R_k}{\partial t} \frac{\partial}{\partial P} + \frac{2}{Z_{\psi,k}} \frac{P_F}{1 + r_F} \frac{\partial [Z_{\psi,k} r_F]}{\partial t} \frac{\partial}{\partial P_F} . \quad (\text{A.4})$$

The bosonic threshold functions read

$$\begin{aligned} l_n^d(w; \eta_\Phi) &= l_n^d(w) - \eta_\Phi \widehat{l}_n^d(w) \\ &= \frac{n + \delta_{n,0}}{2} k^{2n-d} \int_0^\infty dx x^{\frac{d}{2}-1} \left(\frac{1}{Z_{\Phi,k}} \frac{\partial R_k}{\partial t} \right) (P + wk^2)^{-(n+1)} \\ l_{n_1, n_2}^d(w_1, w_2; \eta_\Phi) &= l_{n_1, n_2}^d(w_1, w_2) - \eta_\Phi \widehat{l}_{n_1, n_2}^d(w_1, w_2) \\ &= -\frac{1}{2} k^{2(n_1+n_2)-d} \int_0^\infty dx x^{\frac{d}{2}-1} \frac{\widehat{\partial}}{\partial t} \left\{ (P + w_1 k^2)^{-n_1} (P + w_2 k^2)^{-n_2} \right\} \end{aligned} \quad (\text{A.5})$$

where $n, n_1, n_2 \geq 0$ is assumed. For $n \neq 0$ the functions l_n^d may also be written as

$$l_n^d(w; \eta_\Phi) = -\frac{1}{2} k^{2n-d} \int_0^\infty dx x^{\frac{d}{2}-1} \frac{\widehat{\partial}}{\partial t} (P + wk^2)^{-n} . \quad (\text{A.6})$$

The fermionic integrals $l_n^{(F)d}(w; \eta_\psi) = l_n^{(F)d}(w) - \eta_\psi \check{l}_n^{(F)d}(w)$ are defined analogously as

$$l_n^{(F)d}(w; \eta_\psi) = (n + \delta_{n,0}) k^{2n-d} \int_0^\infty dx x^{\frac{d}{2}-1} \frac{1}{Z_{\psi,k}} \frac{P_F}{1 + r_F} \frac{\partial [Z_{\psi,k} r_F]}{\partial t} (P + wk^2)^{-(n+1)} . \quad (\text{A.7})$$

⁵¹We note that the definition of $P_k(q)$ in section 4.4 obtains from the definition used here by a rescaling with the factor Z_k .

Furthermore one has

$$\begin{aligned}
l_{n_1, n_2}^{(FB)d}(w_1, w_2; \eta_\psi, \eta_\Phi) &= l_{n_1, n_2}^{(FB)d}(w_1, w_2) - \eta_\psi \check{l}_{n_1, n_2}^{(FB)d}(w_1, w_2) - \eta_\Phi \hat{l}_{n_1, n_2}^{(FB)d}(w_1, w_2) \\
&= -\frac{1}{2} k^{2(n_1+n_2)-d} \int_0^\infty dx x^{\frac{d}{2}-1} \widehat{\partial} \left\{ \frac{1}{[P_F(x) + k^2 w_1]^{n_1} [P(x) + k^2 w_2]^{n_2}} \right\} \\
m_{n_1, n_2}^d(w_1, w_2; \eta_\Phi) &\equiv m_{n_1, n_2}^d(w_1, w_2) - \eta_\Phi \hat{m}_{n_1, n_2}^d(w_1, w_2) \\
&= -\frac{1}{2} k^{2(n_1+n_2-1)-d} \int_0^\infty dx x^{\frac{d}{2}} \widehat{\partial} \left\{ \frac{\dot{P}(x)}{[P(x) + k^2 w_1]^{n_1}} \frac{\dot{P}(x)}{[P(x) + k^2 w_2]^{n_2}} \right\} \\
m_4^{(F)d}(w; \eta_\psi) &= m_4^{(F)d}(w) - \eta_\psi \check{m}_4^{(F)d}(w) \\
&= -\frac{1}{2} k^{4-d} \int_0^\infty dx x^{\frac{d}{2}+1} \widehat{\partial} \left(\frac{\partial}{\partial x} \frac{1 + r_F(x)}{P_F(x) + k^2 w} \right)^2 \\
m_{n_1, n_2}^{(FB)d}(w_1, w_2; \eta_\psi, \eta_\Phi) &= m_{n_1, n_2}^{(FB)d}(w_1, w_2) - \eta_\psi \check{m}_{n_1, n_2}^{(FB)d}(w_1, w_2) - \eta_\Phi \hat{m}_{n_1, n_2}^{(FB)d}(w_1, w_2) \\
&= -\frac{1}{2} k^{2(n_1+n_2-1)-d} \int_0^\infty dx x^{\frac{d}{2}} \widehat{\partial} \left\{ \frac{1 + r_F(x)}{[P_F(x) + k^2 w_1]^{n_1}} \frac{\dot{P}(x)}{[P(x) + k^2 w_2]^{n_2}} \right\}. \tag{A.8}
\end{aligned}$$

The dependence of the threshold functions on the anomalous dimensions arises from the t -derivative acting on $Z_{\Phi, k}$ and $Z_{\psi, k}$ within R_k and $Z_{\psi, k} r_F$, respectively. We furthermore use the abbreviations

$$\begin{aligned}
l_n^d(\eta_\Phi) &\equiv l_n^d(0; \eta_\Phi) \quad , \quad l_n^{(F)d}(\eta_\psi) \equiv l_n^{(F)d}(0; \eta_\psi) \\
l_n^d(w) &\equiv l_n^d(w; 0) \quad , \quad l_n^d \equiv l_n^d(0; 0)
\end{aligned} \tag{A.9}$$

etc. and note that in four dimensions the integrals

$$l_2^4(0, 0) = l_2^{(F)4}(0, 0) = l_{1,1}^{(FB)4}(0, 0) = m_4^{(F)4}(0) = m_{1,2}^{(FB)4}(0, 0) = 1 \tag{A.10}$$

are independent of the particular choice of the infrared cutoff.

B Temperature dependent threshold functions

Non-vanishing temperature manifests itself in the flow equations (5.13), (5.16)–(5.18) only through a change to T -dependent threshold functions. In this appendix we will define these functions and discuss some subtleties regarding the definition of the anomalous dimensions and the Yukawa coupling for $T \neq 0$. The corresponding $T = 0$ threshold functions can be found in appendix A where also some of our notation is fixed.

The flow equation (5.13) for the effective average potential involves a bosonic and a

fermionic threshold function whose generalization to finite temperature is straightforward

$$\begin{aligned}
l_n^d(w, \tilde{T}; \eta_\Phi) &= \frac{(n + \delta_{n,0}) v_{d-1}}{2 v_d} k^{2n-d+1} \tilde{T} \sum_{l \in \mathbb{Z}} \int_0^\infty dx x^{\frac{d-3}{2}} Z_{\Phi,k}^{-1} \frac{\partial_t R_k(y)}{[P(y) + k^2 w]^{n+1}}, \\
l_n^{(F)d}(w, \tilde{T}; \eta_\Phi) &= (n + \delta_{n,0}) \frac{v_{d-1}}{v_d} k^{2n-d+1} \\
&\times \tilde{T} \sum_{l \in \mathbb{Z}} \int_0^\infty dx x^{\frac{d-3}{2}} Z_{\psi,k}^{-1} \frac{P_F(y_F)}{1 + r_F(y_F)} \frac{\partial_t [Z_{\psi,k} r_F(y_F)]}{[P_F(y_F) + k^2 w]^{n+1}}
\end{aligned} \tag{B.1}$$

where $\tilde{T} = T/k$ and

$$\begin{aligned}
y &= x + (2l\pi T)^2, \\
y_F &= x + (2l+1)^2 \pi^2 T^2,
\end{aligned} \tag{B.2}$$

The computation of the anomalous dimensions η_Φ , η_ψ and the flow equation for the Yukawa coupling h at non-vanishing temperature requires some care. The anomalous dimensions determine the IR cutoff scale dependence of $Z_{\Phi,k}$ and $Z_{\psi,k}$ according to $\eta_\Phi = -\partial_t \ln Z_{\Phi,k}$, $\eta_\psi = -\partial_t \ln Z_{\psi,k}$ with $t = \ln k/k_\Phi$. It is important to realize that for a computation of the scale dependence of the effective three-dimensional $Z_{\Phi,k}$ and $Z_{\psi,k}$ for $T \neq 0$ momentum dependent wave function renormalization constants of the four-dimensional theory are required. This is a consequence of the fact that in the three-dimensional model each of the infinite number of different Matsubara modes of a four-dimensional bosonic or fermionic field $\phi(Q)$ corresponds to a different value of $Q_0 = 2\pi l T$ or $Q_0 = (2l+1)\pi T$, respectively, with $Q^2 = Q_0^2 + \vec{Q}^2$ and $l \in \mathbb{Z}$. We will therefore allow for momentum dependent wave function renormalizations, i.e. for a kinetic part of Γ_k of the form

$$\Gamma_k^{\text{kin}} = \int \frac{d^d q}{(2\pi)^d} \left\{ Z_{\Phi,k}(q^2) q^2 \text{Tr} \left(\Phi^\dagger(q) \Phi(q) \right) + Z_{\psi,k}(q^2) \bar{\psi}(q) \gamma^\mu q_\mu \psi(q) \right\} \tag{B.3}$$

in momentum space.

In the $O(4)$ -model the evolution equation for $Z_{\Phi,k}(Q)$ may then be obtained by considering a background field configuration with a small momentum dependence,

$$\Phi_j(x) = \varphi \delta_{j1} + \left(\delta\varphi e^{-iQx} + \delta\varphi^* e^{iQx} \right) \delta_{j2}; \quad j = 1, \dots, 4 \tag{B.4}$$

supplemented by

$$\psi_a = \bar{\psi}_a = 0; \quad a = 1, 2. \tag{B.5}$$

Expanding around this configuration at the minimum of the effective average potential U_k we observe that $\delta\varphi$ corresponds to an excitation in the Goldstone boson direction. The exact inverse two-point function $\Gamma_k^{(2)}$ turns out to be block-diagonal with respect to scalar and fermion indices for this configuration. It therefore decays into corresponding matrices $\Gamma_{S_k}^{(2)}$ and $\Gamma_{F_k}^{(2)}$ acting in the scalar and fermion subspaces, respectively. The scale dependence of the scalar wave function renormalization for non-vanishing T is obtained from (2.10)

and (B.3) for the configuration (B.4) as

$$\begin{aligned} \frac{\partial}{\partial t} Z_{\Phi,k}(Q) &= \frac{1}{\vec{Q}^2} \left(\lim_{\delta\varphi\delta\varphi^* \rightarrow 0} \frac{\delta}{\delta(\delta\varphi\delta\varphi^*)} \left\{ \frac{1}{2} \text{Tr} \left[\left(\Gamma_{S^k}^{(2)} + R_k \right)^{-1} \frac{\partial}{\partial t} R_k \right] \right. \right. \\ &\quad \left. \left. - \text{Tr} \left[\left(\Gamma_{F^k}^{(2)} + R_{F^k} \right)^{-1} \frac{\partial}{\partial t} R_{F^k} \right] \right\} - (\vec{Q} \rightarrow 0) \right). \end{aligned} \quad (\text{B.6})$$

In the three-dimensional theory there is now a different scalar wave function renormalization $Z_{\Phi,k}(Q_0, \vec{Q})$ for each Matsubara mode Q_0 . As in the four-dimensional model for $T = 0$ we neglect the momentum dependence of the wave function renormalization constants and evaluate $Z_{\Phi,k}$ for $\vec{Q} = 0$ for each Matsubara mode. We will furthermore simplify the truncation of the effective average action by choosing the Matsubara zero-mode wave function renormalization constant for all Matsubara modes, i.e., approximate

$$Z_{\Phi,k}(\vec{T}) = Z_{\Phi,k}(Q_0^2 = 0, \vec{Q}^2 = 0). \quad (\text{B.7})$$

This is justified by the rapid decoupling of all massive Matsubara modes within a small range of k for fixed T as discussed in section 5.5. This results in the expression (5.18) for η_{Φ} but now with temperature dependent threshold functions ($\vec{T} = T/k$)

$$\begin{aligned} m_{n_1, n_2}^d(w_1, w_2, \vec{T}; \eta_{\Phi}) &= m_{n_1, n_2}^d(w_1, w_2, \vec{T}) - \eta_{\Phi} \hat{m}_{n_1, n_2}^d(w_1, w_2, \vec{T}) \\ &= -\frac{1}{2} k^{2(n_1+n_2-1)-d+1} \frac{dv_{d-1}}{(d-1)v_d} \\ &\quad \times \vec{T} \sum_{l \in \mathbb{Z}} \int_0^{\infty} dx x^{\frac{d-1}{2}} \frac{\widehat{\partial}}{\partial t} \left\{ \frac{\dot{P}(y)}{[P(y) + k^2 w_1]^{n_1}} \frac{\dot{P}(y)}{[P(y) + k^2 w_2]^{n_2}} \right\} \\ m_4^{(F)d}(w, \vec{T}; \eta_{\psi}) &= m_4^{(F)d}(w, \vec{T}) - \eta_{\psi} \check{m}_4^{(F)d}(w, \vec{T}) \\ &= -\frac{1}{2} k^{5-d} \frac{dv_{d-1}}{(d-1)v_d} \vec{T} \sum_{l \in \mathbb{Z}} \int_0^{\infty} dx x^{\frac{d-1}{2}} y_F \frac{\widehat{\partial}}{\partial t} \left(\frac{\partial}{\partial x} \frac{1 + r_F(y_F)}{P_F(y_F) + k^2 w} \right)^2. \end{aligned} \quad (\text{B.8})$$

For further technical details we refer the reader to ref. [].

The fermion anomalous dimension and the flow equation for the Yukawa coupling can be obtained by considering a field configuration

$$\begin{aligned} \Phi_j(x) &= \varphi \delta_{j1}; \quad j = 1, \dots, 4, \\ \psi_a(x) &= \psi_a e^{-iQx}, \\ \bar{\psi}_a(x) &= \bar{\psi}_a e^{iQx}; \quad a = 1, 2. \end{aligned} \quad (\text{B.9})$$

The derivation follows similar lines as for the scalar anomalous dimension discussed above. For computational details we refer the reader to ref. [46]. An important difference as compared to $Z_{\Phi,k}$ relates to the fact that there are no fermionic zero modes. It would

therefore be inconsistent to define $Z_{\psi,k}(\tilde{T})$ or $h_k(\tilde{T})$ at $Q_0 = 0$ if Q denotes the external fermion momentum. Yet, we will again resort to the approximation of using the same wave function renormalization constant and Yukawa coupling for all fermionic Matsubara modes. For the same reason as for $Z_{\Phi,k}(\tilde{T})$ we will use for this purpose the mode with the lowest T -dependent mass, i.e. define

$$\begin{aligned} Z_{\psi,k}(\tilde{T}) &= Z_{\psi,k}(Q_0^2 = \pi^2 T^2, \vec{Q}^2 = 0), \\ h_k(\tilde{T}) &= h_k(Q_0^2 = \pi^2 T^2, \vec{Q}^2 = 0), \end{aligned} \quad (\text{B.10})$$

where we have neglected a possible dependence of h_k on the external scalar momentum of the Yukawa vertex. This yields the expressions (5.17) and (5.18) for the flow of h^2 and η_ψ , respectively, but now with the T -dependent threshold functions

$$\begin{aligned} m_{1,2}^{(FB)d}(w_1, w_2, \tilde{T}; \eta_\psi, \eta_\Phi) &= m_{1,2}^{(FB)d}(w_1, w_2, \tilde{T}) \\ &\quad - \eta_\Phi \hat{m}_{1,2}^{(FB)d}(w_1, w_2, \tilde{T}) - \eta_\psi \check{m}_{1,2}^{(FB)d}(w_1, w_2, \tilde{T}) \\ &= -\frac{1}{2} k^{2(n_1+n_2)-d-1} \frac{dv_{d-1}}{(d-1)v_d} \tilde{T} \sum_{l \in \mathbb{Z}} \int_0^\infty dx x^{\frac{d-1}{2}} \\ &\quad \times \frac{\widehat{\partial}}{\partial t} \left\{ \frac{1 + r_F(y_F)}{[P_F(y_F) + k^2 w_1]^{n_1}} \frac{\dot{P}(y)}{[P(y) + k^2 w_2]^{n_2}} \right\}, \\ l_{n_1, n_2}^{(FB)d}(w_1, w_2, \tilde{T}; \eta_\psi, \eta_\Phi) &= l_{n_1, n_2}^{(FB)d}(w_1, w_2, \tilde{T}) \\ &\quad - \eta_\psi \check{l}_{n_1, n_2}^{(FB)d}(w_1, w_2, \tilde{T}) - \eta_\Phi \hat{l}_{n_1, n_2}^{(FB)d}(w_1, w_2, \tilde{T}) \\ &= -\frac{1}{2} k^{2(n_1+n_2)-d+1} \frac{v_{d-1}}{v_d} \tilde{T} \times \sum_{l \in \mathbb{Z}} \int_0^\infty dx x^{\frac{d-3}{2}} \\ &\quad \frac{\widehat{\partial}}{\partial t} \left\{ \frac{1}{[P_F(y_F) + k^2 w_1]^{n_1} [P(y) + k^2 w_2]^{n_2}} \right\}. \end{aligned} \quad (\text{B.11})$$

C Pole structure of the l_n^d integrals

The integrals

$$\begin{aligned} l_n^d(\omega) &= -n \int_0^\infty dy y^{\frac{d}{2}+1} \frac{\partial r(y)}{\partial y} [y(1+r(y)) + \omega]^{-(n+1)}, \\ \hat{l}_n^d(\omega) &= \frac{n}{2} \int_0^\infty dy y^{\frac{d}{2}} r(y) [y(1+r(y)) + \omega]^{-(n+1)} \end{aligned} \quad (\text{C.1})$$

with

$$r(y) = \frac{e^{-y}}{1 - e^{-y}}, \quad \frac{\partial r(y)}{\partial y} = -\frac{e^{-y}}{(1 - e^{-y})^2} \quad (\text{C.2})$$

exhibit for $d \leq 2(n+1)$ a singularity at $\omega = -1$. The massless dimensionless average propagator $y(1+r(y))$ is a monotonic function of y that takes on its minimum at $y = 0$

with $\lim_{y \rightarrow 0} y(1+r(y)) = 1$. We define new variables δ and z ,

$$\delta = \omega + 1 \quad , \quad z = y(1+r(y)) - 1 \quad (\text{C.3})$$

and substitute in (C.1),

$$\begin{aligned} l_n^d(\delta) &= \int_0^\infty dz G_n^d(z) (z + \delta)^{-(n+1)}, \\ \hat{l}_n^d(\delta) &= \int_0^\infty dz \hat{G}_n^d(z) (z + \delta)^{-(n+1)} \end{aligned} \quad (\text{C.4})$$

with

$$\begin{aligned} G_n^d(z) &= -\frac{ny^{\frac{d}{2}+1} \frac{\partial r(y)}{\partial y}}{1+r(y) + y \frac{\partial r(y)}{\partial y}}, \\ \hat{G}_n^d(z) &= \frac{ny^{\frac{d}{2}} r(y)}{2 \left(1+r(y) + y \frac{\partial r(y)}{\partial y} \right)} \end{aligned} \quad (\text{C.5})$$

and $y = y(z)$. For $d < 2(n+1)$ the integrals (C.4) have a pole at $\delta = 0$. (The singularity becomes logarithmic in δ for $d = 2(n+1)$). In this case for $\delta \rightarrow 0$ the dominant contribution to the integral comes from the region $y \simeq 0$ or equivalently $z \simeq 0$. To find an approximate expression for l_n^d and \hat{l}_n^d near the pole we expand the regular part of G_n^d and \hat{G}_n^d around $z = 0$. With

$$\begin{aligned} r(y) &= \frac{1}{y} \left(1 - \frac{1}{2}y + \frac{1}{12}y^2 + O(y^4) \right), \\ \frac{\partial r(y)}{\partial y} &= -\frac{1}{y^2} \left(1 - \frac{1}{12}y^2 + O(y^4) \right) \end{aligned} \quad (\text{C.6})$$

one obtains

$$\begin{aligned} G_n^d(z) &= ny^{\frac{d}{2}-1} \left(2 - \frac{2}{3}y + \frac{1}{18}y^2 + O(y^3) \right), \\ \hat{G}_n^d(z) &= \frac{n}{2}y^{\frac{d}{2}-1} \left(2 - \frac{5}{3}y + \frac{13}{18}y^2 + O(y^3) \right). \end{aligned} \quad (\text{C.7})$$

The inversion of $z(y)$ given by (C.3) can be done by expanding

$$z = \frac{1}{2}y + \frac{1}{12}y^2 + O(y^4) \quad (\text{C.8})$$

and we find

$$y = 2z - \frac{2}{3}z^2 + \frac{4}{9}z^3 + O(z^4). \quad (\text{C.9})$$

Insertion of (C.9) in (C.7) yields

$$\begin{aligned} G_n^d(z) &= 2n(2z)^{\frac{d}{2}-1} \left(1 - \frac{1}{3} \left(\frac{d}{2} + 1 \right) z + \left[\frac{1}{3} + \frac{1}{18} \left(\frac{d}{2} - 1 \right) \left(\frac{d}{2} + 6 \right) \right] z^2 + O(z^3) \right), \\ \hat{G}_n^d(z) &= n(2z)^{\frac{d}{2}-1} \left(1 - \frac{1}{3} \left(\frac{d}{2} + 4 \right) z + \left[2 + \frac{1}{18} \left(\frac{d}{2} - 1 \right) \left(\frac{d}{2} + 12 \right) \right] z^2 + O(z^3) \right). \end{aligned} \quad (\text{C.10})$$

We consider for $d = 3$ and $n \geq 1$ the zeroth order expression for l_n^d and \hat{l}_n^d that obtains from the first term in (C.10) and the exchange of summation and integration in (C.4). Near the pole one finds

$$\begin{aligned} l_n^3(\delta) &\simeq 2^{3/2} n \int_0^\infty dz z^{1/2} (z + \delta)^{-(n+1)} \\ \hat{l}_n^3(\delta) &= \frac{1}{2} l_n^3(\delta). \end{aligned} \quad (\text{C.11})$$

The leading contributions to l_1^3 , l_2^3 and l_3^3 are therefore given by

$$\begin{aligned} l_1^3(\delta) &= 2^{1/2} \pi \delta^{-1/2}, \\ l_2^3(\delta) &= 2^{-1/2} \pi \delta^{-3/2}, \\ l_3^3(\delta) &= 2^{-5/2} 3 \pi \delta^{-5/2}. \end{aligned} \quad (\text{C.12})$$

We have verified this numerically.

D The quark mass term

In this appendix we determine the source $j = \text{diag}(j_u, j_d, \dots)$ as a function of the average current quark mass \hat{m} . In this context it is important to note that the source j does not depend on the IR cutoff scale k . Since j is determined by the properties of the quark meson model at the compositeness scale k_Φ and also enters directly the value of the pion mass, which is determined at $k = 0$, this relation provides a bridge between the short and long distance properties of the quark meson model. This will allow us to compute the chiral condensate $\langle \bar{\psi}\psi \rangle$ or the parameter B_0 of chiral perturbation theory [3]. (We expect, however, sizeable corrections when going from two to three flavors. They arise because of the relevance of strange quark physics at scales near k_Φ .) In a more general context we need the proportionality coefficient a_q between the source j_q and the current quark mass m_q , $q = u, d, \dots$, taken at the renormalization scale⁵² $\mu = k_\Phi$,

$$j_q = \frac{Z_{\psi, k_\Phi}}{\bar{h}_{k_\Phi}} a_q m_q. \quad (\text{D.1})$$

⁵²We will occasionally use the notation $\hat{m}(\mu)$, $m_q(\mu)$ or $\langle \bar{\psi}\psi \rangle(\mu) \equiv \langle \bar{\psi}\psi \rangle_{k=0}(\mu)$ (not to be confused with $\langle \bar{\psi}\psi \rangle_k \equiv \langle \bar{\psi}\psi \rangle_k(\mu = k_\Phi)$) in order to indicate the renormalization scale μ . If no argument is given $\mu = k_\Phi$ is assumed.

For a computation of the coefficient a_q we need to look into the details of the introduction of composite meson fields in QCD [44, 122]. Let us assume that at the scale k_Φ a part of the QCD average action for quarks $\Gamma_{k_\Phi}[\psi]$ factorizes in the quark bilinear

$$\chi_{ab}(q) = - \int \frac{d^4p}{(2\pi)^4} \tilde{g}(p, q) \bar{\psi}_{Lb}(p) \psi_{Ra}(p + q) \quad (\text{D.2})$$

such that

$$\Gamma_{k_\Phi}[\psi] = -F_{k_\Phi}[\chi] + \Gamma'_{k_\Phi}[\psi] . \quad (\text{D.3})$$

We can then introduce meson fields by inserting the identity

$$N \int D\Phi \exp(-F_{k_\Phi}[\chi + \Phi]) = 1 \quad (\text{D.4})$$

into the path integral which formally defines $\Gamma_{k_\Phi}[\psi]$. (Here N is a field independent normalization factor.) This effectively replaces in (D.3) the term $-F_{k_\Phi}[\chi]$ by⁵³

$$-F_{k_\Phi}[\chi] + F_{k_\Phi}[\chi + \Phi] = \frac{\partial F_{k_\Phi}[\chi]}{\partial \chi_{ab}(q)} \Phi_{ab}(q) + \frac{1}{2} \frac{\partial^2 F_{k_\Phi}[\chi]}{\partial \chi_{ab}(q) \partial \chi_{cd}(q')} \Phi_{ab}(q) \Phi_{cd}(q') + \dots \quad (\text{D.5})$$

The original multi-quark interaction $-F_{k_\Phi}[\chi]$ is canceled by the lowest order term in the Taylor expansion in Φ . Instead, we have substituted mesonic self-interactions $F_{k_\Phi}[\Phi]$ and interactions between mesons and quarks corresponding to the terms in the expansion which contain powers of χ and Φ . In particular, we may specialize to the case where the derivative terms in F_{k_Φ} are small and consider a local form $F_{k_\Phi} = \int d^4x f_{k_\Phi}(\chi)$. A quark mass term is linear in χ and translates into a source term for Φ

$$-\frac{Z_{\psi, k_\Phi}}{\tilde{g}} \text{Tr}(\chi^\dagger m + m^\dagger \chi) \longrightarrow -\frac{Z_{\psi, k_\Phi}}{\tilde{g}} \text{Tr}(\Phi^\dagger m + m^\dagger \Phi) = -\frac{1}{2} \text{Tr}(\Phi^\dagger j + j^\dagger \Phi) \quad (\text{D.6})$$

where $m = \text{diag}(m_u, m_d, \dots)$. A factorizing four fermion interaction yields

$$\bar{m}_{k_\Phi}^2 \text{Tr} \chi^\dagger \chi \longrightarrow \bar{m}_{k_\Phi}^2 \text{Tr} \Phi^\dagger \Phi + \bar{m}_{k_\Phi}^2 \text{Tr}(\Phi^\dagger \chi + \chi^\dagger \Phi) . \quad (\text{D.7})$$

The second term corresponds to the Yukawa interaction with $\bar{h}_{k_\Phi} = \bar{m}_{k_\Phi}^2 \tilde{g}$. We can therefore extract a_q from eq. (D.6) as

$$a_q = 2\bar{m}_{k_\Phi}^2 . \quad (\text{D.8})$$

We note that only the terms linear and quadratic in χ influence the value of a_q . We could either restrict the composite fields from the beginning to the ones contained in the $O(4)$ symmetric linear σ -model or work with all the fields contained in a complex 2×2 matrix Φ . In the latter case the anomaly term would contribute to both the masses and the Yukawa coupling. The net result is the same with $\bar{m}_{k_\Phi}^2$ denoting the relevant mass term for the $O(4)$

⁵³The summation over internal indices as well as the integration over momenta has been suppressed. For complex $\chi_{ab}(q)$ similar terms have to be supplemented in the expansion. See ref. [44, 122] for a more detailed description. In our Euclidean conventions one has $\chi_{ab}^\dagger \sim +\tilde{g}^* \bar{\psi}_{Rb} \psi_{La}$.

vector. For our conventions with $\bar{h}_{k_\Phi} = 1$ we have to normalize with $\tilde{g} = \bar{m}_{k_\Phi}^{-2}$. Finally an eight fermion interaction becomes

$$\frac{1}{2}\bar{\lambda}_{k_\Phi} (\text{Tr}\chi^\dagger\chi)^2 \longrightarrow \frac{1}{2}\bar{\lambda}_{k_\Phi} (\text{Tr}\Phi^\dagger\Phi)^2 + \bar{\lambda}_{k_\Phi} \text{Tr}\Phi^\dagger\Phi \text{Tr}(\chi^\dagger\Phi + \Phi^\dagger\chi) + \dots \quad (\text{D.9})$$

We see here the appearance of terms quadratic in the quarks involving higher powers of Φ .

There is an alternative, equivalent way of understanding the relation between j and m_q : The quark masses in the picture with mesons must be equal at the scale k_Φ to the current quark mass $m_q(k_\Phi)$. Let us consider an $O(4)$ symmetric fermionic interaction $\bar{m}_{k_\Phi}^2 \text{Tr}\chi^\dagger\chi + \frac{1}{2}\bar{\lambda}_{k_\Phi} (\text{Tr}\chi^\dagger\chi)^2$ which leads to a meson potential

$$U_{k_\Phi} = \bar{m}_{k_\Phi}^2 \text{Tr}\Phi^\dagger\Phi + \frac{1}{2}\bar{\lambda}_{k_\Phi} (\text{Tr}\Phi^\dagger\Phi)^2. \quad (\text{D.10})$$

In the mesonic picture the quarks acquire masses through the Yukawa coupling to Φ

$$M_k = \frac{\bar{h}_k}{Z_{\psi,k}} \left(1 + \frac{\bar{\lambda}_k}{\bar{m}_k^2} \text{Tr}\langle\Phi^\dagger\rangle_k \langle\Phi\rangle_k \right) \langle\Phi\rangle_k \quad (\text{D.11})$$

where the second term arises from the higher order coupling in (D.9). Here $\langle\Phi\rangle_k = \text{diag}(\varphi_u, \varphi_d, \dots)$ is the expectation value at the coarse graining scale k in the presence of the source term and $M_k = \text{diag}(M_u, M_d, \dots)$. It is sufficient to specify the dependence of U_{k_Φ} on real diagonal fields Φ_{qq} . Then the φ_q are determined from the condition

$$\frac{\partial U_{k_\Phi}}{\partial \Phi_{qq}}(\varphi_q) = 2 \left(\bar{m}_{k_\Phi}^2 + \bar{\lambda}_{k_\Phi} \sum_{q'} \varphi_{q'}^2 \right) \varphi_q = j_q. \quad (\text{D.12})$$

Identifying $M_{k=k_\Phi}$ in (D.11) with $m(k_\Phi)$ one has

$$a_q \left(1 + \frac{\bar{\lambda}_{k_\Phi}}{\bar{m}_{k_\Phi}^2} \sum_{q'} \varphi_{q'}^2 \right) = \frac{j_q}{\varphi_q} = 2\bar{m}_{k_\Phi}^2 + 2\bar{\lambda}_{k_\Phi} \sum_{q'} \varphi_{q'}^2 \quad (\text{D.13})$$

and we recover (D.8) or, in our normalization with $Z_{\psi,k_\Phi} = 1$, $\bar{h}_{k_\Phi} = 1$,

$$j = 2\bar{m}_{k_\Phi}^2 \hat{m}. \quad (\text{D.14})$$

It is remarkable that higher order terms (e.g. $\sim \bar{\lambda}_{k_\Phi}$) do not influence the relation between j and \hat{m} . Only the quadratic term $\bar{m}_{k_\Phi}^2$ enters which is in our scenario the only relevant coupling. This feature is an important ingredient for the predictive power of the model as far as the absolute size of the current quark mass is concerned. An appearance of higher order couplings in a_q would make it very hard to compute this quantity. We emphasize that within our formalism there is no difference of principle between the current quark mass and the constituent quark mass. Whereas the current quark mass $m_q(k_\Phi)$ at the normalization scale $\mu = k_\Phi$ corresponds to $M_{q,k}$ at the compositeness scale k_Φ the constituent quark mass

is $M_{q,k=0}$. As k is lowered from k_Φ to zero one observes that the quark mass increases, similarly to the running current quark mass. Once chiral symmetry breaking sets in at the scale $k_{\chi SB}$ there is a large increase in the quark masses, especially for M_u and M_d .

The formalism of composite fields also provides the link [44] to the chiral condensate $\langle \bar{\psi}\psi \rangle$ since the expectation value $\langle \Phi \rangle$ is related to the expectation value of a composite quark-antiquark operator. For $\bar{\lambda} = 0$ one has [122]

$$\langle \Phi \rangle_k + \langle \Phi^\dagger \rangle_k = -\frac{1}{\bar{m}_{k_\Phi}^2} \langle \bar{\psi}\psi \rangle_k(k_\Phi) + m_q(k_\Phi) + m_q^\dagger(k_\Phi) \quad (\text{D.15})$$

with $\langle \bar{\psi}\psi \rangle_k(k_\Phi)$ a suitably regularized operator normalized at $\mu = k_\Phi$.

References

- [1] D.J. Gross and F.A. Wilczek, Phys. Rev. Lett. **30** (1973) 1343; H.D. Politzer, Phys. Rev. Lett. **30** (1973) 1346.
- [2] G. 't Hooft, Phys. Rep. **142** (1986) 357.
- [3] J. Gasser and H. Leutwyler, Phys. Rep. **C87** (1982) 77.
- [4] See e.g. A. Pich, Rept. Prog. Phys. **58** (1995) 563 and references therein.
- [5] M. Gell–Mann and M. Levy, Nuovo Cim. **16** (1960) 705.
- [6] D.–U. Jungnickel and C. Wetterich, Phys. Lett. **B389** (1996) 600.
- [7] D.–U. Jungnickel and C. Wetterich, preprint HD–THEP–97–9 (hep-ph/9704345), to appear in Z. Phys. **C**.
- [8] For a review see A.V. Smilga, preprint TPI-MINN-96-23 (hep-ph/9612347).
- [9] See e.g. M. Jacob and H. Satz, eds., *Quark Matter Formation and Heavy Ion Collisions* (World Scientific, Singapore 1982); H.R. Schmidt and J. Schukraft, J. Phys. **G 19** (1993) 1705.
- [10] E.W. Kolb and M.S. Turner, *The Early Universe* (Addison–Wesley 1990).
- [11] J.C. Collins and M.J. Perry, Phys. Rev. Lett. **34** (1975) 1353.
- [12] J. Cleymans, R.V. Gavai and E. Suhonen, Phys. Rep. **130** (1986) 217.
- [13] For a review about lattice approaches to non–zero baryon density see I. Barbour, Nucl. Phys. **B** (Proc. Suppl.) **26** (1992) 22.
- [14] B. Svetitsky and L.G. Yaffe, Nucl. Phys. **B 210** (1982) 423; B. Svetitsky, Phys. Rep. **132** (1986) 1.
- [15] J.B. Kogut et al., Phys. Rev. Lett. **50** (1983) 393, **51** (1983) 869; S.A. Gottlieb et al. Phys. Rev. Lett. **55** (1985) 1958; N.H. Christ and A.E. Terrano, Phys. Rev. Lett. **56** (1986) 111.
- [16] K. Kajantie, M. Laine, K. Rummukainen and M.E. Shaposhnikov, Nucl. Phys. **B466** (1996) 189; M. Laine, Phys. Lett. **385 B** (1996) 249.
- [17] M. Reuter and C. Wetterich, Nucl. Phys. **B408** (1993) 91, **417** (1994) 181, **427** (1994) 291;
- [18] B. Bergerhoff and C. Wetterich, Nucl. Phys. **B440** (1995) 91.
- [19] W. Buchmüller and O. Philipsen, Nucl. Phys. **B443** (1995) 47.

-
- [20] K. Geiger, Phys. Rev. **D46** (1992) 4965, 4986; J. Kapusta, P. Lichard and D. Seibert, Nucl. Phys. **A544** (1992) 485c; E.V. Shuryak, Phys. Rev. Lett. **68** (1992) 3270.
- [21] E.V. Shuryak, Phys. Lett. **B78** (1978) 150.
- [22] J.D. Bjorken, Phys. Rev. **D27** (1983) 140.
- [23] K. Geiger, B. Mueller, Nucl. Phys. **B369** (1992) 600; K. Geiger, Phys. Rev. **D46** (1992) 4965, 4986. T.S. Biró et al., Phys. Rev. **C48** (1993) 1275.
- [24] See e.g. K. Geiger, in *Quark-Gluon Plasma 2*, edited by R. Hwa (World Scientific, 1995) and references therein.
- [25] For a review see H. Meyer–Ortmanns, Rev. Mod. Phys. **68** (1996) 473.
- [26] K. Rajagopal and F. Wilczek, Nucl. Phys. **B399** (1993) 395; **B404** (1993) 577.
- [27] K. Rajagopal, in *Quark-Gluon Plasma 2*, edited by R. Hwa (World Scientific, 1995) (hep-ph/9504310).
- [28] A. A. Anselm, Phys. Lett. **B217** (1988) 169; A. A. Anselm and M. G. Ryskin, Phys. Lett. **B266** (1991) 482; J.–P. Blaizot and A. Krzywicki, Phys. Rev. **D46** (1992) 246; J. D. Bjorken, Int. J. Mod. Phys. **A7** (1992) 4189; Acta Phys. Pol. **B23** (1992) 561; K. L. Kowalski and C. C. Taylor, preprint CWRUTH-92-6 (hep-ph/9211282); J. D. Bjorken, K. L. Kowalski and C. C. Taylor, preprint SLAC-PUB-6109 (hep-ph/9309235).
- [29] C.M.G. Lattes, Y. Fujimoto and S. Hasegawa, Phys. Rep. **65** (1980) 151.
- [30] K.G. Wilson, Phys. Rev. **B4** (1971) 3174; 3184; K.G. Wilson and I.G. Kogut, Phys. Rep. **12** (1974) 75; F. Wegner, in *Phase Transitions and Critical Phenomena*, vol. 6, eds. C. Domb and M.S. Greene (Academic Press, 1976).
- [31] R.D. Pisarski and F. Wilczek, Phys. Rev. **D29** (1984) 338.
- [32] E. Shuryak, Comm. Nucl. Part. Phys. **21** (1994) 235.
- [33] J. Berges, D.–U. Jungnickel and C. Wetterich, preprint HD–THEP–97–20 (hep-ph/9705474).
- [34] See e.g. F. Karsch, preprint BI-TP-97-19 (hep-lat/9706006) and references therein.
- [35] K. Rajagopal, *Disorienting the Chiral Condensate at the QCD Phase Transition*, Hirschegg Workshop 1997, eds. H. Feldmeier et al. (hep-ph/9703258) and references therein.
- [36] C. Bernard et al., Phys. Rev. **D55** (1997) 6861; C. Bernard et al., Nucl. Phys. Proc. Suppl. **53** (1997) 442.

- [37] C. Wetterich, Nucl. Phys. **B352** (1991) 529; Z. Phys. **C57** (1993) 451; **C60** (1993) 461.
- [38] C. Wetterich, Phys. Lett. **B301** (1993) 90.
- [39] F. Wegner and A. Houghton, Phys. Rev. **A8** (1973) 401.
- [40] J.F. Nicoll and T.S. Chang, Phys. Lett. **A62** (1977) 287.
- [41] S. Weinberg in *Critical Phenomena for Field Theorists*, Erice Subnucl. Phys. (1976) 1;
- [42] J. Polchinski, Nucl. Phys. **B231** (1984) 269.
- [43] A. Hasenfratz and P. Hasenfratz, Nucl. Phys. **B270** (1986) 687; P. Hasenfratz and J. Nager, Z. Phys. **C 37** (1988) 477.
- [44] U. Ellwanger and C. Wetterich, Nucl. Phys. **B423** (1994) 137.
- [45] C. Wetterich, Heidelberg preprint HD-THEP-95-2 (hep-th/9501119); Z. Phys. **C72** (1996) 139.
- [46] D.-U. Jungnickel and C. Wetterich, Phys. Rev. **D53** (1996) 5142.
- [47] S. Gottlieb et al., Phys. Rev. Lett. **59** (1987) 1513; Phys. Rev. **D35** (1987) 3972; **D41** (1990) 622; **D47** (1993) 315; M. Fukugita et al., Phys. Rev. Lett. **65** (1990) 816; Phys. Rev. **D42** (1990) 2936; F.R. Brown et al., Phys. Rev. Lett. **65** (1990) 2491; F. Karsch, Phys. Rev. **D 49** (1993) 3791; F. Karsch and E. Laermann, Phys. Rev. **D 50** (1994) 6954; C. Bernard et al., Phys. Rev., **D45** (1992) 3854; **D54** (1996) 4585; G. Boyd et al., preprint IFUP-TH-40-96 (hep-lat/9607046); Y. Iwasaki et al., Phys. Rev. Lett. **78** (1997) 179; A. Ukawa, Nucl. Phys. Proc. Suppl. (1997) 438.
- [48] F.R. Brown et al., Phys. Rev. Lett. **65** (1990) 2491.
- [49] Y. Iwasaki et al., Nucl. Phys. **B** (Proc. Suppl.) **42** (1995) 499; Y. Iwasaki et al., Phys. Rev. **D 54** (1996) 7010.
- [50] F. Wilczek, Int. J. Mod. Phys. **A7** (1992) 3911;
- [51] S. Gavin, A. Gocksch and R.D. Pisarski, Phys. Rev. **D 49** (1994) 3079;
- [52] R.D. Pisarski, preprint BNL-RP-941 (hep-ph/9503330).
- [53] J. Kapusta, *Finite Temperature Field Theory* (Cambridge University Press, 1989).
- [54] P. Ginsparg, Nucl. Phys. **B170** (1980) 388; T. Appelquist and R. Pisarski, Phys. Rev. **D23** (1981) 2305; S. Nadkarni, Phys. Rev. **D27** (1983) 917; N.P. Landsman, Nucl. Phys. **B322** (1989) 498.

-
- [55] N. Tetradis and C. Wetterich, Nucl. Phys. **B398** (1993) 659; Int. J. Mod. Phys. **A9** (1994) 4029.
- [56] K.G. Wilson and M.E. Fisher, Phys. Rev. Lett. **28** (1972) 240.
- [57] G. Parisi, J. Stat. Phys. **23** (1980) 49.
- [58] See e.g. A.J. Guttmann, *Phase Transitions and Critical Phenomena* vol. 13, C. Domb and J. Lebowitz eds. (Academic Press, New York 1989).
- [59] M. Creutz, Phys. Rev. Lett. **45** (1980) 313.
- [60] E. Brezin, D.J. Wallace and K.G. Wilson, Phys. Rev. **B7** (1973) 232.
- [61] D. Toussaint, Phys. Rev. **D55** (1997) 362.
- [62] J. Berges, N. Tetradis and C. Wetterich, Phys. Rev. Lett. **77** (1996) 873.
- [63] J. Adams, J. Berges, S. Bornholdt, F. Freire, N. Tetradis and C. Wetterich, Mod. Phys. Lett. **A10** (1995) 2367.
- [64] J. Berges, *Field Theory near the Critical Temperature*, preprint HD-THEP-96-41 (hep-ph/9610353), appears in Erice Subnucl. Phys., 34th Course, Effective Theories and Fundamental Interactions, 1996.
- [65] M.M. Tsy-pin, preprint FIAN-TD-23-95 (hep-lat/9601021).
- [66] M.M. Tsy-pin, Phys. Rev. Lett. **73** (1994) 2015.
- [67] J. Zinn-Justin, *Quantum Field Theory and Critical Phenomena* (Oxford University Press, 1993).
- [68] J. Berges and C. Wetterich, Nucl. Phys. **B487** (1997) 675.
- [69] J. Berges, N. Tetradis and C. Wetterich, Phys. Lett. **B393** (1997) 387.
- [70] S. Coleman and E. Weinberg, Phys. Rev. **D7** (1973) 1888.
- [71] J. Langer, Ann. Phys. **41** (1967) 108; **54** (1969) 258; Physica **73** (1974) 61.
- [72] S. Coleman, Phys. Rev. **D15** (1977) 2929; C. Callan and S. Coleman, Phys. Rev. **D16** (1977) 1762.
- [73] A.D. Linde, Phys. Lett. **B100** (1981) 37; Nucl. Phys. **B216** (1983) 421.
- [74] J. Berges, D.-U. Jungnickel and C. Wetterich, in preparation.

-
- [75] J. Schwinger, Proc. Nat. Acad. Sci. (US) **37** (1951) 452; J. Goldstone, A. Salam and S. Weinberg, Phys. Rev. **127** (1962) 965; G. Jona-Lasinio, Nuov. Cim. **34** (1964) 1790; K. Symanzik, Comm. Math. Phys. **16** (1970) 48; B. Zumino, Brandeis Lectures, ed. S. Deser (MIT Press, Cambridge 1970); J. Iliopoulos, C. Itzykson and A. Martin, Rev. Mod. Phys. **47** (1975) 165.
- [76] L.P. Kadanoff, Physica **2** (1966) 263.
- [77] C. Wetterich, Z. Phys. **C48** (1990) 693; S. Bornholdt and C. Wetterich, Z. Phys. **C58** (1993) 585.
- [78] M. Reuter and C. Wetterich, Nucl. Phys. **B391** (1993) 147; Heidelberg preprint HD-THEP-94-39 (hep-th/9411227).
- [79] C. Becchi, preprint GEF-TH-96-11 (hep-th/9607188).
- [80] M. Bonini, M. D' Attanasio and G. Marchesini, Nucl. Phys. **B418** (1994) 81; **B421** (1994) 429;
- [81] U. Ellwanger, Phys. Lett. **B335** (1994) 364; U. Ellwanger, M. Hirsch and A. Weber, Z. Phys. **C69** (1996) 687.
- [82] U. Ellwanger, M. Hirsch and A. Weber, preprint LPTHE-ORSAY-96-50 (hep-ph/9606468).
- [83] U. Ellwanger, preprint LPTHE-ORSAY-97-02 (hep-ph/9702309).
- [84] F.J. Dyson, Phys. Rev. **75** (1949) 1736; J. Schwinger, Proc. Nat. Acad. Sci. **37** (1951) 452, 455.
- [85] M. Bonini, M. D' Attanasio and G. Marchesini, Nucl. Phys. **B409** (1993) 441.
- [86] U. Ellwanger, Z. Phys. **C58** (1993) 619; C. Wetterich, Int. J. Mod. Phys. **A9** (1994) 3571.
- [87] G. Keller, C. Kopper and M. Salmhofer, Helv. Phys. Acta **65** (1992) 32; G. Keller and G. Kopper, Phys. Lett. **B273** (1991) 323.
- [88] B. Widom, J. Chem. Phys. **43** (1965) 3898.
- [89] P. Butera and M. Comi, Phys. Rev. **B52** (1995) 6185; preprint IFUM-548-FT (hep-lat/9703018) and references therein.
- [90] T. Reisz, Phys. Lett. **B360** (1995) 77.
- [91] A.D. Linde, Phys. Lett. **B96** (1980) 289; D. Gross, R.D. Pisarski and L. Yaffe, Rev. Mod. Phys. **53** (1981) 43.

- [92] N. Tetradis and C. Wetterich, Nucl. Phys. **B422** (1994) 541.
- [93] T. R. Morris, Phys. Lett. **B329** (1994) 241.
- [94] T. R. Morris, Phys. Lett. **B345** (1995) 139.
- [95] T.R. Morris and M.D. Turner, preprint SHEP-97-06 (hep-th/9704202).
- [96] J. Berges, S. Seide and C. Wetterich, in preparation.
- [97] I. Kondor and T. Temesvari, J. Phys. Lett. (Paris) **39**, L99 (1978).
- [98] G. Baker, D. Meiron and B. Nickel, Phys. Rev. **B17** (1978) 1365, cited in ref. [50].
- [99] P. Butera, M. Comi, Phys. Rev. **E55** (1997) 6391.
- [100] R. Guida and J. Zinn-Justin, Nucl. Phys. **B489** (1997) 626 and references therein.
- [101] F. Wegner, Z. Phys. **B35** (1979) 207; **B38** (1980) 113; Phys. Rep. **67** (1980) 15; K.B. Efetov, A.I. Larkin and D.E. Kheml'nitskii, Sov. Phys. JETP **52** (1980) 568.
- [102] See e.g. P.G. de Gennes and J. Prost, *The physics of liquid crystals*, 2. ed. (Oxford, Clarendon Press, 1995).
- [103] For a review see P. Di Francesco, P. Ginsparg and J. Zinn-Justin, Phys. Rep. **254** (1995) 1.
- [104] D.-U. Jungnickel and C. Wetterich, Heidelberg preprint HD-THEP-96-19 to appear in Z. Phys. **C** (hep-ph/9606483).
- [105] H. Meyer-Ortmanns, H.-J. Pirner and A. Patkos, Phys. Lett. **B295** (1992) 255; Int. J. Mod. Phys. **C3** (1992) 993; D. Metzger, H. Meyer-Ortmanns and H.-J. Pirner, Phys. Lett. **B321** (1994) 66; **B328** (1994) 547; H. Meyer-Ortmanns and B.-J. Schäfer, Phys. Rev. **D53** (1996) 6586.
- [106] A. Ringwald and C. Wetterich, Nucl. Phys. **B334** (1990) 506; N. Tetradis and C. Wetterich, Nucl. Phys. **B383** (1992) 197.
- [107] D.F. Litim, Phys. Lett. **B393** (1997) 103.
- [108] S. Bornholdt, P. Büttner, N. Tetradis and C. Wetterich, preprint CAU-THP-95-38 (cond-mat/9603129); S. Bornholdt, N. Tetradis and C. Wetterich, Phys. Rev. **D53** (1996) 4552.
- [109] M. Alford and J. March-Russell, Nucl. Phys. **B417** (1994) 527.
- [110] A. J. Paterson, Nucl. Phys. **B190** (1981) 188; R. D. Pisarski and D. L. Stein, Phys. Rev. **B23** (1981) 3549; J. Phys. **A14** (1981) 3341.

- [111] B. Bergerhoff, D. Litim, S. Lola and C. Wetterich, *Int. J. Mod. Phys.* **A11** (1996) 4273. B. Bergerhoff, F. Freire, D. Litim, S. Lola and C. Wetterich, *Phys. Rev.* **B53** (1996) 5734.
- [112] P. Dreher, *Phys. Lett.* **B281** (1992) 127; Y. Shen, *Nucl. Phys. B (Proc. Suppl.)* **34** (1994) 712.
- [113] S. Y. Khlebnikov and R. G. Schnathorst, *Phys. Lett.* **B358** (1995) 81.
- [114] F. John, *Partial Differential Equations*, 4. ed. (New York, Springer, 1992).
- [115] N. Tetradis, *Nucl. Phys.* **B488** (1997) 92.
- [116] J. Kripfganz, A. Laser and M.G. Schmidt, *Nucl. Phys.* **B433** (1995) 467; *Z. Phys.* **C73** (1997) 353.
- [117] W. Buchmüller, Z. Fodor, T. Helbig and D. Walliser, *Ann. Phys.* **234** (1994) 260; D. Bödeker, W. Buchmüller, Z. Fodor and T. Helbig, *Nucl. Phys.* **B423** (1994) 171.
- [118] J. Baacke, *Phys. Rev.* **D52** (1995) 6760.
- [119] Proceedings of Quark Matter '96, *Nucl. Phys.* **A610** (1996).
- [120] J. Comellas, Y. Kubyshev and E. Moreno, *Nucl. Phys.* **B490** (1997) 653.
- [121] K.-I. Aoki, K. Morikawa, J.-I. Sumi, H. Terao and M. Tomoyose, *Progr. Theor. Phys.* **97** (1997) 479.
- [122] D.-U. Jungnickel and C. Wetterich, *Nonperturbative flow equations and low-energy QCD*, Workshop on Quantum Chromodynamics: Confinement, Collisions, and Chaos, Paris, France, and QCD 96, Yaroslavl, Russia, 1996 (hep-ph/9610336).
- [123] Y. Nambu and G. Jona-Lasinio, *Phys. Rev.* **122** (1961) 345.
- [124] J. Bijnens, *Phys. Rep.* **265** (1996) 369.
- [125] J. Pawłowski, preprint FSUJ-TPI-05-96 (hep-th/9605037).
- [126] M. Gell-Mann, R.J. Oakes and B. Renner, *Phys. Rev.* **175** (1968) 2195.
- [127] H. Leutwyler, preprint HEP-9609467 (hep-ph/9609467).
- [128] M. Jamin and M. Münz, *Z. Phys.* **C66** (1995) 633; K.G. Chetyrkin, C.A. Dominguez, D. Pirjol and K. Schilcher *Phys. Rev.* **D51** (1995) 5090; J. Bijnens, J. Prades and E. de Rafael, *Phys. Lett.* **B348** (1995) 226.
- [129] K. Kanaya and S. Kaya, *Phys. Rev.* **D51** (1995) 2404.
- [130] S. Gottlieb et al., *Phys. Rev.* **D55** (1997) 6852.

-
- [131] F. Karsch, Phys. Rev. **D49** (1994) 3791; F. Karsch and E. Laermann, Phys. Rev. **D50** (1994) 6954.
- [132] Y. Iwasaki, K. Kanaya, S. Kaya and T. Yoshie, Phys. Rev. Lett. **78** (1997) 179.
- [133] G. Boyd, F. Karsch, E. Laermann and M. Oevers, preprint IFUP-TH-40-96 (hep-lat/9607046).
- [134] A. Ukawa, Nucl. Phys. Proc. Suppl. **53** (1997) 106; S. Aoki, T. Kaneda, A. Ukawa and T. Umemura, Nucl. Phys. Proc. Suppl. **53** (1997) 438.
- [135] J. Gasser and H. Leutwyler, Phys. Lett. **B184** (1987) 83; H. Leutwyler, Nucl. Phys. Proc. Suppl. **B4** (1988) 248.
- [136] C. Bernard et al., Phys. Rev. Lett. **78** (1997) 598.
- [137] J.B. Kogut, J.F. Lagae and D.K. Sinclair, Nucl. Phys. Proc. Suppl. **53** (1997) 269.
- [138] S.F. Edwards, P.W. Anderson, J. Phys. **F5** (1975) 965.
- [139] P.G. de Gennes, Phys. Lett. **A38** (1972) 339.
- [140] Work done with M. Gräter.
- [141] M. Gräter and C. Wetterich, Phys. Rev. Lett. **75** (1995) 378.
- [142] G. Ferretti, Nucl. Phys. **B450** (1995) 713.
- [143] S. Nishigaki, Phys. Lett. **B376** (1996) 73.
- [144] B. Bergerhoff and C. Wetterich, in preparation.